



Technische Universität München

Fakultät für Chemie

Lehrstuhl für Physikalische Chemie

Thermal and Photo-Activated Molecular Mechanisms of Surface Processes on $\text{TiO}_2(110)$ and $\text{GaN}(0001)$

Sebastian Ludwig Kollmannsberger

Vollständiger Abdruck der von der Fakultät für Chemie der Technischen Universität München zur Erlangung des akademischen Grades eines

Doktors der Naturwissenschaften (Dr. rer. nat.)

genehmigten Dissertation.

Vorsitzender: Priv.-Doz. Dr. Friedrich Esch

Prüfende der Dissertation

1. Prof. Dr. Ulrich K. Heiz
2. Hon.-Prof. Dr. Richard W. Fischer

Die Dissertation wurde am 10.04.2018 bei der Technischen Universität München eingereicht und durch die Fakultät für Chemie am 08.05.2018 angenommen.

Gehe ruhig und gelassen durch Lärm und Hast und sei des Friedens eingedenk, den die Stille bergen kann. Stehe, soweit ohne Selbstaufgabe möglich, in freundlicher Beziehung zu allen Menschen. Äußere deine Wahrheit ruhig und klar und höre anderen zu, auch den Geistlosen und Unwissenden; auch sie haben ihre Geschichte.

Meide laute und aggressive Menschen, sie sind eine Qual für den Geist. Wenn du dich mit anderen vergleichst, könntest du bitter werden und dir nichtig vorkommen; denn immer wird es jemanden geben, der größer ist oder geringer als du.

Freue dich deiner Leistungen wie auch deiner Pläne. Bleibe weiter an deinem eigenen Weiterkommen interessiert, wie bescheiden es auch immer sein mag. Es ist ein echter Besitz im wechselnden Glück der Zeit. In deinen geschäftlichen Angelegenheiten lass Vorsicht walten, denn die Welt ist voller Betrug.

Viele Menschen ringen um hohe Ideale; und überall ist das Leben voller falschem Heldentum. Sei du selbst; vor allen Dingen heuchle keine Zuneigung. Noch sei zynisch, was die Liebe betrifft; denn auch im Angesicht aller Dürre und Enttäuschung ist sie doch immerwährend wie wachsendes Gras.

Ertrage freundlich und gelassen den Ratschluss der Jahre, gib die Dinge der Jugend mit Grazie auf. Stärke die Kraft des Geistes, damit sie dich im plötzlich hereinbrechenden Unglück schütze. Und beruhige dich nicht mit Einbildungen. Viele Befürchtungen sind Folge von Erschöpfung und Einsamkeit. Bei einem heilsamen Maß an Selbstdisziplin sei gut zu dir selbst.

Du bist ein Kind des Universums, nicht weniger als die Bäume und die Sterne. Du hast ein Recht, hier zu sein. Und ob es dir nun bewusst ist oder nicht: Es gibt keinen Zweifel, das Universum entfaltet sich wie vorgesehen.

Darum lebe in Frieden mit Gott, was für eine Vorstellung auch immer du von ihm hast und was immer dein Mühen und Sehnen ist. In der lärmenden Wirrnis des Lebens erhalte dir den Frieden mit deiner Seele. Trotz all ihrem Schein, der Plackerei und zerbrochenen Träumen ist diese Welt doch wunderschön. Sei vorsichtig. Strebe danach, glücklich zu sein.

Max Ehrmann (1872–1945) sampled by Christian Steiffen (2013)

Abstract

The influence of semiconductor material properties on thermal and photo-activated surface processes were studied under well-defined conditions in ultra high vacuum. The oxidation of alcohols was investigated as a function of the type of semiconductor, bulk doping, and surface composition. It was shown that the photo-oxidation of alcohols on a $\text{TiO}_2(110)$ surface proceeds via a hole mediated pathway and that a species in α -position of the alcohol functionality is abstracted. Furthermore, it was demonstrated that the therewith associated hydroxylation of the $\text{TiO}_2(110)$ surface is the origin of the poisoning effect in alcohol photo-oxidation. Consequently, it was clarified that the photo-chemistry is mainly determined by the semiconductor surface. Moreover, it was found that the thermal behavior of adsorbates is crucial for the photo-catalytic activity and that even the selectivity of the photo-reaction is determined by temperature.

In addition, the thermal ethanol chemistry was studied in detail on $\text{TiO}_2(110)$, $\text{GaN}(0001)$, and $\text{Ga}_2\text{O}_3(\bar{2}01)$. It was found that in the case of $\text{GaN}(0001)$ all metal sites convert ethanol to acetaldehyde and ethylene, whereas on $\text{TiO}_2(110)$ particularly the defect sites are active and generate the same products as observed on $\text{GaN}(0001)$. The reactivity of the GaN surface was investigated as a function of the native oxide, as it is always present under ambient conditions. It was found that the ethanol conversion vanishes on a fully oxidized surface, which is identically observed on $\text{Ga}_2\text{O}_3(\bar{2}01)$.

The electronic properties of the $\text{GaN}(0001)$ surface were further investigated by adsorption and photon-stimulated desorption of CO . It was demonstrated that the bulk doping level determines the amount of adsorbable CO . Furthermore, the photon-stimulated desorption of CO was strongly inhibited by surface oxidation.

Zusammenfassung

Der Einfluss von Halbleitermaterialeigenschaften auf thermische und photoaktivierte Oberflächenprozesse wurde unter wohl definierten Bedingungen im Ultrahochvakuum erforscht. Dabei wurde die Oxidation von Alkoholen in Abhängigkeit von der Art des Halbleiters, der Dotierung und der Oberflächenbeschaffenheit betrachtet. Es wurde gezeigt, dass die Photooxidation von Alkoholen auf einer $\text{TiO}_2(110)$ Oberfläche über einen lochgetriebenen Reaktionsweg verläuft und dass einer der in α -Position zur Hydroxygruppe stehenden Reste abgespalten wird. Des Weiteren wurde bewiesen, dass die damit einhergehende Hydroxylierung der $\text{TiO}_2(110)$ Oberfläche der Grund der Vergiftung der photoaktivierten Alkoholoxidation ist. Folglich, wurde klargelegt, dass die Halbleiteroberfläche die Photochemie bestimmt. Darüber hinaus wurde herausgefunden, dass das thermische Verhalten der Adsorbate ausschlaggebend für deren photokatalytische Aktivität ist, und sogar die Selektivität der Photoreaktion wird durch die Temperatur bestimmt.

Zusätzlich wurde das thermische Verhalten von Ethanol auf $\text{TiO}_2(110)$, $\text{GaN}(0001)$ und $\text{Ga}_2\text{O}_3(\bar{2}01)$ im Detail untersucht. Es wurde beobachtet, dass auf der $\text{GaN}(0001)$ Oberfläche jegliches Ethanol, welches zu einem Galliumatom gebunden ist, zu Acetaldehyd und Ethylen umgesetzt wird, wohingegen auf $\text{TiO}_2(110)$ vor allem die Defektstellen eine Aktivität aufweisen und das Aldehyd sowie das Alken erzeugen. Die Reaktivität der GaN Oberfläche wurde in Abhängigkeit der natürlichen Oxidschicht, welche unter Umgebungsbedingungen immer vorhanden ist, erforscht. Es wurde gezeigt, dass die Umsetzung von Ethanol auf einer komplett oxidierten Oberfläche verschwindet, identisch zu dem chemischen Verhalten auf $\text{Ga}_2\text{O}_3(\bar{2}01)$.

Außerdem wurden die elektronischen Eigenschaften der $\text{GaN}(0001)$ Oberfläche mit Hilfe von Adsorption und photonenstimulierter CO Desorption erforscht. Es wurde gezeigt, dass der Dotierungsgehalt des Halbleiters die adsorbierbare Menge an CO bestimmt. Darüber hinaus wurde die photonenstimulierte CO Desorption stark von der Oberflächenoxidation blockiert.

Table of contents

| | |
|---|------------|
| Abstract | ii |
| Zusammenfassung | iii |
| 1 Introduction | 1 |
| 1.1 Alcohol Chemistry on the TiO ₂ (110) Surface | 2 |
| 1.1.1 Methanol | 3 |
| 1.1.2 Ethanol | 4 |
| 1.1.3 Isopropanol | 5 |
| 1.1.4 General Consideration of the Photo-Reactive Site | 5 |
| 1.2 Surface Science on GaN(0001) | 6 |
| 1.2.1 Surface Preparation | 6 |
| 1.2.2 Native Surface Oxide | 7 |
| 1.2.3 Reactivity of GaN Surfaces | 8 |
| 2 Experimental Setup | 9 |
| 2.1 Laser Setup | 9 |
| 2.2 Cluster Source | 10 |
| 2.3 Semiconductor Sample Holder | 11 |
| 2.3.1 Sample Holder for Cylindrical Semiconductor Samples | 11 |
| 2.3.2 Sample Holder for Square-Shaped Semiconductor Platelet Samples | 12 |
| 2.3.3 Transfer Sample Holder | 14 |
| 3 Experimental Methods | 17 |
| 3.1 TPD Experiments | 17 |
| 3.2 PSD and PSR Experiments | 20 |
| 3.2.1 Discontinuous PSR | 21 |
| 3.2.2 Continuous PSR | 22 |
| 3.3 Quantitative QMS Analysis | 22 |
| 3.3.1 Calibration of the QMS for One Substance | 23 |
| 3.3.2 Conversion to Other Molecules | 24 |
| 3.3.3 Determination of the QMS Transmission Function | 28 |
| 3.3.4 Disentangling Overlapping Fragment Masses | 28 |

| | | |
|----------|--|-----------|
| 3.4 | Crystal Preparation | 30 |
| 3.4.1 | TiO ₂ (110) | 30 |
| 3.4.2 | GaN | 31 |
| 3.5 | Auger Electron Spectroscopy | 32 |
| 4 | Results - Publication Summaries | 34 |
| 4.1 | Ethanol photocatalysis on rutile TiO ₂ (110): the role of defects and water | 35 |
| 4.2 | Doping-Dependent Adsorption and Photon-Stimulated Desorption of CO on GaN(0001) | 37 |
| 4.3 | Anhydrous Ethanol Dehydrogenation on Metal–Organic Chemical Vapor Deposition Grown GaN(0001) | 39 |
| 4.4 | Ethanol surface chemistry on MBE-grown GaN(0001), GaO _x /GaN(0001), and Ga ₂ O ₃ ($\bar{2}01$) | 41 |
| 4.5 | Photocatalytic selectivity switch to C–C scission: α -methyl ejection of tert-butanol on TiO ₂ (110) | 43 |
| 5 | Bibliographic Details for Complete Publications | 45 |
| 5.1 | Ethanol photocatalysis on rutile TiO ₂ (110): the role of defects and water | 45 |
| 5.2 | Isomer-Selective Detection of Aromatic Molecules in Temperature-Programmed Desorption for Model Catalysis | 46 |
| 5.3 | Doping-Dependent Adsorption and Photon-Stimulated Desorption of CO on GaN(0001) | 47 |
| 5.4 | Anhydrous Ethanol Dehydrogenation on Metal–Organic Chemical Vapor Deposition Grown GaN (0001) | 48 |
| 5.5 | Ethanol surface chemistry on MBE-grown GaN(0001), GaO _x /GaN(0001), and Ga ₂ O ₃ ($\bar{2}01$) | 49 |
| 5.6 | Photocatalytic selectivity switch to C–C scission: α -methyl ejection of tert-butanol on TiO ₂ (110) | 50 |
| 6 | Conclusion and Outlook | 51 |
| | References | 55 |
| | Danksagung | 62 |
| | Appendix A Reprint Permissions | 64 |

| | |
|---|------------|
| Table of contents | vi |
| Appendix B Contributions to the Publications | 73 |
| Appendix C Technical drawings | 74 |
| Appendix D Publications | 92 |
| Appendix E Unpublished Manuscripts | 153 |

1. Introduction

It is discussed in the news on a daily basis, how to react on global warming, particularly when considering the alarming temperature change from year to year[1]. Associated therewith is the increase of natural disasters like droughts, wildfires, storms, and floods[2]. Therefore, it is obvious, that the climate change has to be fought or at least slowed down. But which steps can we take to decrease for example the emission of CO₂, which is responsible for a major part of the greenhouse effect?[3]

If the situation in Germany is considered, about 85% of the annual CO₂ emission results from energy-related emissions.[4] That shows that the actual trend to renewable energy for electricity production is clearly still in the beginning. Only about 38.2% of the produced electricity is currently from renewable energy, while still coal with 39.1% has the biggest proportion of the energy mix.[5]

If we break all this down to emission that we can control self-reliantly, as for example emission from individual transportation, someone may replace a combustion engine vehicle by an electric one. However, one has to realize that the electricity production, still creates a lot of CO₂ emission. An alternative can therefore be a fuel cell car, which uses hydrogen as fuel and oxygen from air. As a result only H₂O is emitted. The problem in this case is to get the energy carrier hydrogen.

A promising approach is the dehydrogenation of ethanol from fermentation of biomass.[6] Thermochemical, electrochemical, photo-biological, and photo-electrochemical technologies are studied to find cheap, stable, low temperature techniques with a fast production rate.[7]

A second option to generate hydrogen is water splitting. Mostly electrochemical studies have been performed,[8–10] but also photo-electrochemical water splitting is heavily studied.[11–13] However, up to now a perfect method does neither exist for dehydrogenation of ethanol nor for water splitting.

Therefore, a further technique, namely the photo-catalytic hydrogen production from ethanol or water, has attracted greatest attention in the last decade.[14–20] This method implies the illumination of a semiconductor with wavelengths shorter than the band gap, which generates charge carrier pairs that subsequently drive the chemical reaction. Thereby no external applied voltage is required. The most heavily studied semiconductor material for the photo-catalytic approach is TiO₂, which is attributed to its high catalytic activity, its stability against photo-corossion, and not at least because of its availability and cost.[21]

While most of the studies in this field try to optimize the performance of a catalyst by, for example, adding diverse metal co-catalysts,[22] changing the amount and the size of the co-catalyst,[23] optimizing the particle size,[24] adding sacrificial reagents,[20] investigations to get insights in molecular mechanisms and to understand the effects of such changes are scarce. Therefore, studies on perfectly defined model systems with the option to change every parameter separately are needed. In order to ensure these terms, studies in the ultra high vacuum (UHV) on single crystalline materials are required. Such studies enable, inter alia, the clarification of surface reactions, the role of the photo-holes and photo-electrons, the function of co-catalysts, and the operating principle of sacrificial reagents.

The goal of this dissertation is to investigate thermal and photo-activated reactions, in particular of ethanol, on TiO₂(110) and GaN(0001) at UHV conditions. Moreover molecular photo-activated mechanisms are investigated to understand the oxidation reaction of alcohols. Furthermore, the influence of bulk doping on surface effects is elucidated and the role of surface states is clarified. In the following, an overview of the literature regarding alcohol chemistry and photo-oxidation on rutile TiO₂(110) as well as surface science studies on GaN(0001) are presented.

1.1 Alcohol Chemistry on the TiO₂(110) Surface

The material rutile TiO₂ and the properties of the (110) surface have to be considered first. The literature values of the TiO₂ band gap vary from 3.0 eV - 3.2 eV.[25, 26] This corresponds to a wavelength of 413 nm - 387 nm, which is in the UV region. The TiO₂(110) surface consists of bridge bonded oxygen (BBO) rows and fivefold coordinated Ti⁴⁺ ions.[27] Annealing of the crystal leads to a bulk reduction and to surface defects in the BBO rows, which play a major role in the thermal and photo-activated surface chemistry. An illustration of the defect-rich TiO₂(110) surface is depicted in figure 1.1.

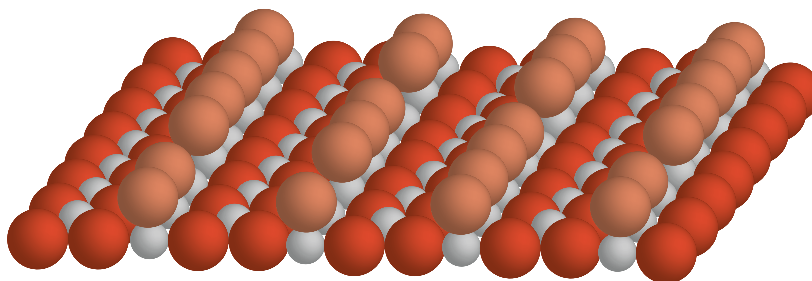


Fig. 1.1 Defect-rich surface of the TiO₂(110) single crystal. The BBO atoms are illustrated in bright orange, the lattice oxygen atoms in dark orange, and the titanium atoms in gray. The missing BBO atoms represent BBO vacancies.

The behavior of various alcohols on this surface was investigated in the last thirty years. The most heavily studied alcohol is methanol, but also diverse studies of ethanol and isopropanol on TiO₂(110) exist. A summary of the literature regarding these three alcohols is given in the next subsections.

1.1.1 Methanol

The thermal methanol chemistry on the TiO₂(110) surface has been experimentally studied since 1998, when Henderson et al. found that methanol dissociates in BBO vacancy sites, whereas molecularly adsorption is predominant on Ti^{4+} sites. The desorption from the TiO₂(110) surface occurs in a low temperature peak or, rather recombinative, in a high temperature peak from the BBO vacancies. Furthermore, they figured out that co-dosed oxygen leads to C-H and O-H bond cleavage.[28, 29] The dissociative adsorption of methanol was later confirmed by TPD and STM studies.[30, 31] Moreover, it was found that methanol starts to diffuse on the surface at 200 K.[32]

The investigations in molecular photo-activated mechanisms of methanol on the TiO₂(110) surface started in the year 2005, when formaldehyde was already figured out as the main reaction product of methanol photo-reforming on powdered TiO₂,[33] The first studies used two-photon photoemission (2PP) spectroscopy to elucidate the electronic structure of methanol on the TiO₂(110) surface.[34, 35] Later it was found with the same technique that methanol can be dissociated with UV light on the TiO₂(110) surface.[36]

In the year 2011 first STM results showed that methanol bound to Ti^{4+} is photo-active and the key catalytic site for photo-induced chemistry, but also that the BBO vacancy concentration has a large effect on the photo-catalytic process.[37] Also in 2011 the group of Henderson clarified that the methoxy is the active species in photo-catalytic hole driven processes. Furthermore, they showed that the reaction products are formaldehyde and BBO-H groups.[38] Since this publication it has been extensively discussed, whether the first step in photo-catalytic methanol oxidation, the methoxy formation, is a thermally driven[38–41] or photo-activated[42–45] one.

On the one hand, the group of Henderson found that a methoxy species can thermally only form at surface imperfections, which means either in a BBO vacancy or, alternatively on a Ti^{4+} -site, if co-adsorbed oxygen adatoms or terminal OH groups are existent.[39] On the other hand, SFG measurements and DFT calculations suggest that methanol can spontaneously dissociate at regular Ti^{4+} -sites.[46]

Apart from this, methyl formate was found as another reaction product by the group of Friend and by the group of Yang.[42, 41, 43] Several studies on the cross coupling mechanism

have been performed, but it is still unclear whether a formyl or a hemiacetal intermediate is formed to produce methyl formate.[45, 47, 40, 48]

The group of Yang claimed that the barrier for water formation from BBO-H groups is lower than the barrier for molecular hydrogen formation. Nevertheless, they observed only a very low H₂ production from methanol photo-reforming on the TiO₂(110) surface.[49]

1.1.2 Ethanol

In the year of 1995 the first study about thermal chemistry of ethanol on the TiO₂(110) surface by the group of Campbell showed that ethoxy is formed on Ti^{4+} -sites upon ethanol adsorption. Furthermore, a recombinative desorption and water formation is observed at low temperature. They concluded that the water formation from the former hydroxyl group leads to a subsequent ethylene formation via a β -hydride elimination and a combined recombinative ethanol desorption at high temperature.[50]

The group of Madix found that similar to methanol two different binding sites are available, resulting in a recombinative low temperature desorption and a high temperature reaction. Although, they observed acetaldehyde from the high temperature channel.[51] Further TPD results elucidated the low and the high temperature reaction channel and showed that a dehydration pathway and a dehydrogenation pathway are possible. The latter one is only observed in the high temperature channel from BBO vacancies.[52]

With STM experiments it can be shown that dissociatively and molecularly adsorbed ethanol exists on regular Ti^{4+} -sites.[53] Furthermore, the diffusion of ethanol is observed at 200 K parallel and perpendicular to the BBO rows.[54]

The photo-activated mechanisms of ethanol on the TiO₂(110) surface were investigated for the first time by the group of Idriss[55] in the year 2007. They were able to show with XPS measurements that ethanol is quickly photo-decomposed with UV light to a reaction intermediate RCOO. They figured out later with TPD that acetaldehyde is the main reaction product of photo-reforming of ethanol with co-dosed O₂. [56].

The group of Yang confirms with 2PP and TPD studies the acetaldehyde production from Ti^{4+} -sites. Furthermore, they found BBO-H as by-product, which leaves as water in TPD experiments. Moreover, they postulate a photo-activated high temperature ethylene formation.[57, 44]

STM studies of the group of Besenbacher[58] confirm that acetaldehyde is formed from ethanol photo-reforming on regular Ti^{4+} -sites. Furthermore, they were able to show that the amount of BBO vacancies increases with the desorption of the by-product water and that the surface is re-oxidized from bulk oxygen.

1.1.3 Isopropanol

The thermal chemistry of isopropanol is very similar to that of ethanol and can be summarized briefly. There exist also two different binding sites, one at the Ti^{4+} -atoms and one at the BBO vacancies. Consequently, two reaction channels as well as a recombinative desorption are possible.[51] The low temperature channel from Ti^{4+} -sites enables dehydration and the high temperature channel from the BBO vacancies enables also dehydrogenation.[59, 60] Furthermore, it is found that pre-dosing of water doubles the yield of the high temperature dehydration pathway.[61]

The investigations in photo-activated mechanisms of isopropanol adsorbed at the TiO₂(110) surface started already comparatively early in the year 1998, which is not the only reason why they are worth mentioning. The group of Engel was able to show that acetone is the main product of photo-reforming on the TiO₂(110) surface. They show a saturation behavior at about 17% of photo-generated acetone. Furthermore, they elucidate the role of BBO vacancies and conclude that they enhance the yield of the reaction but are not the photo-active site.[62–64]

1.1.4 General Consideration of the Photo-Reactive Site

A study of Brinkley and Engel claims that the BBO vacancy cannot be the active site for isopropanol photo-oxidation as a reactivity is observed even under oxidizing conditions, which leads to reoxidation of the BBO vacancies.[62] However, this argument does not take into account that for every reoxidized BBO vacancy site an additional oxygen adatom on a Ti^{4+} -site is created,[65] which may open a new photo-oxidation pathway. Furthermore, it was shown later that with oxygen dosage the reoxidation of BBO vacancy sites is incomplete.[66]

Methanol TPD works of Henderson show that the high temperature peak, which is assigned to the recombinative desorption of methanol from BBO vacancies, is not changed in a TPD after UV illumination.[38, 39] Furthermore, a STM study shows that ethoxy species are present in BBO vacancies after UV illumination at 290 K.[58]

These studies conclude that the BBO vacancy is photo-inactive as alkoxies are observed at those sites after UV illumination. A weakness in this conclusion is, that molecularly adsorbed ethanol or methanol is mobile already at 200 K on a TiO₂(110) surface.[54, 32] Consequently, the alcohol may diffuse into BBO vacancies during a TPD or STM experiment at elevated temperature. Once the molecules are in the vacancies, they could thermally dissociate and will be trapped. If this is the case, the previously mentioned studies do not reflect the true conditions on the surface directly after photo-catalysis.

Another observation is that photo-formed and at low temperature accumulated acetaldehyde or formaldehyde desorbs thermally in a temperature region from 200 K to 300 K in a TPD experiment.[38] This temperature region is assigned to formaldehyde or acetaldehyde desorption from Ti^{4+} -sites in TPD experiments.[67, 68] Consequently, the aldehyde desorption in a TPD experiment following photo-oxidation of the respective alcohol seems to proceed from a Ti^{4+} -site. However, the conditions of an aldehyde TPD and a TPD after an alcohol photo-oxidation are not identically, as the molecules, which are present on the surface are different. Therefore, intermolecular forces could lead to a shift of the desorption temperature.

Moreover, there are also arguments that justify the assignment of the BBO vacancy as the photo-reactive site. A very important fact is that only a fraction of a complete monolayer of adsorbed alcohol can be converted into the oxidation product on a reduced $TiO_2(110)$ surface[62, 49]. Consequently, a conversion of all Ti^{4+} bound alcohol species is ruled out, which could be a hint to a special reactive site.

The photo-oxidation of alcohols is generally believed to be a hole driven process.[38] It is likely that the hole, which is coming to the surface under illumination, is attracted by the negatively charged BBO vacancy (two Ti^{3+} instead of two Ti^{4+} [69]). This is a strong argument for a key role of the BBO vacancy in the photo-oxidation of alcohols.

1.2 Surface Science on GaN(0001)

The first synthetic preparation of GaN, by addition of ammonia gas to metallic gallium at 1173-1273 K, is reported in literature in 1931.[70] Since that time GaN has attracted enormous attention in particular for the use as LED,[71] but also in photo-catalysis.[72] However, the thermal as well as the photo-chemical reactivity of the GaN surface is rarely investigated.

GaN grows in the hexagonal wurtzite structure and has a bandgap of 3.4 eV, which corresponds to photons with a wavelength of 365 nm.[73] The doping level of this semiconductor can be varied from n-type doping to p-type doping. The latter one was investigated for the first time in 1989.[74] The investigations regarding surface preparation, the native surface oxide on GaN and surface reactivity are summarized in the following.

1.2.1 Surface Preparation

Davis et al. achieved no complete removal of carbon and oxygen, neither with wet chemical methods, nor with thermal desorption in vacuum. Even heating in vacuum to temperatures

of a beginning GaN decomposition did not produce a surface free of contaminations.[75] Later, they found that UV/O₃ treatment is the most effective method to remove carbon contamination. In order to subsequently get rid of the oxygen species, they annealed the crystal in NH₃ at 1073 K, which produced an almost contamination free surface. However, with increasing the numbers of cycles of AES measurements, the oxygen signal raised. Consequently, oxidation of the GaN surface by the electron beam was determined.[76] The efficiency of the process of ammonia annealing was confirmed.[77, 78] However, it was found that a significant amount of oxygen is still present on the GaN surface.[79, 80] In contrast to that, the group of Pease postulates that vacuum annealing is more effective than a NH₃ anneal. The chemical pretreatment of the GaN crystal in this case was the exposure to a mixture of 4:1 sulfuric acid to hydrogen peroxide.[81] The group of Roos showed that chemical treatment affects the surface roughness of GaN samples.[82]

An alternative method to chemical etching, vacuum annealing or annealing in NH₃, is ion sputtering. In 1998 it was found that nitrogen sputtering (1 keV) leads to the removal of carbon and oxygen contamination. However, after UHV annealing nitrogen defects are observed. Subsequently, annealing in NH₃ gives a clean and stoichiometric surface.[80] The group of Kahn showed that also vacuum annealing following on nitrogen sputtering with lower energy (0.5 keV) gives a well-ordered and nearly stoichiometric surface.[83] Furthermore, it was found that also the combination of HCl etching and sputtering removes the contaminations.[84]

A comparison of argon and nitrogen sputtering shows that both methods produce a gallium enrichment, though nitrogen sputtering is less damaging, as the sputter gas can compensate for the losses. Furthermore, it is shown that chlorination of such a non-stoichiometric surface can create volatile gallium chlorides.[85]

1.2.2 Native Surface Oxide

Bermudez showed in 1996 that a saturation coverage of 0.4 ML of an ordered oxygen adsorbate layer is obtained, when the GaN surface is exposed to 200 L of oxygen at room temperature.[86] In contrast, the group of Mönch found that oxygen exposure at room temperature leads to 0.79 ± 0.1 ML of dissociative oxygen uptake. In an additional non-dissociative pathway a summed maximum of 2 ML of oxygen was observed.[87] At 823 K even 2.1 ± 0.5 ML of an oxidation layer are obtained, which generate also ordered structures.[88] Such higher values of oxygen uptake are confirmed by a study of the group of Mavrikakis.[79]

The group of Nozawa found that the native oxygen overlayer is mostly in the Ga₂O₃ form. They assumed that reactive dangling bonds are present at the surface, which are the reason

for surface oxidation when exposed to air.[89] An exposure to H₂O and subsequent annealing to 773 K results in the exactly similar oxide-phase as obtained from O₂ exposure.[90] A reduction of a surface re-oxidation of a clean GaN can be achieved by chemisorbed chlorine.[91]

The group of Gao found that the surface oxidation saturates at 10⁸ L of oxygen exposure. They conclude that subsurface oxidation does not occur on GaN samples.[92] Moreover, it was found that the GaN surface is oxidized in a layer by layer mode.[92, 93]

Systematical oxidation of the GaN surface has been examined in dry air[94], in dry oxygen[95], with photo-enhanced wet oxidation in aqueous phosphorous acid[96], and with photo-electrochemical oxidation in glycol and water.[97] It is found that different oxidation rates can be achieved, depending on the applied technique. Furthermore, rough oxide layers as well as uniform ones can be obtained.

1.2.3 Reactivity of GaN Surfaces

The surface processes of some inorganic and organometallic molecules have been investigated on the GaN surface, whereas organic molecules are hardly explored. Concerning inorganic substances, in particular the reaction behavior of hydrogen and ammonia are well known. Shekhar and Jensen found in a temperature programmed desorption (TPD) study that NH₃ adsorbs dissociatively on the GaN(0001) surface. Small amounts of molecular hydrogen desorption were observed after NH₃ adsorption.[98] These results are confirmed by a study of Bermudez.[99] Upon dosage of molecular deuterium at room-temperature a desorption occurs at 700 K.[98] In good agreement with these findings is a study of the group of Henry, who showed that a surface Ga-H species is formed.[100]

Concerning organometallic molecules, the interaction of trimethylgallium, the most common precursor molecule for GaN growing, with the GaN(0001) surface was investigated by the group of Vohs.[101] They observed a dissociation of trimethylgallium to dimethylgallium and monomethylgallium, which desorb between 290 K and 400 K, and the formation of surface-bound methyl groups. The methyl species either desorb as methyl radical or form methane, molecular hydrogen, and surface-bound carbon via a disproportionation pathway.

In the case of organic molecules, as for example alcohols, only a theoretical study of the reactivity of catechol on the GaN surface exists.[102]

2. Experimental Setup

Figure 2.1 shows a schematic illustration of the instrument used for the research obtained during this dissertation. The main parts are the cluster source, the surface preparation and analysis part, as well as the reaction part. The latter one contains the laser setup, the gasline, an electron impact - quadrupole mass spectrometer (EI-QMS), a home built photo-ionisation - time of flight - mass spectrometer (PI-ToF-MS); the latter is described in detail in Winbauer et al.[103].

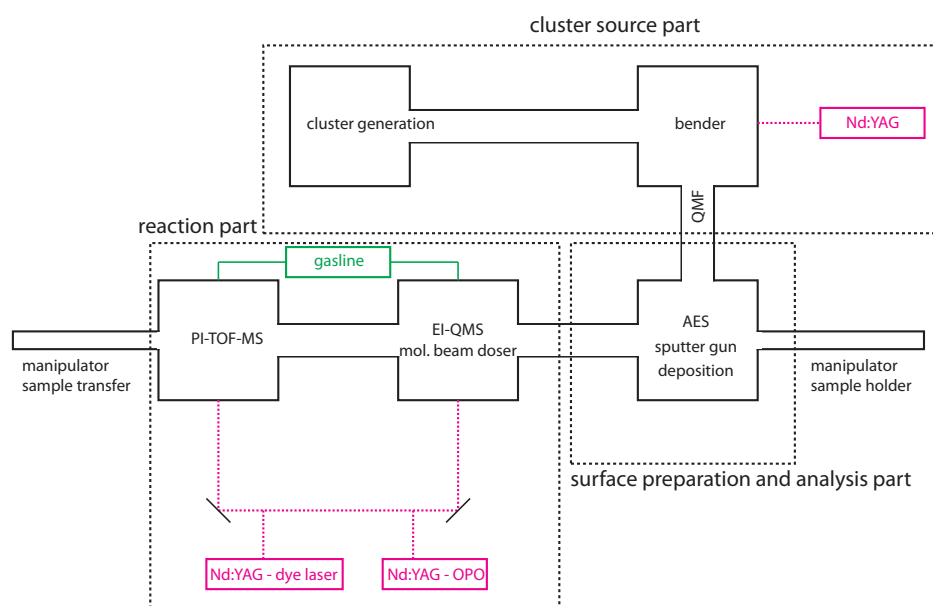


Fig. 2.1 Chamber scheme of the UHV apparatus including the cluster source part, the reaction part, as well as the surface preparation and analysis part.

In order to move the sample to the different stages in the setup a x, y, z, Φ manipulator is used, to which the sample holder is attached. Furthermore, a second manipulator for a fast sample transfer is implemented. In the next sections emphasis is put on the laser setup, the cluster source, and the different sample holders.

2.1 Laser Setup

The laser setup comprises two laser systems, which are tunable in their wavelength. One system consists of a dye laser (SCANMATE 2E, Lambda Physik GmbH), which is pumped by a Nd:YAG (Quanta Ray GCR-3, Spectra-Physics Inc., 20 Hz repetition rate, 10 ns pulse

width). A wavelength of 355 nm is used for pumping the dye laser, which is obtained by frequency sum generation of the fundamental wavelength of 1064 nm and the second harmonic wavelength of 532 nm. The resulting tunable wavelength, which is obtained from the dye laser, is frequency doubled. Afterwards, the laser energy can be adjusted with a graduated gray filter from about 1500 uJ to 50 uJ. For lower laser energies further gray filters can be included in the beam path. The second system also consists of a Nd:YAG laser (Innolas Spitlight HighPower 1200, 20 Hz repetition rate, 7 ns pulse width), which is pumping an optical parametric oscillator (OPO, GWU, premiScan ULD/400). Again, the third harmonic of the Nd:YAG laser is used and guided into the OPO. The obtained wavelength is frequency doubled afterwards and can also be adjusted to lower energies with a graduated gray filter from 800 uJ to 50 uJ as well as with further gray filters. The advantage of the OPO setup is the fast and widely scanable wavelength range (about 300 nm) in comparison to the dye laser, which enables only the scanning of a small wavelength range (about 30 nm) without changing the dye. The advantage of the dye laser setup is the low energy fluctuation from pulse to pulse, the more regular beam profile, the narrower band width, and the higher obtainable pulse energy in comparison to the OPO laser.

For photo experiments, the laser beam is coupled into the reaction chamber with a periscope (CVI Melles Griot GmbH). The semiconductor is illuminated in an angle of 30° off the surface normal, at which complete illumination of the semiconductor surface is achieved. The beam alignment is checked by the observation of the reflection from the semiconductor at the backside of the chamber.

2.2 Cluster Source

The laser vaporization cluster source, which is based on the setup developed by Heiz et al.[104], was built up in the course of this thesis and was attached to the already existing surface preparation and analysis part. The working principle is based on laser ablation (Nd:YAG, 532 nm, 100 Hz, Innolas) of atoms from a rotating metal target, followed by cooling with helium pulses and the expansion into vacuum, which leads to agglomeration of the atoms. From this procedure a mixture of cationic, anionic, and neutral clusters results in the cluster generation chamber. The cationic clusters are separated from the neutral ones with a bender and guided with ion lenses into the quadrupole mass filter (QMF, Extrel, USA), which enables cluster size selection. Alternatively, the QMF can be operated with the AC-potential only; this operation mode acts as a high pass filter. Consequently, a distribution of clusters with several sizes is obtained with this method. In the course of this thesis a Pt-target (99.95% purity, ESG Edelmetalle, Germany) was used for cluster

generation. A final ion lense with an inner aperture of only 6 mm is used to ensure deposition onto the semiconductor surface, only. With a retarding field analysis the soft-landing conditions in cluster deposition ($<1\text{eV/atom}$ in kinetic energy) are confirmed. The cluster current is measured with a picoammeter (Keithley, 6587) to obtain the exact loading of the semiconductor sample.

2.3 Semiconductor Sample Holder

In order to cool and heat the semiconductors, sample holders consisting of a metal heating wire, a metal base plate, and a mounting bracket have been developed. Different sample holders, these are needed depending on the shape of the crystal, are described in detail in the following. Furthermore, if fast exchange of samples is desired, a transfer sample holder for thin square-shape samples can be used.

2.3.1 Sample Holder for Cylindrical Semiconductor Samples

The sample holder for cylindrical semiconductor samples is used for $\text{TiO}_2(110)$ single crystal samples and is described in detail elsewhere.[105] A picture of the sample holder with a freshly mounted $\text{TiO}_2(110)$ single crystal is shown in figure 2.2a, and the sample holder in operation in the UHV chamber is displayed in figure 2.2b.

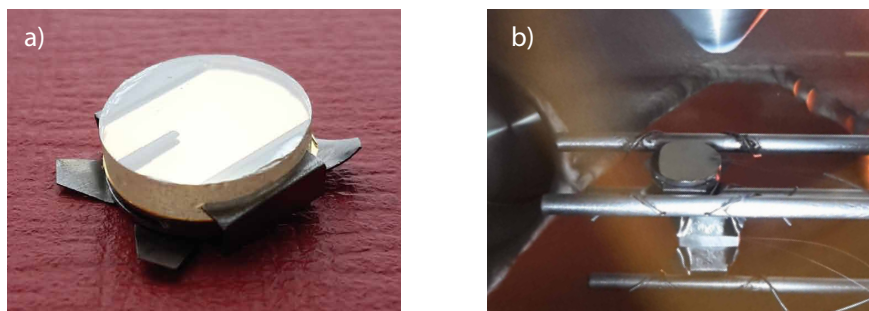


Fig. 2.2 Freshly mounted $\text{TiO}_2(110)$ single crystal in the sample holder for cylindrical semiconductor samples in a) and a readily prepared one in operation in the UHV chamber in b)

In general, the holder consists of a tantalum base plate and two tantalum clamps, which are spot-welded to the base plate. 0.35 mm thick wires made from an alloy of tungsten–26% rhenium (W–26%Re) are used for heating the sample holder and mounting it to the molybdenum rods. This particular material exhibits excellent properties regarding the durable ductility, resistance, and thermal conductance.[103] Furthermore, a gold foil is placed in

between the crystal and the base plate to ensure an optimal thermal contact over the whole area. It is very important to shorten the twisted thermocouple in order to have the entire contacted twisted thermocouple inside the crystal drill hole. Otherwise, a temperature lower than the actual crystal temperature is measured in a heat-up experiment.

Note that the four wings of the tantalum foil, which should prevent the crystal from slipping out, are not needed anymore as the friction between the crystal and the gold foil is large enough. Mechanical stress to the W–26%Re heating wire should be avoided during spot welding. Therefore, the wires should not be bent more than half a turn around the molybdenum rod. In order to optimize the tension of the wire between the molybdenum rods, the latter can be compressed slightly, when bending the wires around them.

2.3.2 Sample Holder for Square-Shaped Semiconductor Platelet Samples

For square-shaped and thin semiconductor samples a new sample holder, which is inspired by the above described design, is developed. An illustration of this sample holder is depicted in figure 2.3.

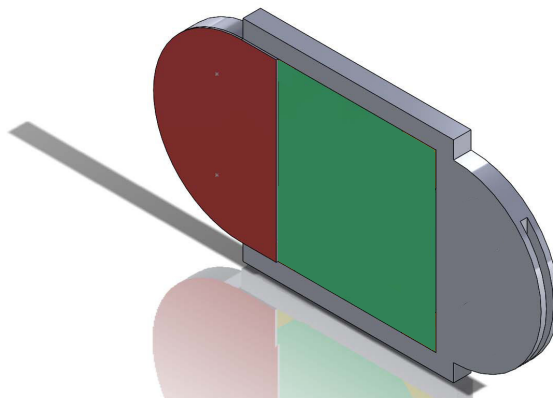


Fig. 2.3 Schematic drawing of the sample holder for square-shaped semiconductor platelets. The tantalum base plate is depicted in gray, the semicircular tantalum retaining plates in red and the semiconductor platelet in green color.

In order to enable an easy mounting, a boat-shaped 1 mm tantalum base plate with a milling groove in the size of the semiconductor platelet is designed. Furthermore, it contains semicircular ends with cut outs for the mounting and heating wires. The distance of the two outer cut outs amounts to 19 mm. Therefore, the distance of the drillings in the molybdenum rods are changed to 18 mm. The other parts are two 0.1 mm thick semicircular retaining plates, which are stamped out from a tantalum foil, and a gold foil for the optimized thermal

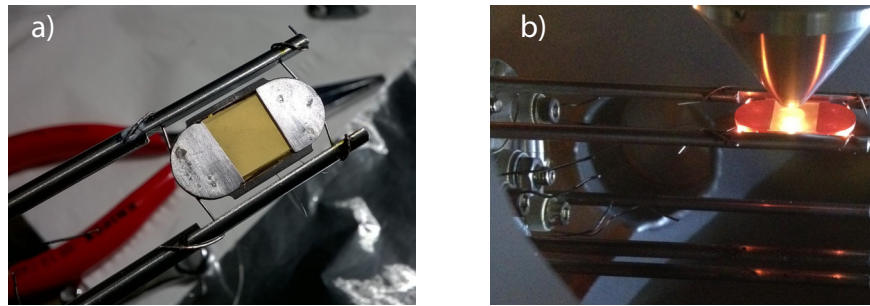


Fig. 2.4 Freshly mounted GaN semiconductor in the sample holder for square-shaped semiconductor platelets in a) and during a high temperature application in the UHV chamber in b).

contact. Technical drawings of the boat-shaped base plate, the retaining plates, and the modified molybdenum rods can be found in the appendix C.1.

An image of the sample holder with a freshly mounted GaN semiconductor sample is shown in figure 2.4a. In figure 2.4b the sample holder during a high temperature application is presented. Note that the complete sample holder glows homogeneously.

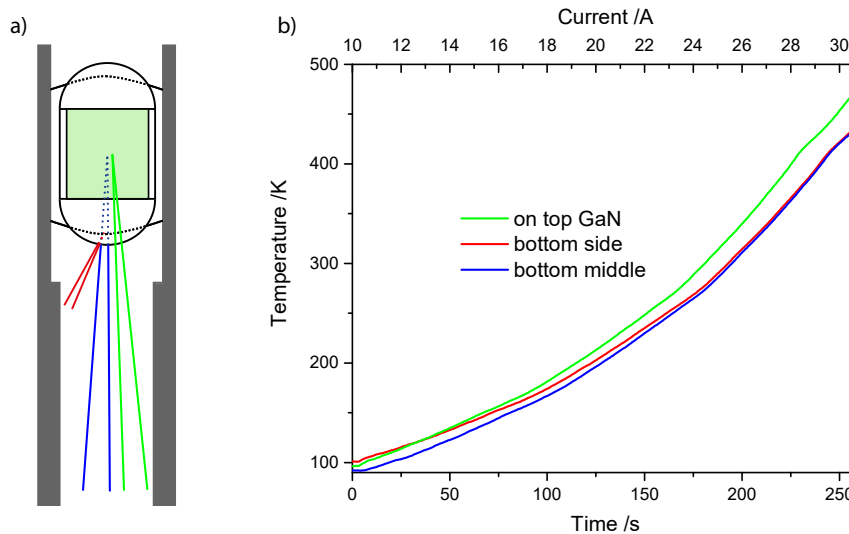


Fig. 2.5 Scheme of the three different thermocouple positions at the sample holder for square-shaped semiconductor platelets in a) and the temperature curves obtained from three heating experiments at three different positions in b). The colors of the temperature curves used in b) reflect the colors of the thermocouples in a). Note that the two x-axes can only be plotted as the current is linearly and identically raising with time in the three different heating experiments.

To proof the temperature distribution, thermocouples are mounted at the bottom middle, the bottom side, and on top of the GaN semiconductor. The positions are illustrated in

figure 2.5a. Furthermore, figure 2.5b shows three different temperature curves, which are from three different thermocouple positions. Note that in one heating experiment only one thermocouple can be measured. A comparison is therefore only possible, when the current is linearly raising with time and identical in the three measurements. It can clearly be seen that the deviation of the temperature at the three positions is less than 20 K over the whole investigated temperature region. Consequently, a measurement of the temperature at the bottom middle position at the base plate does not differ significantly from the surface temperature of the semiconductor sample. Therefore, this thermocouple position can be used for all experiments.

2.3.3 Transfer Sample Holder

A transfer sample holder for square-shaped semiconductor platelets has been developed in order to change samples without breaking the vacuum. The most desired properties were: its mechanical stability, an effective cooling and heating, as well as an easy sample transfer. The transfer sample holder consists in general of two different parts, a fixed one and a transfer unit.

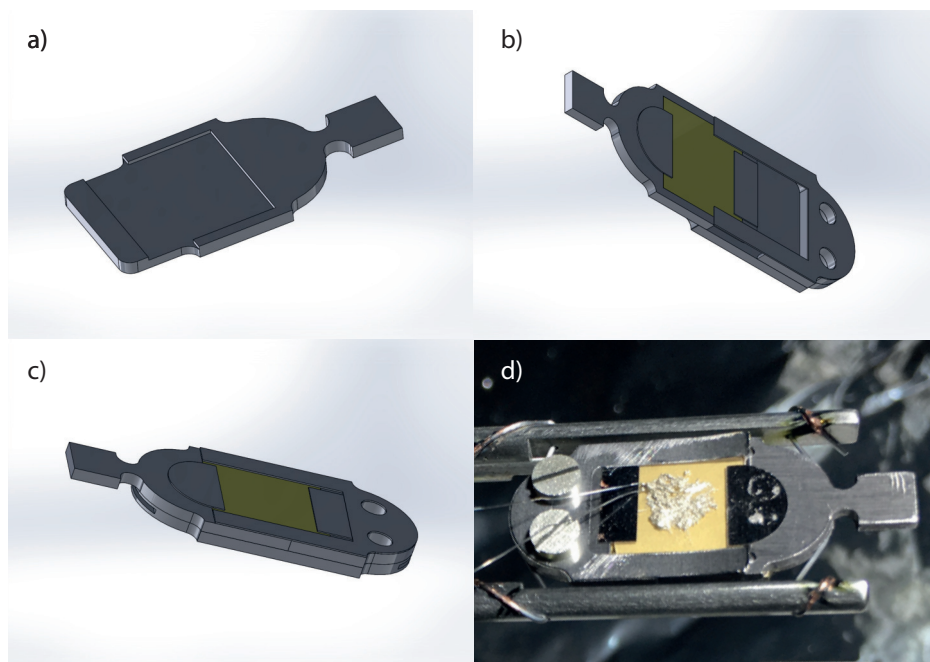


Fig. 2.6 Schematic drawings of the transfer unit in a) and of the complete transfer sample holder in b) and c). A photo of the readily installed transfer sample holder in d).

In figure 2.6a) a schematic drawing of the tantalum base plate of the transfer unit, which is inspired by the above described sample holder for platelets, is depicted. The crucial

changes are the omitted semicircular end at the left side and the added rectangular adapter at the right end. This adapter is needed for the sample rotation-locking mechanism of the applied transfer tool (SH2/12 ISR from SPECS Surface Nano Analysis GmbH). The tantalum retaining plates are reduced in order to avoid a blocking with the fixed unit. In figure 2.6b)-c) two schematic drawings of the complete holder are shown. The fixed unit, which is also completely built from tantalum, consists of a base plate, a semicircular ended intermediate piece, and a retaining spring. These three parts are tied together with screws, and the spring is spot welded at the sides to the intermediate piece, which guarantees a high mechanical stability. It can clearly be seen, how the transfer unit is plugged into the fixed unit from figure 2.6b) to figure 2.6c). The photo in figure 2.6d) shows the readily installed transfer sample holder with the plugged in transfer unit, which has a thermocouple glued to the surface of the semiconductor. Technical drawings of the various parts of the transfer sample holder can be found in the appendix C.2.

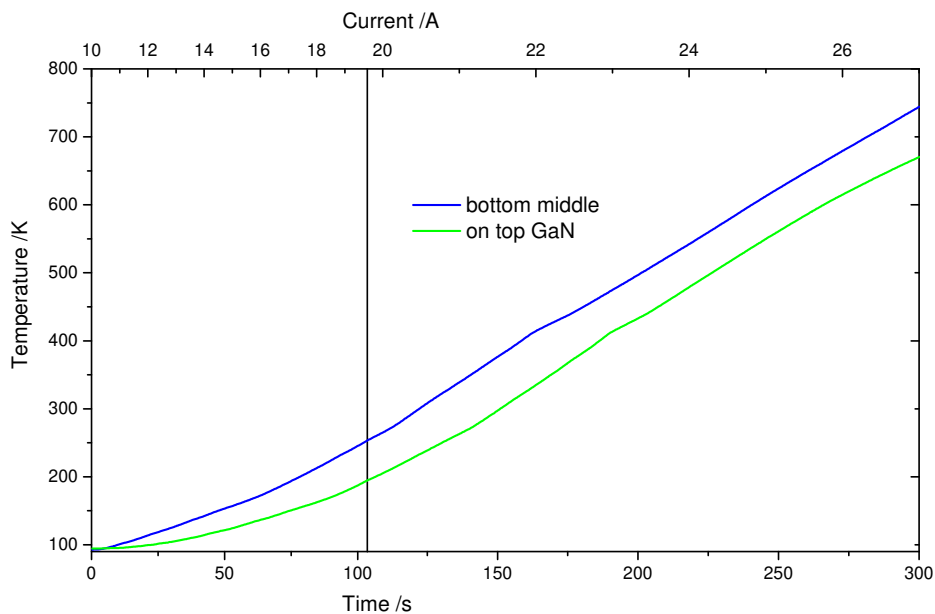


Fig. 2.7 The temperature curves obtained by two heating experiments from the thermocouple at the bottom middle and the thermocouple on top of the GaN semiconductor. Note that the two x-axes can only be plotted as the current is linearly - with a lower slope from about 106 s on - and identically raised with time in the two different heating experiments.

Figure 2.7 shows the temperature curves obtained from a thermocouple at the bottom and one on top of the GaN semiconductor. The heating experiments are identically performed as described for the non-transferable sample holder. A deviation of about 60 K from bottom to top is determined. Consequently, the transfer sample holder exhibits a stronger temperature deviation than the above described non-transferable one. This deviation is not anymore

negligible. Therefore, an internal temperature calibration with known desorption features from TPD measurements is recommended for future measurements. Another disadvantage is that the lowest achievable temperature is about 95 K. In comparison to that the non-transferable sample holder for square-shaped semiconductor platelets reaches about 80 K. The cooling efficiency could be optimized by lowering the mass of the complete system by the use of thinner materials, drills through the base plates or a better thermal contact between the base plate of the transfer unit and the base plate of the fixed unit. The latter could be achieved by the use of a harder spring. This could impair the desired easy transfer though.

3. Experimental Methods

The temperature programmed desorption (TPD), the photon-stimulated desorption (PSD), and the photon-stimulated reaction (PSR), which are the main techniques used in order to obtain the results presented in this dissertation, are explained in the following. Regarding the quantification of the results from these techniques, the evaluation of quadrupole mass spectrometry (QMS) experiments is introduced. Moreover, the crystal preparation is described, and the evaluation of the surface sensitive auger electron spectroscopy (AES) is presented.

3.1 TPD Experiments

TPD is a powerful tool to elucidate the physical and chemical behavior of adsorbates at surfaces. Typical information, which are accessible with this method, are the adsorption sites, type of binding, binding energies, and thermal surface reactions. Furthermore, it is possible to distinguish between different substances, when they exhibit different desorption temperatures.

In order to adsorb gaseous substances the sample is cooled to low, for example liquid nitrogen temperatures. The dosage is then applied by background dosing or with a molecular beam-doser. The advantage of background dosage is its simplicity, as only a leak valve has to be opened, and the sample can stay at the final position for a TPD measurement. The disadvantage is that the gas will adsorb at every site being at low temperature, in particular at the sample holder and the manipulator. Consequently, a background will result in subsequent TPD experiments. In comparison to that, the application of a molecular beam-doser requires to move the sample around, but only a small area is exposed to the gas, resulting in a negligible TPD background. For the desorption or thermal reaction of the adsorbate, the temperature is linearly raised. Therefore, a PID controller (2408, Eurotherm, Invensys Systems GmbH) is programmed with respect to the linearity of the temperature ramp and the current steps, which would lead to artificial desorption features. Indirectly heated semiconductor samples are, compared to directly heated metal samples, thermally inert. Consequently, a controlled fast heat-up with the commonly used $1-2 \frac{K}{s}$ is only possible, when the PID controller is set to a zero current, which is a function of the heating wire, the sample holder, and the sample. That means, by switching on the heating-current supply, immediately a certain temperature decrease results and bridges the onset control. Nevertheless, a linear, reproducible temperature ramp free of currents steps can hardly be obtained with this method.

An alternative to a PID control is the direct application of different current gradients, if the thermal behavior of the combination of heating wire, sample holder, and sample is well-known.

The desorbing substances in a TPD experiment can enter the QMS through a skimmer, which is used for background minimization. A scheme of a TPD experiment with adsorbed ethanol and the thermal reaction products ethylene and acetaldehyde is shown in figure 3.1.

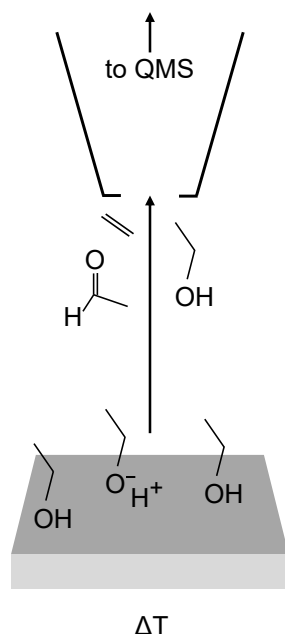


Fig. 3.1 Scheme of a TPD experiment with the semiconductor sample, the skimmer, and the adsorbate ethanol in the non-dissociative and the dissociative binding mode, as well as the desorbing thermal reaction products ethylene and acetaldehyde.

If background desorption features cannot be avoided by molecular beam-dosage or the skimmer, a background correction of the TPD results is required. In the following, by means of two examples, two different typical corrections are introduced. The first one is a rising non-peaking background with temperature, which can usually be assigned to an unspecific heat-up of the sample holder, the rods, and the manipulator. The raw data of such an example is shown as the blue curve in figure 3.2. It can clearly be seen that this background is perfectly fitted with an exponential function. Note that it is important to fit only the temperature region, in which no specific desorption occurs. A subtraction of this exponential fit leads to the corrected green curve, which is also shown in figure 3.2.

The second example is the correction for a peaking overlapping desorption feature, which can be assigned to the desorption from one specific part or material. A TPD spectra exhibiting this background at 150 K to 300 K is shown in 3.3. For a quantitative statement this feature

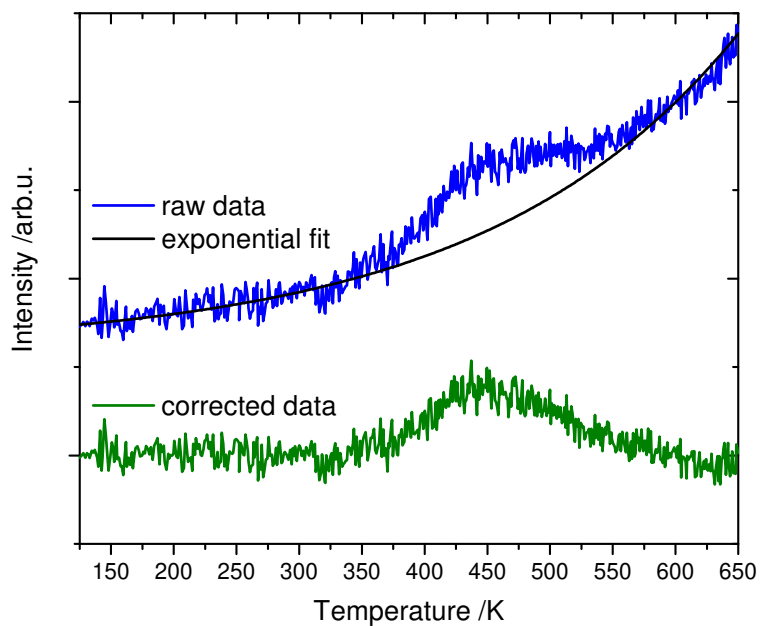


Fig. 3.2 Background correction for a rising non peaking background. The exponential curve fits the raw data background from 250 K to 350 K and 550 K to 695 K. Subtraction of this exponential background leads to the corrected curve depicted in green.

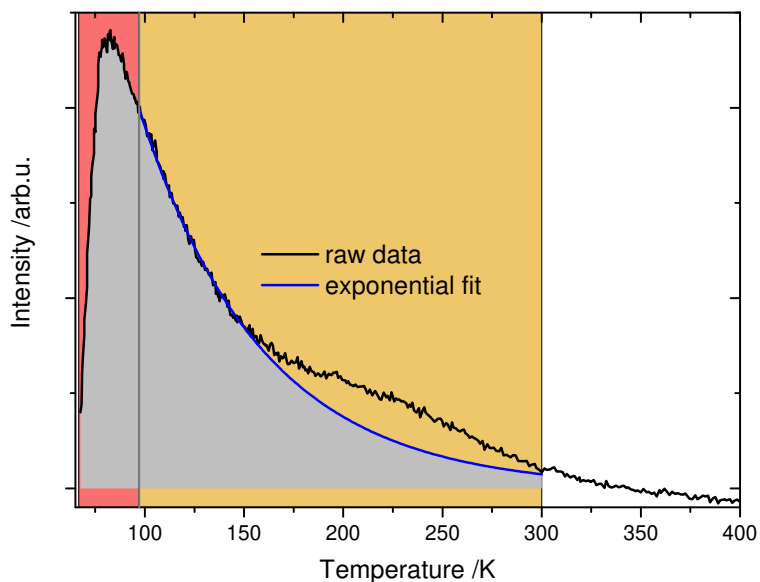


Fig. 3.3 Background correction for a peaking overlapping desorption feature. The exponential curve (in blue) fits the decay of the original desorption feature. A corrected amount of desorption is obtained from a combined integration as depicted in red and orange.

must not be integrated. Therefore, the decay of the original desorption with the peak at 80 K has to be fitted with an exponential function. In this case only the part from 80 K to 150 K, in which no additional desorption occurs can be considered, resulting in the blue curve in figure 3.3. For the integration of the entire peak a combined approach is chosen. For the first part from 70 K to 96 K, which is depicted in red in figure 3.3, the raw data is integrated. For the second part from 96 K to 300 K, which is depicted in orange in figure 3.3, the exponential decay has to be integrated.

3.2 PSD and PSR Experiments

In the field of photo-activated experiments the desorption technique (PSD) and the reaction technique (PSR) are distinguished. While with PSD information about special surface sites and surface composition are obtained, with PSR molecular mechanisms and catalytic insights can be elucidated, as well. Within the PSR the discontinuous and the continuous method can be applied, which is explained in detail in the following. In general a substrate is adsorbed on a semiconductor surface and either desorbs or reacts when the illumination is turned on. Subsequently, the products are measured with a QMS, which is in our case the same setup as for TPD experiments. An illustration of a PSD experiment, in which CO desorbs with UV illumination, is depicted in figure 3.4. The setup has to be adjusted in a way that the whole crystal surface is illuminated with light.

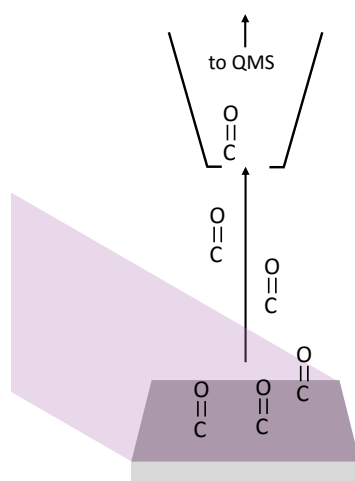


Fig. 3.4 Scheme of a PSD experiment with the semiconductor sample, the illumination, the skimmer, and adsorbed CO, as well as CO desorbing from photon-stimulation.

3.2.1 Discontinuous PSR

An adsorption of substrate at cold temperature with a subsequent photon-stimulation can be compared with a batch reactor model as a substrate replenishment does not occur. One has to distinguish between photon-stimulation with product accumulation at cold temperature followed by a TPD and photon-stimulation with direct product desorption at elevated temperature.

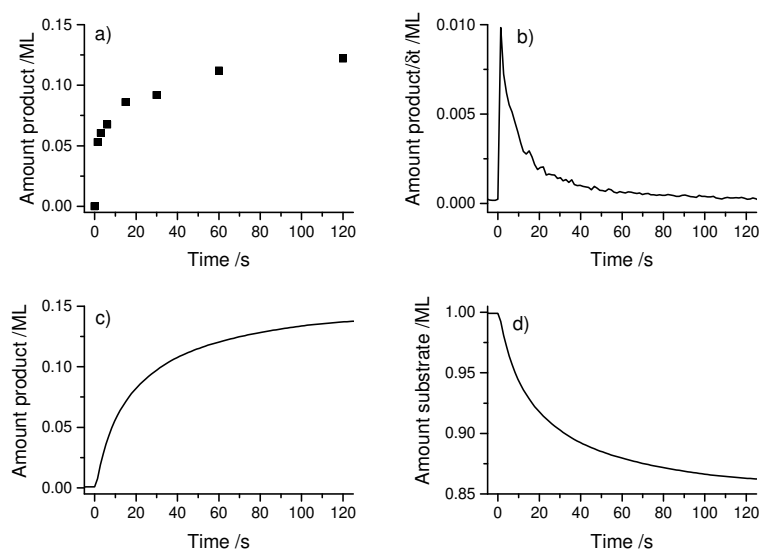


Fig. 3.5 Discontinuous PSR type measurements. In a) is displayed the accumulation case and in b) the direct product desorption case at elevated temperatures. c) shows the amount of product, which is obtained by integration of b) and d) indicates the decrease of substrate, which is obtained by subtraction of the formed product from the initial coverage.

In the first case, a plot of the product formation against illumination time is obtained by changing the duration of illumination and integration of the resulting desorption feature in the TPD experiment (see figure 3.5a). In the second case, an integration of the product decay curve produces a similar plot (see figure 3.5b-c). Note that the results are not identical as surface diffusion has to be considered and the active sites are not equally available. Furthermore, the decay in the amount of substrate can be determined from the increase in the amount of product, and the resulting plot is shown in figure 3.5d. The reaction rate constants k can be derived from kinetic simulation of the underlying reaction and are included in the integral curves as well as in the PSD product decay curve.

3.2.2 Continuous PSR

In contrast to the discontinuous PSD a steady replenishment of substrate is enabled by constant background gas flow in the case of continuous PSD. If the catalyst temperature is high enough for desorption of the photo-reaction product or the product is active for PSD and poisoning of the catalyst does not occur, a constant product gas flow will be measured with the QMS. An example of a continuous PSR measurement, which shows the substrate and product signal and their changes with illumination, is depicted in figure 3.6. It can clearly be seen that a constant turnover is present during illumination. Consequently, a turnover frequency (TOF) can be determined from a continuous PSR.

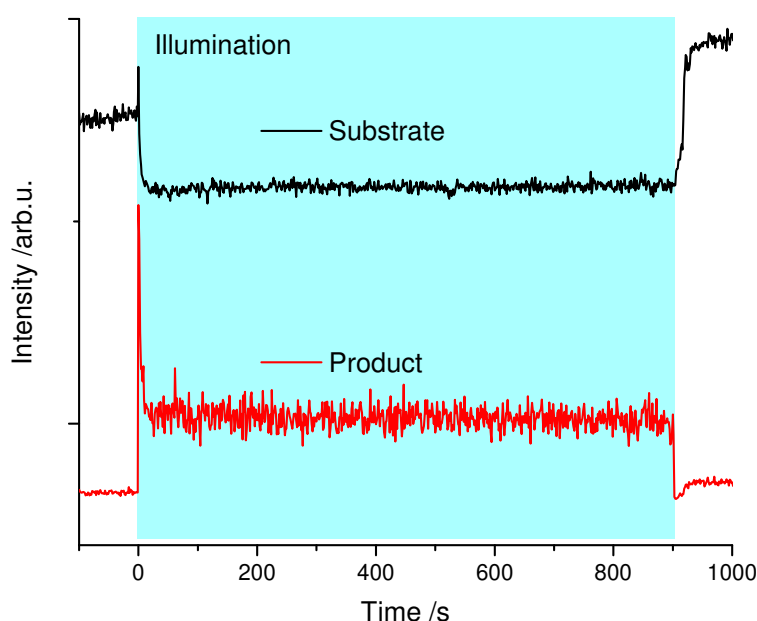


Fig. 3.6 Continuous PSR measurement with the substrate and the product signal intensity. The time of illumination is depicted in blue.

3.3 Quantitative QMS Analysis

In order to obtain quantitative values from QMS measurements, the QMS can either be calibrated for every single substance. Alternatively, the substance and the mass specific parameters have to be considered when a calibration is used from a different molecule. For the latter pathway the ionization efficiency has to be considered first. If a substance interacts with electrons, it ionizes with a certain substance-specific probability, which is the electron impact ionization cross section (ICS). This parameter can be found for the most common substances and electron energies in literature (see table 3.1). In most cases, the ionization is

a dissociative process, resulting in a variety of cationic fragments with different masses. The transmission through the QMS is mass dependent, hence a transmission function must be determined, which is described in the next subsection. The last parameter is the probability for the formation of a specific fragment from a substance. This probability can be determined from the fragmentation pattern.

3.3.1 Calibration of the QMS for One Substance

In order to obtain quantitative values from a measured ion intensity, the QMS has to be calibrated. Therefore, the desorption signal of a known amount of one substance has to be detected. One possibility to carry out this calibration method is the thermal desorption of precisely one monolayer of an inert substance from a perfectly defined surface with known adsorption sites.

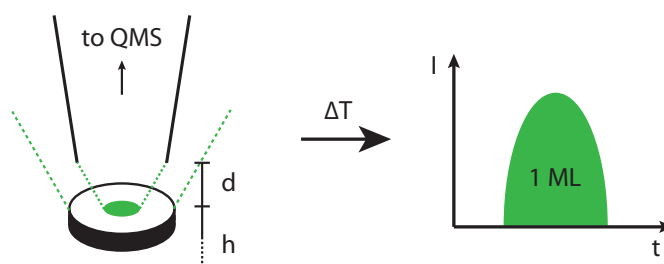


Fig. 3.7 Scheme of a calibration experiment with the setup and the resulting calibration plot. The distance from the skimmer to the sample is denoted with d and the height of the sample in the UHV chamber with h .

In figure 3.7 an illustration of such an calibration experiment is shown. Since the molecules desorb from the entire surface and each direction (with the exception of into the crystal), not all molecules reach the skimmer. Consequently, the area of desorption is not exactly known. Under the assumption that the adsorption is identical over the whole area of the crystal, the signal can be calculated to an exact number of molecules with the adsorption sites and the area of the crystal surface. This is independent of the overall size of the surface, though the area from where molecules desorb and reach the ionisation has to be kept constant in later experiments. Consequently, the distance d , which is illustrated in figure 3.7, of the surface to the skimmer must remain the same for one calibration. In the UHV system a determination of the distance d is not easily feasible. Therefore, the height h (see figure 3.7) is adjusted and kept constant. The integral of the intensity versus time corresponds in this case to the electric charge recorded at the QMS detector, when one monolayer of the investigated substance desorbs from the surface of interest. The system,

which has been chosen for the calibration of this apparatus, is methan-d3-ol on a $\text{TiO}_2(110)$ surface. The number of methanol adsorption sites of a $\text{TiO}_2(110)$ surface equals the Ti^{4+} concentration, which is $5.2 \cdot 10^{14} \text{ cm}^{-2}$. [106] Consequently, the surface concentration c_A of methanol molecules is $5.2 \cdot 10^{14} \text{ molecules} \cdot \text{cm}^{-2}$. The averaged electric charge of one monolayer desorption Q_{ML} , which is measured for a height $h = 41 \text{ mm}$ at a m/z ratio of 33, amounts to $4.5 \cdot 10^{-9} \text{ A} \cdot \text{s}$. The surface area A of the TiO_2 crystal is 0.79 cm^2 . With equation 3.1 we can determine $Q_{molecule}$, a quasi electric charge per molecule at a certain m/z ratio:

$$Q_{molecule_{m/z=k}} = \frac{Q_{ML}}{c_A \times A} \quad (3.1)$$

With the value $Q_{methan-d3-ol_{m/z=33}} = 1.1 \cdot 10^{-23} \frac{\text{A} \cdot \text{s}}{\text{molecule}}$ any other electric charge formed by ionization of methan-d3-ol measured at $m/z = 33$ can be calculated to a number of molecules.

3.3.2 Conversion to Other Molecules

As described previously a transfer of the calibration from one molecule to another can be achieved by the consideration of the transmission, fragmentation, and electron impact ionization cross section. The exact approach is explained in this section, starting with the fundamental equation 3.2 for the transfer from the calibration molecule (CM) to a quantity N_X of another molecule X.

$$N_X = \frac{Q_{X_{m/z=k}}}{ICS_X \times Tr_{m/z=k} \times F_{X_{m/z=k}}} / \frac{Q_{CM_{molecule_{m/z=l}}}}{ICS_{CM} \times Tr_{m/z=l} \times F_{CM_{m/z=l}}} \quad (3.2)$$

$Q_{X_{m/z=k}}$ is the measured electric charge from an unknown amount of molecules X at a m/z ratio k and, accordingly, $Q_{CM_{molecule_{m/z=l}}}$ is the measured quasi electric charge from one molecule of the calibration molecule at a m/z ratio l. ICS is the electron impact ionization cross section of the respective molecule. F is the probability that the measured fragment is formed from the specific molecule. $Tr_{m/z=k,l}$ is the transmission through the QMS at the considered m/z ratio. The ICS values, which are used in this work, are presented in table 3.1. Note that the methanol and methan-3d-ol ICS can be assumed as equal as deuteration does not lead to a significant change in this value.

The mass-to-charge dependent transmission through the QMS has to be determined experimentally. The exact approach is described in the next subsection 3.3.3. The probability factor F can be determined in two different ways from a mass spectra of the respective molecule. On the one hand, equation 3.3 can be applied,

Table 3.1 ICS literature values (at 70 eV) applied in this thesis

| substance | ICS [\AA^2] | reference |
|-------------------------|------------------------|------------|
| methanol (methan-3d-ol) | 4.61 | [107, 108] |
| formaldehyde | 4.14 | [109] |
| ethanol | 7.6 | [107] |
| acetaldehyde | 6.7 | [107] |
| ethylene | 5.115 | [110] |
| benzaldehyde | 20.1 | [111] |
| cyclohexanone | 17.6 | [111] |
| tert-butanol | 13.41 | [107] |
| methyl-radical | 2.99 | [112] |
| acetone | 9.0 | [107] |
| isobutene | 11.889 | [110] |
| water | 2.275 | [110] |
| hydrogen | 1.021 | [110] |
| methyl formate | 6.8 | [113] |

$$F_{X_{m/z=k}} = \frac{S_{m/z=k}}{\sum_{k=1}^n S_{m/z=k}} \quad (3.3)$$

for which $S_{m/z=k}$ is the signal of a fragment with the m/z ratio k . $F_{X_{m/z=k}}$ is the probability that the fragment with the m/z ratio k is measured at the detector of the QMS in relation to all measured fragments. This approach neglects the different transmission of the various fragments. On the other hand, a transmission-corrected factor $F_{X_{m/z=kTr}}$ can be determined with equation 3.4,

$$F_{X_{m/z=kTr}} = \frac{S_{m/z=kTr}}{\sum_{k=1}^n S_{m/z=kTr}} \quad (3.4)$$

where $S_{m/z=kTr}$ is the transmission-corrected signal of a fragment with the m/z ratio k . This correction can be performed with equation 3.5, where $Tr_{m/z=k}$ stands for the transmission through the QMS at $m/z = k$

$$S_{m/z=kTr} = S_{m/z=k} / Tr_{m/z=k} \quad (3.5)$$

Consequently, the factor $F_{X_{m/z=kTr}}$ is the probability that the fragment with the m/z ratio k is formed by the electron impact ionization. It is obvious that the transmission function must be known for the determination of this factor, but this function is mostly not available for mass spectra from data bases.

With equation 3.6 a transmission-corrected total signal, which corresponds to a number of formed fragments after ionization, of a molecule X can be determined. $S_{X_{meas_{m/z=k_{Tr}}}}$ stands for the transmission-corrected measured signal of a molecule X at a m/z ratio k. $F_{X_{m/z=k_{Tr}}}$ is the probability that a fragment of molecule X measured at a m/z ratio k occurs.

$$S_{X_{Tr_{total}}} = S_{X_{meas_{m/z=k_{Tr}}}} / F_{X_{m/z=k_{Tr}}} \quad (3.6)$$

To prove that the application of the factor $F_{X_{m/z=k_{Tr}}}$ leads to the correct conclusion a simple thought experiment with a molecule M is made. It is assumed that M cracks into fragments A, B, and C. The m/z ratios, the appearance probabilities, and the transmission values of the three fragments, are given in the following table 3.2.

Table 3.2 m/z ratios, fragment probabilities, and transmission values of the thought experiment molecule M

| fragments | A | B | C |
|----------------------|-----|-----|-----|
| m/z | 18 | 45 | 70 |
| fragment probability | 0.2 | 0.7 | 0.1 |
| transmission | 1.5 | 0.8 | 0.4 |

The theoretically measured mass spectra of one molecule M can be obtained by multiplying the fragment probability and the transmission of the respective fragment. The spectra of our molecule M would look like shown in figure 3.8.

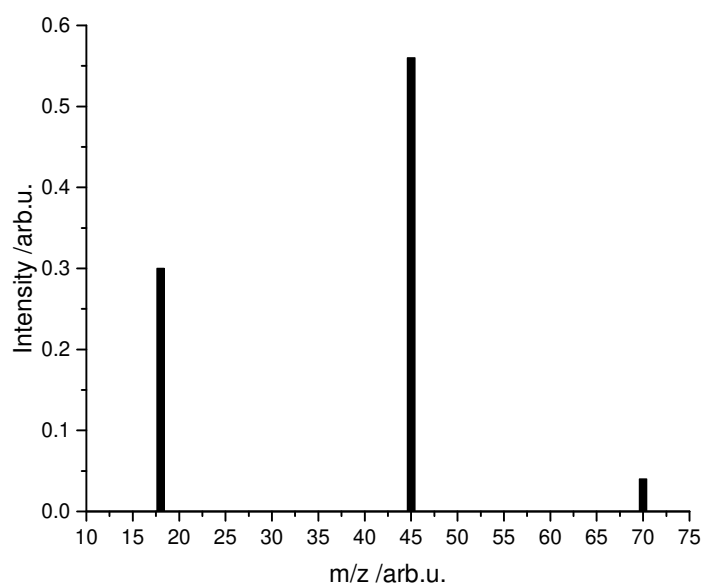


Fig. 3.8 Thought experiment for a mass spectrum of molecule M

From a mass spectral database like the National Institute of Standards and Technology (NIST) one would get for the most intense fragment, which is in our case B, for example a relative intensity of $S_{m/z=45} = 9968$. The relative intensity of A will then result with $S_{m/z=18} = 5340$ and C with $S_{m/z=70} = 712$. If we find fragment C as unique fragment and measure a signal intensity of $S_{meas_{m/z=70}} = 65000$, the absolute number of a molecule M can be determined.

First, the transmission-corrected data base signals have to be calculated with equation 3.5, resulting in $S_{Mdb_{m/z=18Tr}} = 3560$, $S_{Mdb_{m/z=45Tr}} = 12460$, and $S_{Mdb_{m/z=70Tr}} = 1780$. Second, the probability factor $F_{M_{m/z=70}}$ has to be determined with equation 3.4. For the fragment C a value of 0.1 is obtained. In the next step the transmission-corrected total signal of the molecule M can be calculated with equation 3.6, resulting in $S_{MTr_{total}} = 1625000$. In our thought experiment we can prove that this is correct by multiplying the obtained value with the probability factor $F_{M_{m/z=70}}$ and the transmission $Tr_{m/z=70}$, which gives the measured signal of C $S_{meas_{m/z=70}} = 65000$.

The difference of the two probability factors $F_{X_{m/z=k}}$ and $F_{X_{m/z=kTr}}$ is illustrated in figure 3.9b and 3.9d for methan-3d-ol. Figure 3.9a shows a methan-3d-ol mass spectra.[114] Normalization of this spectra leads to 3.9b. Hence, the factor $F_{X_{m/z=k}} = 0.3578$ follows. When the transmission through the QMS is considered, the spectrum in figure 3.9c is obtained. Note that the sum of relative abundances for all masses is not 1 anymore in 3.9c. An additional normalization of this spectrum leads to 3.9d, hence the factor $F_{X_{m/z=kTr}} = 0.3759$ follows.

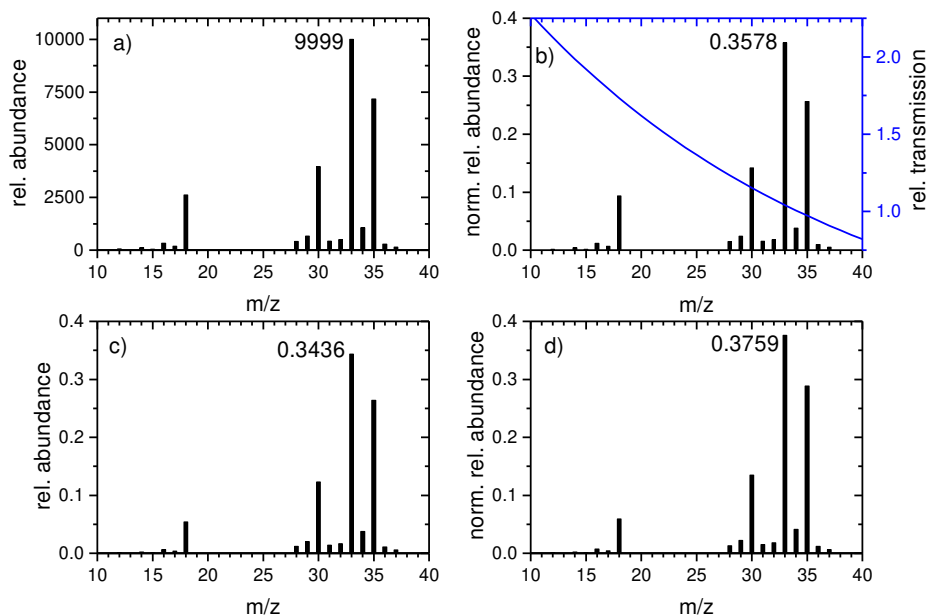


Fig. 3.9 Methan-3d-ol mass spectra in a), the normalization b), the transmission correction c), and the subsequent second normalization resulting in d).

Nevertheless, the fragmentation uncorrected method is used, as the transmission function of the mass spectra from data bases are unknown. However, this can be done, because the error resulting from this method is negligible small. This holds for molecules fragmenting similar to the calibration molecule, for which the errors are reduced, when the conversion with the calibration molecule is performed, and also for hardly fragmenting molecules as for example H₂.

3.3.3 Determination of the QMS Transmission Function

For the determination of the QMS transmission function the background pressure of diverse gases with different masses is compared to the generated signal at the QMS detector. The background pressure is measured with a hot-cathode (Varian, UHV-24) and corrected with the gas correction factor for the specific substance.[115] The gases used for the determination of the transmission function of the described setup are D₂, O₂, CO, and Ar. In table 3.3 the relative transmission values, corrected for the fragmentation pattern and the ICS, at background pressures of $1 \cdot 10^{-9}$ mbar, $5 \cdot 10^{-9}$ mbar, $1 \cdot 10^{-8}$ mbar, and $4 \cdot 10^{-8}$ mbar are shown.

Table 3.3 Relative transmission values for D₂, O₂, CO, and Ar normalized to CO and averaged from background pressures of $1 \cdot 10^{-9}$ mbar, $5 \cdot 10^{-9}$ mbar, $1 \cdot 10^{-8}$ mbar, and $4 \cdot 10^{-8}$ mbar.

| substance | m/z | rel. transmission |
|----------------|-----|-------------------|
| D ₂ | 4 | 2.8 |
| CO | 28 | 1.0 |
| O ₂ | 32 | 0.8 |
| Ar | 40 | 1.3 |

Those transmission values can be fitted with an exponential decay function, resulting in an $m/z = k$ dependent transmission function as shown in equation 3.7.

$$Tr(k) = 3.198 \times e^{-0.034 \times k} \quad (3.7)$$

3.3.4 Disentangling Overlapping Fragment Masses

If a mixture of different molecules, resulting from a reaction, is measured with the QMS, a quantitative evaluation of the reaction products is often desired. Before this can be achieved a qualitative analysis of the mass spectra has to be performed. As several molecules may exhibit fragments with a same m/z value, a direct assignment of the m/z ratios to only one

molecule can be wrong. When all molecules are known, an unique m/z ratio has to be found at best for every type of molecule. If this is not possible, enough m/z ratios must be found, so that the determination of the molecule quantities is not underdetermined. An often occurring example is illustrated in figure 3.10, where one unique m/z ratio and two mixed m/z ratios are found for three molecules.

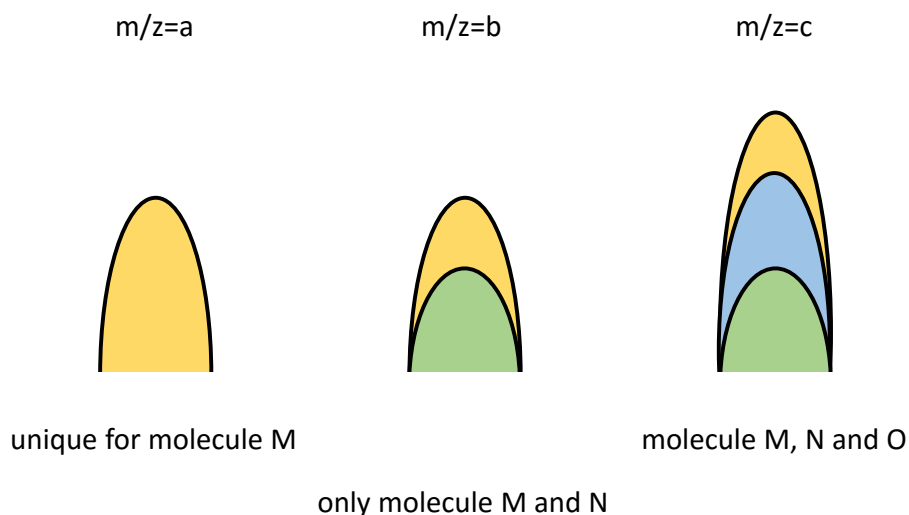


Fig. 3.10 Illustration of a system of three molecules and three m/z ratios

When the exact number of different molecules and the m/z ratios are analyzed, the measured m/z ratio intensities can be separated for the different molecules. Therefore, an exact fragmentation pattern of the investigated molecules in the applied experimental setup is needed. This can be achieved by a mass scan either of the background-filled chamber or by a multilayer signal of the respective molecule. If none of these methods are possible, a fragmentation pattern from a data base can be used. Note that the fragmentation pattern is dependent on a variety of parameters such as e.g. the incident electron energy, the geometry of the ionization area, and the transmission through the QMS.

When two molecules with only one unique m/z ratio desorb at a different temperature in a TPD experiment, the accuracy of the correction can be proven. In figure 3.11 the different cases of correction are illustrated. If we apply too low fragment intensities of A, molecule B is under-corrected, as it is observable in the small shoulder at about 300 K in figure 3.11a. In contrast to that, an over-correction is observed, when too high fragment intensities of A are used, which can clearly be seen by the negative peak at about 350 K in figure 3.11b. An accurate correction of molecule B from molecule A is shown in figure 3.11c.

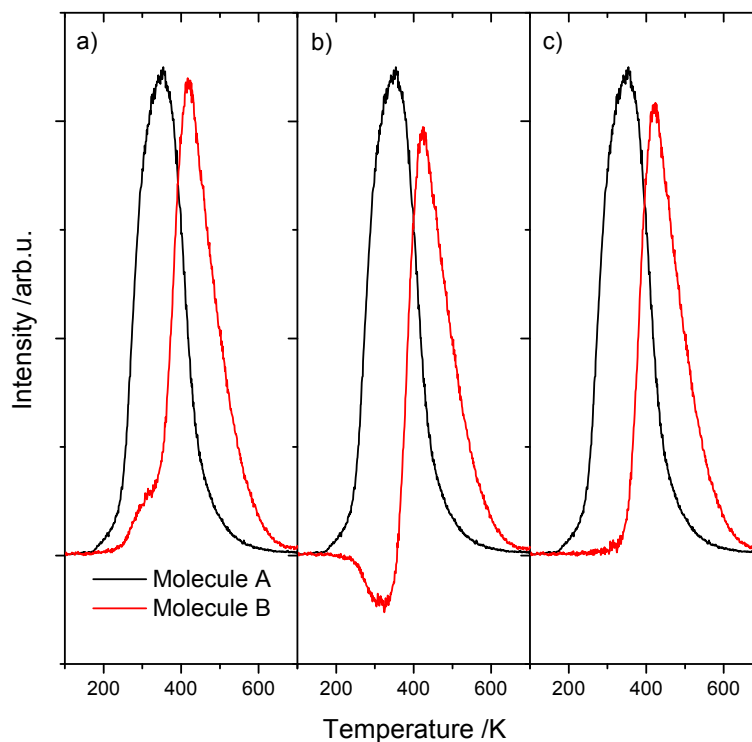


Fig. 3.11 Different types of correction in a TPD experiment for the molecules A and B. The m/z ratio of A is unique, and the m/z ratio of B has a contribution of molecule A. In a) an under-correction, in b) an over-correction, and in c) an accurate correction of the molecule B from molecule A is shown.

3.4 Crystal Preparation

The topics bulk preparation and surface preparation are discussed in this chapter for TiO_2 and GaN. In order to elucidate mechanistic details of surface reactions, the condition of the crystal surface has to be exactly determined and must be reproducible. This means that contaminations have to be removed prior to reaction measurements. Furthermore, the defect concentration of the $\text{TiO}_2(110)$ surface has to be prepared. In the case of GaN, the oxygen proportion of the surface has to be determined. Finally, the surface can be modified with pre-adsorbed species.

3.4.1 $\text{TiO}_2(110)$

The untreated rutile $\text{TiO}_2(110)$ single crystal (SurfaceNet GmbH) is colorless and transparent as depicted in figure 2.4a. Cycles of argon sputtering (1.5 keV, 1×10^{-5} mbar, 30 min), oxygen annealing (800 K, 1×10^{-6} mbar, 20 min), and vacuum annealing (800 K, 10 min) lead to a light blue color reflecting the reduction state of the crystal.[116] Furthermore, the

surface contaminations are removed upon this treatment and an oxygen defective, reduced r-TiO₂ surface is achieved. These oxygen defects are created in the bridge bonding oxygen (BBO) rows and can be titrated with H₂O TPD.[117] The number of BBO vacancies (BBO_{vac}) is stable over a long term upon the above-described preparation method and amounts to 6 ± 1 . An oxidized o-TiO₂ surface with oxygen adatoms (O_{ad}) can be obtained by the exposure of the r-TiO₂ surface at 300 K to oxygen[118] or by the exposure of the r-TiO₂ surface to oxygen at liquid nitrogen temperature and subsequent heating to 300 K.[39] Hydroxylation of the r-TiO₂ surface is achieved by the exposure to water at 400 K[118] or alternatively by the exposure at liquid nitrogen temperature and subsequent heating to 400 K.[119]

3.4.2 GaN

Semiconductor GaN crystals can be grown with metalorganic chemical vapor deposition (MOCVD), plasma-induced molecular beam epitaxy (PIMBE) or with hydrogen vapor phase epitaxy (HVPE). The doping level of this semiconductor can be varied from n-type doping to p-type doping. The three growing processes produce different surfaces and, consequently, have to be considered separately in terms of crystal preparation. PIMBE grown GaN samples are etched in concentrated HCl for 30 s to remove Ga droplets and rinsed with Milli-Q water twice before their transfer into the UHV chamber. MOCVD and HVPE grown GaN samples do not need any pretreatment. Prior to UHV cleaning the surface composition obtained from the three types of samples is different. While the PIMBE samples show comparatively small carbon and chlorine contaminations from the etching process, the MOCVD samples are covered with carbon, which can be assigned to residues from the organometallic precursors. The HVPE samples exhibit the least contamination. In order to clean the surfaces a high temperature evaporation and a combined argon sputter and annealing cycle are tested. The first mentioned approach leads to the evaporation of gallium and nitrogen at temperatures above 1000 K resulting in an uneven surface destruction, which is too rough for subsequent surface science experiments. The latter one, a combination of Ar⁺-sputtering (0.5 keV, 1×10^{-6} mbar, $I_{sputter} = 2.0 \mu A$, 100 K) and 800 K annealing enables to clean the surface non-destructively from all contamination besides oxygen. The amount of oxidation accumulates at the surface with the number of sputtering cycles. The required number of cleaning cycles for a carbon free surface varies from the initial contamination and is thus different for the samples from the three growing processes.

3.5 Auger Electron Spectroscopy

To analyze the crystal preparation, Auger Electron Spectroscopy (AES), as surface sensitive technique is applied. In the following, the evaluation of AES spectra for substances containing more than one element is described. In order to determine the composition of the surface, some assumptions have to be made. The first one is that the analyzed substrate is grown perfectly flat. Then, the number of layers contributing to the detected signal have to be determined. Therefore, the electron inelastic mean free path is considered. This is the distance electrons with a certain energy can overcome in a solid. In literature values for elements[120] and inorganic compounds[121] can be found. In combination with the monolayer thickness of the investigated substrate, the detectable layers are specified. The second assumption is that the signal decays exponentially with the number of layers (l). The proportion of the signal of one layer $S_p(l)$ to the overall signal of the detectable layers can therefore be determined with equation 3.8.

$$S_p(l) = \frac{e^{-l}}{\sum_{l=1}^n e^{-l}} \quad (3.8)$$

The proportion of the signal from the first four layers to the overall signal, which results from equation 3.8, is shown in table 3.4.

Table 3.4 Signal distribution for the contribution of atoms from the first four layers to the overall signal, resulting from an exponential decay

| layer | signal proportion |
|-------|-------------------|
| 1 | 0.64 |
| 2 | 0.24 |
| 3 | 0.09 |
| 4 | 0.03 |

It can be seen that the proportion of the 3rd and the 4th layer is relatively small. Consequently, the mean value of the inelastic mean free path of the elements of a composite material can be used. If we consider for example the N_{KLL} and the Ga_{LMM} Auger electrons of GaN, an inelastic mean free path of 8.4 Å and 14 Å is used in literature.[122] With the height of 2.6 Å of a GaN monolayer[123] electrons from about 4 monolayers can be detected.

In the next step, the intensity (I) of an AES signal is taken as the difference of the respective elemental peak, which is recorded as its derivative. For the comparison of signals from different elements the sensitivity factors (SF) have to be taken into account.[124] The resulting values give a relative composition of the detectable layers. From a perfect GaN crystal one would for example get an intensity of $I_{N_{KLL}} = 12000 \text{ arb.u.}$ and $I_{Ga_{LMM}} = 16740 \text{ arb.u.}$

Corrected with the sensitivity factors of $SF_{N_{KLL}} = 0.600$ and $SF_{Ga_{LMM}} = 0.837$, [124] the identical values would be obtained for both elements. This means a stoichiometric 50/50 proportion is present. An even distribution to the different layers would follow in this simplified and perfect case with the assumption of a perfect stoichiometric, as far as it is possible from the bulk to the surface. Usually, the surface composition of a single crystal is not perfect and non-stoichiometric. If this is the case, further assumptions have to be made, which concern the terminal layer. For example, an overlayer surface enrichment by one element, could be present. Another possibility is the layer-by-layer surface oxidation, which occurs for example on GaN semiconductor samples. [92, 93]

If we consider for example a surface-oxidized GaN sample, three elements, oxygen, nitrogen, and gallium are detected in AES spectra. The sensitivity-corrected proportion of N/O/Ga could be 0.393/0.128/0.479. With the above-mentioned layer-by-layer oxidation the oxygen would fill up from the surface, and the bulkier layers would be stoichiometric GaN. The elements would then follow a distribution as shown in table 3.5.

Table 3.5 Signal proportion of nitrogen, oxygen, and gallium in the first four layers of surface oxidized GaN

| signal proportion layer | N | O | Ga | Σ layer signal |
|---------------------------|-------|-------|-------|-----------------------|
| 1 | 0.215 | 0.128 | 0.301 | 0.64 |
| 2 | 0.118 | 0.000 | 0.118 | 0.24 |
| 3 | 0.044 | 0.000 | 0.044 | 0.09 |
| 4 | 0.016 | 0.000 | 0.016 | 0.03 |
| Σ elemental signal | 0.393 | 0.128 | 0.479 | |

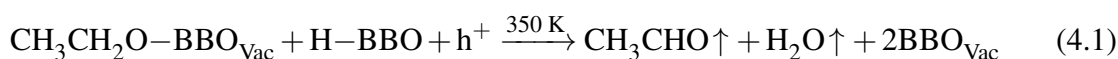
4. Results - Publication Summaries

This chapter includes short summaries of the publications achieved during the course of this thesis. Focus is hereby set on the chemical and physical insights gained from the results.

4.1 Ethanol photocatalysis on rutile TiO₂(110): the role of defects and water

In the beginning of the research project, the molecular mechanisms of photo-catalytic ethanol oxidation and especially the role of surface defects and water on TiO₂(110) have been elucidated.

A hole mediated α -H abstraction of a dissociatively bound ethanol leads to the formation of acetaldehyde and the by-product hydrogen bound to BBO atoms on the TiO₂ surface, which is in accordance with findings for methanol.[38] The hydrogen BBO species can eventually react with each other, producing H₂O, which desorbs at about 350 K from the TiO₂(110) surface, leading to an increased amount of BBO-vacancies.[58] The overall reaction equation is given in eq. 4.1:



If this surface is heated to temperatures higher than 500 K a bulk reduction occurs, rebuilding the initial BBO-vacancy concentration. The complete cycle with the detailed molecular mechanism is illustrated in figure 4.1.

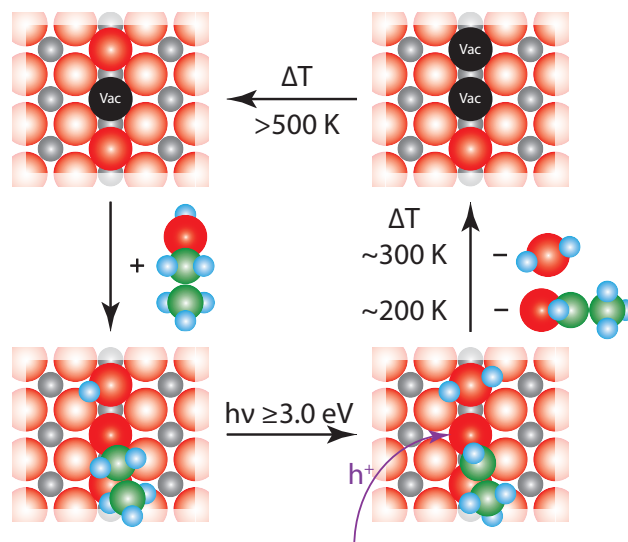


Fig. 4.1 Illustration of the cycle of ethanol photo-oxidation on the TiO₂(110) surface. The color code of the balls representing the different atoms is: Ti-grey, O-red (BBO-intense red), C-green, H-blue. In black the BBO-vacancies are depicted.

Only a limited amount of about 15%, which corresponds well to the amount of BBO-vacancies of 1 ML of adsorbed ethanol, can be converted to the aldehyde. This is in good accordance with findings for other alcohols.[62, 49] When the photo-reaction is carried out at a temperature at which the desorption of one of the reaction products (i.e. acetaldehyde) is enabled, a decay curve of this molecule upon illumination is observed. However, a subsequent ethanol coverage and photo-activation on the same sample does not lead to a further reaction. Consequently, the active sites are poisoned, which occurs by steric or electronic blocking by the BBO-H. In addition, the photo-chemical reactivity of an oxidized $\text{TiO}_2(110)$ surface is elucidated, and the formation of acetaldehyde is observed in absence of the water formation from BBO-H species. Figure 4.2 illustrates the reaction scheme with the photo-activation at the TiO_2 single crystal and the blocking of a subsequent reaction.

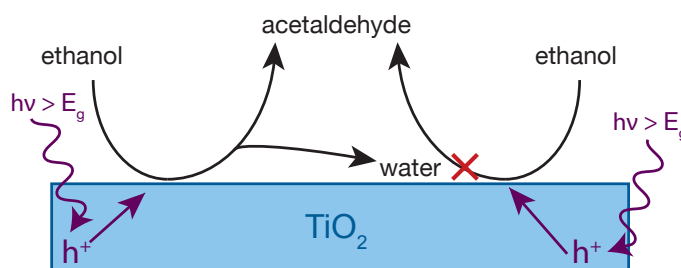


Fig. 4.2 Scheme of the photo-oxidation of ethanol on $\text{TiO}_2(110)$ with the substrate, the reaction products, the photo-activation, and the hole as charge carrier responsible for the oxidation reaction. Furthermore, the blocking by water for subsequent reactions is depicted. *Phys. Chem. Chem. Phys.*, **2015**, *17*, 22809-22814 - Published by the PCCP Owner Societies.

Reference: C. A. Walenta, **S. L. Kollmannsberger**, J. Kiermaier, A. Winbauer, M. Tschurl, U. Heiz *Phys. Chem. Chem. Phys.*, **2015**, *17*, 22809-22814, doi: 10.1039/c5cp03550c.

4.2 Doping-Dependent Adsorption and Photon-Stimulated Desorption of CO on GaN(0001)

CO is used as a probe molecule for PSD and TPD studies on three differently n-type doped PIMBE grown GaN(0001) samples with variable degree of surface oxidation. TPD experiments show that the electron donor CO is only physisorbed on the semiconductor surface, with a desorption maximum at 100 K. The evaluation of various CO coverages on the three differently n-type doped samples shows that the thermal desorption peak position does not change with doping. However, the amount of adsorbed CO reflects the GaN(0001) semiconductor dopant concentration and is not influenced by surface oxidation.

While the doping does not affect the surface morphology, as shown with atomic force microscopy (AFM) measurements, the space charge region (SCR) is shortened with higher dopant concentration, which results in an electron accumulation at the surface. This causes a lower amount of physisorbable CO. Figure 4.3 illustrates this model.

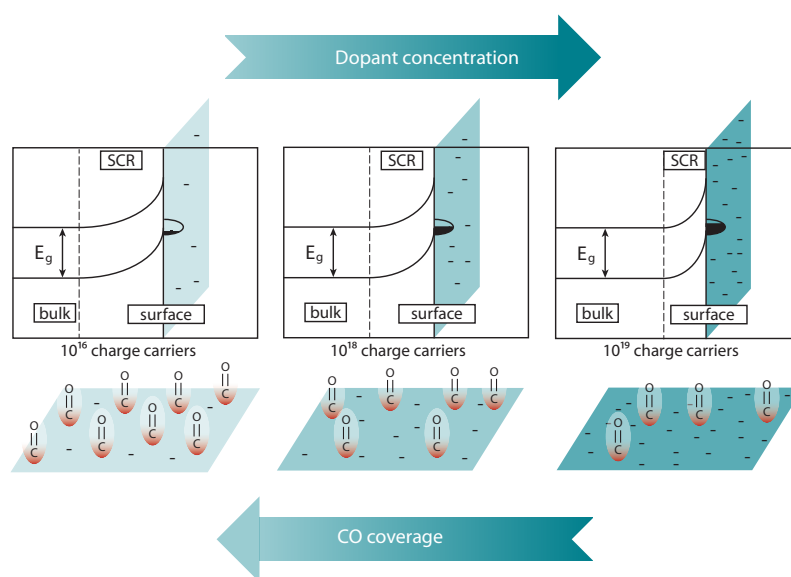


Fig. 4.3 Illustration of the effect of n-type bulk doping of GaN(0001) semiconductor samples on adsorption of the electron donor CO. The increase in charge carrier concentration is depicted with a darkening of the blue color.

Reprinted with permission from *J. Phys. Chem. C*, **2017**, *121*, 8473-8479. Copyright 2017 American Chemical Society.

It is observed that a fraction of the physisorbed CO can be photo-desorbed from the GaN(0001) surface. A strong influence of the surface oxidation degree of the semiconductor sample on the intensity of the PSD is identified, while the kinetics of the PSD remain

identical. The drop in intensity with surface oxidation is attributed to the depletion of photo-active sites.

The mechanistics of the CO PSD is discussed based on findings from semiconductor physics. In an illuminated n-type semiconductor the holes preferentially move to the surface, while the electrons favor a migration into the other direction. Consequently, on the investigated semiconductors the holes should lead to a charge redistribution at the surface. This results in a weakening of the CO-GaN bond, which effects the CO PSD. A desorption based on local heating effects is excluded by the comparison of an identical experiment with CO₂ instead of CO, which desorbs thermal similarly but is not active in photo-desorption.

Reference: **S. L. Kollmannsberger**, C. A. Walenta, A. Winnerl, S. Weiszer, R. N. Pereira, M. Tschurl, M. Stutzmann, U. Heiz *J. Phys. Chem. C*, **2017**, *121*, 8473-8479, doi: 10.1021/acs.jpcc.7b01570.

4.3 Anhydrous Ethanol Dehydrogenation on Metal–Organic Chemical Vapor Deposition Grown GaN(0001)

The thermal-chemistry and photo-chemistry of ethanol on unintentionally doped MOCVD grown GaN(0001) is compared to the reactivity of a light blue, bulk reduced TiO₂(110) with about 10% BBO-vacancies. This is the first study of ethanol reactivity on a GaN surface. The comparative system TiO₂(110) has been studied extensively, and mechanistic details of thermal reactivity are well known.[125, 51, 52]

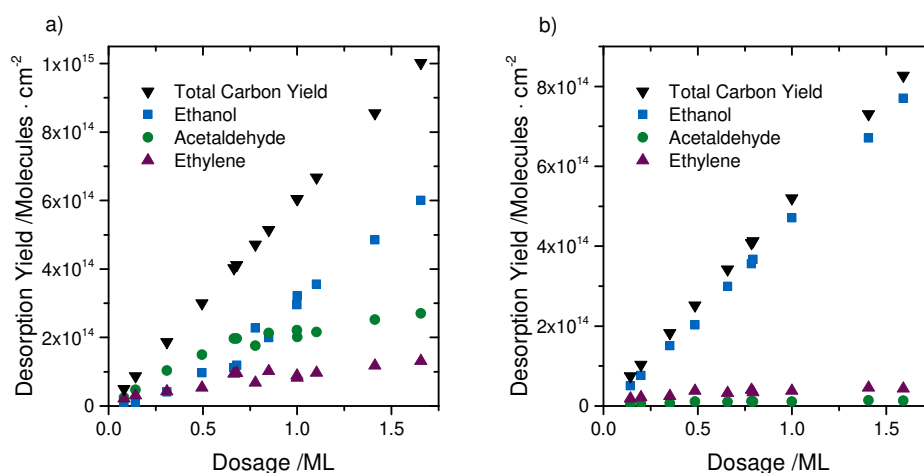


Fig. 4.4 Thermal carbon-containing products of ethanol conversion on GaN(0001) and on TiO₂(110): the species are ethanol (blue rectangles), acetaldehyde (green dots), and ethylene (purple triangles). The sum of the species is depicted in black triangles.

Reprinted with permission from *J. Phys. Chem. C*, **2017**, *121*, 16393-16398. Copyright 2017 American Chemical Society.

Low coverages of ethanol on GaN(0001) lead to the complete conversion of the alcohol. Ethylene, acetaldehyde, and hydrogen are identified as thermal reaction products at 450 K in a TPD experiment. For higher coverages an ethanol desorption feature is observed at 400 K, shifting to lower temperatures with rising coverage. The amount of products rises linearly until an initial ethanol coverage of 0.68 ML is reached, for which the conversion saturates. The yields of carbon-containing species from TPD experiments as a function of initial ethanol coverage are shown in figure 4.4a for the GaN(0001) surface and in figure 4.4b for the TiO₂(110) one. It is evident that the GaN(0001) surface exhibits a higher thermal reactivity and that the selectivity of the reaction is switched to the dehydrogenation pathway in comparison to the TiO₂(110) system. It is demonstrated with AES that coking does not

occur upon ethanol conversion.

For TiO₂(110) the amount of converted ethanol matches with the number of BBO-vacancies and is about 10%. In contrast to that, about 50% of the adsorbed ethanol is converted on GaN(0001). For TiO₂(110) it is known from literature that the thermally reactive species is dissociatively bound ethanol.[52, 125] In analogy to that, it is concluded that dissociative adsorption occurs on the Ga³⁺ surface atoms, which can be assigned to the oxophilicity of Ga.

While on the TiO₂(110) surface the by-product is H₂O, along with a reduction of the crystal,[52] a desorption of H₂ is observed in the case of ethanol conversion on GaN(0001), and no H₂O desorption occurs. Consequently, it is expected that surface amines are less stable than surface hydroxyls, which makes nitrides promising candidates for photo-catalytic hydrogen evolution. However, while GaN(0001) exhibits interesting thermal reaction properties in the conversion of alcohols, it is inert in the photo-chemical alcohol reforming.

Reference: C. A. Walenta, **S. L. Kollmannsberger**, R. N. Pereira, M. Tschurl, M. Stutzmann, U. Heiz *J. Phys. Chem. C*, **2017**, *121*, 16393-16398,
doi: 10.1021/acs.jpcc.7b04946.

4.4 Ethanol surface chemistry on MBE-grown GaN(0001), GaO_x/GaN(0001), and Ga₂O₃($\bar{2}01$)

The thermal ethanol chemistry is investigated on two MBE grown GaN(0001) samples with different degree of surface oxidation and on Ga₂O₃($\bar{2}01$). The amount of native oxide is determined with AES to be 0.18 ML for the GaN(0001) sample and 1.05 ML for the surface oxidized GaO_x/GaN(0001) sample.

The MBE grown GaN(0001) surface shows thermal reactivity to acetaldehyde at 470 K in a TPD experiment. This reactivity vanishes for the surface oxidized sample, while the high temperature desorption feature of ethanol expands to exactly the temperature, at which acetaldehyde is detected on the GaN(0001) surface. It is generally known that for thermal reactivity of ethanol on metal oxides the existence of ethoxys as precursor for a dehydrogenation reaction is necessary.[126] Consequently, the desorbing acetaldehyde is formed via a α -H abstraction from dissociatively bound ethanol on the GaN(0001) surface. This reaction does not occur on the GaO_x/GaN(0001) sample, and the ethanol desorbs associatively at the high temperature peak. In case of the Ga₂O₃($\bar{2}01$) crystal, no thermal reactivity is observed, and the high temperature desorption feature also ends already at 300 K, which indicates that no dissociative adsorption occurs. The reactivity and the type of binding is illustrated for the three samples in figure 4.5

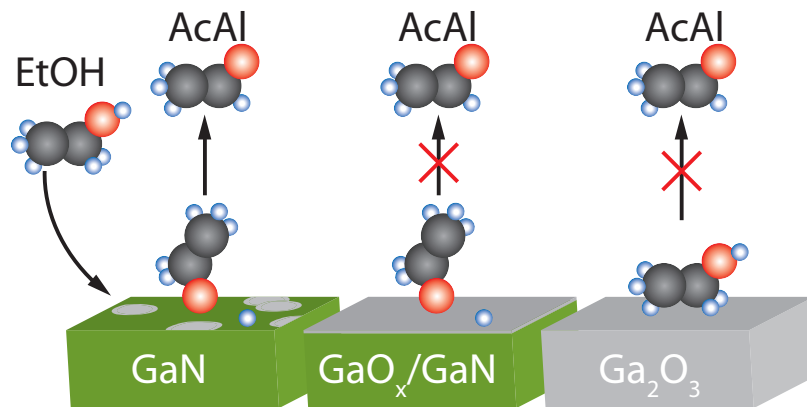


Fig. 4.5 Illustration of the three different materials GaN(0001), GaO_x/GaN(0001), Ga₂O₃($\bar{2}01$), and the substrate ethanol. The type of binding is schematically displayed and the resulting reactivity is shown.

The non-existent reactivity of the surface oxidized GaN(0001) sample demonstrates the key role of the surface nitrogen in the α -H abstraction. Furthermore, the surface states, which are populated by negative charges in n-type semiconductors,[127] are removed upon oxidation of the GaN(0001) surface.[128, 86] This change is connected to the absence of the α -H

abstraction. In case of the Ga₂O₃($\bar{2}01$) the other bulk structure causes that not even the precursor species ethoxy is formed.

Reference: **S. L. Kollmannsberger**, C. A. Walenta, A. Winnerl, F. Knoller, R. N. Pereira, M. Tschurl, M. Stutzmann, U. Heiz *J. Chem. Phys.*, **2017**, *147*, 124704, doi: 10.1063/1.4994141.

4.5 Photocatalytic selectivity switch to C–C scission: α -methyl ejection of tert-butanol on $\text{TiO}_2(110)$

It is known for alcohols containing a hydrogen atom in an α position that photo-oxidation on $\text{TiO}_2(110)$ leads to abstraction of this afore mentioned hydrogen, which results in the formation of the respective aldehyde or ketone.[129, 63, 44] Photo-conversion of tert-butanol on $\text{TiO}_2(110)$ is investigated to clarify the photo-abstraction of this α -bound species.

While the thermal chemistry of tert-butanol shows a dehydration forming isobutene, no oxidation reaction and thus no abstraction of a α -species occurs.[52] The situation changes with UV-illumination, which leads instantaneously to a hole driven methyl radical ejection even at 100 K with the associated formation of acetone. The latter one is detected in subsequent TPD experiments, in which the thermal dehydration product isobutene is also observed at 400 K. When the photo-conversion is carried out at 293 K, surprisingly all of the three reaction products are observed simultaneous. However, their PSR curves decay differently and enable conclusions to the reaction kinetics and mechanisms. The intensity of methyl ejection shows a temperature dependence, which can be related to diffusion and the clearance of reactive sites. However, this reaction is clearly a photon induced process. Isobutene exhibits the fastest decay curve, originating from a PSD process,[130] but occurs only at elevated temperature, which is assigned to an energy barrier of a transition state. The acetone decay is the slowest one, which reflects the thermal desorption. In general, for all three species thermal as well as photo-chemical steps are involved.

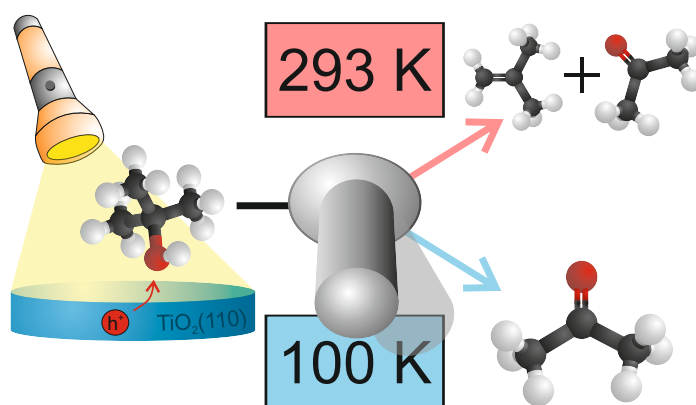


Fig. 4.6 The photo-conversion of tert-butanol, which is a hole mediated process, is illustrated and the influence of temperature on the two reaction channels is depicted. At 100 K only the photo-formation of acetone is possible, while at 293 K both pathways are accessible. Reproduced from *Phys. Chem. Chem. Phys.*, **2018**, 20, 7105-7111 with permission from the PCCP Owner Societies.

Performing the PSR at different temperatures enables to switch the selectivity of the reaction. This is due to the energy barrier of isobutene formation, a faster diffusion of tert-butanol to the photo-active sites with higher temperature, and an enhanced thermal desorption of acetone with higher temperature. Figure 4.6 shows an illustrative graphic of the possibility to change selectivity of tert-butanol photo-conversion by adjustment of temperature.

The photon-activated splitting of a C-C-bond of tertiary alcohols is a new mechanistic pathway, which opens up entirely new options in synthetic chemistry.

Reference: C. A. Walenta, **S. L. Kollmannsberger**, C. Courtois, M. Tschurl, U. Heiz *Phys. Chem. Chem. Phys.*, **2018**, *20*, 7105-7111,
doi: 10.1039/c8cp00223a.

5. Bibliographic Details for Complete Publications

5.1 Ethanol photocatalysis on rutile TiO₂(110): the role of defects and water

C. A. Walenta,[†] **S. L. Kollmannsberger**,[†] J. Kiermaier, A. Winbauer, M. Tschurl, U. Heiz*

Phys. Chem. Chem. Phys., **2015**, *17*, 22809-22814

doi: 10.1039/c5cp03550c

Chair of Physical Chemistry, Department of Chemistry and Catalysis Research Center, Technische Universität München, Lichtenbergstr. 4, 85748 Garching, Germany

[†] Contributed equally to this work.

*Corresponding author, E-mail: ulrich.heiz@mytum.de

Phys. Chem. Chem. Phys., **2015**, *17*, 22809-22814 - Published by the PCCP Owner Societies.

5.2 Isomer-Selective Detection of Aromatic Molecules in Temperature-Programmed Desorption for Model Catalysis

A. Winbauer, **S. L. Kollmannsberger**, C. A. Walenta, P. Schreiber, J. Kiermaier, M. Tschurl,*
U. Heiz

Anal. Chem., **2016**, 88, 5392-5397

doi: 10.1021/acs.analchem.6b00717

Chair of Physical Chemistry, Department of Chemistry and Catalysis Research Center, Technische
Universität München, Lichtenbergstr. 4, 85748 Garching, Germany

*Corresponding author, E-mail: ulrich.heiz@mytum.de

Reprinted with permission from *Anal. Chem.*, **2016**, 88, 5392-5397. Copyright 2016
American Chemical Society.

5.3 Doping-Dependent Adsorption and Photon-Stimulated Desorption of CO on GaN(0001)

S. L. Kollmannsberger,^{†,1} C. A. Walenta,^{†,1,2} A. Winnerl,³ S. Weiszer,³ R. N. Pereira,³
M. Tschurl¹, M. Stutzmann,^{2,3} U. Heiz^{*,1,2}

J. Phys. Chem. C, **2017**, *121*, 8473-8479

doi: 10.1021/acs.jpcc.7b01570

¹ Chair of Physical Chemistry, Department of Chemistry & Catalysis Research Center, Technische Universität München, Lichtenbergstr. 4, 85748 Garching, Germany

² Nanosystems Initiative Munich, Schellingstr. 4, 80799 München, Germany

³ Walter Schottky Institute and Physics Department, Technische Universität München, Am Coulombwall 4, 85748 Garching, Germany

[†] Contributed equally to this work.

*Corresponding author, E-mail: ulrich.heiz@mytum.de

Reprinted with permission from *J. Phys. Chem. C*, **2017**, *121*, 8473-8479. Copyright 2017 American Chemical Society.

5.4 Anhydrous Ethanol Dehydrogenation on Metal–Organic Chemical Vapor Deposition Grown GaN(0001)

C. A. Walenta,^{†,1,2} S. L. Kollmannsberger,^{†,1} R. N. Pereira,³ M. Tschurl,¹ M. Stutzmann,^{2,3}
U. Heiz^{*,1,2}

J. Phys. Chem. C, **2017**, *121*, 16393-16398

doi: 10.1021/acs.jpcc.7b04946

¹ Chair of Physical Chemistry, Department of Chemistry & Catalysis Research Center, Technische Universität München, Lichtenbergstr. 4, 85748 Garching, Germany

² Nanosystems Initiative Munich, Schellingstr. 4, 80799 München, Germany

³ Walter Schottky Institute and Physics Department, Technische Universität München, Am Coulombwall 4, 85748 Garching, Germany

[†] Contributed equally to this work.

*Corresponding author, E-mail: ulrich.heiz@mytum.de

Reprinted with permission from *J. Phys. Chem. C*, **2017**, *121*, 16393-16398. Copyright 2017 American Chemical Society.

5.5 Ethanol surface chemistry on MBE-grown GaN(0001), GaO_x/GaN(0001), and Ga₂O₃($\bar{2}01$)

S. L. Kollmannsberger,^{†,1} C. A. Walenta,^{†,1} A. Winnerl,³ F. Knoller,¹ R. N. Pereira,³
M. Tschurl,¹ M. Stutzmann,^{2,3} U. Heiz^{*,1,2}

J. Chem. Phys., **2017**, *147*, 124704

doi: 10.1063/1.4994141

¹ Chair of Physical Chemistry, Department of Chemistry and Catalysis Research Center, Technische Universität München, Lichtenbergstr. 4, 85748 Garching, Germany

² Nanosystems Initiative Munich, Schellingstr. 4, 80799 München, Germany

³ Walter Schottky Institute and Physics Department, Technische Universität München, Am Coulombwall 4, 85748 Garching, Germany

[†] Contributed equally to this work.

*Corresponding author, E-mail: ulrich.heiz@mytum.de

Reprinted from *J. Chem. Phys.*, **2017**, *147*, 124704, with the permission of AIP Publishing.

5.6 Photocatalytic selectivity switch to C–C scission: α -methyl ejection of tert-butanol on TiO₂(110)

C. A. Walenta,[†] S. L. Kollmannsberger,[†] C. Courtois, M. Tschurl, U. Heiz*

Phys. Chem. Chem. Phys., **2018**, *20*, 7105-7111

doi: 10.1039/c8cp00223a

Chair of Physical Chemistry, Department of Chemistry and Catalysis Research Center, Technische Universität München, Lichtenbergstr. 4, 85748 Garching, Germany

[†] Contributed equally to this work.

*Corresponding author, E-mail: ulrich.heiz@mytum.de

Reproduced from *Phys. Chem. Chem. Phys.*, **2018**, *20*, 7105-7111 with permission from the PCCP Owner Societies.

6. Conclusion and Outlook

The results obtained during the course of this thesis yield important aspects of thermal and photo-activated molecular mechanisms of surface processes on semiconductors. Firstly, *mechanistic details* of the *photo-oxidation of alcohols* including the scission of the α -bond species were elucidated. Regarding this, the influence of thermal steps prior to the photo-reaction was emphasized. Secondly, the *thermal ethanol pathways* depending on the semiconductor material and the *surface composition* were compared. Thirdly, the *semiconductor doping* and the *role of surface states* on the CO adsorption as well as photo-activated desorption were investigated. All in all, the enormous importance of individual surface properties of the different semiconductor materials to thermal as well as photo-activated processes was demonstrated.

The mechanism of hole mediated alcohol photo-oxidation on the $\text{TiO}_2(110)$ surface was clarified. It was found that a thermal dissociation of the alcohol is a necessary step for subsequent photo-reforming. In this regard, the photo-abstraction of an species in α -position of the alcohol functionality was shown, even if no hydrogen is available in case of a tertiary alcohol. This results in the formation of acetone from tert-butanol and the formation of acetaldehyde from ethanol. In the first case the abstracted α -species is a methyl radical, which is directly ejected, while in the second one it is hydrogen, which hydroxylates the $\text{TiO}_2(110)$ surface. In this regard, it was demonstrated that the hydroxylation is the origin of the poisoning effect in alcohol photo-oxidation. In contrast to that, the activating influence of co-dosed oxygen was elucidated. Furthermore, for tert-butanol photo-oxidation it was found that a second pathway yielding isobutene exists, which is only available at elevated temperatures. Consequently, the thermal behavior of the adsorbates is a crucial aspect for photo-activated processes.

Therefore, the thermal ethanol chemistry was not only investigated on $\text{TiO}_2(110)$ but also on $\text{Ga}_2\text{O}_3(\bar{2}01)$ and $\text{GaN}(0001)$. For the latter one, the surface composition was varied, not only from the growing process of the GaN semiconductor but also by surface oxidation. It was found that $\text{TiO}_2(110)$ and $\text{GaN}(0001)$ exhibit a rich thermal chemistry. Both semiconductors enable the thermal formation of acetaldehyde and ethylene. For $\text{TiO}_2(110)$ it is known, that the preliminary step to those thermal reaction products is dissociative adsorption. In the case of $\text{GaN}(0001)$ thermal ethanol chemistry was not yet been investigated, however dissociative

adsorption was known for the molecules H_2 , NH_3 and trimethylgallium. Differently to the reaction on TiO_2 we found that all metal sites of the GaN(0001) surface enable dissociative binding. Consequently, the overall product yield is about a factor of five higher for MOCVD grown GaN(0001) than on $TiO_2(110)$. Moreover, H_2 formation is observed from the MOCVD GaN(0001) surface. The increase in native oxide, which is always present on GaN, leads to loss of thermal reactivity. However, dissociative adsorption of ethanol is still observed even on a fully oxidized GaN(0001) surface. This is different to the bulk oxide $Ga_2O_3(\bar{2}01)$, which only enables molecularly adsorption of ethanol.

To study the electronic properties of the GaN(0001) surface as a function of bulk doping and surface oxidation, the adsorption and photon stimulated desorption of CO was investigated. It was found, that the amount of adsorbable CO changes with the doping level. This is related to the number of negative charges in surface states, which increases with the shortening of the space charge region. However, the surface oxidation does not have an influence on the CO adsorption. By illumination of the semiconductor a charge redistribution at the surface occurs, which leads to a photon stimulated desorption of a fraction of the adsorbed CO. This effect is strongly influenced by surface oxidation, as it leads to a decrease in the intensity of the CO PSD. This can be related to a loss of photo-active sites accompanied by surface oxidation.

Furthermore, the results also emphasize the key role of the semiconductor surface on thermal and photo-activated processes. Consequently, the surface preparation of a photo-catalyst is of enormous importance for its catalytic activity. Regarding the photo-activated dehydrogenation of ethanol to generate molecular hydrogen, it is shown, that a bare semiconductor surface does not enable an H_2 formation. However, it could be demonstrated, that the photo-oxidation proceeds on reactive sites at the $TiO_2(110)$ surface. Consequently, the dehydrogenation reaction is mainly determined from the semiconductor surface. Another insight is, that only one photo-generated hole is needed to oxidize an alcohol to the respective aldehyde. Therefore, it seems obvious, that also only one electron is necessary for a catalytic cycle producing the aldehyde and molecular hydrogen. To answer this assumption, the next step is to investigate the photo-reforming of alcohols on semiconductor surfaces decorated with metal clusters. In case of $TiO_2(110)$ a co-catalyst enabling the hydrogen recombination instead of the formation of water has to be found. Whereas the GaN(0001) supported catalyst may be advantageous for a H_2 formation from N-H bonds, a co-catalyst opening the photo-oxidation pathway is required.

Figure 6.1 shows preliminary results for ethanol photo-reforming on a $\text{TiO}_2(110)$ surface decorated with 1% ML Pt clusters, respective to the number of surface atoms. It can clearly be seen that the ethanol trace declines immediately upon illumination and the formation of acetaldehyde and stoichiometric molecularly hydrogen occurs. Furthermore, the removed surface hydroxylation enables to perform the reaction under steady state conditions in a constant ethanol background. Identical intensities are observed in the three illumination periods. From such measurements, turn over frequencies can be obtained and their dependence upon cluster loading, background pressure, surface temperature and illumination intensity can be investigated. Such co-catalyst loaded semiconductors open a wide field of research options in

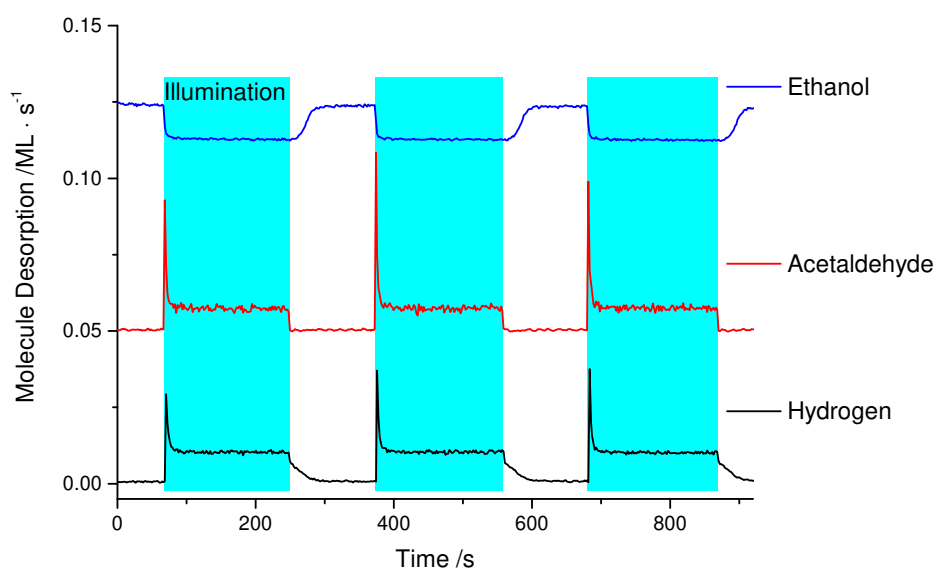


Fig. 6.1 Signals of ethanol, acetaldehyde and hydrogen upon photo-reforming of 1×10^{-7} mbar ethanol background at 257 K on a $\text{TiO}_2(110)$ surface decorated with Pt clusters. The blue region highlights the time of illumination. The ethanol and the acetaldehyde traces are offset for better transparency.

order to understand mechanistic details of hydrogen formation and the role of the co-catalysts. From our findings, the latter one is expected only to enable the recombination of hydrogen. If this is the case, the generally believed requirement for hydrogen evolution, which is that the semiconductor's conduction band edge has to lie above the electrochemical potential of hydrogen, would be irrelevant. Consequently, the number of semiconductor materials, which are worth considering for this reaction, would increase strongly. Furthermore, the efficiency may show a maximum at very low metal loadings, as the surface hydroxyl is very mobile and too high metal loadings will block the photo-active sites of the semiconductor surface. Another interesting option is the photo-catalytic gasphase synthesis of water-free aldehydes and ketons, which opens new pathways with high selectivities and low reaction

temperatures. At the same time, the selectivity may change with temperature, as it was found for the photo-reaction of tert-butanol (see appendix E).

References

- [1] Rahmstorf, S.; Foster, G.; Cahill, N. *Environ. Res. Lett.* **2017**, *12*, 054001.
- [2] Berlemann, M.; Steinhardt, M. F. *CESifo Econ. Stud.* **2017**, *63*, 353–385.
- [3] Rodhe, H. *Science* **1990**, *248*, 1217–1219.
- [4] Wilke, S. Treibhausgas-Emissionen in Deutschland. <https://www.umweltbundesamt.de/daten/klima/treibhausgas-emissionen-in-deutschland#textpart-3> requested 2018, March 14, 2017; Umweltbundesamt.
- [5] Burger, B. energy charts - Stromerzeugung in Deutschland in 2017. https://www.energy-charts.de/energy_pie_de.htm?year=2017 requested 2018, March 14, 2017; Fraunhofer-Institut für Solare Energiesysteme ISE.
- [6] Fatsikostas, A. N.; Kondarides, D.; Verykios, X. E. *Catal. Today* **2002**, *75*, 145 – 155.
- [7] Haryanto, A.; Fernando, S.; Murali, N.; Adhikari, S. *Energy Fuels* **2005**, *19*, 2098–2106.
- [8] Doyle, R. L.; Godwin, I. J.; Brandon, M. P.; Lyons, M. E. G. *Phys. Chem. Chem. Phys.* **2013**, *15*, 13737–13783.
- [9] Zhang, J.; Dai, L. *Angew. Chem.* **2016**, *128*, 13490–13494.
- [10] Wang, J.; Cui, W.; Liu, Q.; Xing, Z.; Asiri, A. M.; Sun, X. *Adv. Mater.* **2016**, *28*, 215–230.
- [11] Hisatomi, T.; Kubota, J.; Domen, K. *Chem. Soc. Rev.* **2014**,
- [12] Su, J.; Guo, L.; Bao, N.; Grimes, C. A. *Nano Lett.* **2011**, *11*, 1928–1933.
- [13] Wang, G.; Wang, H.; Ling, Y.; Tang, Y.; Yang, X.; Fitzmorris, R. C.; Wang, C.; Zhang, J. Z.; Li, Y. *Nano Lett.* **2011**, *11*, 3026–3033.
- [14] Shimura, K.; Yoshida, H. *Energy Environ. Sci.* **2011**, *4*, 2467–2481.
- [15] Murdoch, M.; Waterhouse, G. I. N.; Nadeem, M.; Metson, J. B.; Keane, M. A.; Howe, R. F.; Llorca, J.; Idriss, H. *Nat. Chem.* **2011**, *3*, 489 – 492.
- [16] Strataki, N.; Antoniadou, M.; Dracopoulos, V.; Lianos, P. *Catal. Today* **2010**, *151*, 53 – 57.
- [17] Montini, T.; Gombac, V.; Sordelli, L.; Delgado, J. J.; Chen, X.; Adami, G.; Fornasiero, P. *ChemCatChem* **2011**, *3*, 574–577.
- [18] Sampaio, M. J.; Oliveira, J. W.; Sombrio, C. I.; Baptista, D. L.; Teixeira, S. R.; Carabineiro, S. A.; Silva, C. G.; Faria, J. L. *Appl. Catal., A* **2016**, *518*, 198 – 205.
- [19] Yu, J.; Qi, L.; Jaroniec, M. *J. Phys. Chem. C* **2010**, *114*, 13118–13125.

- [20] Galińska, A.; Walendziewski, J. *Energy Fuels* **2005**, *19*, 1143–1147.
- [21] Ni, M.; Leung, M. K.; Leung, D. Y.; Sumathy, K. *Renew. Sustain. Energy Rev.* **2007**, *11*, 401 – 425.
- [22] Yang, Y.; Chang, C.-H.; Idriss, H. *Appl. Catal., B* **2006**, *67*, 217 – 222.
- [23] Majeed, I.; Nadeem, M. A.; Al-Oufi, M.; Nadeem, M. A.; Waterhouse, G.; Badshah, A.; Metson, J.; Idriss, H. *Appl. Catal., B* **2016**, *182*, 266 – 276.
- [24] Nadeem, M.; Murdoch, M.; Waterhouse, G.; Metson, J.; Keane, M.; Llorca, J.; Idriss, H. *J. Photochem. Photobiol., A* **2010**, *216*, 250 – 255.
- [25] Linsebigler, A. L.; Lu, G.; Yates, J. T. *Chem. Rev.* **1995**, *95*, 735 – 758.
- [26] Umebayashi, T.; Yamaki, T.; Itoh, H.; Asai, K. *Appl. Phys. Lett.* **2002**, *81*, 454–456.
- [27] Diebold, U. *Surf. Sci. Rep.* **2003**, *48*, 53 – 229.
- [28] Henderson, M.; Otero-Tapia, S.; Castro, M. *Surf. Sci.* **1998**, *412-413*, 252 – 272.
- [29] Henderson, M.; Otero-Tapia, S.; Castro, M. *Faraday Discuss.* **1999**, *114*, 313–329.
- [30] Farfan-Arribas, E.; Madix, R. J. *Surf. Sci.* **2003**, *544*, 241 – 260.
- [31] Zhang, Z.; Bondarchuk, O.; White, J. M.; Kay, B. D.; Dohnálek, Z. *J. Am. Chem. Soc.* **2006**, *128*, 4198–4199.
- [32] Shen, M.; Acharya, D. P.; Dohnálek, Z.; Henderson, M. A. *J. Phys. Chem. C* **2012**, *116*, 25465–25469.
- [33] Chuang, C.-C.; Chen, C.-C.; Lin, J.-L. *J. Phys. Chem. B* **1999**, *103*, 2439–2444.
- [34] Onda, K.; Li, B.; Zhao, J.; Petek, H. *Surf. Sci.* **2005**, *593*, 32–37.
- [35] Li, B.; Zhao, J.; Onda, K.; Jordan, K. D.; Yang, J.; Petek, H. *Science* **2006**, *311*, 1436–1440.
- [36] Zhou, C. et al. *Chem. Sci.* **2010**, *1*, 575–580.
- [37] Zhou, C.; Ma, Z.; Ren, Z.; Mao, X.; Dai, D.; Yang, X. *Chem. Sci.* **2011**, *2*, 1980–1983.
- [38] Shen, M.; Henderson, M. A. *J. Phys. Chem. Lett.* **2011**, *2*, 2707–2710.
- [39] Shen, M.; Henderson, M. A. *J. Phys. Chem. C* **2012**, *116*, 18788–18795.
- [40] Kolesov, G.; Vinichenko, D.; Tritsarlis, G. A.; Friend, C. M.; Kaxiras, E. *J. Phys. Chem. Lett.* **2015**, *6*, 1624–1627.
- [41] Phillips, K. R.; Jensen, S. C.; Baron, M.; Li, S.-C.; Friend, C. M. *J. Am. Chem. Soc.* **2013**, *135*, 574–577.
- [42] Guo, Q.; Xu, C.; Ren, Z.; Yang, W.; Ma, Z.; Dai, D.; Fan, H.; Minton, T. K.; Yang, X. *J. Am. Chem. Soc.* **2012**, *134*, 13366–13373.

- [43] Guo, Q.; Xu, C.; Yang, W.; Ren, Z.; Ma, Z.; Dai, D.; Minton, T. K.; Yang, X. *J. Phys. Chem. C* **2013**, *117*, 5293–5300.
- [44] Ma, Z.; Guo, Q.; Mao, X.; Ren, Z.; Wang, X.; Xu, C.; Yang, W.; Dai, D.; Zhou, C.; Fan, H.; Yang, X. *J. Phys. Chem. C* **2013**, *117*, 10336–10344.
- [45] Yuan, Q.; Wu, Z.; Jin, Y.; Xu, L.; Xiong, F.; Ma, Y.; Huang, W. *J. Am. Chem. Soc.* **2013**, *135*, 5212–5219.
- [46] Liu, S.; an Liu, A.; Wen, B.; Zhang, R.; Zhou, C.; Liu, L.-M.; Ren, Z. *J. Phys. Chem. Lett.* **2015**, *6*, 3327–3334.
- [47] Cremer, T.; Jensen, S. C.; Friend, C. M. *J. Phys. Chem. C* **2014**, *118*, 29242–29251.
- [48] Lang, X.; Wen, B.; Zhou, C.; Ren, Z.; Liu, L.-M. *J. Phys. Chem. C* **2014**, *118*, 19859–19868.
- [49] Xu, C.; Yang, W.; Guo, Q.; Dai, D.; Chen, M.; Yang, X. *J. Am. Chem. Soc.* **2013**, *135*, 10206–10209.
- [50] Gamble, L.; Jung, L. S.; Campbell, C. T. *Langmuir* **1995**, *11*, 4505–4514.
- [51] Farfan-Arribas, E.; Madix, R. J. *J. Phys. Chem. B* **2002**, *106*, 10680–10692.
- [52] Kim, Y. K.; Kay, B. D.; White, J. M.; Dohnálek, Z. *J. Phys. Chem. C* **2007**, *111*, 18236–18242.
- [53] Hansen, J. Ø.; Huo, P.; Martinez, U.; Lira, E.; Wei, Y. Y.; Streber, R.; Lægsgaard, E.; Hammer, B.; Wendt, S.; Besenbacher, F. *Phys. Rev. Lett.* **2011**, *107*, 136102–136106.
- [54] Huo, P.; Hansen, J. Ø.; Martinez, U.; Lira, E.; Streber, R.; Wei, Y.; Lægsgaard, E.; Hammer, B.; Wendt, S.; Besenbacher, F. *J. Phys. Chem. Lett.* **2012**, *3*, 283–288.
- [55] Jayaweera, P. M.; Quah, E. L.; Idriss, H. *J. Phys. Chem. C* **2007**, *111*, 1764 – 1769.
- [56] Nadeem, A. M.; Muir, J. M. R.; Connelly, K. A.; Adamson, B. T.; Metson, B. J.; Idriss, H. *Phys. Chem. Chem. Phys.* **2011**, *13*, 7637 – 7643.
- [57] Ma, Z.; Zhou, C.; Mao, X.; Ren, Z.; Dai, D.; Yang, X. *Chi. J. Chem. Phys.* **2013**, *26*, 1–7.
- [58] Hansen, J. Ø.; Bebensee, R.; Martinez, U.; Porsgaard, S.; Lira, E.; Wei, Y.; Lam-mich, L.; Li, Z.; Idriss, H.; Besenbacher, F.; Hammer, B.; Wendt, S. *Sci. Rep.* **2016**, *6*, 21990.
- [59] Bondarchuk, O.; Kim, Y. K.; White, J. M.; Kim, J.; Kay, B. D.; Dohnalek, Z. *J. Phys. Chem. C* **2007**, *111*, 11059 – 11067.
- [60] Zhang, Z.; Bondarchuk, O.; Kay, B. D.; White, J. M.; Dohnálek, Z. *J. Phys. Chem. C* **2007**, *111*, 3021–3027.
- [61] Kim, Y. K.; Kay, B. D.; White, J.; Dohnálek, Z. *Surf. Sci.* **2008**, *602*, 511 – 516.

- [62] Brinkley, D.; Engel, T. *J. Phys. Chem. B* **1998**, *102*, 7596 – 7605.
- [63] Brinkley, D.; Engel, T. *Surf. Sci.* **1998**, *415*, L1001 – L1006.
- [64] Brinkley, D.; Engel, T. *J. Phys. Chem. B* **2000**, *104*, 9836 – 9841.
- [65] Henderson, M. A. *J. Phys. Chem. B* **2004**, *108*, 18932–18941.
- [66] Du, Y.; Deskins, N. A.; Zhang, Z.; Dohnalek, Z.; Dupuis, M.; Lyubinetsky, I. *Phys. Chem. Chem. Phys.* **2010**, *22*, 6337–6344.
- [67] Yu, X.; Zhang, Z.; Yang, C.; Bebensee, F.; Heissler, S.; Nefedov, A.; Tang, M.; Ge, Q.; Chen, L.; Kay, B. D.; Dohnálek, Z.; Wang, Y.; Wöll, C. *J. Phys. Chem. C* **2016**, *120*, 12626–12636.
- [68] Zehr, R.; Henderson, M. *Surf. Sci.* **2008**, *602*, 2238–2249.
- [69] Zhang, Z.; Bondarchuk, O.; Kay, B. D.; White, J. M.; Dohnálek, Z. *J. Phys. Chem. B* **2006**, *110*, 21840–21845.
- [70] Johnson, W. C.; Parson, J. B.; Crew, M. C. *J. Phys. Chem.* **1931**, *36*, 2651–2654.
- [71] Krames, M. R.; Shchekin, O. B.; Mueller-Mach, R.; Mueller, G. O.; Zhou, L.; Harbers, G.; Craford, M. G. *J. Disp. Technol.* **2007**, *3*, 160–175.
- [72] Maeda, K.; Takata, T.; Hara, M.; Saito, N.; Inoue, Y.; Kobayashi, H.; Domen, K. *J. Am. Chem. Soc.* **2005**, *127*, 8286 – 8287.
- [73] Maruska, H. P.; Tietjen, J. *J. Appl. Phys. Lett.* **1969**, *15*, 327 – 329.
- [74] Amano, H.; Kito, M.; Hiramatsu, K.; Akasaki, I. *Jpn. J. Appl. Phys.* **1989**, *28*, L2112.
- [75] Smith, L.; King, S.; Nemanich, R.; Davis, R. *J. Elec. Mater.* **1996**, *25*, 805–810.
- [76] King, S. W.; Barnak, J. P.; Bremser, M. D.; Tracy, K. M.; Ronning, C.; Davis, R. F.; Nemanich, R. J. *J. Appl. Phys.* **1998**, *84*, 5248–5260.
- [77] Lee, K. N.; Donovan, S. M.; Gila, B.; Overberg, M.; Mackenzie, J. D.; Abernathy, C. R.; Wilson, R. G. *J. Electrochem. Soc.* **2000**, *8*, 3087–3090.
- [78] Tracy, K. M.; Mecouch, W. J.; Davis, R. F.; Nemanich, R. J. *J. Appl. Phys.* **2003**, *94*, 3163–3172.
- [79] Grabow, L.; Uhlrich, J.; Kuech, T.; Mavrikakis, M. *Surf. Sci.* **2009**, *603*, 387–399.
- [80] Bermudez, V.; Koleske, D.; Wickenden, A. *Appl. Surf. Sci.* **1998**, *126*, 69–82.
- [81] Machuca, F.; Liu, Z.; Sun, Y.; Pianetta, P.; Spicer, W. E.; Pease, R. F. W. *J. Vac. Sci. Technol., A* **2002**, *50*, 1784–1786.
- [82] Diale, M.; Auret, F.; van der Berg, N.; Odendaal, R.; Roos, W. *Appl. Surf. Sci.* **2005**, *246*, 279–389.

- [83] Wu, C. I.; Kahn, A.; Taskar, N.; Dorman, D.; Gallagher, D. *J. Appl. Phys.* **1998**, *83*, 4249–4252.
- [84] Shalish, I.; Shapira, Y.; Burstein, L.; Salzman, J. *J. Appl. Phys.* **2001**, *89*, 390–395.
- [85] Lai, Y.-H.; Yeh, C.-T.; Hwang, J.-M.; Hwang, H.-L.; Chen, C.-T.; Hung, W.-H. *J. Phys. Chem. B* **2001**, *105*, 10029–10036.
- [86] Bermudez, V. M. *J. Appl. Phys.* **1996**, *80*, 1190–1200.
- [87] Janzen, O.; Hahn, C.; Mönch, W. *Eur. Phys. J. B* **1999**, *9*, 315–321.
- [88] Dong, Y.; Feenstra, R. M.; Northrup, J. E. *J. Vac. Sci. Technol., B* **2006**, *24*, 2080–2086.
- [89] Prabhakaran, K.; Andersson, T. G.; Nozawa, K. *Appl. Phys. Lett.* **1996**, *69*, 3212–3214.
- [90] Bermudez, V.; Long, J. *Surf. Sci.* **2000**, *450*, 98–105.
- [91] Uhrich, J.; Grabow, L.; Mavrikakis, M.; Kuech, T. *J. Electron. Mater.* **2008**, *37*, 439–447.
- [92] Watkins, N. J.; Wicks, G. W.; Gao, Y. *Appl. Phys. Lett.* **1999**, *75*, 2602–2604.
- [93] Hollinger, G.; Skheyta-Kabbani, R.; Gendry, M. *Phys. Rev. B* **1994**, *49*, 11159–11167.
- [94] Wolter, S. D.; Luther, B. P.; Waltemyer, D. L.; Önnby, C.; Mohny, S. E.; Molnar, R. J. *Appl. Phys. Lett.* **1997**, *70*, 2156–2158.
- [95] Chen, P.; Zhang, R.; Xu, X.; Chen, Z.; Zhou, Y.; Xie, S.; Shi, Y.; Shen, B.; Gu, S.; Huang, Z.; Hu, J.; Zheng, Y. *MRS Internet J. Nitride Semicond. Res.* **2000**, *5*, 866–872.
- [96] Peng, L.-H.; Liao, C.-H.; Hsu, Y.-C.; Jong, C.-S.; Huang, C.-N.; Ho, J.-K.; Chiu, C.-C.; Chen, C.-Y. *Appl. Phys. Lett.* **2000**, *76*, 511–513.
- [97] Shiozaki, N.; Sato, T.; Hashizume, T. *Jpn. J. Appl. Phys.* **2007**, *46*, 1471.
- [98] Shekhar, R.; Jensen, K. F. *Surf. Sci.* **1997**, *381*, L581–L588.
- [99] Bermudez, V. *Chem. Phys. Lett.* **2000**, *317*, 290–295.
- [100] Bellitto, V.; Thoms, B.; Koleske, D.; Wickenden, A.; Henry, R. *Surf. Sci.* **1999**, *430*, 80–88.
- [101] Lam, H.-T.; Vohs, J. *Surf. Sci.* **1999**, *426*, 199 – 211.
- [102] Calzolari, A.; Ruini, A.; Catellani, A. *J. Phys. Chem. C* **2012**, *116*, 17158–17163.
- [103] Winbauer, A. REMPI-ToF als isomerenselektive Analyseverfahren in der heterogenen Katalyse. Ph.D. thesis, Technische Universität München, 2014.
- [104] Heiz, U.; Vanolli, F.; Trento, L.; Schneider, W.-D. *Rev. Sci. Instrum.* **1997**, *68*, 1986–1994.

- [105] Kiermaier, J. Entwicklung und Aufbau einer Apparatur zur Bestimmung der photokatalytischen Eigenschaften von halbleiterbasierten Modellsystem im Ultrahochvakuum - Photodesorption von Sauerstoff auf (110)-TiO₂-Einkristallen. Ph.D. thesis, Technische Universität München, 2013.
- [106] Li, Z.; Smith, R. S.; Kay, B. D.; Dohnálek, Z. *J. Phys. Chem. C* **2011**, *115*, 22534–22539.
- [107] Bull, J. N.; Harland, P. W.; Vallance, C. *J. Phys. Chem. A* **2012**, *116*, 767–777.
- [108] Straub, H. C.; Lindsay, B. G.; Smith, K. A.; Stebbings, R. F. *J. Chem. Phys.* **1998**, *108*, 109–116.
- [109] Gupta, D.; Antony, B. *J. Chem. Phys.* **2014**, *141*, 054303.
- [110] Kim, Y.-K.; Irikura, K. K.; Rudd, M. E.; Ali, M. A.; Stone, P. M.; Chang, J.; Coursey, J. S.; Dragoset, R. A.; Kishore, A. R.; Olsen, K. J.; Sansonetti, A. M.; Wiersma, G. G.; Zucker, D. S.; Zucker, M. A. Electron-Impact Ionization Cross Section for Ionization and Excitation Database. <http://physics.nist.gov/ionxsec> requested 2018, February 12, 2004 version 3.0; National Institute of Standards and Technology.
- [111] Harrison, A. G.; Jones, E. G.; Gupta, S. K.; Nagy, G. P. *Can. J. Chem.* **1966**, *44*, 1967–1973.
- [112] Peng, X.; Viswanathan, R.; Smudde Jr., G. H.; Stair, P. C. *Rev. Sci. Instrum.* **1992**, *63*, 3930–3935.
- [113] Hudson, J. E.; Weng, Z. F.; Vallance, C.; Harland, P. W. *Int. J. Mass Spectrom.* **2006**, *248*, 42 – 46.
- [114] Linstrom, P., Mallard, W., Eds. *NIST Chemistry WebBook, NIST Standard Reference Database Number 69*, retrieved December 12, 2017 ed.; National Institute of Standards and Technology: Gaithersburg MD, 20899, 2017.
- [115] Varian, UHV-24/UHV-24p Ionization Gauge. Instruction Manual, 2004.
- [116] Li, M.; Hebenstreit, W.; Diebold, U.; Tyryshkin, A. M.; Bowman, M. K.; Dunham, G. G.; Henderson, M. A. *J. Phys. Chem. B* **2000**, *104*, 4944–4950.
- [117] Henderson, M. A. *Langmuir* **1996**, *12*, 5093–5098.
- [118] Petrik, N. G.; Zhang, Z.; Du, Y.; Dohnálek, Z.; Lyubinetsky, I.; Kimmel, G. A. *J. Phys. Chem. C* **2009**, *113*, 12407–12411.
- [119] Kim, B.; Li, Z.; Kay, B. D.; Dohnalek, Z.; Kim, Y. K. *Phys. Chem. Chem. Phys.* **2012**, *14*, 15060–15065.
- [120] Tanuma, S.; Powell, C. J.; Penn, D. R. *Surf. Interface Anal.* **1991**, *17*, 911–926.
- [121] Tanuma, S.; Powell, C. J.; Penn, D. R. *Surf. Interface Anal.* **1991**, *17*, 927–939.
- [122] Asif Khan, M.; Kuznia, J. N.; Olson, D. T.; Kaplan, R. *J. Appl. Phys.* **1993**, *73*, 3108–3110.

-
- [123] Heying, B.; Tarsa, E. J.; Elsass, C. R.; Fini, P.; DenBaars, S. P.; Speck, J. S. *J. Appl. Phys.* **1999**, *85*, 6470–6476.
- [124] Childs, K. D.; Carlson, B. A.; Vanier, L. A.; Moulder, J. F.; Paul, D. F.; Stickle, W. F.; Watson, D. G. *Handbook of Auger Electron Spectroscopy*; Physical Electronics Industries, 1995.
- [125] Gamble, L.; Jung, L. S.; Campbell, C. T. *Surf. Sci.* **1996**, *348*, 1–16.
- [126] Idriss, H.; Seebauer, E. *J. Mol. Catal. A: Chem.* **2000**, *152*, 201–212.
- [127] Winnerl, A.; Pereira, R. N.; Stutzmann, M. *J. Appl. Phys.* **2015**, *118*.
- [128] Winnerl, A.; Garrido, J. A.; Stutzmann, M. *Appl. Phys. Lett.* **2017**, *110*, 101602.
- [129] Henderson, M. A.; Lyubinetsky, I. *Chem. Rev.* **2013**, *113*, 4428 – 4455.
- [130] Henderson, M. A. *J. Phys. Chem. C* **2013**, *117*, 14113 – 14124.

Danksagung

Zu aller erst möchte ich mich bei Prof. Dr. Ulrich K. Heiz bedanken, für die Möglichkeit mich schon früh im Studium in der Physikalischen Chemie einzubringen, dies hat meine Motivation auf ein neues Level gehoben. Des Weiteren möchte ich mich bedanken für die Möglichkeit an seinem Lehrstuhl zu promovieren, für die herausragend gute Atmosphäre, für die sehr gute Betreuung, die gewährten Freiheiten und nicht zuletzt für den Kicker der Arbeitsgruppe.

Ich bedanke mich bei Martin Tschurl für die herausragende Unterstützung, die Wertschätzung meiner Arbeit und die Möglichkeit über alles zu reden und Lösungen zu finden, für die Ratschläge und Gespräche egal ob beruflicher oder privater Natur. Ich danke meinem Laborkollegen Constantin Walenta für seine motivierende Art, seine Hilfsbereitschaft, die Labormatches, die Literaturvorschläge und die Kompromissbereitschaft aber vor allem für die besondere Freundschaft die sich in den letzten Jahren entwickelt hat. Insbesondere möchte ich Martin und Constantin aber für die genialen Momente neben der Arbeit, bei Christian Steiffen Konzerten, beim Weggehen oder auf Konferenzen danken. Vor allem ihr Beide habt meine Zeit am Lehrstuhl geprägt und diese zu einer unvergesslichen gemacht.

Außerdem möchte ich mich bei Carla Courtois bedanken für die sehr gute Unterstützung im Labor, für die Hilfe mit Abbildungen, für die guten Gespräche während dem Arbeitsweg und die herausragenden Abwehrleistungen am Kicker.

Ich danke Kim Vetter und Moritz Eder für die Hilfe im Labor und die gute und humorvolle Atmosphäre die ihr jederzeit in das Photocat Labor gebracht habt.

Außerdem bedanke ich mich bei Sophie Mader, Michael Röhl, Kevin Maik Jablonka, Jeryl Jep, Nicolas Hadisurya und Dennis Meier, die ich während meiner Promotion betreuen durfte. Vielen Dank für die Unterstützung und die guten Ergebnisse die wir zusammen erarbeitet haben.

Vielen Dank an Dr. Andreas Winbauer und Dr. Josef Kiermaier. Ohne euch hätte ich diesen Weg vermutlich nie eingeschlagen. Ihr habt mich in eurem Labor aufgenommen und mir immer das Gefühl gegeben am richtigen Platz zu sein.

Ich möchte mich bei Fabian Knoller für die gute Zeit und die guten Unterhaltungen während des schweißtreibenden Arbeitsweges auf dem Fahrrad bedanken.

Ich danke meinen Labornachbarn Maximilian Krause und Marian Rötzer dafür, dass ihr die extrem laute und nicht immer gute Musik ertragen habt und jederzeit zu Kicker-Matches, die ihresgleichen suchen zur Verfügung standet.

Allen anderen Mitarbeitern des Lehrstuhls möchte ich für die außerordentlich gute Atmosphäre und die Hilfsbereitschaft danken.

Mario Bilobrk möchte ich besonders dafür danken, dass er mir gelehrt hat wie Schraubverbindungen professionell mit Hanf gedichtet werden.

Ich danke den Werkstätten für Feinmechanik und für Elektronik für die herausragend gute Unterstützung. Meine Forschung wäre ohne eure Leistung so nicht möglich gewesen.

Besonders danke ich meinen Eltern, die mich zu jederzeit unterstützt haben egal welche Wege ich gehen wollte. Außerdem danke ich meinem Bruder für sensationelle Badmintonmatches, die ein wichtiger Ausgleich zu Studium und Promotion waren.

Ich danke meiner Frau Julia für ihr Verständnis, ihre Geduld und dafür, dass sie mein Leben so wundervoll bereichert. Außerdem danke ich meiner Tochter Luisa, die mich so oft mit ihren strahlenden Augen und ihrer fröhlichen Art nach der Arbeit begrüßt hat.

A. Reprint Permissions

A.1 Ethanol photocatalysis on rutile TiO₂(110): the role of defects and water

This article is licensed under a Creative Commons Attribution 3.0 Unported Licence. Material from this article can be used in other publications provided that the correct acknowledgement is given with the reproduced material.

Reproduced material should be attributed as follows:

- For reproduction of material from NJC:
[Original citation] - Published by The Royal Society of Chemistry (RSC) on behalf of the Centre National de la Recherche Scientifique (CNRS) and the RSC.
- For reproduction of material from PCCP:
[Original citation] - Published by the PCCP Owner Societies.
- For reproduction of material from PPS:
[Original citation] - Published by The Royal Society of Chemistry (RSC) on behalf of the European Society for Photobiology, the European Photochemistry Association, and RSC.
- For reproduction of material from all other RSC journals:
[Original citation] - Published by The Royal Society of Chemistry.

Information about reproducing material from RSC articles with different licences is available on our [Permission Requests](#) page.

A.2 Isomer-Selective Detection of Aromatic Molecules in Temperature-Programmed Desorption for Model Catalysis



RightsLink®

Home

Create Account

Help



Title: Isomer-Selective Detection of Aromatic Molecules in Temperature-Programmed Desorption for Model Catalysis
Author: Andreas Winbauer, Sebastian L. Kollmannsberger, Constantin A. Walenta, et al
Publication: Analytical Chemistry
Publisher: American Chemical Society
Date: May 1, 2016
Copyright © 2016, American Chemical Society

LOGIN
If you're a **copyright.com user**, you can login to RightsLink using your copyright.com credentials. Already a **RightsLink user** or want to [learn more?](#)

PERMISSION/LICENSE IS GRANTED FOR YOUR ORDER AT NO CHARGE

This type of permission/license, instead of the standard Terms & Conditions, is sent to you because no fee is being charged for your order. Please note the following:

- Permission is granted for your request in both print and electronic formats, and translations.
- If figures and/or tables were requested, they may be adapted or used in part.
- Please print this page for your records and send a copy of it to your publisher/graduate school.
- Appropriate credit for the requested material should be given as follows: "Reprinted (adapted) with permission from (COMPLETE REFERENCE CITATION). Copyright (YEAR) American Chemical Society." Insert appropriate information in place of the capitalized words.
- One-time permission is granted only for the use specified in your request. No additional uses are granted (such as derivative works or other editions). For any other uses, please submit a new request.

BACK

CLOSE WINDOW

A.3 Doping-Dependent Adsorption and Photon-Stimulated Desorption of CO on GaN(0001)



RightsLink®

Home

Create Account

Help



Title: Doping-Dependent Adsorption and Photon-Stimulated Desorption of CO on GaN(0001)
Author: Sebastian L. Kollmannsberger, Constantin A. Walenta, Andrea Winnerl, et al
Publication: The Journal of Physical Chemistry C
Publisher: American Chemical Society
Date: Apr 1, 2017
Copyright © 2017, American Chemical Society

LOGIN
If you're a **copyright.com user**, you can login to RightsLink using your copyright.com credentials. Already a **RightsLink user** or want to [learn more?](#)

PERMISSION/LICENSE IS GRANTED FOR YOUR ORDER AT NO CHARGE

This type of permission/license, instead of the standard Terms & Conditions, is sent to you because no fee is being charged for your order. Please note the following:

- Permission is granted for your request in both print and electronic formats, and translations.
- If figures and/or tables were requested, they may be adapted or used in part.
- Please print this page for your records and send a copy of it to your publisher/graduate school.
- Appropriate credit for the requested material should be given as follows: "Reprinted (adapted) with permission from (COMPLETE REFERENCE CITATION). Copyright (YEAR) American Chemical Society." Insert appropriate information in place of the capitalized words.
- One-time permission is granted only for the use specified in your request. No additional uses are granted (such as derivative works or other editions). For any other uses, please submit a new request.

BACK

CLOSE WINDOW

A.4 Anhydrous Ethanol Dehydrogenation on Metal–Organic Chemical Vapor Deposition Grown GaN(0001)



RightsLink®



Title: Anhydrous Ethanol
Dehydrogenation on Metal–
Organic Chemical Vapor
Deposition Grown GaN(0001)
Author: Constantin A. Walenta,
Sebastian L. Kollmannsberger,
Rui N. Pereira, et al
Publication: The Journal of Physical
Chemistry C
Publisher: American Chemical Society
Date: Aug 1, 2017

Copyright © 2017, American Chemical Society

LOGIN
If you're a **copyright.com**
user, you can login to
RightsLink using your
copyright.com credentials.
Already a **RightsLink user** or
want to [learn more?](#)

PERMISSION/LICENSE IS GRANTED FOR YOUR ORDER AT NO CHARGE

This type of permission/license, instead of the standard Terms & Conditions, is sent to you because no fee is being charged for your order. Please note the following:

- Permission is granted for your request in both print and electronic formats, and translations.
- If figures and/or tables were requested, they may be adapted or used in part.
- Please print this page for your records and send a copy of it to your publisher/graduate school.
- Appropriate credit for the requested material should be given as follows: "Reprinted (adapted) with permission from (COMPLETE REFERENCE CITATION). Copyright (YEAR) American Chemical Society." Insert appropriate information in place of the capitalized words.
- One-time permission is granted only for the use specified in your request. No additional uses are granted (such as derivative works or other editions). For any other uses, please submit a new request.

BACK

CLOSE WINDOW

A.5 Ethanol surface chemistry on MBE-grown GaN(0001), GaO_x/GaN(0001), and Ga₂O₃($\bar{2}01$)

AIP PUBLISHING LICENSE TERMS AND CONDITIONS

Mar 14, 2018

This Agreement between Mr. Sebastian Kollmannsberger ("You") and AIP Publishing ("AIP Publishing") consists of your license details and the terms and conditions provided by AIP Publishing and Copyright Clearance Center.

| | |
|--|---|
| License Number | 4307481279664 |
| License date | Mar 14, 2018 |
| Licensed Content Publisher | AIP Publishing |
| Licensed Content Publication | Journal of Chemical Physics |
| Licensed Content Title | Ethanol surface chemistry on MBE-grown GaN(0001), GaO _x /GaN(0001), and Ga ₂ O ₃ ($\bar{2}01$) |
| Licensed Content Author | Sebastian L. Kollmannsberger, Constantin A. Walenta, Andrea Winnerl, et al |
| Licensed Content Date | Sep 28, 2017 |
| Licensed Content Volume | 147 |
| Licensed Content Issue | 12 |
| Type of Use | Thesis/Dissertation |
| Requestor type | Author (original article) |
| Format | Print and electronic |
| Portion | Excerpt (> 800 words) |
| Will you be translating? | No |
| Title of your thesis / dissertation | Thermal and Photo-Activated Molecular Mechanisms on TiO ₂ (110) and GaN(0001) |
| Expected completion date | May 2018 |
| Estimated size (number of pages) | 200 |
| Requestor Location | Mr. Sebastian Kollmannsberger TUM Department of Chemistry Chair of Physical Chemistry Lichtenbergstraße 4 Garching, Bavaria 85748 Germany Attn: Mr. Sebastian Kollmannsberger |
| Billing Type | Invoice |
| Billing Address | Mr. Sebastian Kollmannsberger TUM Department of Chemistry Chair of Physical Chemistry Lichtenbergstraße 4 Garching, Germany 85748 Attn: Mr. Sebastian Kollmannsberger |
| Total | 0.00 EUR |

Terms and Conditions

AIP Publishing -- Terms and Conditions: Permissions Uses

AIP Publishing hereby grants to you the non-exclusive right and license to use and/or distribute the Material according to the use specified in your order, on a one-time basis, for the specified term, with a maximum distribution equal to the number that you have ordered. Any links or other content accompanying the Material are not the subject of this license.

1. You agree to include the following copyright and permission notice with the reproduction of the Material: "Reprinted from [FULL CITATION], with the permission of AIP Publishing." For an article, the credit line and permission notice must be printed on the first page of the article or book chapter. For photographs, covers, or tables, the notice may appear with the Material, in a footnote, or in the reference list.
2. If you have licensed reuse of a figure, photograph, cover, or table, it is your responsibility to ensure that the material is original to AIP Publishing and does not contain the copyright of another entity, and that the copyright notice of the figure, photograph, cover, or table does not indicate that it was reprinted by AIP Publishing, with permission, from another source. Under no circumstances does AIP Publishing purport or intend to grant permission to reuse material to which it does not hold appropriate rights.
You may not alter or modify the Material in any manner. You may translate the Material into another language only if you have licensed translation rights. You may not use the Material for promotional purposes.
3. The foregoing license shall not take effect unless and until AIP Publishing or its agent, Copyright Clearance Center, receives the Payment in accordance with Copyright Clearance Center Billing and Payment Terms and Conditions, which are incorporated herein by reference.
4. AIP Publishing or Copyright Clearance Center may, within two business days of granting this license, revoke the license for any reason whatsoever, with a full refund payable to you. Should you violate the terms of this license at any time, AIP Publishing, or Copyright Clearance Center may revoke the license with no refund to you. Notice of such revocation will be made using the contact information provided by you. Failure to receive such notice will not nullify the revocation.
5. AIP Publishing makes no representations or warranties with respect to the Material. You agree to indemnify and hold harmless AIP Publishing, and their officers, directors, employees or agents from and against any and all claims arising out of your use of the Material other than as specifically authorized herein.
6. The permission granted herein is personal to you and is not transferable or assignable without the prior written permission of AIP Publishing. This license may not be amended except in a writing signed by the party to be charged.
7. If purchase orders, acknowledgments or check endorsements are issued on any forms containing terms and conditions which are inconsistent with these provisions, such inconsistent terms and conditions shall be of no force and effect. This document, including the CCC Billing and Payment Terms and Conditions, shall be the entire agreement between the parties relating to the subject matter hereof.

This Agreement shall be governed by and construed in accordance with the laws of the State of New York. Both parties hereby submit to the jurisdiction of the courts of New York County for purposes of resolving any disputes that may arise hereunder.

V1.2

Questions? customer@copyright.com or +1-855-239-3415 (toll free in the US) or +1-978-646-2777.

A.6 Photocatalytic selectivity switch to C–C scission: α -methyl ejection of tert-butanol on TiO₂(110)

Authors contributing to RSC publications (journal articles, books or book chapters) do not need to formally request permission to reproduce material contained in this article provided that the correct acknowledgement is given with the reproduced material.

Reproduced material should be attributed as follows:

- For reproduction of material from NJC:
Reproduced from Ref. XX with permission from the Centre National de la Recherche Scientifique (CNRS) and The Royal Society of Chemistry.
- For reproduction of material from PCCP:
Reproduced from Ref. XX with permission from the PCCP Owner Societies.
- For reproduction of material from PPS:
Reproduced from Ref. XX with permission from the European Society for Photobiology, the European Photochemistry Association, and The Royal Society of Chemistry.
- For reproduction of material from all other RSC journals and books:
Reproduced from Ref. XX with permission from The Royal Society of Chemistry.

If the material has been adapted instead of reproduced from the original RSC publication "Reproduced from" can be substituted with "Adapted from".

In all cases the Ref. XX is the XXth reference in the list of references.

If you are the author of this article you do not need to formally request permission to reproduce figures, diagrams etc. contained in this article in third party publications or in a thesis or dissertation provided that the correct acknowledgement is given with the reproduced material.

Reproduced material should be attributed as follows:

- For reproduction of material from NJC:
[Original citation] - Reproduced by permission of The Royal Society of Chemistry (RSC) on behalf of the Centre National de la Recherche Scientifique (CNRS) and the RSC

- For reproduction of material from PCCP:
[Original citation] - Reproduced by permission of the PCCP Owner Societies
- For reproduction of material from PPS:
[Original citation] - Reproduced by permission of The Royal Society of Chemistry (RSC) on behalf of the European Society for Photobiology, the European Photochemistry Association, and RSC
- For reproduction of material from all other RSC journals:
[Original citation] - Reproduced by permission of The Royal Society of Chemistry

If you are the author of this article you still need to obtain permission to reproduce the whole article in a third party publication with the exception of reproduction of the whole article in a thesis or dissertation.

Information about reproducing material from RSC articles with different licences is available on our [Permission Requests](#) page.

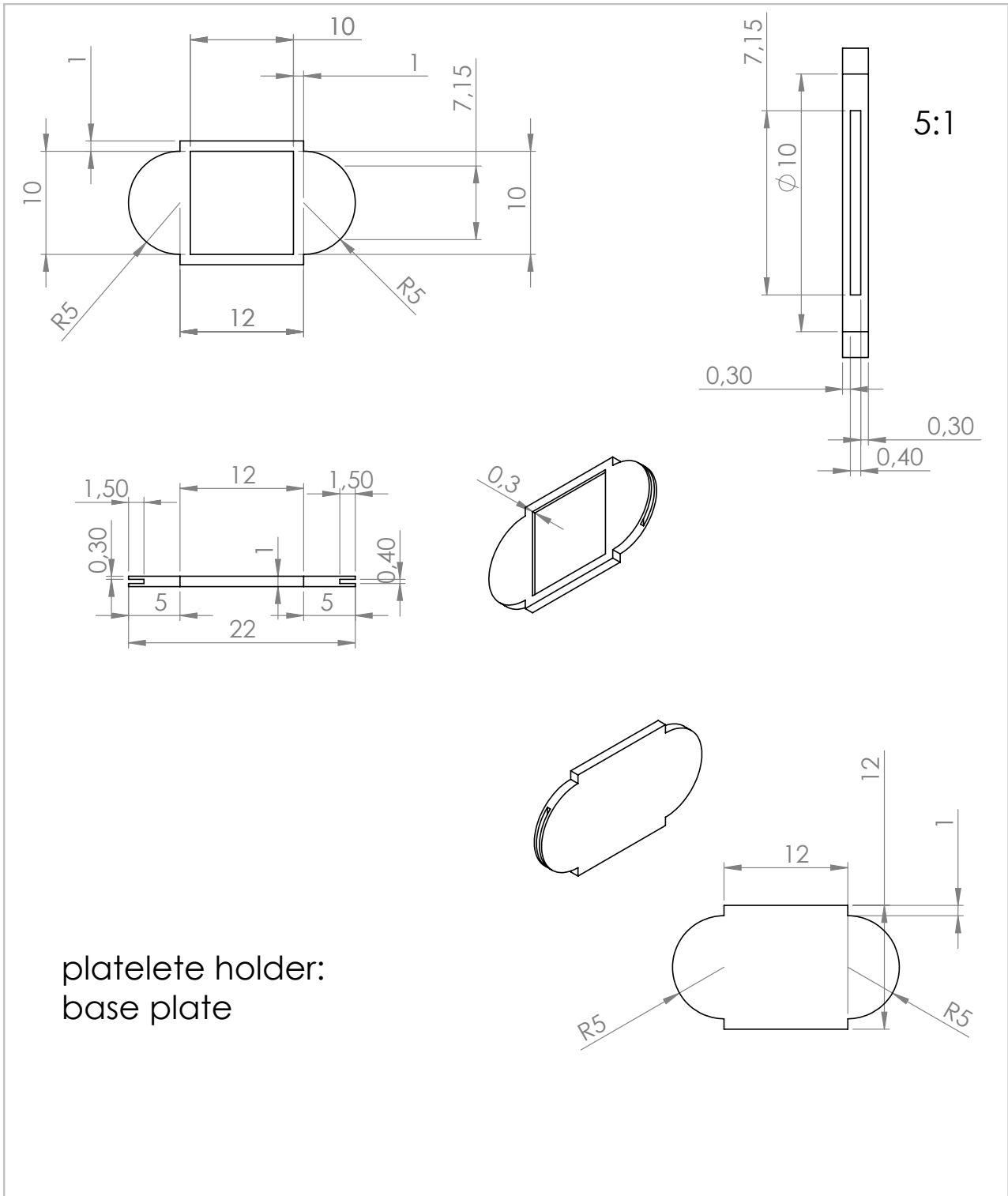
B. Contributions to the Publications

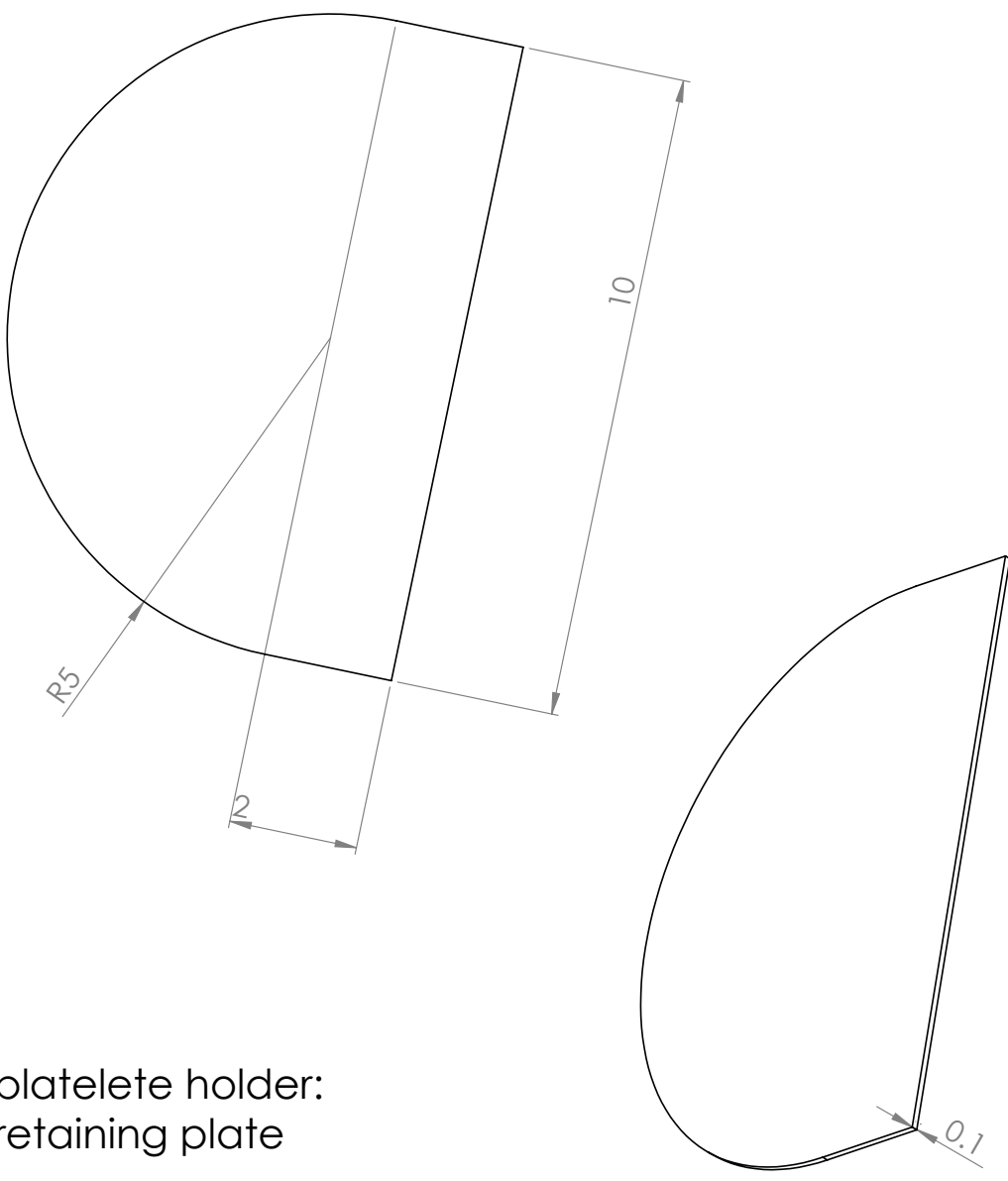
Table B.1 Overview of the contributions of Ph.D. candidate S. L. Kollmannsberger to the publications (\dagger = equally contributing as first author)

| Publication | Reference | Contribution |
|---|---|---|
| Ethanol photocatalysis on rutile TiO ₂ (110): the role of defects and water | C. A. Walenta, \dagger S. L. Kollmannsberger , \dagger J. Kiermaier, A. Winbauer, M. Tschurl, U. Heiz <i>Phys. Chem. Chem. Phys.</i> , 2015 , <i>17</i> , 22809-22814 | Performance and evaluation of experiments in a team of two, preparation of figures, discussion and interpretation of results |
| Isomer-Selective Detection of Aromatic Molecules in Temperature-Programmed Desorption for Model Catalysis | A. Winbauer, S. L. Kollmannsberger , C. A. Walenta, P. Schreiber, J. Kiermaier, M. Tschurl, U. Heiz <i>Anal. Chem.</i> , 2016 , <i>88</i> , 5392-5397 | Preparation of experiments, performance of experiments in a team of three, discussion and interpretation of results |
| Doping-Dependent Adsorption and Photon-Stimulated Desorption of CO on GaN(0001) | S. L. Kollmannsberger , \dagger C. A. Walenta, \dagger A. Winnerl, S. Weiszer, R. N. Pereira, M. Tschurl, M. Stutzmann, U. Heiz <i>J. Phys. Chem. C</i> , 2017 , <i>121</i> , 8473-8479 | Performance of experiments in a team of two, evaluation of experiments, preparation of figures, discussion and interpretation of results, co-writing of manuscript and SI |
| Anhydrous Ethanol Dehydrogenation on Metal–Organic Chemical Vapor Deposition Grown GaN(0001) | C. A. Walenta, \dagger S. L. Kollmannsberger , \dagger R. N. Pereira, M. Tschurl, M. Stutzmann, U. Heiz <i>J. Phys. Chem. C</i> , 2017 , <i>121</i> , 16393-16398 | Performance of experiments in a team of two, evaluation of experiments, preparation of figures, discussion and interpretation of results |
| Ethanol surface chemistry on MBE-grown GaN(0001), GaO _x /GaN(0001), and Ga ₂ O ₃ ($\bar{2}01$) | S. L. Kollmannsberger , \dagger C. A. Walenta, \dagger A. Winnerl, F. Knoller, R. N. Pereira, M. Tschurl, M. Stutzmann, U. Heiz <i>J. Chem. Phys.</i> , 2017 , <i>147</i> , 124704 | Performance of experiments in a team of two, evaluation of experiments, preparation of figures, discussion and interpretation of results, writing of manuscript and SI |
| Photocatalytic selectivity switch to C–C scission: α -methyl ejection of tert-butanol on TiO ₂ (110) | C. A. Walenta, \dagger S. L. Kollmannsberger , \dagger C. Courtois, M. Tschurl, U. Heiz <i>Phys. Chem. Chem. Phys.</i> , 2018 , <i>20</i> , 7105-7111 | Discussion and interpretation of results, evaluation of experiments, preparation of figures |

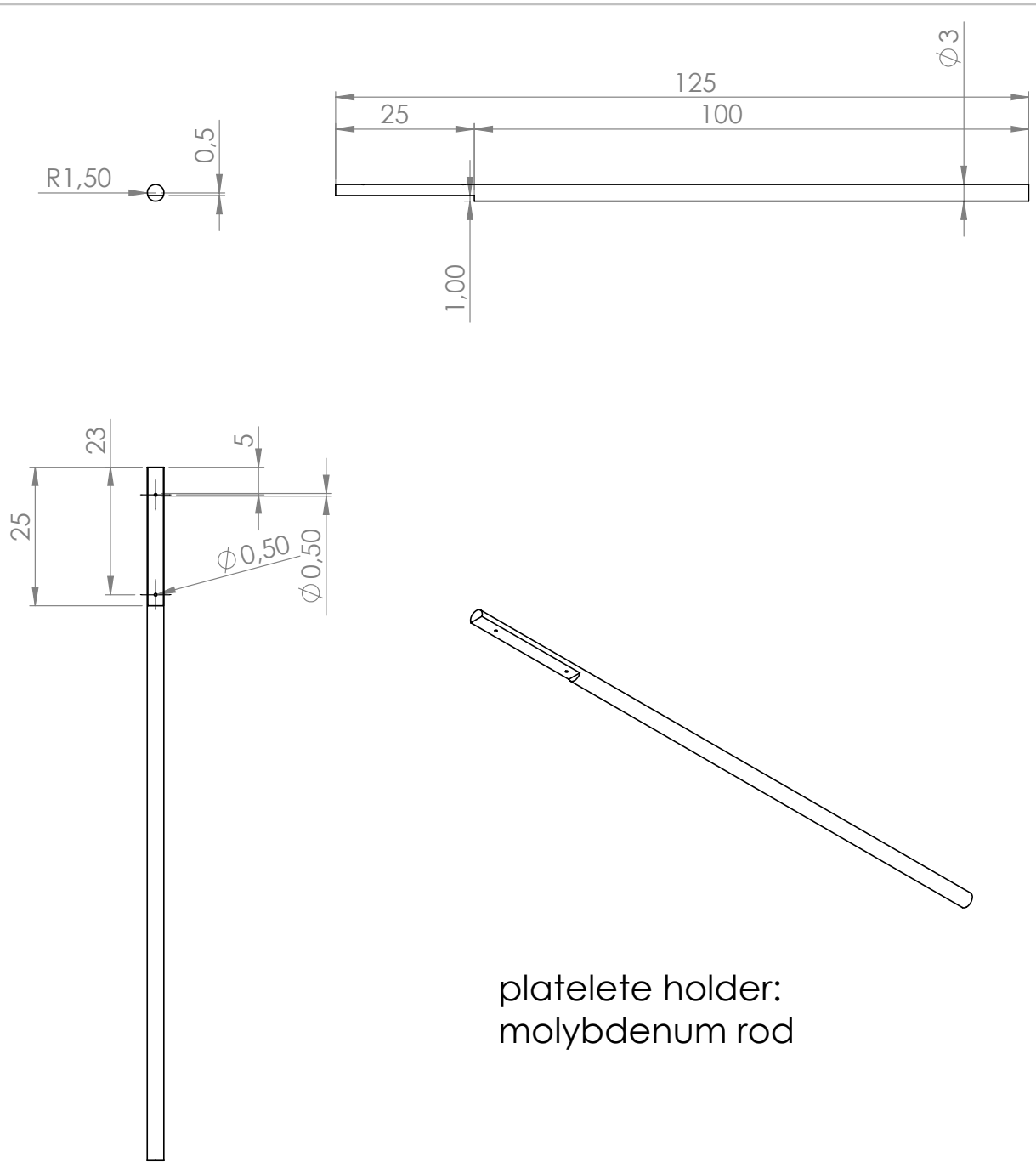
C. Technical drawings

C.1 Platelete holder



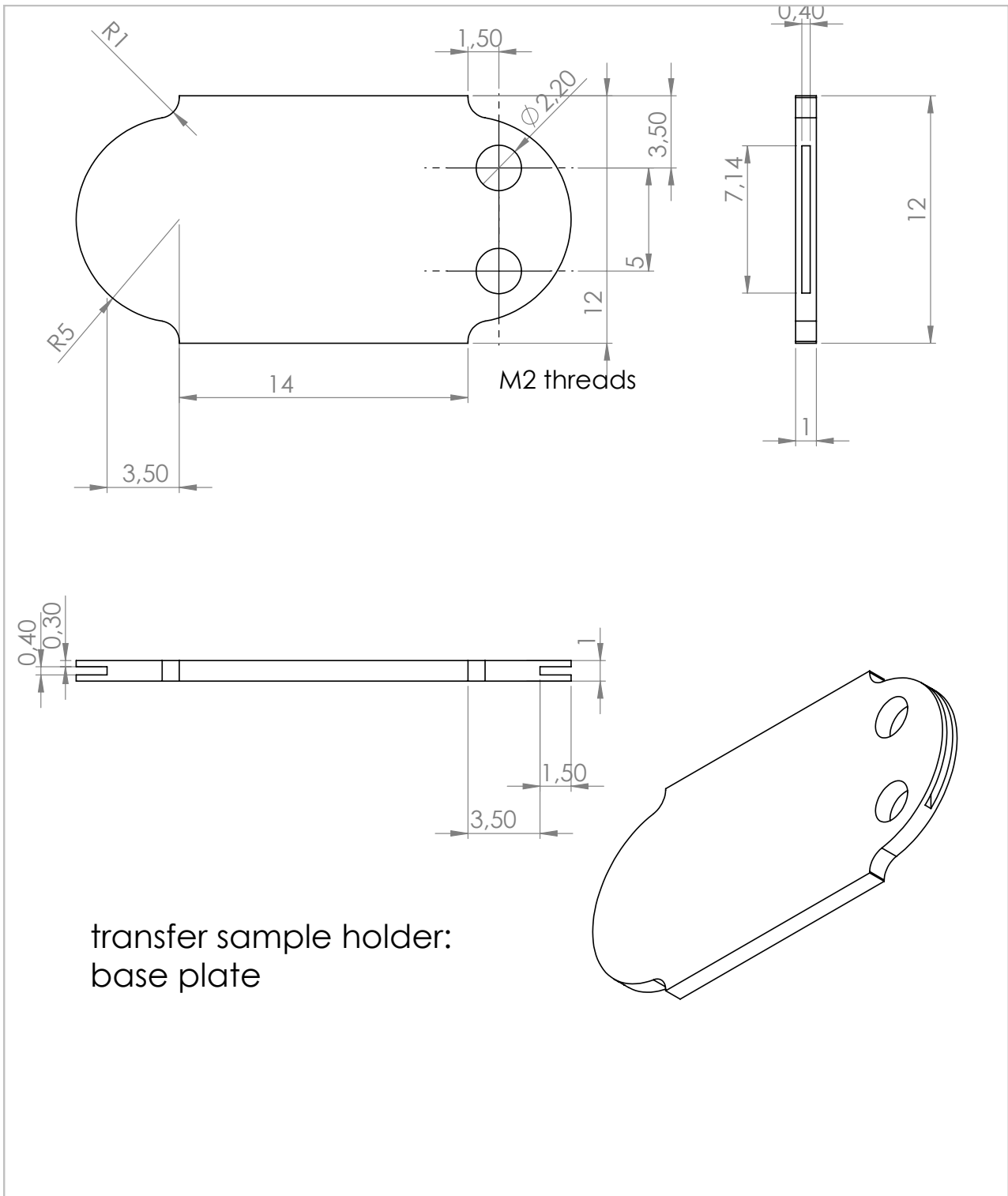


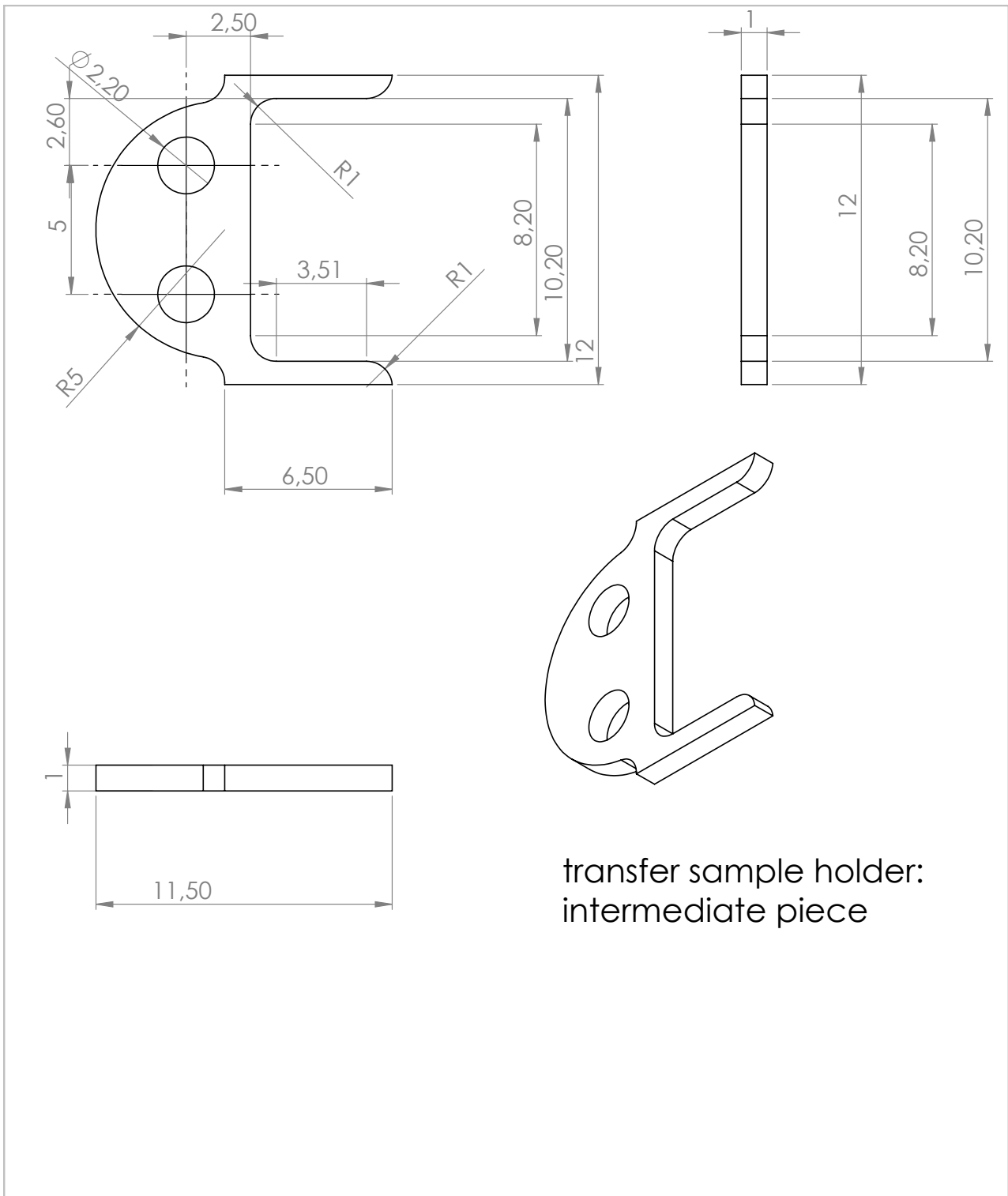
platelete holder:
retaining plate

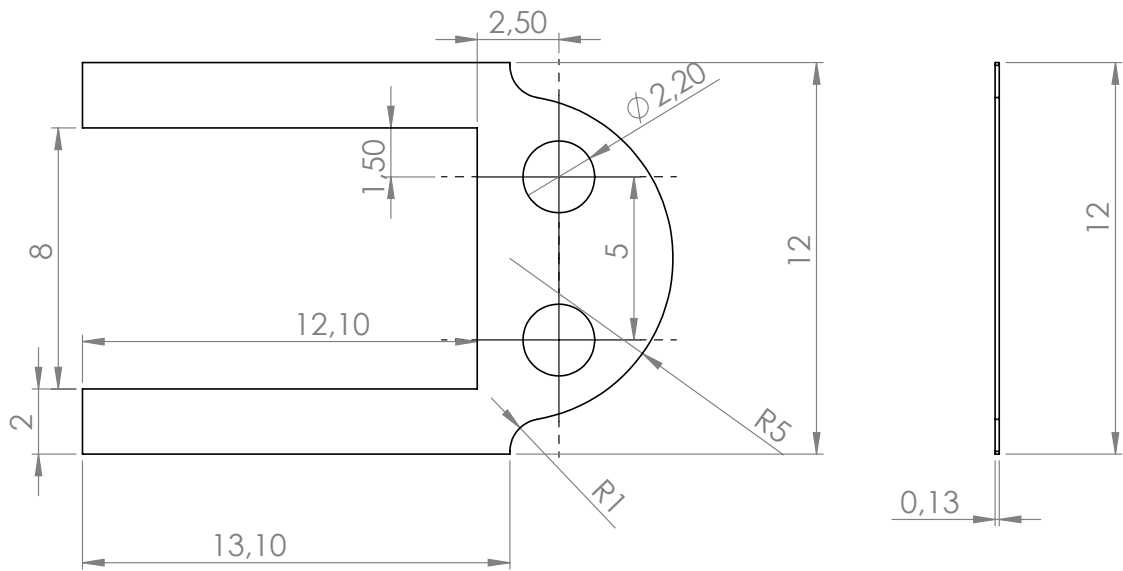


platelete holder:
molybdenum rod

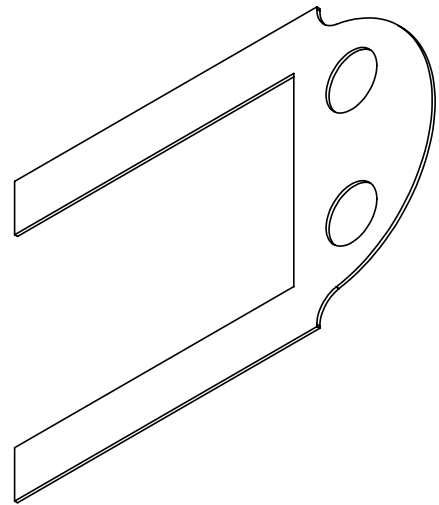
C.2 Transfer platelete holder

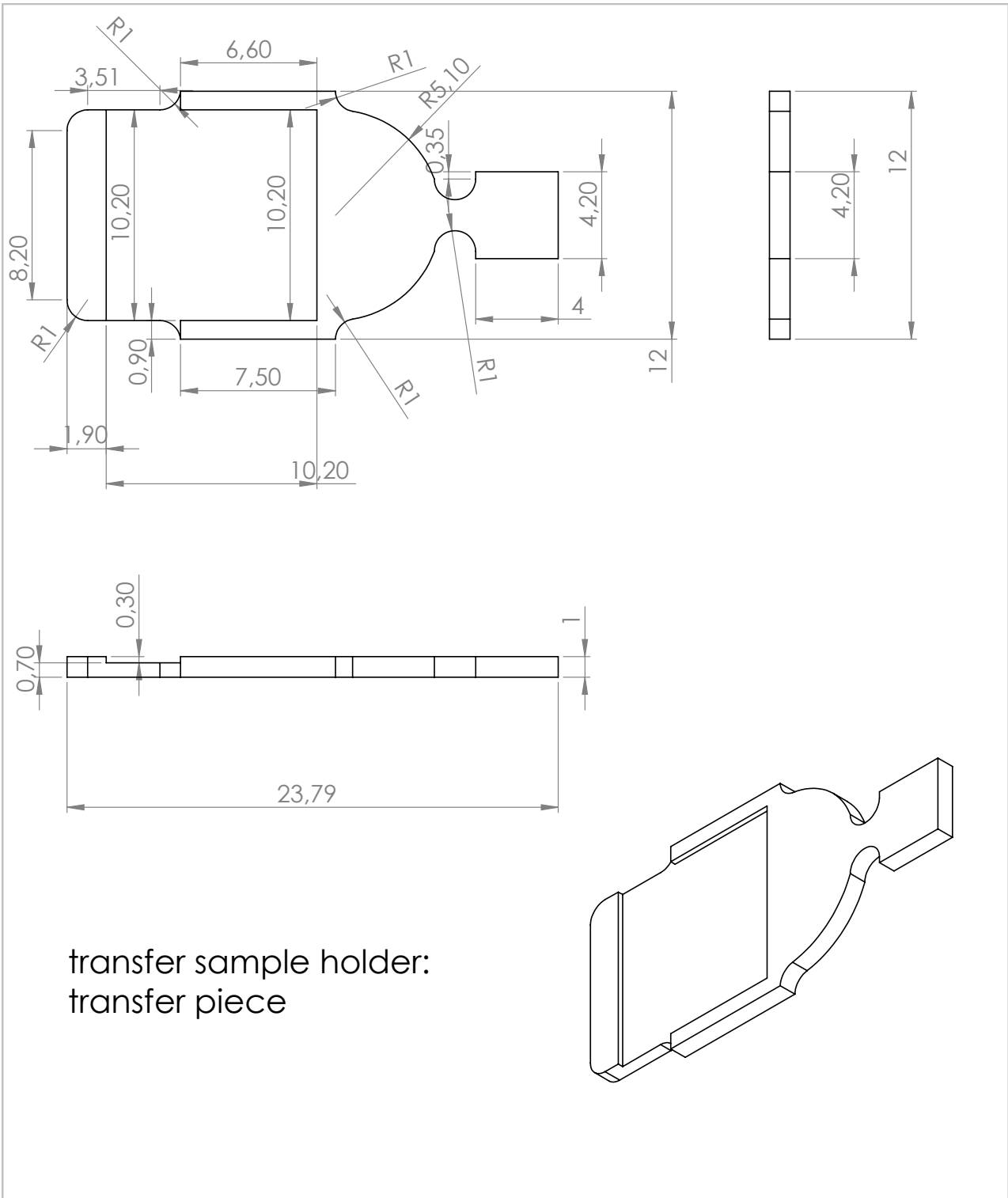


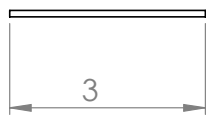
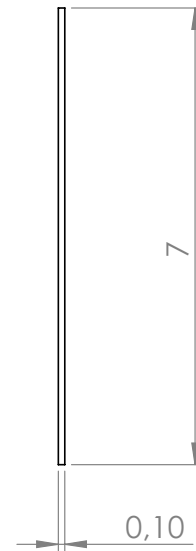
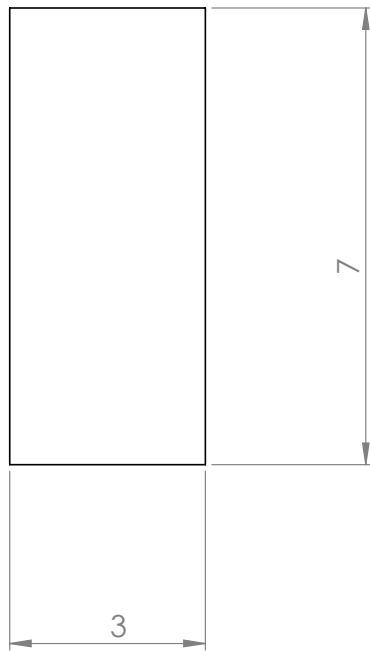




transfer sample holder:
retaining spring

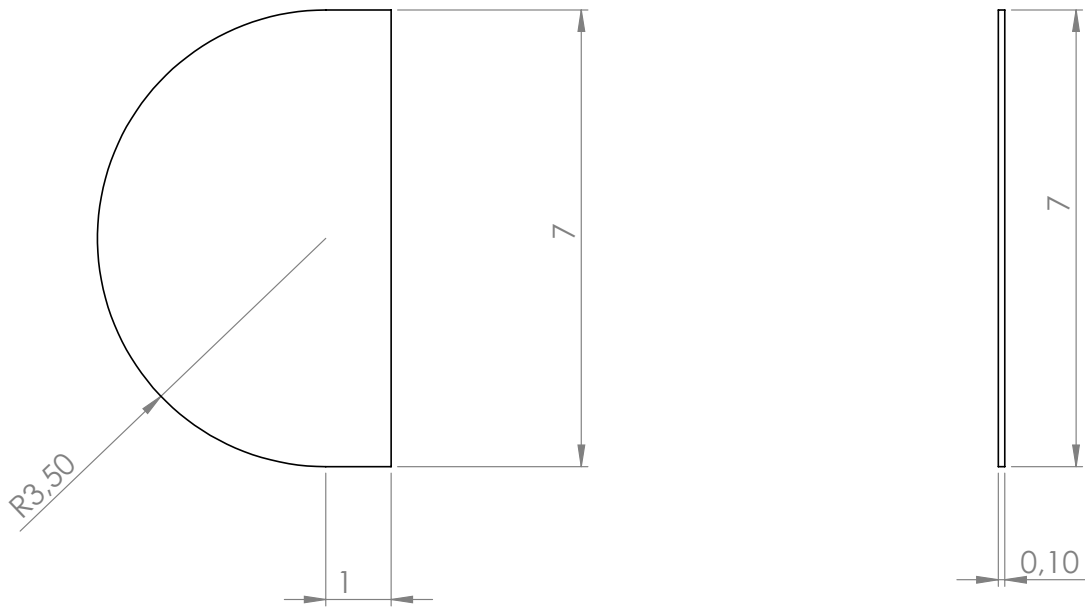




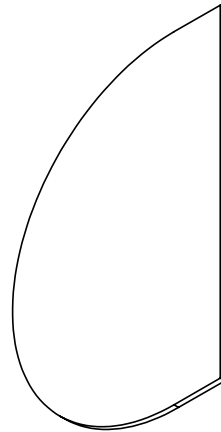


transfer sample holder:
retaining plate 1

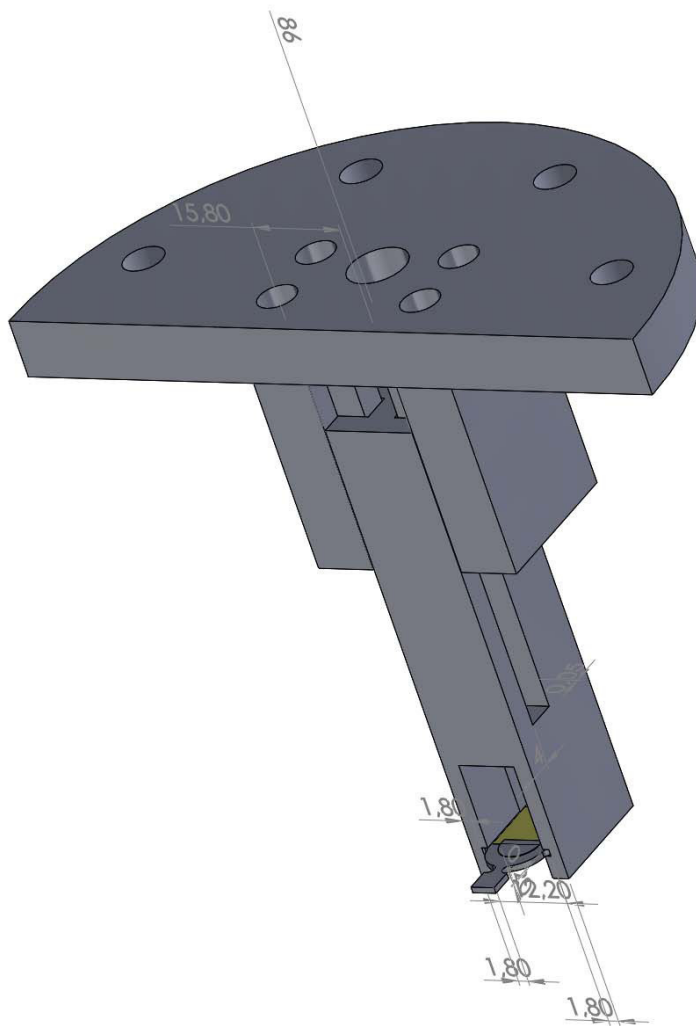


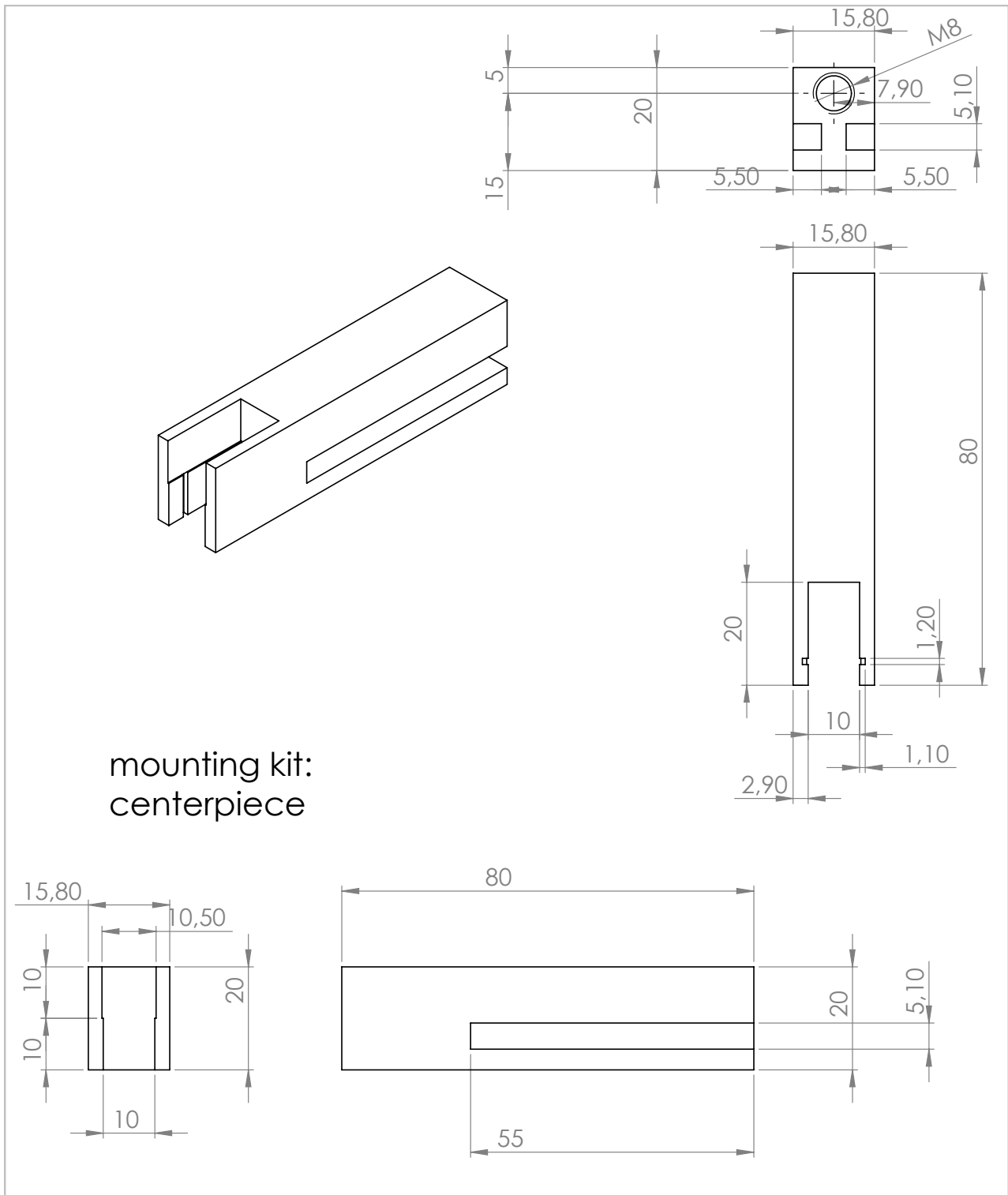


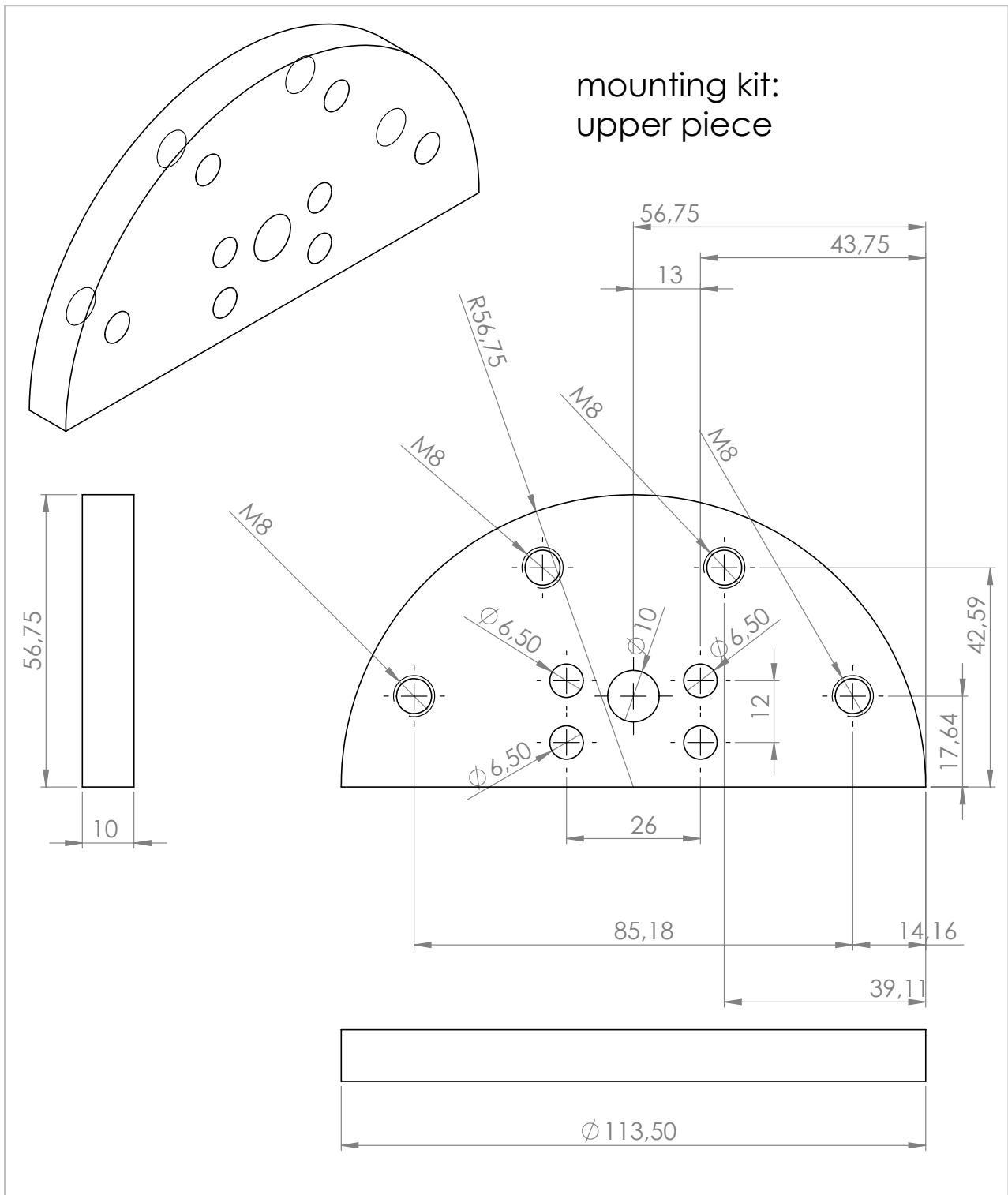
transfer sample holder:
retaining plate 2

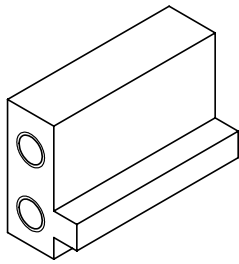


C.3 Mounting kit

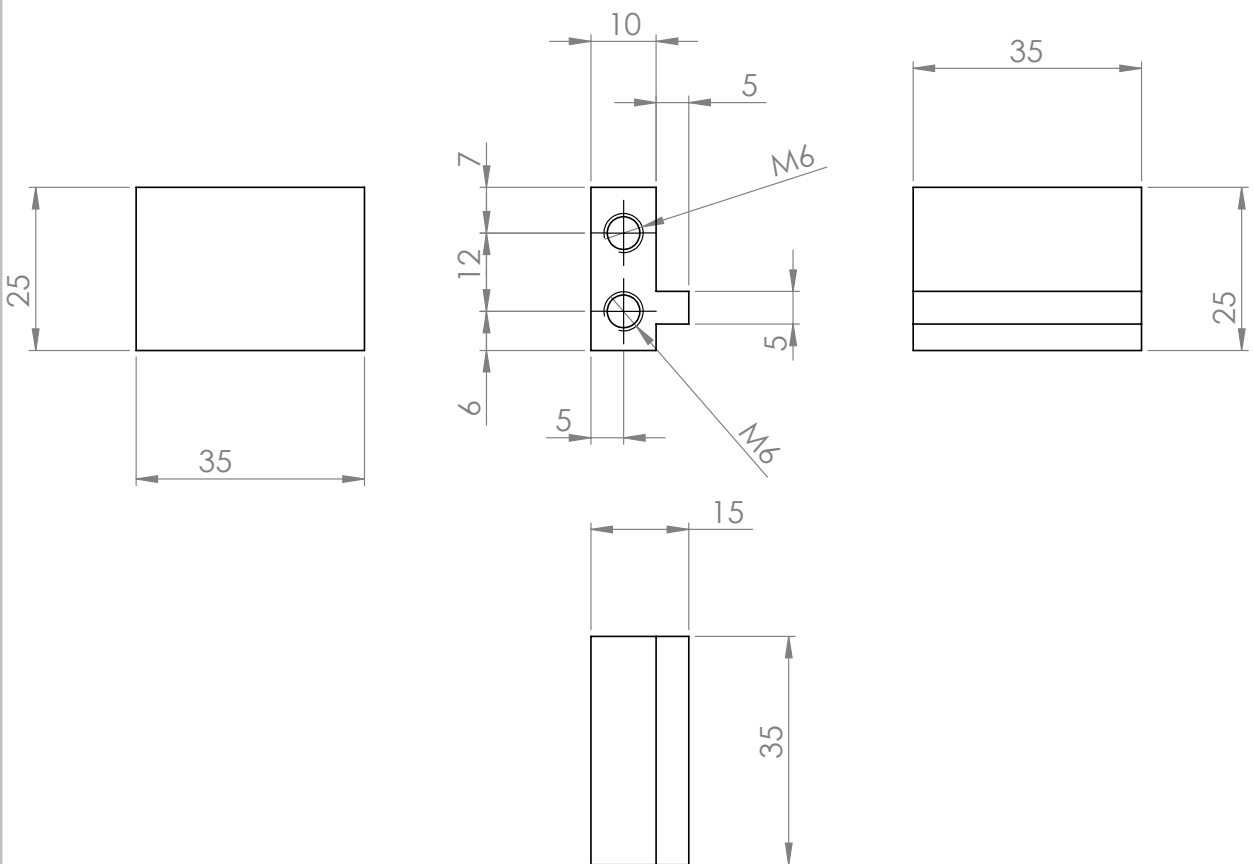




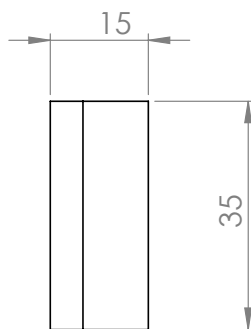
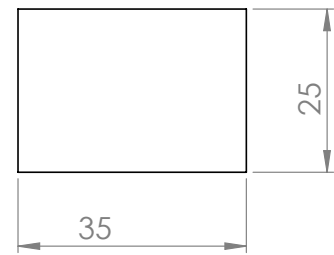
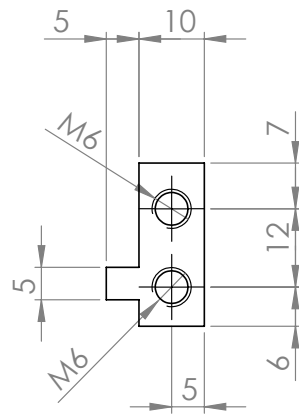
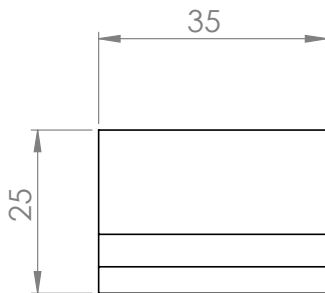
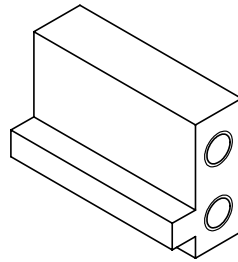




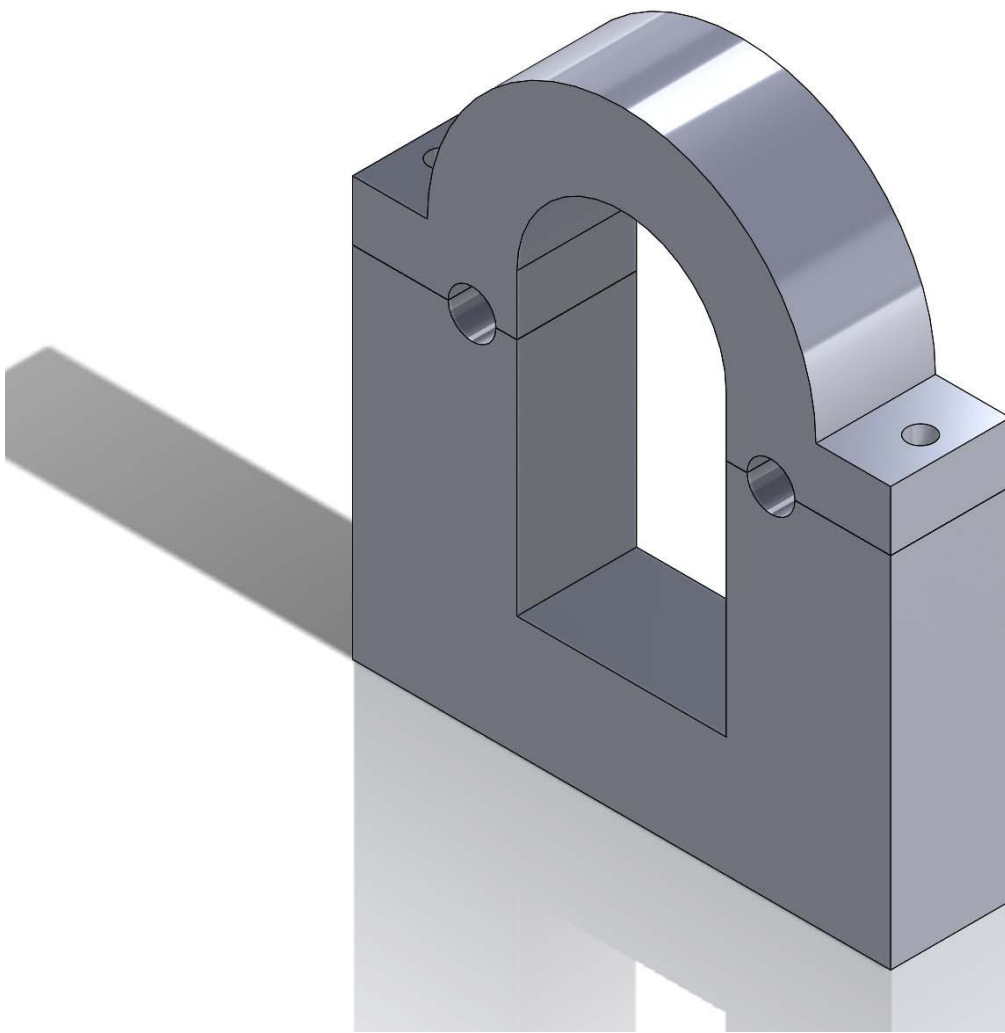
mounting kit:
left rail

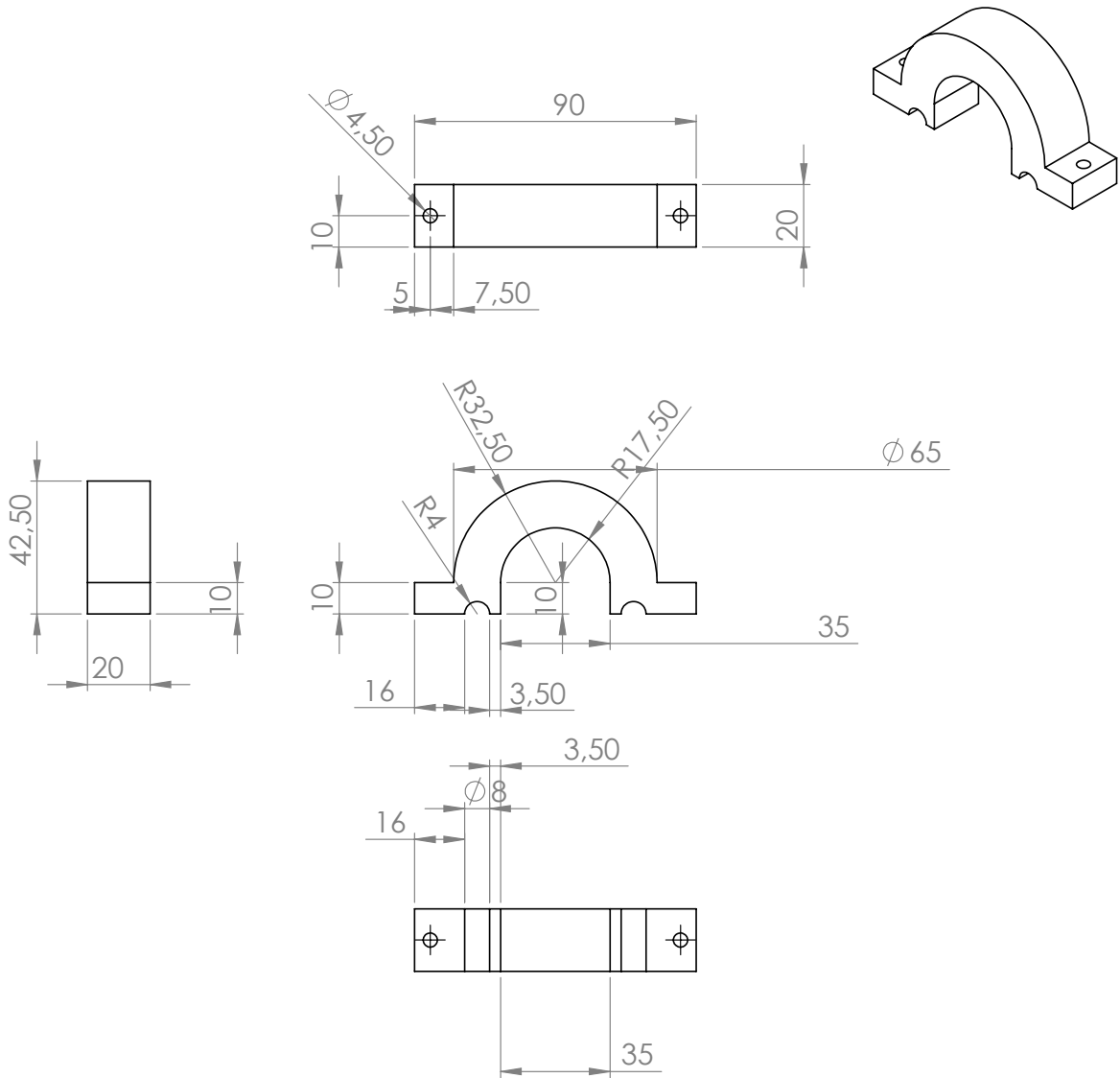


mounting kit:
right rail

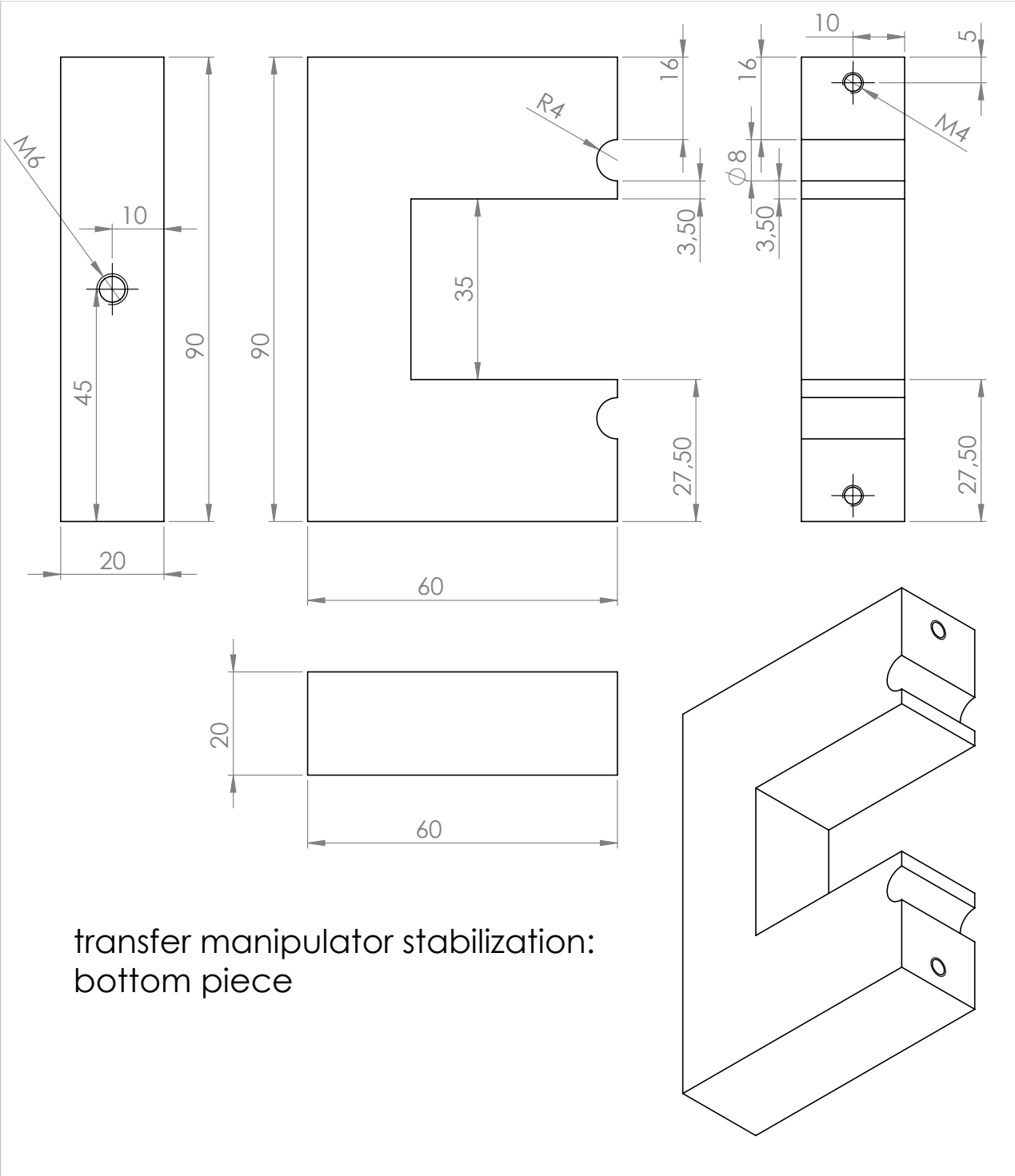


C.4 Transfer manipulator stabilization kit





transfer manipulator stabilization:
upper piece



transfer manipulator stabilization:
bottom piece

D. Publications

D.1. Ethanol photocatalysis on rutile TiO₂(110): the role of defects and water



PCCP

PAPER

View Article Online
View Journal | View IssueCite this: *Phys. Chem. Chem. Phys.*,
2015, 17, 22809

Ethanol photocatalysis on rutile TiO₂(110): the role of defects and water

Constantin A. Walenta,[†] Sebastian L. Kollmannsberger,[†] Josef Kiermaier,
Andreas Winbauer, Martin Tschurl and Ueli Heiz*

In this work we present a stoichiometric reaction mechanism for the photocatalytic ethanol oxidation on TiO₂(110). The reaction products are analyzed either under reaction conditions or after irradiation at lower temperatures. Water is identified as a quantitative by-product, which resides in a defect site. These water molecules cause a blocking of the defect sites which results in poisoning of the catalyst. By different preparation techniques of the TiO₂(110) surface, the role of surface defects is further elucidated and the role of molecular oxygen is investigated. Based on the investigation, a complete photochemical reaction mechanism is given, which provides insights into general photon driven oxidation mechanisms on TiO₂.

Received 19th June 2015,
Accepted 30th July 2015

DOI: 10.1039/c5cp03550c

www.rsc.org/pccp

Introduction

The thermodynamically stable rutile TiO₂(110) surface is among the most studied oxide model systems in surface science. Since the discovery of its photocatalytic activity, TiO₂ has become the most explored heterogeneous photocatalyst to date.^{1–5} While photocatalytic mechanisms of simple model reactions (as the CO-oxidation, or the O₂-photon stimulated desorption [PSD]) on the surface are well understood,^{6–9} the photochemical mechanisms of small organic molecules on bare TiO₂(110) remain unclear. For almost any reaction not even all reaction products have so far been identified.^{10–17} The understanding of the exact photocatalytic processes for such reactions will, however, be highly beneficial, since a fundamental understanding will allow for improvement of titania-based photocatalysts, in general. This is also the reason why the photochemistry of such systems has attracted considerable attention within the last few years.^{5,18,19} In this regard, ethanol is in particular of significant interest, because this molecule serves as a precursor for biomass fuels, due to its C–C bond.²⁰ Furthermore, its functional group makes ethanol a potential precursor for the green photocatalytic hydrogen production, especially since alcohols can be obtained as a renewable feedstock from biomass.^{21–23} Therefore, the elucidation of the ethanol chemistry on TiO₂ represents an important step towards the understanding of the H₂-production from renewable sources with light on metal-semiconductor hybrid materials.

Considering the reaction pathway, it is known that alcohols generally undergo a hole-mediated oxidation process on a rutile TiO₂(110) surface.^{5,8,10,11,16} Idriss and coworkers observed the photoreaction of ethanol to acetaldehyde with a strong dependency on the oxygen pressure on an oxygen covered surface. In a more recent study, however, Yang and co-workers have reported a photo-oxidation of ethanol under exclusion of oxygen, focussing on its photocatalyzed dissociation.²⁴ For adsorbed propanol, analogous production of propanal was observed and a similar dependence on the O₂ concentration was found as well.^{10,25} The group of Henderson reported the oxidation of methanol to formaldehyde on a defect-rich crystal surface in the absence of any O₂ and determined the surface-bound methoxy as the active reactant.^{16,26} Consecutive photocatalyzed coupling reactions have also been reported in the literature.^{27,28}

All studies up to date have only investigated the main photo-product and postulated mechanisms based on plausible assumptions. Thus, the stoichiometric reaction equations have been made without the analysis of any by-products and unknown charge states. For the total reaction pathway, the role of defects in the reaction still remains unclear, especially when oxygen is added as a reactant. In this work stoichiometric mechanisms for the photochemistry of ethanol on rutile TiO₂ are presented. The mechanisms unravel the role of oxygen and surface defects and are supported by studies based on different preparation conditions for the titania crystal and on the analysis of water as one of the main products of the photoreaction.

Experimental

All experiments were carried out in a home built ultra-high vacuum setup as seen in Fig. 1 with a base pressure of

Chair of Physical Chemistry, Department of Chemistry and Catalysis Research Center, Technische Universität München, Lichtenbergstrasse 4, 85748 Garching, Germany. E-mail: ulrich.heiz@mytum.de; Fax: +49 (0)89 289 13389; Tel: +49 (0)89 289 13391

[†] Contributed equally to this work.



Paper

View Article Online

PCCP

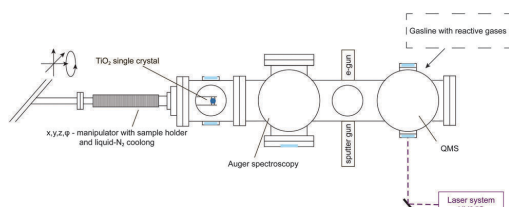


Fig. 1 Overview of the apparatus including methods for surface characterization and preparation as well as product analysis.

8.0×10^{-11} mbar. Briefly, it consists of a liquid-N₂ cooled, x, y, z, ϕ -manipulator (VAB Vakuum GmbH), an Auger Spectrometer (CMA 100, Omicron Nanotechnology GmbH), a sputter gun (IQE 11/35, SPECS GmbH), a QMS (QMA 430, Pfeiffer Vacuum GmbH), leak valves (Pfeiffer Vacuum GmbH), a home-built gasoline (base pressure of 5.0×10^{-9} mbar) and an e-gun of in-house design.

The rutile TiO₂(110) crystal was purchased from Surface-net GmbH and is of cylindrical shape with a diameter of 10 mm and a thickness of 2 mm. At two sides of the crystal symmetrical grooves were cut for mounting the crystal on a 1 mm thick tantalum plate. The interface between the metal and the single crystal is covered with a thin (0.025 mm) gold foil to ensure good thermal conductivity. The heating of the crystal was performed indirectly *via* resistive heating of two tungsten wires (0.38 mm in diameter), which were fixed on the sides of the tantalum holder. For the photochemical measurement, the sample holder was cooled by contact to a reservoir of liquid nitrogen to achieve temperatures of around 100 K. The temperature of the crystal was controlled by the calibrated readout of a twisted type-C thermocouple,²⁹ which was inserted into a hole located on the side of the rutile single crystal without any adhesive. Crystal cleaning was done by repeated cycles of Ar⁺-sputtering, oxygen annealing and vacuum annealing and confirmed by AES. With this procedure a reduced, dark blue, conductive crystal was obtained which has a constant surface defect density of usually 10 to 15%.^{3,30,31}

Ethanol (absolute, HPLC grade, $\geq 99.8\%$, Sigma-Aldrich) was purified by pump-thaw cycles and flushing cycles of the gasoline prior to use. Purity was confirmed by chamber back-filling and analysis with the QMS. The ethanol dosage was performed at a crystal temperature below 150 K and TPD experiments were conducted by heating the crystal with 1.2 K s^{-1} to 700 K. For the photochemical measurements a Nd:YAG-pumped (Spectra GCR 4, ~ 10 ns pulse length) dye laser (Lambda Physics) with a wavelength of 266.5 nm is used to excite electron-hole pairs. The laser spot lights the entire single crystal plane and the intensity was chosen with a pulse energy of 600 μJ per pulse, so no laser induced thermal heating effects were observed. Mass signals in the QMS of thermal and photochemically desorbing species were identified by cracking pattern analysis and were corrected by the different ionization sensitivities.

Results

For the elucidation of the mechanisms for the photocatalytic ethanol oxidation reaction, different desorption experiments were performed. The temperature programmed desorption (TPD) spectrum of 1 L of pure ethanol in the absence of UV light is shown in Fig. 2a. From the fragmentation pattern analysis, the traces were assigned to species. The trace ($m/z = 31$) corresponds to the main fragment of ethanol and ($m/z = 29$) to that of acetaldehyde. For the latter, it has to be taken into account that this mass appears in the main fragmentation pattern of ethanol as well. The TPD spectra of the pure alcohol have already been extensively discussed in the literature.^{32–34} In general agreement, it is found that the majority of ethanol molecules desorb at temperatures below 300 K and, besides other features,

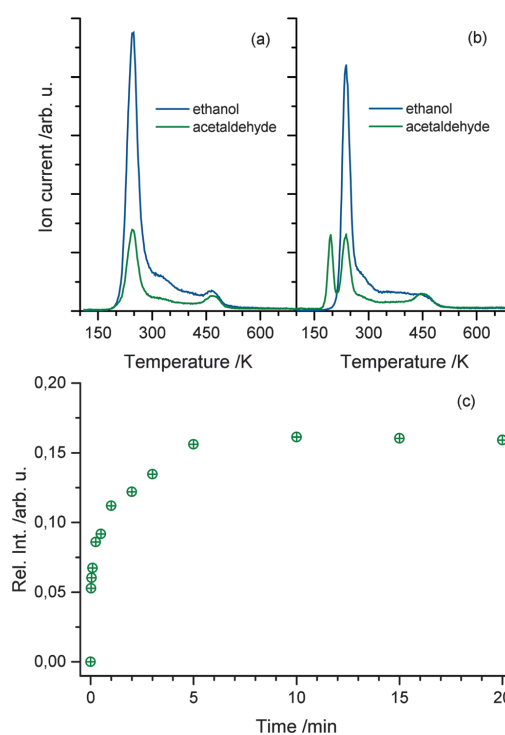


Fig. 2 (a) The thermal desorption mass signal of acetaldehyde and ethanol without photoexcitation. Note that the trace assigned to acetaldehyde is a fragment of either ethanol or acetaldehyde. Due to the constant ratio of both traces, the origin of the first peak is assigned to ethanol desorption, while acetaldehyde production only occurs at temperatures above 400 K. (b) The thermal desorption mass signal of acetaldehyde and ethanol after 10 min of UV excitation at 110 K. The consecutive TPD run shows another feature at 195 K, resulting from molecular acetaldehyde. (c) The integral over acetaldehyde production normalized to the overall ethanol dosage. The signal shows a rapid rise in acetaldehyde production within 1 s of photoexcitation and a saturation of acetaldehyde is found after 5 min of photoexcitation.



View Article Online

PCCP

Paper

another distinct peak above 400 K occurs. The trace representing acetaldehyde follows the same trend, but is proportionally lower in intensity. This trend only deviates at higher temperatures indicating that the signal only originates from the fragmentation pattern of ethanol with the exception of temperatures above 400 K, where also ethene is produced from dehydration.^{32–34}

Upon irradiation of photons with energies above the band gap, another feature at 195 K appears in the spectrum depicted in Fig. 2b. This peak can solely be assigned to acetaldehyde, because no desorption of ethanol is observed at this temperature. This clearly shows that in the absence of O₂, photo-excitation at 110 K results in the accumulation of acetaldehyde at the surface. In agreement with the literature for highly covered crystal surfaces, the desorption of acetaldehyde occurs at lower temperature due to the repulsive interactions of the molecule with ethanol and other surface species.^{13,24} In contrast to the study of Idriss and coworkers performed at 300 K¹² and in agreement with Yang and co-workers,²⁴ oxygen dosing is not a prerequisite for a substantial yield in the ethanol photooxidation at lower temperatures. The amount of acetaldehyde produced is strongly dependent on the illumination time. Fig. 2c shows the integrated mass signal of acetaldehyde trace normalized to the ethanol coverage *versus* illumination time at 110 K. A rapid rise with the photoexcitation is observed, which results in saturation at about 15% with respect to ethanol after 5 min.

Since the desorption of acetaldehyde takes place at lower temperatures than that of ethanol, the photochemical reaction can be monitored *in situ*. Fig. 3a demonstrates the formation and the direct desorption of the aldehyde under UV illumination at 222 K, which is well below the desorption temperature of the alcohol. Since this method enables the recording of any product that leaves the surface at this temperature, the H₂ mass can also be monitored. However, only a small change in the

signal with UV excitation is seen, which is rather attributed to cracking in the QMS than to the production of molecular hydrogen during reaction. Furthermore, no ethanol desorption is observed as is expected at this temperature. As seen in Fig. 3b the integral of the photoproduct matches the amount of acetaldehyde produced at cold temperatures (Fig. 2c), showing that the reaction is charge carrier driven and desorption only occurs *via* a thermal process. After another dosage of ethanol at lower temperatures and subsequent irradiation at 222 K, a strong decrease in the acetaldehyde production is observed. The photochemical yield gets even lower for all successive dosage cycles, which hints to a deactivation mechanism of the catalyst. However, after ramping up the temperature to about 500 K, the activity of the catalyst can be completely restored.

While no significant H₂ production is found in the photo-reaction, it is observed that water molecules (*m/z* = 18) are leaving the surface in the TPD experiments in good agreement to Yang and co-workers.²⁴ However, such water molecules may either originate from the photochemical reaction or the co-adsorption of residual water molecules from ethanol dosage. Thus, Fig. 4 shows a comparison of the H₂O trace of 1 L ethanol after 5 min UV illumination (a) and after the same time in the dark (b), to enable the discrimination between water formed by the photoreaction and water from co-adsorption. In both cases, an identical feature at 210 K is found, which can be attributed to H₂O desorbing from O-bridge atoms of the semiconductor. However, in the case of the photoexcitation (Fig. 4a) another distinct feature between 280 K and 400 K occurs, which is assigned to water coordinated on Ti⁴⁺-sites in the TiO₂ lattice.³⁴ Fig. 4c demonstrates that the integral of the peak from these Ti sites *versus* time shows a similar behavior to the acetaldehyde formation (Fig. 2c). Thus, the production of water in this defect sites is clearly associated with the photochemical process and is identified as a quantitative by-product of the photoreaction.

To elucidate the role of defects in the reaction in more detail, a surface defect-free crystal is produced by annealing the crystal in oxygen at 300 K.^{35,36} The absence of any photon stimulated desorption (PSD) of O₂ indicated that no O₂-species is bonded to remaining defect sites.^{2,35,37} The resulting TPD after 1 min of photoexcitation (Fig. 5) shows a slight shift of 30 K to higher temperatures for the ethanol desorption in comparison to the desorption from a defect-rich TiO₂(110) surface. A similar behavior is observed for the desorption of acetaldehyde, which is in good agreement with the literature for molecular acetaldehyde.¹³ In contrast to the defect-rich surface, only the H₂O desorbing from bridging O-atoms is observed. Although the photoreaction of ethanol takes place, a higher temperature signal of H₂O as on the defect rich surface is not observed. This further demonstrates that the surface of the crystal is indeed defect free. The integral for the peak of 210 K significantly exceeds the one in Fig. 4a, which shows that water is again formed during the photoreaction. In addition, the total amount of H₂O desorbing from the surface after the same time of illumination is similar for both surfaces, the defect-free and the defect-rich ones.

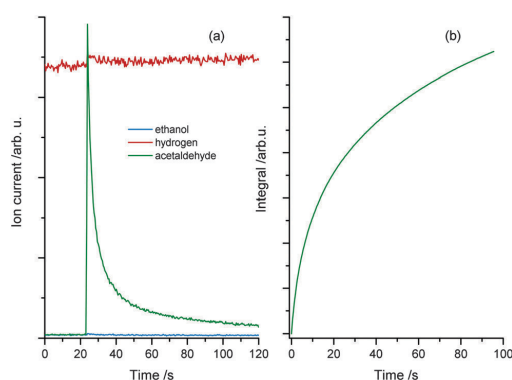


Fig. 3 (a) Isothermal photoreaction at 222 K. Prior to reaction, 1 L ethanol is dosed at a temperature of 120 K. UV excitation starts at 23 seconds and an immediate increase in acetaldehyde production is observed, while the ethanol trace remains unchanged. Note that the slight change in the molecular hydrogen trace is attributed to cracking in the QMS rather than to the production of H₂. Part (b) shows the integrated mass signal of figure (a), which shows the same trend as Fig. 2(c).



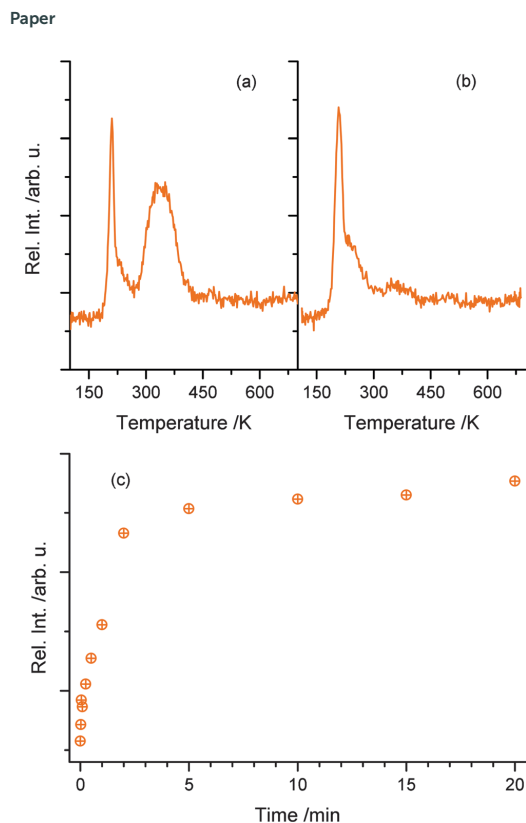
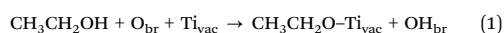


Fig. 4 The upper parts (a) and (b) show the water mass traces in TPD experiments of 1 L ethanol after 5 min of photoexcitation (a) and 5 min of waiting without photoexcitation (b). In both cases, a sharp feature of water at 210 K is observed. However, only with UV illumination, a high temperature feature between 290 K and 420 K occurs, which demonstrates that water is formed during the photoreaction. Part (c) shows the integral of high temperature water in dependence of the photoexcitation time probed by TPD. Similar to Fig. 2(c), a rapid rise occurs with a saturation at a UV-excitation time of 5 min.

Discussion

Defect rich surface

Based on our findings and the existing studies in the literature, we propose the mechanism illustrated in Fig. 6 for the photochemical reaction on rutile. It is widely accepted that ethanol adsorbs preferentially in a dissociative way on rutile TiO₂(110) and always dissociatively in an oxygen vacancy.^{22,38,39} Thus, in the defect a chemical reaction according to eqn (1) takes place, which results in the formation of an ethoxy species and a protonated O_{br}.



When the semiconductor is irradiated by photons with energies above the band gap electron hole pairs are created (eqn (2)).

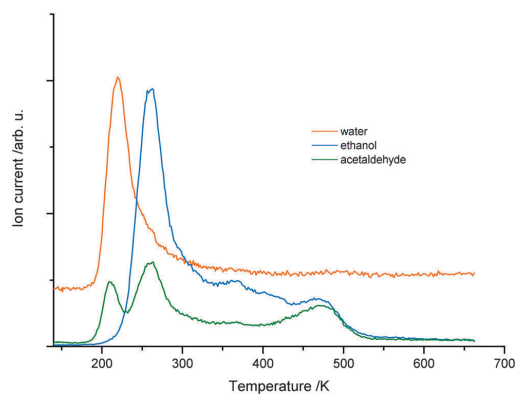
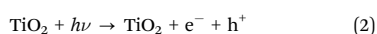


Fig. 5 TPD after 1 min of UV excitation at 130 K for 1 L ethanol on a surface-oxidized crystal. On this surface the desorption features of the monitored species are observed at slightly higher temperatures. After the photoreaction, the production of acetaldehyde is found again. The water trace, however, shows only a more intense feature at around 225 K and no high temperature signal occurs.

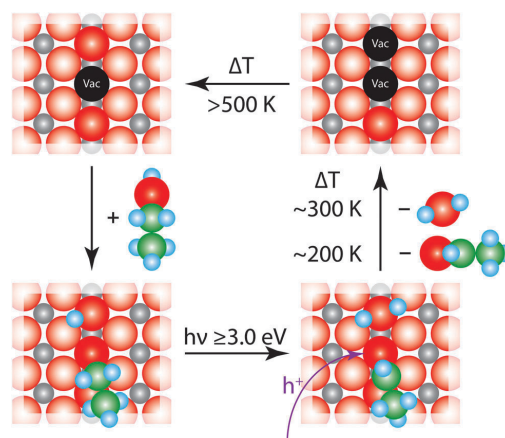


Fig. 6 Photochemical reaction mechanism of ethanol on a defect-rich TiO₂(110) surface. The figure illustrates four different reaction steps. After the dissociative ethanol adsorption, an ethoxy and a neighboring surface hydroxyl are formed. Under UV-illumination, charge carriers are generated in the semiconductor and the photoholes travel to the surface. There they react with ethanol under α -H-abstraction to give acetaldehyde and water; the latter is in equilibrium with two surface hydroxyl groups. When the crystal is heated to elevated temperatures, the reaction products are desorbing at the corresponding temperatures and formally two oxygen vacancies remain. The surface is eventually reoxidized by bulk diffusion leading to a similar surface-defect density as before the photoreaction. (The grey balls resemble the Ti atoms and the red ones O atoms. The intense colored red balls indicate bridging oxygen atoms in the rows of the TiO₂(110) surface. Shown in black are vacancies in those bridging atoms, also referred to as surface defect. Green balls are associated with C atoms and light blue resemble H atoms.)

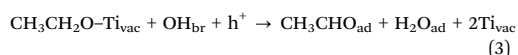
Depending on the type of photochemical reaction, either electrons or holes govern the yield in the surface chemistry.^{8,37,40,41}

View Article Online

PCCP

Paper

The oxidation of alcohols is a hole mediated process.^{10,12,16,42} It can be described by eqn (3), in which a formal h⁺ reacts with the partly negatively charged ethoxy species, which undergoes an α-H elimination.



The resulting acetaldehyde is still bound on the surface *via* the oxygen atom,⁴³ and can desorb at 195 K. The abstracted hydrogen either moves to the neighboring hydroxyl group to form water or results in the formation of another intermediate hydroxyl species, which eventually reacts to water and a bridging oxygen atom.⁴⁴ In both cases, water molecules in an oxygen vacancy are produced, which block the defect and deactivate the catalyst. This mechanism fully supports the observed surface chemistry. The amount of water desorbing from defect sites shows a similar behavior to the formation of acetaldehyde (Fig. 2c and 4c). The reaction saturates, when all the surface defects are blocked by the reaction products. This is supported by studies for alcohols, where no diffusion effects have been reported at cryogenic temperatures below 200 K.^{45,46} In addition, it is observed that the amount for acetaldehyde saturation lies in the range of the density of defect states on the surface. At a temperature around 200 K the aldehyde is leaving the surface site. However, water molecules, which are in equilibrium with two hydroxyl species,⁴⁷ still reside in the defects and cause a deactivation of the catalyst. This deactivation is observed after the consecutive dosing of ethanol after the photoreaction. If the water is eventually thermally removed above 450 K, the trap sites are accessible again. In addition, it is also well known that the surface is reoxidized from the bulk at these temperatures, so that the same percentage of surface defects is reobtained.^{30,48} Site blocking of the oxygen vacancies by the water molecule formed is also indicated by the absence of PSD of O₂ even after the thermal removal of ethanol and acetaldehyde and the subsequent dosage of oxygen at low temperatures. Furthermore, it should be noted that no coking is observed, as the Auger spectra did not reveal transitions for carbon, even for temperatures of up to 800 K.

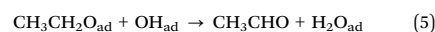
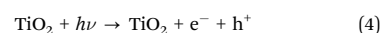
The role of defects in the photochemical reaction is also in good agreement with the fact that the defects such as oxygen vacancies lead to a stabilization of negative charges at the surface, which further results in an upward band bending in the semiconductor.^{41,42} This causes a preferential movement of photoholes to the defects, while the electrons travel into the bulk.⁴¹

Similar reaction and saturation behavior has been reported previously for methanol¹⁶ and 2-propanol¹⁰ and are a strong indication that the proposed mechanism may play an important role even in the photochemistry of other alcohols.

Oxidized surface

Fig. 5 demonstrates that the photooxidation of ethanol can also be performed at the surface of an oxidized crystal. Due to the absence of oxygen vacancies, which is also reflected in the

absence of any water desorption between 290 K and 420 K, another reaction pathway must be responsible for the acetaldehyde formation on this surface. In this respect, it is well established that dosing of O₂ at 300 K results in the formation of dissociated O_{ad}-atoms, which fill the vacancies and populate the surface.^{36,48,49}



Instead of filling vacancies, ethanol adsorbs on the oxide surface and dissociates, resulting in the ethoxy species and an adsorbed hydroxyl species. After the light-induced creation of electron hole pairs, photoholes initiate the formation of acetaldehyde. The reaction takes place *via* the abstraction of an α-hydrogen atom of the ethanol and water is formed at the surface, eqn (5). This is supported by the increase in the water desorption at around 225 K. A similar desorption temperature is found for water that is bound molecularly to a bridging oxygen atom.³⁴

Conclusion

In summary, we propose a stoichiometric reaction mechanism for the illumination-dependent photochemical oxidation of ethanol to acetaldehyde on TiO₂(110) surfaces. The mechanism explicitly addresses the role of surface defects (such as oxygen vacancies) and the role of water as a by-product of the reaction. With this mechanism the experimental observations of the role of oxygen in surface preparation and deactivation as well as saturation of the reaction can be explained. This is facilitated by two different experimental methods. The first one uses TPD as a probe for the accumulation of photo-products at cold temperatures and the second one investigates the photoreaction at elevated temperatures above the desorption temperature of the photo-product. Our mechanism can not only be extended to other alcohols of different chemical structures, but may even supply potential reaction pathways for metal particle loaded semiconductor systems.

Acknowledgements

The authors thank the DFG (HE3435/22-1), the ERC under grant ERC-2009-AdG 246645-ASC3 and the BMBF through IC⁴ for financial support. C.A.W. thanks the Nano Initiative Munich (NIM) for support.

References

- 1 A. Fujishima and K. Honda, *Nature*, 1972, **238**, 37–38.
- 2 A. L. Linsebigler, G. Lu and J. T. Yates, *Chem. Rev.*, 1995, **95**, 735–758.
- 3 U. Diebold, *Surf. Sci. Rep.*, 2003, **48**, 53–229.
- 4 A. Fujishima, X. Zhang and D. A. Tryk, *Surf. Sci. Rep.*, 2008, **63**, 515–582.
- 5 M. A. Henderson, *Surf. Sci. Rep.*, 2011, **66**, 185–297.



[View Article Online](#)

Paper

PCCP

- 6 A. Linsebigler, G. Lu and J. T. Yates, *J. Phys. Chem.*, 1996, **100**, 6631–6636.
- 7 T. L. Thompson and J. T. Yates, *Chem. Rev.*, 2006, **106**, 4428–4453.
- 8 Z. Zhang and J. T. Yates, *J. Phys. Chem. Lett.*, 2010, **1**, 2185–2188.
- 9 N. G. Petrik and G. A. Kimmel, *J. Phys. Chem. Lett.*, 2010, **1**, 1758–1762.
- 10 D. Brinkley and T. Engel, *J. Phys. Chem. B*, 1998, **102**, 7596–7605.
- 11 P. M. Jayaweera, E. L. Quah and H. Idriss, *J. Phys. Chem. C*, 2007, **111**, 1764–1769.
- 12 A. M. Nadeem, J. M. R. Muir, K. A. Connelly, B. T. Adamson, B. J. Metson and H. Idriss, *Phys. Chem. Chem. Phys.*, 2011, **13**, 7637–7643.
- 13 R. Zehr and M. Henderson, *Surf. Sci.*, 2008, **602**, 2238–2249.
- 14 M. A. Henderson, *J. Phys. Chem. C*, 2013, **117**, 14113–14124.
- 15 M. A. Henderson, *J. Phys. Chem. C*, 2013, **117**, 23840–23847.
- 16 M. Shen and M. A. Henderson, *J. Phys. Chem. Lett.*, 2011, **2**, 2707–2710.
- 17 X. Mao, Z. Wang, X. Lang, Q. Hao, B. Wen, D. Dai, C. Zhou, L.-M. Liu and X. Yang, *J. Phys. Chem. C*, 2015, **119**, 6121–6127.
- 18 C. M. Friend, *Chem. Rec.*, 2014, **14**, 944–951.
- 19 P. M. Clawin, C. M. Friend and K. Al-Shamery, *Chem. – Eur. J.*, 2014, **20**, 7665–7669.
- 20 R. M. Navarro, M. C. Sanchez-Sanchez, M. C. Alvarez-Galvan, F. d. Valle and J. L. G. Fierro, *Energy Environ. Sci.*, 2009, **2**, 35–54.
- 21 S. Kim and B. E. Dale, *Biomass Bioenergy*, 2004, **26**, 361–375.
- 22 K. A. Connelly and H. Idriss, *Green Chem.*, 2012, **14**, 260–280.
- 23 S. Atsumi, T. Hanai and J. C. Liao, *Nature*, 2008, **451**, 86–89.
- 24 Z. Ma, Q. Guo, X. Mao, Z. Ren, X. Wang, C. Xu, W. Yang, D. Dai, C. Zhou, H. Fan and X. Yang, *J. Phys. Chem. C*, 2013, **117**, 10336–10344.
- 25 D. Brinkley and T. Engel, *J. Phys. Chem. B*, 2000, **104**, 9836–9841.
- 26 M. Shen and M. A. Henderson, *J. Phys. Chem. C*, 2012, **116**, 18788–18795.
- 27 Q. Yuan, Z. Wu, Y. Jin, L. Xu, F. Xiong, Y. Ma and W. Huang, *J. Am. Chem. Soc.*, 2013, **135**, 5212–5219.
- 28 K. R. Phillips, S. C. Jensen, M. Baron, S.-C. Li and C. M. Friend, *J. Am. Chem. Soc.*, 2013, **135**, 574–577.
- 29 V. S. Smentkowski and J. T. Yates, *J. Vac. Sci. Technol., A*, 1996, **14**, 260–265.
- 30 G. Lu, A. Linsebigler and J. T. Yates, *J. Phys. Chem.*, 1994, **98**, 11733–11738.
- 31 M. A. Henderson, *J. Phys. Chem. C*, 2008, **112**, 11433–11440.
- 32 L. Gamble, L. S. Jung and C. T. Campbell, *Surf. Sci.*, 1996, **348**, 1–16.
- 33 E. Farfan-Arribas and R. J. Madix, *J. Phys. Chem. B*, 2002, **106**, 10680–10692.
- 34 Z. Li, R. S. Smith, B. D. Kay and Z. Dohnálek, *J. Phys. Chem. C*, 2011, **115**, 22534–22539.
- 35 J.-M. Pan, B. L. Maschhoff, U. Diebold and T. E. Madey, *J. Vac. Sci. Technol., A*, 1992, **10**, 2470–2476.
- 36 N. G. Petrik, Z. Zhang, Y. Du, Z. Dohnálek, I. Lyubinetsky and G. A. Kimmel, *J. Phys. Chem. C*, 2009, **113**, 12407–12411.
- 37 T. L. Thompson and J. T. Yates, *Top. Catal.*, 2005, **35**, 197–210.
- 38 Y. K. Kim, B. D. Kay, J. M. White and Z. Dohnálek, *J. Phys. Chem. C*, 2007, **111**, 18236–18242.
- 39 J. Ø. Hansen, P. Huo, U. Martinez, E. Lira, Y. Y. Wei, R. Streber, E. Lægsgaard, B. Hammer, S. Wendt and F. Besenbacher, *Phys. Rev. Lett.*, 2011, **107**, 136102.
- 40 J. T. Yates, Jr., *Surf. Sci.*, 2009, **603**, 1605–1612.
- 41 Z. Zhang and J. T. Yates, *Chem. Rev.*, 2012, **112**, 5520–5551.
- 42 T. L. Thompson and J. T. Yates, *J. Phys. Chem. B*, 2005, **109**, 18230–18236.
- 43 J. J. Plata, V. Collico, A. M. Márquez and J. F. Sanz, *J. Phys. Chem. C*, 2011, **115**, 2819–2825.
- 44 M. A. Henderson, *Langmuir*, 1996, **12**, 5093–5098.
- 45 M. Shen, D. P. Acharya, Z. Dohnálek and M. A. Henderson, *J. Phys. Chem. C*, 2012, **116**, 25465–25469.
- 46 P. Huo, J. Ø. Hansen, U. Martinez, E. Lira, R. Streber, Y. Wei, E. Lægsgaard, B. Hammer, S. Wendt and F. Besenbacher, *J. Phys. Chem. Lett.*, 2012, **3**, 283–288.
- 47 S. Wendt, J. Matthiesen, R. Schaub, E. K. Vestergaard, E. Lægsgaard, F. Besenbacher and B. Hammer, *Phys. Rev. Lett.*, 2006, **96**, 066107.
- 48 M. A. Henderson, W. S. Epling, C. L. Perkins, C. H. F. Peden and U. Diebold, *J. Phys. Chem. B*, 1999, **103**, 5328–5337.
- 49 Y. Du, N. A. Deskins, Z. Zhang, Z. Dohnálek, M. Dupuis and I. Lyubinetsky, *Phys. Chem. Chem. Phys.*, 2010, **22**, 6337–6344.



D.2. Isomer-Selective Detection of Aromatic Molecules in Temperature-Programmed Desorption for Model Catalysis

analytical
chemistry

Article

pubs.acs.org/ac

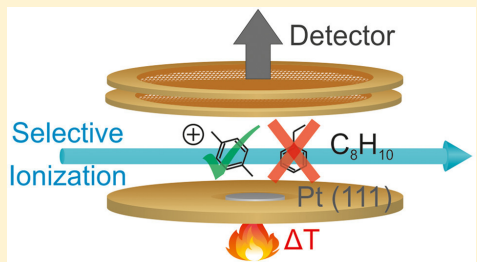
Isomer-Selective Detection of Aromatic Molecules in Temperature-Programmed Desorption for Model Catalysis

Andreas Winbauer, Sebastian L. Kollmannsberger, Constantin A. Walenta, Patrick Schreiber, Josef Kiermaier, Martin Tschurl,* and Ueli Heiz

Chair of Physical Chemistry, Department of Chemistry and Catalysis Research Center, Technische Universität München, Lichtenbergstrasse 4, 85748 Garching, Germany

Supporting Information

ABSTRACT: Based on three different molecules dosed on a Pt(111) single crystal the selectivity and sensitivity of REMPI-TPD in UHV is investigated for a potential application in heterogeneous catalysis. It is shown that the two structural isomers ethylbenzene and *p*-xylene can be discriminated by REMPI in a standard TPD experiment. The latter is not possible for the ionization with electrons in a Q-MS. It is further demonstrated by benzene TPD studies that the sensitivity of the REMPI-TOF-MS is comparable to commercial EI-Q-MS solutions and enables the detection of less than 0.6% molecules of a monolayer.



Almost all relevant basic chemicals in the chemical industry are produced in large scale via heterogeneous catalytic reactions.¹ In an atom-efficient process, high selectivities of the catalyst are of paramount importance.² Prominent reactions are the hydrogenation of α,β -unsaturated aldehydes and ketones^{3–5} or the epoxidation of ethylene.^{6–8} For the chemoselective hydrogenation the desired product usually is the unsaturated alcohol and the formation of the saturated aldehyde or ketone shall be avoided. For the epoxidation to ethylene oxide an unwanted formation of CO₂ is observed. In both cases the reactions proceed via the formation of products of the same mass, which either excludes the product analysis via mass spectrometry or makes it cumbersome.⁹ The problem is usually circumvented by the use of other methods as gas chromatography, as it was for example used in the epoxidation reaction.¹⁰ However, for a good time resolution or vacuum studies, mass spectrometry is the method of choice for many different analyte molecules. Studies of model systems are often conducted under ultrahigh vacuum (UHV) conditions to reveal detailed insights into reaction mechanisms.² For temperature-programmed desorption (TPD) or even temperature-programmed reaction (TPR), which are powerful and often applied methods for catalyst characterization, the application of mass spectrometry is particularly advantageous.

One way to overcome the problem of isobaric interferences in mass spectrometry is to use selective ionization techniques, such as resonant-enhanced multiphoton ionization (REMPI). As the ionization by the absorption of several photons is strongly enhanced by resonant states of the analyte molecules, a difference in the optical properties of the molecules can be exploited for their mass spectrometric analysis. Furthermore, REMPI is usually a very soft ionization technique and can be coupled

with highly sensitive product detection by time-of-flight mass spectrometry (TOF-MS). These properties have already led to several applications of this analytic technique, as e.g. for process analysis.^{11,12} Consequently, ionization with photons has also been applied in surface science.^{13–16} One example is the state-selective analysis of thermally desorbing molecules.^{17–21} In one recent study resonant ionization was even used in combination with TPD (“REMPI-TPD”) to investigate the desorption of physisorbed hydrogen molecules.²² The study was performed at very low temperature (below 30 K) with molecular hydrogen. However, an evaluation of this method as a technique for the analysis of products in a typical catalytic temperature regime (room temperature and above) and for larger molecules has so far not been performed. In particular, the physical demands of the TPD measurements for surface science studies are challenging. TPD experiments usually feature temperature ramps of one to several Kelvins per seconds,¹ and the number of data points per temperature is limited to the repetition rate of the laser. Furthermore, the temperature of the molecules, which in many cases is above room temperature, results in a lower ionization yield due to the broad peaks in the REMPI spectra. Especially in surface science detection with high sensitivity is very much desired, because most of the studies start at coverages significantly below one monolayer. In this respect the investigation of the desorption of larger molecules in a UHV environment is particularly challenging. Such molecules exhibit a high steric demand on the catalyst’s surface, and their large

Received: February 23, 2016

Accepted: April 14, 2016

Published: April 14, 2016

Analytical Chemistry

Article

number of states is significantly populated at elevated temperatures. In addition, ionization pathways have to be considered in order to enable the spectroscopic separation even at high desorption temperatures.

In this work it is demonstrated that REMPI-TPD can successfully be performed for molecules with an aromatic ring system, which represent precursors for selective hydrogenation reactions of larger molecules.^{23,24} It is shown that the discrimination by spectroscopy enables the selective detection of structural isomers in typical TPD experiments. Furthermore, the sensitivity of REMPI-TPD is determined for benzene and compared to that of a commercial quadrupole mass spectrometer (Q-MS) with electron ionization (EI), which is the standard technique for such measurements.¹ The obtained results demonstrate the potential of REMPI-TOF-MS for its application in heterogeneous catalysis, if the analyte molecules exhibit accessible electronically allowed transitions, which can be exploited for their ionization.

■ EXPERIMENTAL SETUP

All experiments were carried out in a home-built ultrahigh vacuum setup, which is described in more detail elsewhere.²⁵ The apparatus consists of an Auger spectrometer for surface analysis as well as of a sputter- and e-gun for surface cleaning. The sample crystals are mounted with heating wires to molybdenum rods (diameter: 3 mm), which are attached to the sample holder. The holder can carry three different sample crystals simultaneously (see Figure 1) and is further attached to a x, y, z, φ -manipulator by a silver block, which enables the cooling of the sample to 80 K with liquid-N₂. The samples can be heated resistively by tungsten–rhenium heating wires (W26Re, Omega Newport Electronics GmbH, diameter = 0.38 mm) up to 1200 K. Analysis of the desorption products is either performed with a commercial Q-MS (QMA 430, Pfeiffer Vacuum GmbH) equipped with an EI source or in a REMPI-TOF-MS, which is shown in Figure 1. The entire mass spectrometer is mounted by three treaded bars to a flange with a linear translation stage (LD 100-50, Vab Vakuum-Anlagenbau GmbH), which enables the precise adjustment in vertical direction. The acceleration stage of TOF-MS consists of one gold-covered repeller plate (diameter: 80 mm, thickness: 1 mm), which has a hole in the middle. Depending on the purpose the diameter of the hole can be changed by the replacement of the repeller plate. If it is desired to reduce the contribution from the background, which arises from desorption for components other than the sample, a small hole is chosen (i.e., 5 mm in diameter). If the aim is to enable the detection with highest sensitivity, a rather large hole (i.e., with a diameter of 20 mm) is chosen so that the entire crystal can be placed inside the acceleration region of the TOF-MS. Above the repeller plate two copper meshes (80% transmission, Precision Eforming LLC) are placed in a distance of 10.5 mm and 6 mm, respectively, to each other. In the first section of the drift region (total length about 470 mm) an Einzel lens enables the focusing of the ions onto a Chevron MCP-detector (S3040-10-D60-MA, SI Scientific Instruments GmbH). The data is acquired by an oscilloscope (WaveRunner 44Xi-A, Teledyne LeCroy GmbH). The TOF-MS typically has a resolution of better than 150.

The ionization is performed by a Nd:YAG (Quanta Ray GCR-3, Spectra-Physics Inc.) pumped dye laser (Scanmate 2E, Lambda Physik GmbH), whose output beam is frequency doubled. The laser system works with a repetition rate of 20 Hz. The laser beam is guided into the UHV chamber right to enable ionization in between the repeller plate and the first grid. The

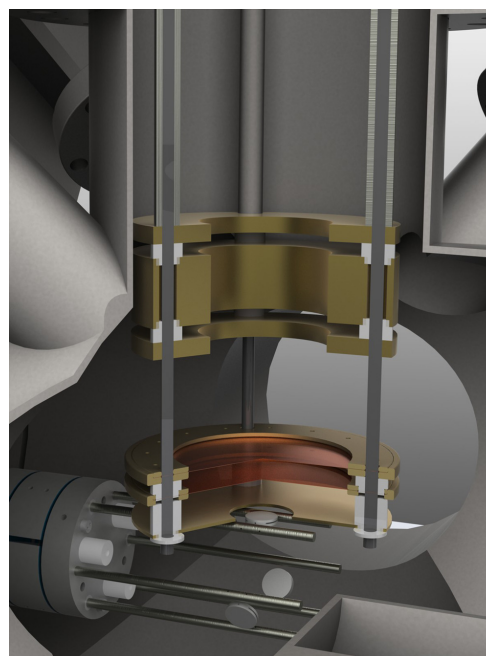


Figure 1. CAD drawing of the TOF-MS. The liquid N₂-cooled sample holder is heatable and carries up to three sample crystals at once. The manipulator enables the movement of the sample crystal below or into the acceleration region of the TOF-MS. The crystal can be set to a defined voltage to guarantee proper extract fields. The ions are extracted into a Wiley–McLaren type TOF-MS with an Einzel lens to focus the ions onto the detector. The mass spectrometer has a total ion drift region of 470 mm and supplies a mass resolution better than 150. Typical values for the voltages: $U_{\text{repeller}} = +1000$ V, $U_{\text{grid}} = +853$ V, $U_{\text{lens}} = +300$ V.

laser's pulse energy is optimized to the highest value, at which only minor fragmentation is observed (usually 3 to 4 mJ/cm² per pulse). One data point represents an average over 20 measurement points.

TPD measurements are controlled by a PID controller (2408, Eurotherm, Invensys Systems GmbH). The temperature is measured by a type C-thermocouple, which is spot-welded onto the crystal. The thermocouple was calibrated to a standard procedure²⁶ and referenced to TPD measurements of benzene. The read-out of the thermocouple is converted (Dat4135AC, Datexel S.R.L.) and fed into the PID controller. All TPD experiments were performed with a heating rate of 2.35 K/s. All these electronic components are connected to the power via an insulating transformer. This setup enables the sample crystal to be set to a particular voltage, which ensures proper electric fields in the acceleration region of the TOF-MS.

■ RESULTS AND DISCUSSION

Due to the relevance of the material in catalysis, a Pt (111) single crystal (Surface Preparation Laboratory B. V.) was chosen as model system. The crystal was cleaned following existing procedures^{27,28} until no contamination was observed in the Auger electron spectra (AES). In the following the critical aspects

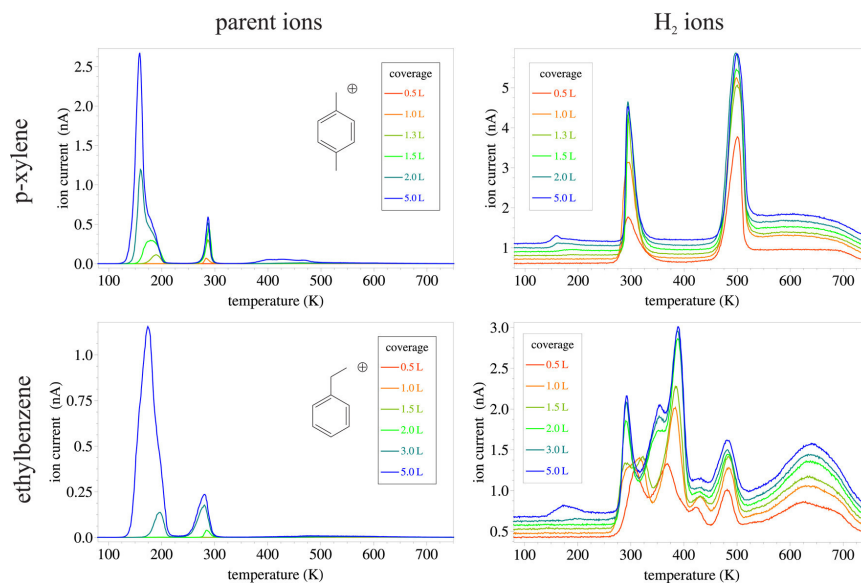


Figure 2. TPD measurements with a commercial EI-Q-MS for different coverages of *p*-xylene (top row) and ethylbenzene (bottom row, both C_8H_{10}). The desorption behavior for both molecules is very similar, which can be seen by their TPD measurements on their parent mass (left column). The only significant difference is seen in the hydrogen evolution (right column), which occurs at different temperatures.

of REMPI-TPD are addressed. First, the selectivity of the REMPI-TOF-MS is demonstrated by the measurement of mixtures of two structural isomers. Second, the sensitivity of the technique is evaluated and compared to that of a commercial Q-MS with EI.

■ SELECTIVITY

For the demonstration of the selectivity *p*-xylene and ethylbenzene (both C_8H_{10}) were chosen as model systems. Both isomers exhibit an almost identical fragmentation pattern by EI with only small deviations in the relative abundance in some fragment masses.²⁹ Thus, discrimination between these two molecules by EI is almost completely excluded. Furthermore, both molecules show similar desorption behaviors in their TPD measurements.

In good agreement with previous studies,^{30,31} *p*-xylene shows two desorption features at coverages above 1 L. The low temperature peak between 120 and 200 K can be assigned to multilayer physisorption of *p*-xylene molecules on top of a monolayer of molecules, which are directly bound to the Pt(111) surface. The latter desorb at temperatures between 260 and 320 K. In contrast to the multilayer peak, the feature for the chemisorbed monolayer already appears at a coverage of 1 L and reaches its saturation between 2 and 5 L. The monolayer peak only represents a small fraction of *p*-xylene molecules covering the surface, as only a small fraction of molecules (about 10%) leaves the Pt-surface intact.³⁰ The reason for that is that *p*-xylene undergoes dehydrogenation on the Pt-surface, which causes an increase in the H_2 signal (Figure 2). There are three temperature regions, where hydrogen molecules leave the surface. Between 260 and 350 K hydrogen atoms from the methyl groups form H_2 .³⁰ At temperatures above 450 K all C–H bonds are subsequently broken.³⁰ The hydrogen atoms recombine and

leave the surface, while carbon still remains on the surface of the crystal,³⁰ which is also confirmed by AES.

For ethylbenzene a very similar TPD spectrum with two desorption temperatures (between 120 and 220 K as well as 240 and 320 K, respectively) is obtained by the detection of the molecule on its parent mass (Figure 2). The monolayer peak can only be detected at a coverage of 2 L and above, which indicates that a higher steric demand results in a lower adsorption probability. The only significant difference of the TPD spectra of the two molecules is found in their H_2 desorption spectra. Similarly to *p*-xylene, molecular hydrogen starts to leave the surface at around 300 K. However, in contrast to *p*-xylene, ethylbenzene exhibits a complex desorption pattern from 300 to 450 K, which indicates the C–H bonds from the ethyl group are subsequently cracked prior to those of the aromatic ring. H_2 evolution originating from hydrogen atoms of the aromatic ring analogously starts at temperatures above 450 K.

While a direct discrimination of the two molecules is almost impossible by EI, REMPI as an ionization technique can be used to overcome the difficulties. In Figure 3 the 1+1 REMPI spectra of both molecules are shown at conditions similar to those of the TPD experiment (i.e., an effusive beam at room temperature). The results are in good agreement with previous ones from a supersonic jet^{32,33} and show the difference in the 0_0^0 position of the excited electronic state. Based on this scan two wavelengths are chosen: At a wavelength of 266.5 nm both molecules are detected simultaneously, while at 272.2 nm only *p*-xylene molecules are ionized. Note that the ionization yield of ethylbenzene is lower than that of *p*-xylene, which leads to a more sensitive detection of the latter molecule.

The selectivity of REMPI for TPD experiments is demonstrated by mixtures of *p*-xylene and ethylbenzene obtained by the subsequent dosage of 3 L of the respective molecules. As

Analytical Chemistry

Article

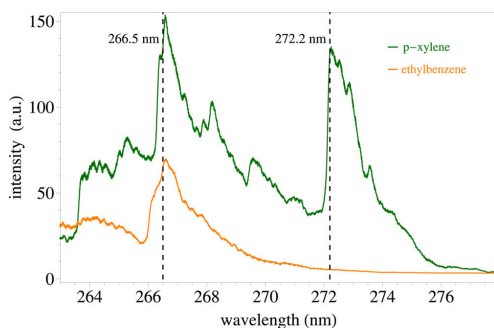


Figure 3. Wavelength scan of an effusive beam of *p*-xylene and ethylbenzene at room temperature (pressure in the chamber: 1×10^{-6} mbar). Two wavelengths are identified, which enable the discrimination between the two isomers. At 272.2 nm *p*-xylene is exclusively ionized, while at 266.5 nm both molecules are detected.

illustrated in Figure 4, either ethylbenzene (right) or *p*-xylene (left) therefore dosed on top of the other molecules. As a consequence, three different layers are formed: a saturated chemisorbed monolayer of the molecule dosed first, a physisorbed layer of the same molecule, and further layers caused from physisorption of the second molecule.

Depending on this sequence of the dosing at around 100 K, differences are observed in the TPD experiments (Figure 5). For the measurements with EI-Q-MS these differences are small. When ethylbenzene was dosed directly on the Pt(111) surface, the multilayer peaks (at 142 and 165 K) at higher temperatures exhibit an additional shoulder at about 180 K. The differences in the monolayer peak, however, are even less pronounced. The peak is somewhat broader and slightly shifted to lower temperatures (279 K instead of 283 K). Almost the same spectrum is obtained by REMPI-TOF-MS recorded at a wavelength of 266.5 nm, which causes the ionization of both molecules. However, the spectra at an ionization wavelength of 272.2 nm exhibit significant differences. If *p*-xylene is dosed first, a monolayer desorption peak is clearly visible in the TPD measurement but does not appear in the measurement with a dosage of ethylbenzene prior to *p*-xylene. The result clearly demonstrates the selectivity of REMPI also in surface science

studies. Furthermore, it is seen that no detectable diffusion to the surface occurs and that the layers remain at 100 K according to their dosing sequence.

SENSITIVITY

In contrast to EI-Q-MS, which is usually operated in a continuous way, REMPI-TOF-MS is a pulsed technique. While the measurement in a TOF-MS allows for the simultaneous detection of several masses, the intensity of specific ion is certainly higher for continuous measurements due to the longer measurement time. On the other hand, the ionization by REMPI leads to a very sensitive detection, and it has been shown that very small quantities of aromatic molecules can be detected using this technique (see for example Boesl et al.³⁴ and references therein). In the following the TPD of benzene of Pt(111) is to evaluate the sensitivity of the REMPI-TOF setup, because this system is very well-studied^{35–39} and the ionization via electronic states of the aromatic ring can be exploited for many different organic molecules. Moreover, benzene often represents a precursor for selective hydrogenation reactions of larger molecules.^{23,24}

Ionization of benzene is performed by a 1+1 REMPI process at a wavelength of 252.935 nm (see the spectrum in Figure S1 in the Supporting Information). The obtained REMPI-TPD measurements in comparison with the measurement with a conventional EI-Q-MS are shown in Figure 6. It can be seen that the REMPI-TPD exhibits a somewhat higher background level, which originates from benzene desorption from parts other than the sample crystal. In contrast to the EI-Q-MS the shielding of these parts is less efficient, which results in the higher background of the signal. Nevertheless, a coverage of 0.5 L can easily be detected with REMPI-TPD and yields the same signal as by the measurement with the commercial EI-Q-MS. The sensitivity of REMPI-TPD is also in the same order of magnitude and only somewhat worse than for the EI-Q-MS, as it can be seen for a coverage of 0.25 L.

According to Campbell et al., a saturation of the surface coverage is obtained at 0.16 benzene molecules per surface atom for a dosage at 120 K.³⁷ Taking the integral ion current from the EI-Q-MS measurements at a coverage of 0.5 L and the integral current of the saturation coverage (coverage of 2 L, see Figure S2 in the Supporting Information), it is found that only 8% of the saturation coverage is obtained by a benzene dosage of 0.5 L. Taking into account that only 45% of the molecules desorb intact

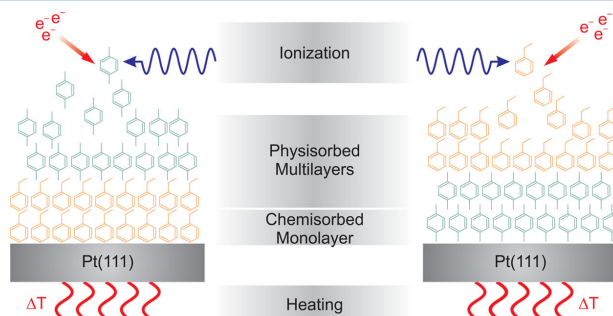


Figure 4. Illustration of the mixing experiment with ethylbenzene and *p*-xylene (both: C_8H_{10}). The dosage of *p*-xylene on top of a layer of ethylbenzene leads to the formation of a structure as displayed on the left side, while a vice versa procedure results in the scheme on the right. Note that in this model diffusion of the molecules is excluded, which is also found experimentally (see text).

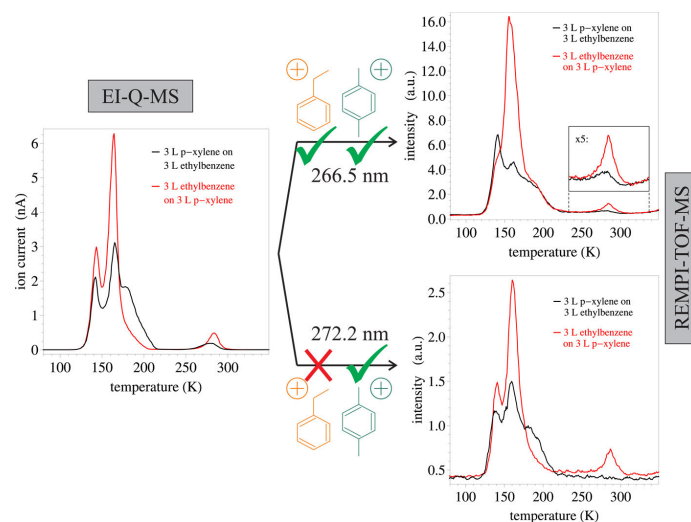


Figure 5. Selectivity by the detection with REMPI TOF-MS (right) in comparison to the detection with EI Q-MS (left). Depending on the sequence of dosing, the TPD measurements exhibit only a small difference if the desorbing molecules are detected with EI Q-MS. However, for ionization with REMPI these differences are clearly more pronounced. As seen for the ionization with 272.2 nm (bottom) only a monolayer desorption peak is visible, if *p*-xylene was dosed prior to ethylbenzene; otherwise this peak is absent. This result also demonstrates for the dosage at 100 K no significant diffusion of the molecules to the surface is observed. Note that the ionization yield for ethylbenzene is lower than that of *p*-xylene at a detection wavelength of 266.5 nm.

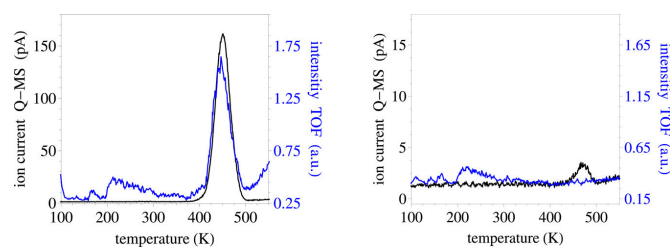


Figure 6. Sensitivity of the detection with REMPI TOF-MS in comparison to the detection with a commercial EI Q-MS. Based on the TPDs of benzene on Pt(111) it is seen that a dosage of 0.5 L at 190 K can clearly be detected by REMPI TOF-MS (figure on the left). Only at a coverage of 0.25 L it is found that the detection limit of the EI Q-MS is better than that of the REMPI TOF-MS.

and do not undergo dehydrogenation,³⁷ it is found that less than 0.0057 (0.57%) desorbing benzene molecules per surface atom can easily be detected by REMPI-TPD. While the achieved sensitivity is more than sufficient for most of the experiments, even further improvements may be obtained by modification of the laser system, as for example by an increase of the interaction region of the laser with the molecules or by the use of lasers with a higher repetition rate.

CONCLUSION

In this work it is shown that REMPI-TOF-MS can be used as a detection technique complementary to EI-Q-MS in TPD and TPR experiments. These experiments are powerful tools in heterogeneous catalysis, and REMPI enables the selective ionization and supplies the time resolution, which is needed for in situ product analysis. As demonstrated for *p*-xylene and ethylbenzene, the isomer-selective detection can be achieved by

REMPI-TOF-MS. Furthermore, the sensitivity of the method is found to be more than sufficient to detect analyte molecules with similar ionization efficiencies as benzene in heterogeneous catalysis, even for systems with low catalyst loading as for example of size-selected cluster catalysts.

ASSOCIATED CONTENT

Supporting Information

The Supporting Information is available free of charge on the ACS Publications website at DOI: 10.1021/acs.analchem.6b00717.

1+1 REMPI spectra of an effusive beam of benzene at room temperature and coverage-dependent TPD measurements of benzene desorbing from a Pt(111) single crystal recorded by a Q-MS (PDF)

Analytical Chemistry

Article

■ AUTHOR INFORMATION

Corresponding Author

*E-mail: tschurl@tum.de.

Notes

The authors declare no competing financial interest.

■ ACKNOWLEDGMENTS

The authors thank the DFG (HE3454/23-1) and the ERC (ERC-2009-AdG 246645-ASC3) for financial support. We acknowledge Ulrich Boesl for his helpful discussions at the beginning of the project.

■ REFERENCES

- (1) Chorkendorff, L.; Niemantsverdriet, J. W. *Concepts of Modern Catalysis and Kinetics*; WILEY-VCH: Weinheim, 2007.
- (2) Somorjai, G. A.; Park, J. Y. *Angew. Chem., Int. Ed.* **2008**, *47*, 9212–9228.
- (3) Gallezot, P.; Richard, D. *Catal. Rev.: Sci. Eng.* **1998**, *40*, 81–126.
- (4) Maki-Arvela, P.; Hajek, J.; Salmi, T.; Murzin, D. Y. *Appl. Catal., A* **2005**, *292*, 1–49.
- (5) Claus, P. *Top. Catal.* **1998**, *5*, 51–62.
- (6) Sajkowski, D. J.; Boudart, M. *Catal. Rev.: Sci. Eng.* **1987**, *29*, 325–360.
- (7) Bailey, J. E.; Ullmann, F. *Ullmann's Encyclopedia of Industrial Chemistry*; Wiley-VCH: Weinheim [u.a.], 2001.
- (8) Christopher, P.; Lincic, S. J. *Am. Chem. Soc.* **2008**, *130*, 11264–11265.
- (9) Bocklein, S.; Gunther, S.; Reichelt, R.; Wyrwich, R.; Joas, M.; Hettstedt, C.; Ehrensperger, M.; Sicklinger, J.; Wintterlin, J. *J. Catal.* **2013**, *299*, 129–136.
- (10) Campbell, C. T. *J. Catal.* **1985**, *94*, 436–444.
- (11) Boesl, U. *J. Mass Spectrom.* **2000**, *35*, 289–304.
- (12) Streibel, T.; Zimmermann, R. *Annu. Rev. Anal. Chem.* **2014**, *7*, 361–381.
- (13) Horwitz, J. S.; Villa, E.; Hsu, D. S. Y. *J. Phys. Chem.* **1990**, *94*, 7214–7219.
- (14) Jackson, R. C.; Polanyi, J. C.; Sjoval, P. *J. Chem. Phys.* **1995**, *102*, 6308–6326.
- (15) Elg, A.-P.; Andersson, M.; Rosén, A. *Appl. Phys. B: Lasers Opt.* **1997**, *64*, 573–578.
- (16) Wilson, D. P.; Sporleder, D.; White, M. G. *J. Phys. Chem. C* **2012**, *116*, 16541–16552.
- (17) Peremans, A.; Fukutani, K.; Mase, K.; Murata, Y. *Surf. Sci.* **1993**, *283*, 189–194.
- (18) Schroter, L.; Trame, C.; Gauer, J.; Zacharias, H.; David, R.; Brenig, W. *Faraday Discuss.* **1993**, *96*, 55–65.
- (19) Ferkel, H.; Hodgson, L.; Singleton, J. T.; Blass, P. M.; Reisler, H.; Wittig, C. *J. Chem. Phys.* **1994**, *100*, 9228–9237.
- (20) Fukutani, K.; Murata, Y.; Schwarzwald, R.; Chuang, T. *J. Surf. Sci.* **1994**, *311*, 247–256.
- (21) Zimmermann, F. M.; Ho, W. *Surf. Sci. Rep.* **1995**, *22*, 127–247.
- (22) Sugimoto, T.; Fukutani, K. *Phys. Rev. Lett.* **2014**, *112*, 146101.
- (23) Nishimura, S. *Handbook of Heterogeneous Catalytic Hydrogenation for Organic Synthesis*; Wiley: 2001.
- (24) Schwab, F.; Lucas, M.; Claus, P. *Angew. Chem., Int. Ed.* **2011**, *50*, 10453–10456.
- (25) Walenta, C. A.; Kollmannsberger, S. L.; Kiermaier, J.; Winbauer, A.; Tschurl, M.; Heiz, U. *Phys. Chem. Chem. Phys.* **2015**, *17*, 22809–22814.
- (26) Smentkowski, V. S.; Yates, J. T. *J. Vac. Sci. Technol., A* **1996**, *14*, 260–265.
- (27) Campbell, C. T.; Ertl, G.; Kuipers, H.; Segner, J.; Molecular-Beam, A. *Surf. Sci.* **1981**, *107*, 220–236.
- (28) Powell, C. J.; Madey, T. E.; Czanderna, A. W. *Specimen Handling, Preparation, and Treatments in Surface Characterization*; Plenum Press: New York; London, 1998.
- (29) Stein, S. E. Nist Chemistry Webbook. <http://webbook.nist.gov> (accessed October 29).
- (30) Wilk, D. E.; Stanners, C. D.; Shen, Y. R.; Somorjai, G. A. *Surf. Sci.* **1993**, *280*, 298–312.
- (31) Lutterloh, C.; Biener, J.; Schenk, A.; Kuppers, J. *Surf. Sci.* **1995**, *331–333*, 261–266.
- (32) Blease, T. G.; Donovan, R. J.; Langridgesmith, P. R. R.; Ridley, T. *Laser Chem.* **1988**, *9*, 241–263.
- (33) Gunzer, F.; Grotemeyer, J. *Phys. Chem. Chem. Phys.* **2002**, *4*, 5966–5972.
- (34) Boesl, U.; Zimmermann, R.; Weickhardt, C.; Lenoir, D.; Schramm, K. W.; Ketrup, A.; Schlag, E. W. *Chemosphere* **1994**, *29*, 1429–1440.
- (35) Tsai, M. C.; Muetterties, E. L. *J. Am. Chem. Soc.* **1982**, *104*, 2534–2539.
- (36) Garfunkel, E. L.; Farias, M. H.; Somorjai, G. A. *J. Am. Chem. Soc.* **1985**, *107*, 349–353.
- (37) Campbell, J. M.; Seimanides, S.; Campbell, C. T. *J. Phys. Chem.* **1989**, *93*, 815–826.
- (38) Xu, C.; Tsai, Y. L.; Koel, B. E. *J. Phys. Chem.* **1994**, *98*, 585–593.
- (39) Breitbach, J.; Franke, D.; Hamm, G.; Becker, C.; Wandelt, K. *Surf. Sci.* **2002**, *S07–S10*, 18–22.

Supporting Information

Isomer-Selective Detection of Aromatic Molecules in Temperature-Programmed Desorption for Model Catalysis

*Andreas Winbauer,^a Sebastian L. Kollmannsberger,^a Constantin A. Walenta,^a Patrick Schreiber,^a
Josef Kiermaier,^a Martin Tschurl,^a Ueli Heiz^a*

^a Chair of Physical Chemistry, Department of Chemistry and Catalysis Research Center,
Technische Universität München, Lichtenbergstrasse 4, 85748 Garching, Germany.

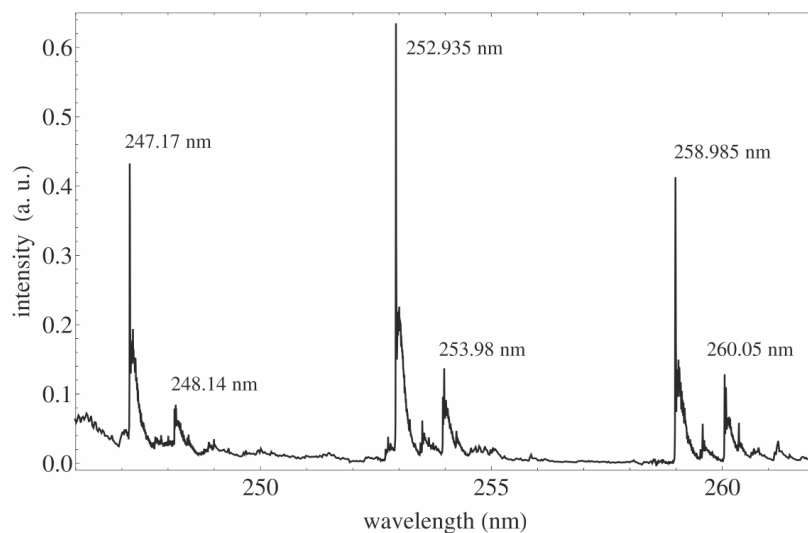


Figure S1. 1+1 REMPI scan of an effusive beam of benzene at room temperature (pressure in the chamber: $1 \cdot 10^{-8}$ mbar).

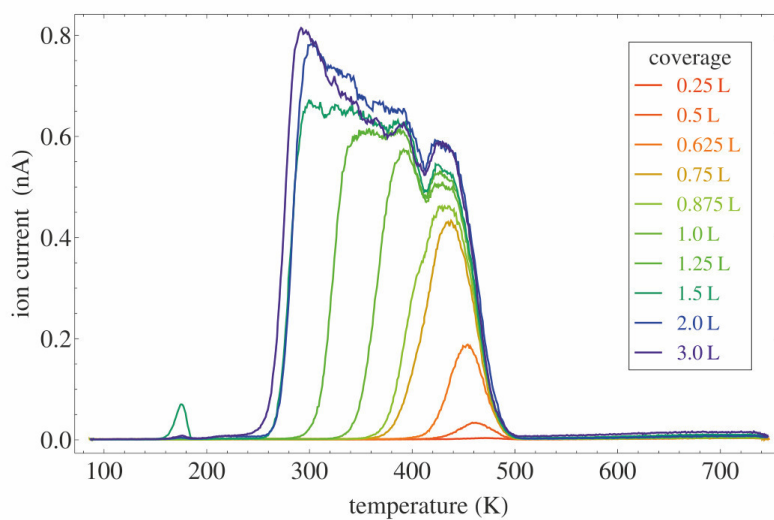


Figure S2. Coverage-dependent TPD measurements of benzene desorbing from a Pt(111) single crystal recorded by a Q-MS. At 2.0 L the saturation for monolayer coverage is reached.

D.3. Doping-Dependent Adsorption and Photon-Stimulated Desorption of CO on GaN(0001)

THE JOURNAL OF
PHYSICAL CHEMISTRY C

Article

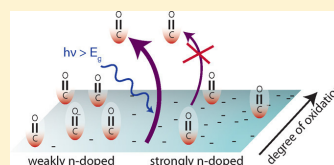
pubs.acs.org/JPC

Doping-Dependent Adsorption and Photon-Stimulated Desorption of CO on GaN(0001)

Sebastian L. Kollmannsberger,^{†,||} Constantin A. Walenta,^{†,‡,||} Andrea Winnerl,[§] Saskia Weiszer,[§] Rui N. Pereira,[§] Martin Tschurl,[†] Martin Stutzmann,^{§,‡} and Ueli Heiz^{*,†,‡}[†]Chair of Physical Chemistry, Department of Chemistry & Catalysis Research Center, Technische Universität München, Lichtenbergstr. 4, 85748 Garching, Germany[‡]Nanosystems Initiative Munich, Schellingstr. 4, 80799 München, Germany[§]Walter Schottky Institute and Physics Department, Technische Universität München, Am Coulombwall 4, 85748 Garching, Germany

Supporting Information

ABSTRACT: CO is used as a chemical probe molecule to elucidate the properties of differently n-type doped GaN(0001) surfaces under ultrahigh vacuum conditions. Doping-dependent sticking of CO is observed by temperature-programmed desorption, which is not influenced by the surface composition of the semiconductor substrates. By the excitation of the semiconductor with UV photons a low-temperature desorption of CO is stimulated. The absolute photon-stimulated desorption intensity strongly depends on the surface composition. However, the desorption kinetics do not significantly depend on the surface composition, semiconductor doping, or UV excitation wavelength. A model is introduced, which is based on the electronic characteristics of the GaN substrates and describes the doping-dependent adsorption as well as the photochemical behavior.



INTRODUCTION

Heterogeneous photocatalysis is believed to be a viable pathway to H₂ production from renewable energy sources and sunlight.^{1–3} Since their discovery as suitable catalysts, group III–V materials such as gallium nitride (GaN) have proven to be stable heterogeneous photocatalysts when decorated with cocatalysts.^{4–6} The most explored reactions in photocatalysis on GaN are the H₂ evolution from water^{6–11} and the CO oxidation.^{12–16}

Pure GaN is a semiconductor with an energy gap of 3.4 eV.¹⁷ In contrast with other semiconductors used in photocatalysis such as ZnO and TiO₂, it can be n-type- as well as p-type-doped to alter the charge-carrier concentration and the sign of charge accumulated at the illuminated surface.¹⁸ Additionally, solid solutions of GaN with other wurtzite-type structures such as ZnO can be prepared. Because in such systems the energy of the valence band edge is shifted upward with respect to ZnO, the band gap is moved into the visible part of the solar spectrum.^{19,20} Despite these promising properties the surface chemistry even of bare GaN is not well known, which is different from other catalysts such as TiO₂.^{21,22} Previous surface science studies mainly have focused on the building process during epitaxial growth^{23–25} and surface reconstructions^{26–28} for applications in devices.^{29,30} However, a better understanding of the surface chemistry of the bare semiconductor helps in identifying and avoiding undesirable side reactions in heterogeneous (photo)catalysis. O₂ photon-stimulated desorption (PSD) from TiO₂(110) is a powerful tool to determine the photochemical activity of the bare semiconductor surface.^{31,32}

While the detailed mechanism of O₂ PSD from TiO₂ has been investigated during the last 30 years,^{33–38} no other PSD experiments without a previous chemical reaction on semiconductors are known.

In metal nanoparticle/semiconductor hybrid materials it has been shown that the p-type or n-type doping has an influence on the charge state of the metal nanoparticle as well as on the charge carrier dynamics. Consequently, the reactivity during catalysis is also affected by semiconductor doping.^{15,39} The common assumption of those studies is that the chemical properties of the semiconductor surface are doping-independent, as doping only alters the bulk charge-carrier concentration.

In this work, we present a ultrahigh vacuum (UHV) study of the effect of bulk semiconductor n-type doping on the CO adsorption on the GaN(0001) surface and investigate the PSD of CO from that surface.

EXPERIMENTAL SECTION

Different GaN samples were studied in the UHV using an apparatus that is equipped with standard methods for surface science to perform thermal and photochemical reaction studies. This apparatus is described in detail elsewhere.⁴⁰ The Si-doped GaN(0001) epitaxial layers with a thickness of ~550 nm were deposited by plasma-induced molecular beam epitaxy (PIMBE). As substrates Fe-doped semi-insulating Ga-polar

Received: February 17, 2017

Revised: March 28, 2017

Published: March 31, 2017

GaN MOCVD templates (thickness 4 μm) on $\alpha\text{-Al}_2\text{O}_3(0001)$ from Lumilog were used. The samples were grown in the Ga-droplet regime. During the process, the substrate temperature was kept at 1143 K. The Ga source was heated to 1253 K, which corresponds to a beam equivalent pressure of 1.3×10^{-6} mbar. For the silicon doping, the source was operated at 1273 and 1373 K. The plasma source was operated at 300 W with a nitrogen flux of 0.15 sccm. These conditions were chosen because it is well known that atomically flat surfaces can be achieved in this way.⁴¹ Furthermore, it is known that for the range of silicon dopant concentrations employed in this study the dopant profile in the homoepitaxial layers is constant because it has been confirmed by SIMS profiles.⁴² The free electron concentration of all of these samples was determined by Hall effect measurements.⁴³ The GaN samples were cut to a rectangular shape with a size of 10 mm \times 10 mm for being mounted onto a sample holder, which consists of a 1 mm thick tantalum plate with a 0.3 mm deep cutout of the size of the GaN sample. A thin (0.025 mm) gold foil is placed between the base plate of the sample holder and the semiconductor to ensure good thermal conductivity. The fixation of the semiconductor samples is achieved by two spot-welded 0.1 mm thick tantalum clamps. The heating of the sample is performed indirectly via resistive heating of two tungsten-rhenium wires (0.38 mm in diameter), which are mounted on the sides of the tantalum holder. This setup has been developed on the basis of TiO₂ sample holders.^{40,44} Cooling of the sample to temperatures of around 100 K is achieved by contact to a reservoir of liquid nitrogen (LN₂). The temperature is measured by the calibrated readout of a twisted type-C thermocouple spot-welded to the bottom of the tantalum sample holder. The deviation of the temperature of the GaN surface to the base plate was determined to be <5 K over the entire temperature range. The in situ GaN treatment before measurements includes a single vacuum annealing to 800 K for 10 min and a cycle of Ar⁺ sputtering at 80 K (0.5 keV, 1×10^{-6} mbar, $I_{\text{sputter}} = 2.0 \mu\text{A}$) with a subsequent vacuum annealing flash to 800 K, so that no carbon contamination is observed with Auger electron spectroscopy (AES). The surface morphology and roughness were checked ex situ with atomic force microscopy (AFM) (Figure S1).

For the photochemical measurements a Nd:YAG-pumped dye laser (Spectra GCR 4, ~ 10 ns pulse length) (Lambda Physics) with a wavelength of 266.5 nm is used to excite electron-hole pairs close to the GaN surface. The laser spot is adjusted to illuminate the entire GaN sample. The intensity is set to a pulse energy of 600 μJ /pulse, so that no laser-induced thermal heating effects are observed. All PSD experiments were performed at LN₂ temperature.

RESULTS

Thermal Adsorption and Desorption. CO temperature-programmed desorption (TPD) measurements were performed on three differently doped MBE GaN samples to monitor the influence of doping on the adsorption effects at the GaN surface. Sample a is nominally undoped (5.2×10^{16} charge carriers (cc)/cm³), sample b is weakly n-type doped ($1.3 \times 10^{18} \pm 1.2 \times 10^{16}$ cc/cm³), and sample c is strongly n-type doped ($2.1 \times 10^{19} \pm 2.2 \times 10^{18}$ cc/cm³).

Figure 1 presents a series of TPD spectra from various CO exposures on sample c ($2.1 \times 10^{19} \pm 2.2 \times 10^{18}$ cc/cm³). For lower coverages only one desorption peak is observed at ~ 100 K. A second peak, which appears at ~ 225 K, is observed for

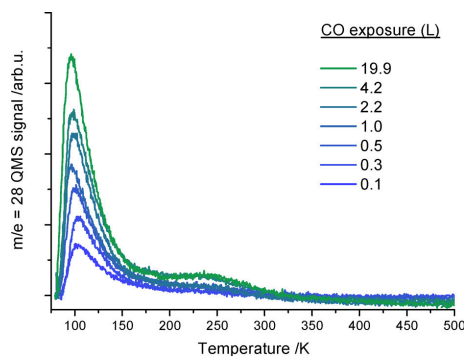


Figure 1. TPD spectra from various coverages of CO dosed on a GaN(0001) surface, sample c, at 80 K.

coverages of 1 langmuir (L) and more. Control experiments indicate that this feature originates from CO desorption from the sample holder. The low-temperature peak is assigned to thermal desorption of physisorbed CO from the GaN surface. Because the relative change in the desorption signal is low for high coverages a saturation behavior is already suggested. Hence it can be seen that no multilayer adsorption occurs in this temperature range. The CO desorption from a multilayer for a nonmetal is expected to occur at ~ 30 K.^{45,46} The GaN samples with the lowest charge-carrier concentrations also show a similar behavior concerning the peak position. However, if the absolute integrals of the 100 K desorption peak at identical exposures are regarded, then a difference between the three GaN samples is observed. The resulting saturation graphs from exposures of 0.1 to 9.0 L are shown in Figure 2. The exposures were determined by background-corrected integration of the $m/e = 28$ signal of the quadrupole mass spectrometer (QMS) during dosage.

As shown in Figure 2, the total saturation coverage is decreasing with increasing n-type doping of the GaN samples. Furthermore, for the smallest exposures to CO, a steeper rise in

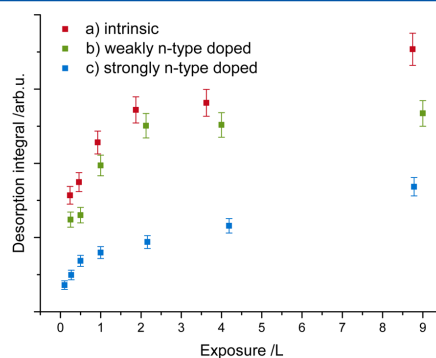


Figure 2. CO desorption integral series of three differently doped GaN samples from exposures of 0.1 to 9.0 L. The higher the charge carrier concentration, the slower the CO coverage rises and the lower is the maximum CO coverage.

the desorption integral is observed for weaker n-type-doped samples.

Photon-Stimulated Processes. After illumination of a 2.0 L CO-covered GaN surface by UV light at 80 K a considerably smaller thermal desorption signal is observed in TPD compared with that without previous illumination (Figure 3a). With the

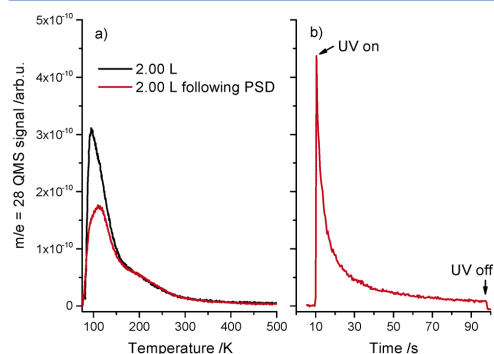


Figure 3. (a) TPD spectra of 2.0 L CO with and without UV illumination after CO exposure on a nonintentionally doped GaN(0001). The desorption following the illumination is considerably smaller than the “dark” one. (b) Photon-stimulated desorption spectra of CO at 80 K. UV excitation starts at 10 s and an immediate CO desorption is observed. Note that panels a and b have the same scale in the $m/e = 28$ QMS signal and that the sum of the integrated red curves matches the “dark” desorption quantitatively.

exception of the high-temperature feature due to the sample holder, the TPD signal decreases as a whole and not at a specific temperature. This indicates that all binding sites are affected similarly by the photostimulation. During the illumination process, desorption of CO occurs (Figure 3b), which stops within the time resolution of the desorption experiment when illumination ends. The absolute amount of CO desorbed via the PSD and the consecutive TPD quantitatively matches the regular desorption of 2.0 L in a “dark” only TPD experiment within the experimental accuracy.

Figure 4 illustrates the normalized intensities of PSD curves for differently n-type-doped samples. It is found that no appreciable difference in the decay curves is observed, which shows that the photon-stimulated desorption kinetics does not change with the semiconductor doping. After an initial rise in intensity, the signal decay can be described by a sum of two stretched exponential functions, one with a fast time constant in the range of some seconds and one with a slow time constant about 1 order of magnitude higher. A change in the irradiation wavelength to 355 nm resulted in the same desorption kinetics (Figure S2). Furthermore, the kinetics were also found to be independent of the surface oxidation state. It is well known that intermediate gallium oxide species (GaO_x) and stoichiometric Ga_2O_3 are always present on GaN surfaces,⁴⁷ and even repeated AES measurements can oxidize the surface.⁴⁸ Long cycles of Ar^+ sputtering reduce the N/Ga ratio, and nitrogen vacancies are formed.^{49,50} Oxygen impurities from the sputter gas or the background pressure lead to an oxidation of the free Ga surface species. The evolution of the surface oxidation can be tuned by the sputtering time and is determined by AES, corrected for the elemental sensitivities.⁵¹ For the calculation of the percentage

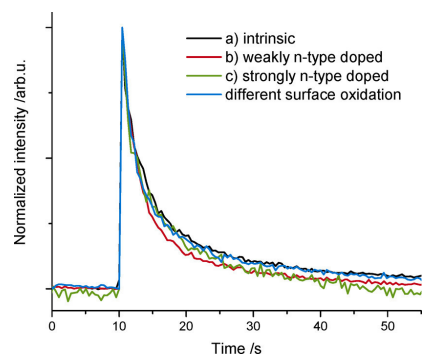


Figure 4. Intensity-normalized PSD signal of three differently doped GaN samples with the same surface oxidation as well as of a differently oxidized GaN surface. The various decay curves do not exhibit any significant differences. Hence the kinetics of the PSD is independent of doping and surface oxidation.

of respective atoms it is assumed that the oxidation occurs only at the surface, as it is described in the literature.⁵²

In Figure 5a, it can be seen that the photoactivity decreases with a decrease in the N percentage on the surface. Figure 5b

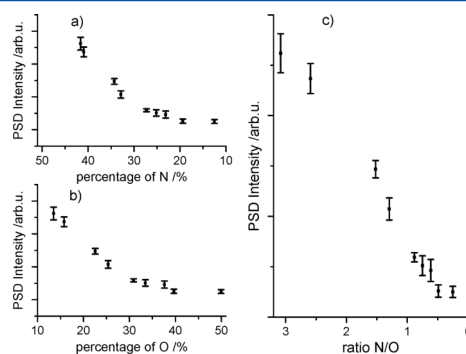


Figure 5. (a) Decrease in PSD intensity with decreasing percentage of nitrogen. (b) Decrease in PSD intensity with increasing percentage of oxygen. (c) Sigmoidal PSD intensity trend as a function of N/O ratio. All Ga, N, and O percentage values were obtained from AES measurements, corrected for the corresponding elemental sensitivities.⁵¹ The percentage of gallium decreases from 45 to 38% with increasing O coverage in the indicated range.

demonstrates the decline in PSD intensity with rising oxygen content. If the PSD intensity is plotted versus the N/O ratio (Figure 5c), then a sigmoidal curve with a linear transition region results. Thus it can be concluded that the presence of oxygen atoms and the decrease in nitrogen lead to a decrease in the PSD intensity. However, the kinetics of the PSD remain unaltered, and similarly the thermal desorption is also found to stay unaffected by the surface oxidation process (Figure 4).

DISCUSSION

Thermal CO Adsorption and Desorption. The binding of CO to GaN(0001) only occurs via physisorption, which is

indicated by the low desorption temperature of ~ 100 K (Figure 1). It is found that the sticking of CO is dependent on the dopant concentration. The intensity of the desorption signal for same dosages decreases with increasing n-type doping. The effect is significant but is not as pronounced as the change of the dopant concentration: An increase in the charge-carrier concentration by a factor of one thousand only results in a maximum decrease in the desorption signal by a factor of 2. While doping results in different electronic properties of the semiconductor, its surface morphology is preserved, as can be seen in the respective AFM images (Figure S1). The saturation coverage behavior shown in Figure 2 and the same desorption temperature of CO also allow us to exclude the formation of different surface defects for different doping levels. In such a case, a difference in the binding of CO to the surface would result, which would be reflected in different TPD peaks. However, such an effect is not observed. Furthermore, the sticking of CO does not significantly depend on the surface composition, as GaN samples with identical doping but different degrees of surface oxidation exhibit identical CO desorption characteristics in TPD experiments. To explain these effects, we propose the following adsorption model, which is sketched in Figure 6 and considers the dependence of the CO sticking on the semiconductor doping.

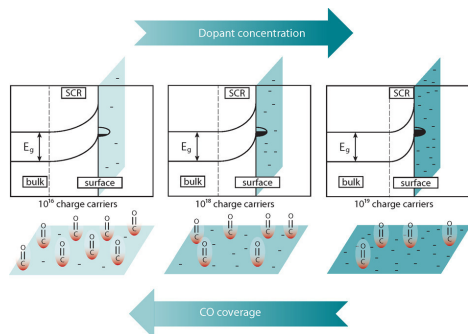


Figure 6. Influence of bulk doping on the CO adsorption on GaN(0001). Because samples with the same surface morphology are obtained by epitaxy, bulk doping only significantly affects the space charge region (SCR) below the GaN surface. Consequently a different degree of electron accumulation in the surface states is obtained. The occupation of surface states and the negative surface charges in the figure are for illustrative purposes only. A higher n-doping results in a higher negative charge density at the semiconductor's surface, which enables the adsorption of only a few electron donors such as CO. Therefore, less CO is bound on higher n-doped GaN samples, whereas on nonintentionally n-doped GaN the highest CO coverage is observed.

All of the investigated semiconductors are n-type and therefore exhibit accumulation of electrons in surface sites, which results in an upward band bending.⁵³ Moreover, from surface photovoltage experiments it is known that this band bending at the surface occurs in a very similar manner for all of the samples.⁵⁴ However, a different amount of doping results in a different depth of the space charge region (SCR) and a different degree of electron accumulation in the surface sites. From calculations similar to those previously reported,⁵⁴ performed with the nextnano software package,⁵⁵ we estimate

that the surface charge density increases by about 1 order of magnitude when the doping is changed from the value of sample a (nominally undoped) to that of sample c (highly n-type-doped).

CO is considered to be an electron donor, and it is expected that the physisorbed molecule donates some negative charge to the semiconductor. Thus CO is expected to adsorb on surface sites sufficiently far away from the negatively charged, electronically active surface defects, which are responsible for the upward band bending. A similar phenomenon was observed for NH_3 on $\text{TiO}_2(110)$, where the ammonia molecules are repelled by an increased number of negative surface states of the n-type semiconductor.⁵⁶ This is also in very good agreement with our simulations and shows that doping itself is indeed changing the surface charge density and thus the adsorption properties of the molecules. Consequently, on the surface of a highly n-doped GaN, where the density of negatively charged surface states is higher, less CO would be adsorbed in comparison with a nominally undoped GaN sample with less negative charge.

Photon-Stimulated Desorption of CO. Figure 3 shows that upon UV illumination a fraction of the adsorbed CO desorbs from the GaN(0001) surface. It is found that the kinetics of this process is not influenced by semiconductor doping, as it can be seen in Figure 4. Because the SCR changes with the degree of doping, it can be concluded that the size of the SCR does not significantly affect the desorption rate. Similarly, the same exponential decay is also observed for GaN surfaces with different degrees of oxidation. However, and in contrast with the CO adsorption, the presence of oxygen instead of nitrogen reduces the PSD intensity. As a consequence, it can be concluded that certain adsorption sites exist, which promote the photodesorption of CO (photoactive sites). These sites diminish for higher degrees of oxidation, which is accompanied by the release of nitrogen. As a result of the existence of these photoactive sites, only a fraction of CO can be photodesorbed, while the remaining molecules can only be removed from the GaN surface thermally (Figure 3). We note that it is observed that the photoactive sites are again accessible after the PSD, as subsequent dosing of CO without any thermal cleaning step results in the same PSD signal as before. Comparing the fast and the slow time constants of the PSD decay with previous photo decay and contact potential difference (CPD) measurements of GaN,⁵⁴ similar time constants of a few seconds and minutes are obtained. The CPD decay has been assigned to the transfer of photogenerated holes to the surface and subsequent capture in electron-filled surface sites,⁵⁴ leading to compensation of the negative charge accumulated at the surface. That the desorption process in PSD experiments is indeed a photochemical one, based on the extinction of charge transferred from CO to the semiconductor, is evidenced by the desorption behavior of CO_2 , which has also been investigated. The TPD of CO_2 on GaN(0001) is very similar to that of CO (Figure S3), and desorption of both molecules is observed at roughly the same temperature. However, no photoinitiated desorption occurs for carbon dioxide. Consequently, local thermal effects originating from the recombination of charge carriers in the vicinity of the adsorbed molecules can be excluded for the PSD of CO, as these would also lead to the desorption of other weakly bound species, for example, CO_2 . In general, upon illumination of an n-type semiconductor, holes move to the surface and neutralize the negatively charged electronic surface states. Immediately

after UV excitation, CO desorbs from the GaN surface (Figure 3b). Detailed mechanisms for photon-stimulated desorption on the atomic scale are still largely unknown and under discussion.^{36,37,57–59} However, it is known that a charge redistribution at the surface alters the electrostatics of the molecule–surface interaction and gives rise to a PSD.⁵⁸ Under the assumption that CO binds with a negative partial charge redistribution to the GaN surface, the molecule–surface interaction can only be weakened when the charge donation is neutralized and consequently a PSD arises. Because in an illuminated n-type semiconductor only holes from the SCR move to the surface, only negative charge states in surface vicinity can be involved. In this picture minority and majority charge carriers may contribute to the atomic PSD mechanism.^{59,60} Experimental data provide evidence that the CO PSD can also occur on p-doped GaN; however, only a very small quantity of CO can be photodesorbed (Figure S4). Consequently both electrons and holes seem to be able to activate the photon-stimulated desorption of CO.

CONCLUSIONS

We demonstrate for the model system CO on GaN(0001) that the adsorption of molecules on semiconductors can be doping-dependent. The change of the n-type doping of GaN results in different amounts of CO on the semiconductors' surface and eventually different saturation coverages. We introduce a model based on the electronic characteristics of the semiconductor, which is capable of explaining this effect qualitatively. With higher n-type doping less carbon monoxide can be adsorbed due to a higher density of negatively charged surface states. Furthermore, the first observation of a photodesorption on GaN is reported. It is found that the kinetics of the PSD are independent of the degree of doping or the surface oxidation state. However, the surface composition influences the PSD intensity, which is related to the existence of photoactive sites. The number of these sites can be reduced by a higher degree of oxidation of the GaN semiconductor surface. Furthermore, by a comparative study of CO₂, local thermal heating effects originating from charge-carrier recombination can be ruled out as the origin of the photon-stimulated desorption. We propose that the CO PSD is indeed a process based on the compensation of transferred charge density from the molecule to the semiconductor, which can be facilitated by electrons and holes.

ASSOCIATED CONTENT

Supporting Information

The Supporting Information is available free of charge on the ACS Publications website at DOI: 10.1021/acs.jpcc.7b01570.

AFM pictures of differently doped PIMBE GaN(0001) surfaces, CO PSD signals of different excitation wavelengths and intensities, TPD spectrum of CO₂ dosed on GaN, and CO PSD signal of the p-type doped GaN sample. (PDF)

AUTHOR INFORMATION

Corresponding Author

*E-mail: ulrich.heiz@mytum.de. Tel: +49 (0) 89 289 13391. Fax: +49 (0) 89 289 13389.

ORCID

Martin Tschurl: 0000-0001-6618-7312

Author Contributions

^{||}S.L.K. and C.A.W. contributed equally to this work.

Notes

The authors declare no competing financial interest.

ACKNOWLEDGMENTS

We thank the DFG through grants HE3435/22-1 and STU139/12-1 for financial support.

REFERENCES

- (1) Shimura, K.; Yoshida, H. Heterogeneous Photocatalytic Hydrogen Production from Water and Biomass Derivatives. *Energy Environ. Sci.* **2011**, *4*, 2467–2481.
- (2) Takanabe, K.; Domen, K. Toward Visible Light Response: Overall Water Splitting Using Heterogeneous Photocatalysts. *Green* **2011**, *1*, 313–322.
- (3) Chen, X.; Shen, S.; Guo, L.; Mao, S. S. Semiconductor-Based Photocatalytic Hydrogen Generation. *Chem. Rev. (Washington, DC, U. S.)* **2010**, *110*, 6503–6570.
- (4) Hayashi, T.; Deura, M.; Ohkawa, K. High Stability and Efficiency of GaN Photocatalyst for Hydrogen Generation from Water. *Jpn. J. Appl. Phys.* **2012**, *51*, 112601.
- (5) Kida, T.; Minami, Y.; Guan, G.; Nagano, M.; Akiyama, M.; Yoshida, A. Photocatalytic Activity of Gallium Nitride for Producing Hydrogen from Water under Light Irradiation. *J. Mater. Sci.* **2006**, *41*, 3527–3534.
- (6) Ohno, T.; Bai, L.; Hisatomi, T.; Maeda, K.; Domen, K. Photocatalytic Water Splitting Using Modified GaN:ZnO Solid Solution under Visible Light: Long-Time Operation and Regeneration of Activity. *J. Am. Chem. Soc.* **2012**, *134*, 8254–8259.
- (7) Maeda, K.; Takata, T.; Hara, M.; Saito, N.; Inoue, Y.; Kobayashi, H.; Domen, K. GaN:ZnO Solid Solution as a Photocatalyst for Visible-Light-Driven Overall Water Splitting. *J. Am. Chem. Soc.* **2005**, *127*, 8286–8287.
- (8) Maeda, K.; Teramura, K.; Lu, D.; Takata, T.; Saito, N.; Inoue, Y.; Domen, K. Photocatalyst Releasing Hydrogen from Water. *Nature* **2006**, *440*, 295–295.
- (9) Maeda, K.; Xiong, A.; Yoshinaga, T.; Ikeda, T.; Sakamoto, N.; Hisatomi, T.; Takashima, M.; Lu, D.; Kanehara, M.; Setoyama, T.; et al. Photocatalytic Overall Water Splitting Promoted by Two Different Cocatalysts for Hydrogen and Oxygen Evolution under Visible Light. *Angew. Chem.* **2010**, *122*, 4190–4193.
- (10) Lu, X.; Bandara, A.; Katayama, M.; Yamakata, A.; Kubota, J.; Domen, K. Infrared Spectroscopic Study of the Potential Change at Cocatalyst Particles on Oxynitride Photocatalysts for Water Splitting by Visible Light Irradiation. *J. Phys. Chem. C* **2011**, *115*, 23902–23907.
- (11) Jung, H. S.; Hong, Y. J.; Li, Y.; Cho, J.; Kim, Y.-J.; Yi, G.-C. Photocatalysis Using GaN Nanowires. *ACS Nano* **2008**, *2*, 637–642.
- (12) Ji, X. Z.; Somorjai, G. A. Continuous Hot Electron Generation in Pt/TiO₂, Pd/TiO₂, and Pt/GaN Catalytic Nanodiodes from Oxidation of Carbon Monoxide. *J. Phys. Chem. B* **2005**, *109*, 22530–22535.
- (13) Park, J. Y.; Somorjai, G. A. Energy Conversion from Catalytic Reaction to Hot Electron Current with Metal-Semiconductor Schottky Nanodiodes. *J. Vac. Sci. Technol., B* **2006**, *24*, 1967–1971.
- (14) Park, J. Y.; Renzas, J. R.; Hsu, B. B.; Somorjai, G. A. Interfacial and Chemical Properties of Pt/TiO₂, Pd/TiO₂, and Pt/GaN Catalytic Nanodiodes Influencing Hot Electron Flow. *J. Phys. Chem. C* **2007**, *111*, 15331–15336.
- (15) Kim, S. M.; Lee, S. J.; Kim, S. H.; Kwon, S.; Yee, K. J.; Song, H.; Somorjai, G. A.; Park, J. Y. Hot Carrier-Driven Catalytic Reactions on Pt-CdSe-Pt Nanodumbbells and Pt/GaN under Light Irradiation. *Nano Lett.* **2013**, *13*, 1352–1358.
- (16) Park, J. Y.; Baker, L. R.; Somorjai, G. A. Role of Hot Electrons and Metal-Oxide Interfaces in Surface Chemistry and Catalytic Reactions. *Chem. Rev. (Washington, DC, U. S.)* **2015**, *115*, 2781–2817.
- (17) Khan, M. A.; Kuznia, J. N.; Olson, D. T.; Van Hove, J. M.; Blasingame, M.; Reitz, L. F. High-Responsivity Photoconductive

Ultraviolet Sensors Based on Insulating Single-Crystal GaN Epilayers. *Appl. Phys. Lett.* **1992**, *60*, 2917–2919.

(18) Long, J. P.; Bermudez, V. M. Band Bending and Photoemission-Induced Surface Photovoltages on Clean n- and p-GaN (0001) Surfaces. *Phys. Rev. B: Condens. Matter Mater. Phys.* **2002**, *66*, 121308–121311.

(19) Hirai, T.; Maeda, K.; Yoshida, M.; Kubota, J.; Ikeda, S.; Matsumura, M.; Domen, K. Origin of Visible Light Absorption in GaN-Rich ($\text{Ga}_{1-x}\text{Zn}_x$)(N_{1-x}O_x) Photocatalysts. *J. Phys. Chem. C* **2007**, *111*, 18853–18855.

(20) Oshima, C.; Nishiyama, H.; Chatterjee, A.; Uchida, K.; Sato, K.; Inoue, Y.; Hisatomi, T.; Domen, K. Photocatalytic Activity of $\text{ZnO}/\text{GaP}_{1-x}\text{N}_x$ for Water Splitting. *J. Mater. Chem. A* **2015**, *3*, 18083–18089.

(21) Diebold, U. The Surface Science of Titanium Dioxide. *Surf. Sci. Rep.* **2003**, *48*, 53–229.

(22) Henderson, M. A. A Surface Science Perspective on TiO_2 Photocatalysis. *Surf. Sci. Rep.* **2011**, *66*, 185–297.

(23) Shekhar, R.; Jensen, K. F. Temperature Programmed Desorption Investigations of Hydrogen and Ammonia Reactions on GaN. *Surf. Sci.* **1997**, *381*, L581–L588.

(24) Xie, M. H.; Seutter, S. M.; Zhu, W. K.; Zheng, L. X.; Wu, H.; Tong, S. Y. Anisotropic Step-Flow Growth and Island Growth of GaN(0001) by Molecular Beam Epitaxy. *Phys. Rev. Lett.* **1999**, *82*, 2749–2752.

(25) Ambacher, O.; Brandt, M. S.; Dimitrov, R.; Metzger, T.; Stutzmann, M.; Fischer, R. A.; Miehler, A.; Bergmaier, A.; Dollinger, G. Thermal Stability and Desorption of Group III Nitrides Prepared by Metal Organic Chemical Vapor Deposition. *J. Vac. Sci. Technol., B: Microelectron. Process. Phenom.* **1996**, *14*, 3532–3542.

(26) Smith, A. R.; Feenstra, R. M.; Greve, D. W.; Neugebauer, J.; Northrup, J. E. Reconstructions of the GaN(000 $\bar{1}$) Surface. *Phys. Rev. Lett.* **1997**, *79*, 3934–3837.

(27) Smith, A. R.; Feenstra, R. M.; Greve, D. W.; Shin, M. S.; Skowronski, M.; Neugebauer, J.; Northrup, J. E. Reconstructions of GaN(0001) and (000 $\bar{1}$) Surfaces: Ga-rich Metallic Structures. *J. Vac. Sci. Technol., B: Microelectron. Process. Phenom.* **1998**, *16*, 2242–2249.

(28) Schulz, C.; Kuhr, S.; Geffers, H.; Schmidt, T.; Flege, J. I.; Aschenbrenner, T.; Hommel, D.; Falta, J. Cleaning of GaN($\bar{2}$ 110) Surfaces. *J. Vac. Sci. Technol., A* **2011**, *29*, 011013.

(29) Morkoç, H.; Mohammad, S. N. High-Luminosity Blue and Blue-Green Gallium Nitride Light-Emitting Diodes. *Science* **1995**, *267*, 51–55.

(30) Shur, M. S. GaN Based Transistors for High Power Applications. *Solid-State Electron.* **1998**, *42*, 2131–2138.

(31) Zhang, Z.; Yates, J. T. Electron-Mediated CO Oxidation on the TiO_2 (110) Surface During Electronic Excitation. *J. Am. Chem. Soc.* **2010**, *132*, 12804–12807.

(32) Green, I. X.; Tang, W.; Neurock, M.; Yates, J. T. Insights into Catalytic Oxidation at the Au/ TiO_2 Dual Perimeter Sites. *Acc. Chem. Res.* **2014**, *47*, 805–815.

(33) Yanagisawa, Y.; Ota, Y. Thermal and Photo-Stimulated Desorption of Chemisorbed Oxygen Molecules from Titanium Dioxide Surfaces. *Surf. Sci.* **1991**, *254*, L433–L436.

(34) Thompson, T. L.; Yates, J. T. Monitoring Hole Trapping in Photoexcited TiO_2 (110) Using a Surface Photoreaction. *J. Phys. Chem. B* **2005**, *109*, 18230–18236.

(35) Petrik, N. G.; Kimmel, G. A. Electron- and Hole-Mediated Reactions in UV-Irradiated O_2 Adsorbed on Reduced Rutile TiO_2 (110). *J. Phys. Chem. C* **2011**, *115*, 152–164.

(36) Petrik, N. G.; Kimmel, G. A.; Shen, M.; Henderson, M. A. Quenching of Electron Transfer Reactions through Coadsorption: A Study of Oxygen Photodesorption from TiO_2 (110). *Surf. Sci.* **2016**, *652*, 183.

(37) Rusu, C. N.; Yates, J. T. Photochemistry of NO Chemisorbed on TiO_2 (110) and TiO_2 Powders. *J. Phys. Chem. B* **2000**, *104*, 1729–1737.

(38) Shapira, Y.; McQuistan, R. B.; Lichtman, D. Relationship Between Photodesorption and Surface Conductivity in ZnO. *Phys. Rev. B* **1977**, *15*, 2163–2169.

(39) Winnerl, A.; Pereira, R. N.; Stutzmann, M. Kinetics of Optically Excited Charge Carriers at the GaN Surface: Influence of Catalytic Pt Nanostructures. *J. Appl. Phys.* **2015**, *118*, 155704.

(40) Walenta, C. A.; Kollmannsberger, S. L.; Kiermaier, J.; Winbauer, A.; Tschurl, M.; Heiz, U. Ethanol Photocatalysis on Rutile TiO_2 (110): the Role of Defects and Water. *Phys. Chem. Chem. Phys.* **2015**, *17*, 22809–22814.

(41) Heying, B.; Averbeck, R.; Chen, L. F.; Haus, E.; Riechert, H.; Speck, J. S. Control of GaN Surface Morphologies Using Plasma-Assisted Molecular Beam Epitaxy. *J. Appl. Phys.* **2000**, *88*, 1855–1860.

(42) Schuster, F.; Winnerl, A.; Weiszer, S.; Hetzl, M.; Garrido, J. A.; Stutzmann, M. Doped GaN Nanowires on Diamond: Structural Properties and Charge Carrier Distribution. *J. Appl. Phys.* **2015**, *117*, 044307.

(43) Karrer, U.; Ambacher, O.; Stutzmann, M. Influence of Crystal Polarity on the Properties of Pt/GaN Schottky Diodes. *Appl. Phys. Lett.* **2000**, *77*, 2012–2014.

(44) Lu, G.; Linsebigler, A.; Yates, J. T. The Photochemical Identification of Two Chemisorption States for Molecular Oxygen on TiO_2 (110). *J. Chem. Phys.* **1995**, *102*, 3005–3008.

(45) Schlichting, H.; Menzel, D. Techniques for Attainment, Control, and Calibration of Cryogenic Temperatures at Small Single-Crystal Samples under Ultrahigh Vacuum. *Rev. Sci. Instrum.* **1993**, *64*, 2013–2022.

(46) Dohnálek, Z.; Kimmel, G. A.; Joyce, S. A.; Ayotte, P.; Smith, R. S.; Kay, B. D. Physisorption of CO on the MgO(100) Surface. *J. Phys. Chem. B* **2001**, *105*, 3747–3751.

(47) Grabow, L.; Uhlrich, J.; Kuech, T.; Mavrikakis, M. Effectiveness of in situ NH_3 Annealing Treatments for the Removal of Oxygen from GaN Surfaces. *Surf. Sci.* **2009**, *603*, 387–399.

(48) King, S. W.; Barnak, J. P.; Bremser, M. D.; Tracy, K. M.; Ronning, C.; Davis, R. F.; Nemanich, R. J. Cleaning of AlN and GaN Surfaces. *J. Appl. Phys.* **1998**, *84*, 5248–5260.

(49) Ishikawa, H.; Kobayashi, S.; Koide, Y.; Yamasaki, S.; Nagai, S.; Umezaki, J.; Koike, M.; Murakami, M. Effects of Surface Treatments and Metal Work Functions on Electrical Properties at p-GaN/Metal Interfaces. *J. Appl. Phys.* **1997**, *81*, 1315–1322.

(50) Hunt, R.; Vanzetti, L.; Castro, T.; Chen, K.; Sorba, L.; Cohen, P.; Gladfelter, W.; Van Hove, J. M.; Kuznia, J.; Khan, M.; et al. Electronic Structure, Surface Composition and Long-Range Order in GaN. *Phys. B* **1993**, *185*, 415–421.

(51) Childs, K. D.; Carlson, B. A.; Vanier, L. A.; Moulder, J. F.; Paul, D. F.; Stickle, W. F.; Watson, D. G. *Handbook of Auger Electron Spectroscopy*; Physical Electronics Industries: Chanhassen, MN, 1995.

(52) Watkins, N. J.; Wicks, G. W.; Gao, Y. Oxidation Study of GaN Using X-ray Photoemission Spectroscopy. *Appl. Phys. Lett.* **1999**, *75*, 2602–2604.

(53) Zhang, Z.; Yates, J. T. Band Bending in Semiconductors: Chemical and Physical Consequences at Surfaces and Interfaces. *Chem. Rev. (Washington, DC, U. S.)* **2012**, *112*, 5520–5551.

(54) Winnerl, A.; Pereira, R. N.; Stutzmann, M. Kinetics of Optically Excited Charge Carriers at the GaN Surface. *Phys. Rev. B: Condens. Matter Mater. Phys.* **2015**, *91*, 075316–075327.

(55) Birner, S.; Zibold, T.; Andlauer, T.; Kubis, T.; Sabathil, M.; Trellakis, A.; Vogl, P. Nextnano: General Purpose 3-D Simulations. *IEEE Trans. Electron Devices* **2007**, *54*, 2137–2142.

(56) Kim, B.; Li, Z.; Kay, B. D.; Dohnálek, Z.; Kim, Y. K. The Effect of Oxygen Vacancies on the Binding Interactions of NH_3 with Rutile TiO_2 (110)-1 \times 1. *Phys. Chem. Chem. Phys.* **2012**, *14*, 15060–15065.

(57) Henderson, M. A. Visible Light Induced Photodesorption of NO from the $\alpha\text{-Cr}_2\text{O}_3$ (0001) Surface. *Surf. Sci.* **2012**, *606*, 505–509.

(58) Henderson, M. A.; Mu, R.; Dahal, A.; Lyubinetsky, I.; Dohnálek, Z.; Glezakou, V.-A.; Rousseau, R. Light Makes a Surface Banana-Bond Split: Photodesorption of Molecular Hydrogen from RuO_2 (110). *J. Am. Chem. Soc.* **2016**, *138*, 8714–8717.

(59) Petrik, N. G.; Kimmel, G. A. Probing the Photochemistry of Chemisorbed Oxygen on TiO₂(110) with Kr and Other Co-Adsorbates. *Phys. Chem. Chem. Phys.* **2014**, *16*, 2338–2346.

(60) Linsebigler, A.; Lu, G.; Yates, J. T. CO Photooxidation on TiO₂(110). *J. Phys. Chem.* **1996**, *100*, 6631–6636.

Supporting information for:
Doping-Dependent Adsorption and
Photon-Stimulated Desorption of CO on
GaN(0001)

Sebastian L. Kollmannsberger,^{†,§} Constantin A. Walenta,^{†,‡,§} Andrea Winnerl,[¶]
Saskia Weiszer,[¶] Rui N. Pereira,[¶] Martin Tschurl,[†] Martin Stutzmann,^{¶,‡} and Ueli
Heiz^{*,†,‡}

*Chair of Physical Chemistry, Department of Chemistry & Catalysis Research Center,
Technische Universität München, Lichtenbergstr. 4, 85748 Garching, Germany,
Nanosystems Initiative Munich, Schellingstr. 4, 80799 München, Germany, and Walter
Schottky Institute and Physics Department, Technische Universität München, Am
Coulombwall 4, 85748 Garching, Germany*

E-mail: ulrich.heiz@mytum.de

Phone: +49 (0) 89 289 13391. Fax: +49 (0) 89 289 13389

*To whom correspondence should be addressed

[†]Chair of Physical Chemistry, Department of Chemistry & Catalysis Research Center, Technische Universität München, Lichtenbergstr. 4, 85748 Garching, Germany

[‡]Nanosystems Initiative Munich, Schellingstr. 4, 80799 München, Germany

[¶]Walter Schottky Institute and Physics Department, Technische Universität München, Am Coulombwall 4, 85748 Garching, Germany

[§]The authors contributed equally to this work

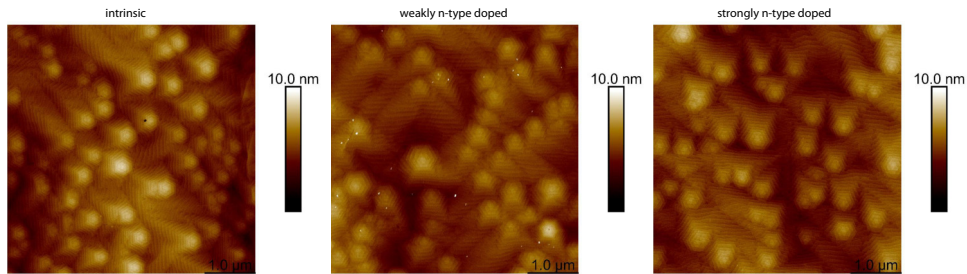


Figure S1: AFM images of differently doped PIMBE GaN(0001) surfaces. The images show that the surface morphology is unaffected by doping.

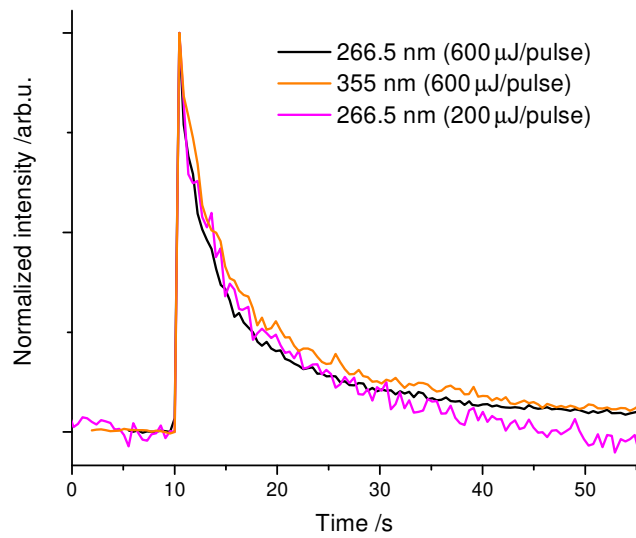


Figure S2: Intensity normalized PSD signal of different UV wavelength (266.5 nm or 355 nm) and UV intensities (200 $\mu\text{J}/\text{pulse}$ or 600 $\mu\text{J}/\text{pulse}$). The decays show no appreciable differences, which indicates that the kinetics of the PSD do not change significantly with the variation of UV wavelength and UV intensity.

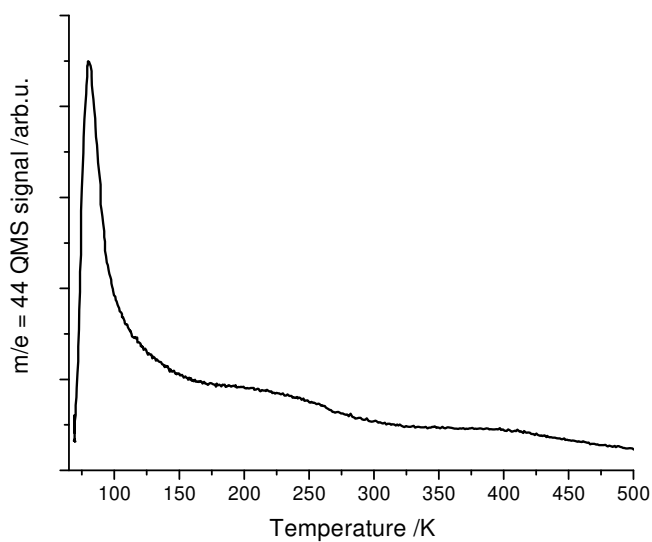


Figure S3: TPD spectrum from CO₂ dosed on a GaN(0001) surface. The low temperature peak is very similar to that of CO on GaN. Analogously, the small high temperature features originate from CO₂ desorption from the sample holder.

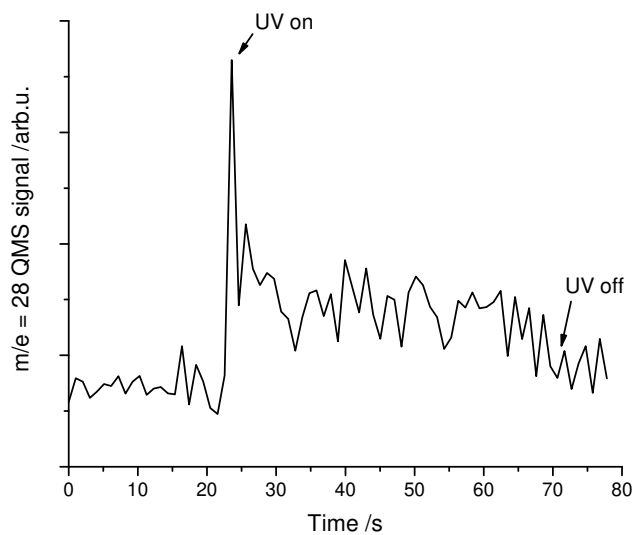


Figure S4: CO PSD spectrum of p-type GaN(0001). Note that the signal is comparably small since the surface has a low N/O ratio. The PSD is carried out at LN₂ temperature after 4 L CO exposure. By illumination with 266.5 nm UV light, a rise in the CO intensity is observed.


D.4. Anhydrous Ethanol Dehydrogenation on Metal–Organic Chemical Vapor Deposition Grown GaN (0001)

THE JOURNAL OF
PHYSICAL CHEMISTRY C

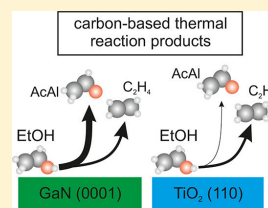
Article

pubs.acs.org/JPC

Anhydrous Ethanol Dehydrogenation on Metal–Organic Chemical Vapor Deposition Grown GaN(0001)

Constantin A. Walenta,^{†,‡,||} Sebastian L. Kollmannsberger,^{†,||} Rui N. Pereira,[§] Martin Tschurl,^{†,⊕}
Martin Stutzmann,^{‡,§} and Ueli Heiz^{*,†,‡}[†]Chair of Physical Chemistry, Department of Chemistry & Catalysis Research Center, Technische Universität München, Lichtenbergstrasse 4, 85748 Garching, Germany[‡]Nanosystems Initiative Munich, Schellingstrasse 4, 80799 München, Germany[§]Walter Schottky Institute and Physics Department, Technische Universität München, Am Coulombwall 4, 85748 Garching, Germany Supporting Information

ABSTRACT: In this ultrahigh vacuum study, temperature-programmed desorption, Auger electron spectroscopy, and ex-situ atomic force microscopy are used to evaluate the surface chemistry of ethanol on the GaN(0001) surface. Ethanol undergoes dehydration and dehydrogenation reactions on the GaN(0001) surface to a larger extent than on the TiO₂(110) surface. This enhanced reactivity is attributed to a higher amount of metal-bound ethoxy. In addition, molecular H₂ has been identified as a byproduct of the ethanol dehydrogenation to acetaldehyde. We attribute the reactivity, including the formation of molecular hydrogen, to the combination of wurtzite structure and nitride chemistry, since surface amines are considered to be less stable than surface hydroxyls on other model oxides.



INTRODUCTION

The reforming of ethanol has recently attracted attention, as this alcohol may act as hydrogen sources and renewable feedstocks in heterogeneous^{7–9} and photocatalysis.^{7–10} While hydrogen generation is feasible on noble metals supported on various oxides, new noble-metal-free catalysts are limited in selectivity and activity, so far.^{4,11–14} On the one hand, ethanol dehydrogenation on many oxides leads to the formation of water instead of H₂¹¹ and is accompanied by side reactions such as further oxidations of the acetaldehyde. On the other hand, supported metal catalysts even exhibit more complex reaction networks and show deactivation by coking.¹⁴ In order to understand the reactivity of materials and the underlying reaction mechanisms at the atomic scale, ultrahigh vacuum (UHV) studies have been conducted with the aim to eventually overcome a reduction of efficiencies by undesired side reactions and avoid catalyst deactivation under applied conditions. However, mostly oxide model systems, e.g., TiO₂(110), have so far been considered in such fundamental studies.^{15–20} Additionally, a variety of surfaces of catalytic active metals have been investigated, such as Ru(0001),²¹ Pt(111),²² Pd(110),²³ and Pd(111).²³ On all of these metal surfaces ethanol decomposition to CO accompanied by the evolution of H₂ is observed. At the same time the surface is passivated by the formation of carbon deposits.^{14,21} Despite the use of GaN in semiconductor technology^{24,25} and photocatalysis,^{26,27} the surface chemistry of nitrides has hitherto been rather neglected. In this work, we investigate the reaction pathways of ethanol on a gallium nitride model system. The GaN(0001) surface is

compared with a TiO₂(110) one, for which the mechanistic details of alcohol surface chemistry have been studied extensively.^{16–20,28} Most prominently, the major reaction pathway on TiO₂(110) is the dehydration to ethylene and water.^{16,18} The dehydrogenation reaction to acetaldehyde is only a minor reaction channel for which water is again the byproduct, instead of molecular hydrogen formation, which would be expected from stoichiometry.^{17,29}

EXPERIMENTAL SECTION

Unintentionally doped GaN(0001) grown on sapphire by metal–organic chemical vapor deposition (MOCVD) is obtained from Lumilog and a charge carrier concentration of $1.4 \times 10^{17} \text{ cm}^{-3}$ is determined by Hall measurements.³⁰ The apparatus for studies in the UHV has been described previously.^{29,31} In short, the sample is mounted in a cutout of a tantalum heating plate and fixed by thin tantalum clamps to ensure good thermal and electrical conductivity to the liquid N₂ cooled manipulator. The chamber is equipped with a differentially pumped quadrupole mass spectrometer (QMS, QMA 430, Pfeiffer Vacuum GmbH), a molecular beam doser, a sputter gun (IQE 11/35, SPECS GmbH), and an Auger electron spectrometer (AES, CMA 100, Omicron Nanotechnology GmbH). Typically, a base pressure of 8.0×10^{-11} mbar is reached. The temperature is monitored using a twisted

Received: May 22, 2017

Revised: June 29, 2017

Published: July 7, 2017

type-C thermocouple.³² The GaN(0001) surface was cleaned by annealing at 800 K and sputtering until a carbon-free surface was obtained. The surface cleaning and morphology was monitored by AES and ex-situ AFM measurements. The surface morphology of the sample [see Figure S5 of the Supporting Information (SI)] exhibits the typical characteristics known from the literature.^{33–36} The TiO₂(110) single-crystal surface (Surface-Net GmbH) was cleaned by repeated cycles of Ar⁺-sputtering, oxygen annealing, and vacuum annealing until a dark blue surface with a bridge-bonding oxygen (BBO) defect density of about 10% [*r*-TiO₂(110)] was obtained.^{29,37} Ethanol (absolute, HPLC grade, ≥99.8%, Sigma-Aldrich) was purified by several pump–freeze cycles. The adsorption temperature for ethanol on the sample was 110 K, and temperature-programmed desorption (TPD) experiments were conducted with a constant heating rate of 1.2 K/s to 700 K. The monolayer coverage is normalized to the number of metal surface atoms, being 1 ML ≡ 5.2 × 10¹⁴ cm⁻² for the Ti⁴⁺ concentration on the TiO₂(110) surface^{19,37} and 1 ML ≡ 6.0 × 10¹⁴ cm⁻² for the Ga³⁺ concentration on the GaN(0001) surface. The gallium surface atom density is calculated from the unit cell and the bulk lattice constants, assuming a perfectly flat surface.^{19,38} The cracking pattern analysis accounts for ionization cross sections, transmission coefficients, cracking patterns, and the respective fragment intensities.^{39–41}

RESULTS

The desorption of ethanol from a MOCVD-grown n-type GaN(0001) surface (Figure 1) exhibits the following character-

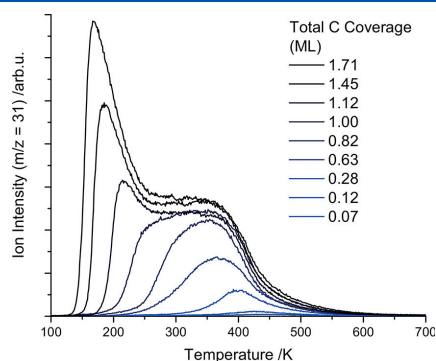


Figure 1. TPD spectra of ethanol adsorbed at 110 K. While for the lowest coverage desorption is not observed, eventually two features evolve for higher coverages, which can be attributed to desorption from different binding sites.

istics: At very low coverages, all ethanol molecules undergo reaction, as desorption of the intact molecule is not observed. Increasing coverages result in an ethanol desorption feature at around 420 K, which eventually shifts to 350 K. Such a shift of the leading edge of the desorption feature with increasing coverages can be attributed to second-order desorption kinetics, which generally results from dissociative adsorption.^{42,43}

At coverages greater than one monolayer, an additional low-temperature peak around 200 K is observed and growing in intensity, while the high-temperature feature remains constant. This second peak is attributed to desorption of ethanol from

nitrogen surface atoms, in analogy to the behavior of metal oxides.^{19,43} The absence of carbon deposits in AES data after TPD runs evidenced that coking does not occur on GaN(0001).

The product analysis (Figure 2) of different TPD measurements (Figure S1, SI) with accounted sensitivities and cracking

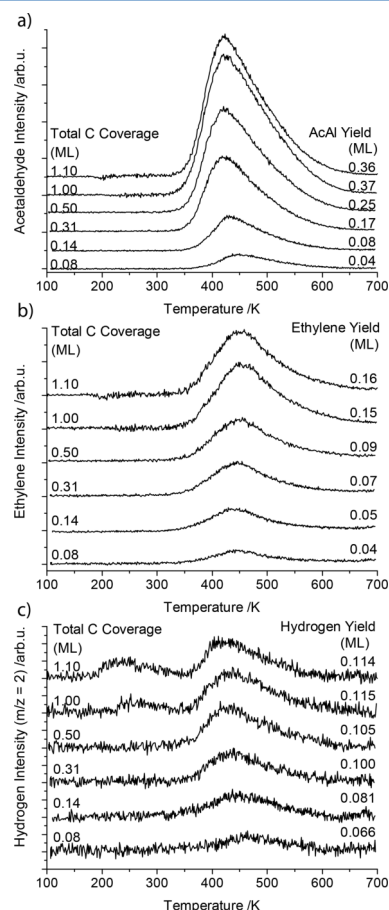


Figure 2. Fragmentation-corrected TPD spectra of acetaldehyde (a), ethylene (b), and molecular hydrogen (c) from ethanol adsorbed at 110 K. For the lowest ethanol coverage of 0.07 ML, the molecules are converted to acetaldehyde and ethylene. The acetaldehyde and ethylene yields saturate at 0.6 ML of the initial dosage. The bump at 220 K is caused by the very high ethanol coverages and originates from the ethanol-cracking pattern.

patterns for all carbon-containing species shows that all alcohol molecules undergo dehydration to ethylene or dehydrogenation to acetaldehyde for the lowest coverage. At a higher dosage of 0.14 ML still the vast majority of ethanol molecules react and only coverages above ≈0.3 ML exhibit significant desorption of the intact molecule. Ethanol dosages exceeding 0.6 ML result in the saturation of the acetaldehyde, ethylene, and hydrogen

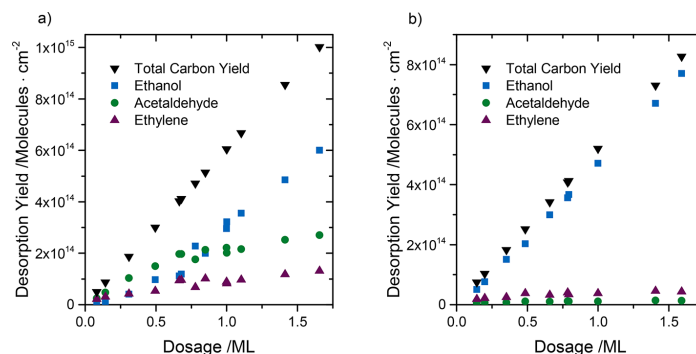


Figure 3. Integrated amounts of molecules desorbing from (a) MOCVD-grown GaN(0001) and for (b) rutile TiO₂(110) for different coverages. Ethanol is depicted in blue rectangles, acetaldehyde in green dots, and ethylene in purple triangles. The sum of all carbon-containing molecules desorbing is plotted in black triangles. Since no coking is observed (AES), the total carbon yield scales linearly with the dosage of ethanol. As it can be seen in the case of GaN, for coverages below 0.5 ML, acetaldehyde and ethylene are the main reaction channels. At higher coverages, these reaction channels are saturated and intact ethanol desorbs from the surface. The reactivity of ethanol is in very good agreement with the literature.^{16–18} The reactivity of ethanol toward ethylene on the r-TiO₂-surface is closely associated with bridge-bonding oxygen vacancies and the acetaldehyde production is on the same order of magnitude.^{17,18}

yields. Desorption of all these products is observed at 450 K. For higher coverages, their desorption maxima shifts to 400 K with a tail at the high-temperature side, indicating a consecutive reaction. As ethanol desorption generally occurs at lower temperatures than the desorption of the reaction products, the existence of a strongly bound ethanol intermediate (i.e., ethoxy species) is suggested, which undergoes reaction instead of desorption.

Although not stoichiometric, the yield in molecular hydrogen formation increases with a higher conversion to the products and also saturates at acetaldehyde and ethylene saturation coverages. Water as potential byproduct was also monitored, but no water formation could be detected (Figure S2, SI). All yields of carbon-containing species as a function of coverage are summarized in Figure 3a. It is found that ethanol reacts to acetaldehyde and ethylene until the yield saturates at 0.68 ML of ethanol dosage. Higher coverages only result in the desorption of ethanol and not in a further chemical reaction.

The reactivity of the GaN(0001) surface is compared to that of TiO₂(110) in the following, as the reaction mechanisms of alcohols are best investigated at the atomic scale on this surface. The integrated amounts (Figure 3b) from TPD experiments (Figure S3, SI) of ethanol on rutile TiO₂ are obtained in the same way as for GaN and are in good agreement with previous ones from the literature.^{16–20} Ethylene production on the surface has been attributed to a dehydration of ethanol in bridge-bonding oxygen (BBO) vacancies via a β -H-activation.^{16,18} Acetaldehyde formation from the dehydrogenation of ethanol molecules was also observed,¹⁷ although no yield of molecular hydrogen is observed from the TiO₂(110) surface.^{16,17} All reaction mechanisms, which also holds true for photochemical acetaldehyde production,^{29,44} involve surface hydroxyl formation, as they are known to be stable in a broad temperature range.^{45,46} This finally leads to water formation upon heating to high temperatures.^{20,45,47} The amount of converted ethanol on TiO₂(110) is in very good agreement with the number of oxygen vacancies on the crystal.^{18,29} However, the GaN(0001) surface is much more reactive and about 50% of 1 ML of ethanol is converted (Figure 4). The

major reaction channel is the dehydrogenation to acetaldehyde, while ethylene formation is only a side reaction.

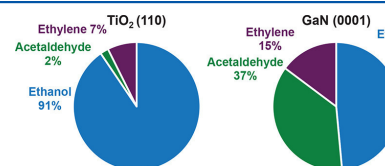


Figure 4. Selectivity for the respective coverages of 1 ML of GaN(0001) and TiO₂(110). For 1 ML of ethanol on TiO₂(110), about 90% of the ethanol desorbs while the rest undergoes dehydration and dehydrogenation to ethylene and acetaldehyde, respectively. While the former is the major reaction channel,^{16,18} the latter is the minor one.¹⁷ The total amount of conversion products is in very good agreement with the amount of BBO defect sites. However, the GaN(0001) surface proves to be very reactive toward the dehydrogenation and the dehydration channel and about half of the 1 ML coverage is converted to acetaldehyde and ethylene.

In contrast to TiO₂, no photochemical activity for the reaction with ethanol is observed on GaN(0001).²⁹ Irradiation with the above-band-gap wavelengths at liquid N₂ temperature results in neither a desorption of any molecules nor a change in a subsequent TPD scan (Figure S4, SI). The inertness of GaN toward ethanol in photoreactions may be attributed to the higher energetic position of the valence band with respect to the vacuum level in comparison to TiO₂.⁴⁸ Therefore, no matching energy states exist that enable a photo-oxidation channel.

DISCUSSION

The high-temperature desorption peak of an initial dose of 1.0 ML ethanol (Figure 1) can be assigned to originate from ethanol binding to Ga³⁺ atoms of the GaN(0001) surface. Its integral agrees with the calculated metal surface atom concentration from the unit cell. From the second-order desorption behavior, we infer that at least a part of the ethanol

molecules are adsorbed dissociatively and bound as ethoxy. The latter is a well-known intermediate in dehydrogenation and dehydration pathways via α -H and β -H elimination, respectively.^{16–18,49} The higher desorption temperatures of ethylene and acetaldehyde suggest that they are formed from a more strongly bound intermediate, as the main ethanol desorption occurs at lower temperatures. In analogy to previous reactivity studies for TiO₂(110)^{16–18,28} and also ZnO,^{50,51} we assign these stronger intermediates to ethoxy species.

From the saturation behavior in Figure 3, we estimate that about 50% of the adsorbed ethanol of the monolayer is bound dissociatively. Product analysis demonstrates that the dehydrogenation of ethanol is favored over the dehydration reaction on the GaN(0001) surface. In contrast, only a small fraction of ethanol on the TiO₂(110) surface undergoes dehydration and dehydrogenation, and the reactions are known to take only place in defect sites.^{17,18} The reactivity of GaN(0001) may instead be expected to be similar to that of ZnO(0001), which also exhibits a wurtzite structure. Indeed, for ZnO it is observed that dehydrogenation of ethanol is also favored over dehydration. However, it is known that the reactivity is limited to only occur on defects and step edges.^{15,51,52} An alternative interpretation is that the activity of the material is related to triangular structures on the wurtzite surface.⁵³ These structures may produce high concentrations of oxygen-terminated steps, which lead to a stabilization of charges on the surface that may facilitate ethoxy formation on the surface.⁵⁰ In contrast to the limited reactivity on ZnO, the conversion of products only saturates at 0.6 monolayers on the GaN(0001) surface. This supplies evidence that the reactivity of the surface does not occur in special defect sites and that ethanol does not exhibit preferential adsorption. The high amount of ethoxy intermediates may arise due to the oxophilicity of Ga and the peculiar binding of hydrogen atoms to the GaN surface.^{54–56} Figure 2 shows that some H₂ is detected around 400 K. This is similar to ZnO(0001), for which very small quantities of H₂ formation from ethanol on ZnO(0001) were reported.⁵⁰ The formation of molecular hydrogen occurs at the same temperature as the acetaldehyde generation but is lower than expected from stoichiometry. Therefore, it can be attributed to originate from the dehydrogenation reaction, as would be expected from stoichiometry. However, full stoichiometry and water formation is also not obtained, in agreement with previous studies.^{50–52} On most oxides, H₂ formation is hindered by a stable surface hydroxyl formation, which generally leads to water formation at high temperatures.^{20,29,45,47,57} The formation of molecular hydrogen can be an indication that potential formation of surface amines is less stable than that of surface hydroxyls, as for example on TiO₂(110).^{43,58} For this surface it is reported that hydroxyls remain at the surface even to very high temperatures,⁵⁹ while desorption of D₂ from a GaN film was observed to occur at significantly lower temperatures in a TPD experiment.⁶⁰ This suggests that nitrides in general may be prospective support materials for hydrogen formation, in particular if they exhibit a wurtzite structure. Furthermore, they may exhibit higher selectivities and no deactivation in comparison to metal-based catalysts.

CONCLUSION

In summary it is found that the GaN(0001) surface is very active toward dehydrogenation and dehydration pathways of ethanol. At a coverage of around 1 ML, 50% of the dosed ethanol amount is converted to either acetaldehyde or ethylene.

Similar to previous studies on oxides and in agreement with the higher desorption temperature, we attribute the Ga-bound ethoxy to be the active intermediate that is more strongly bound.^{16–18,28} The dehydrogenation of ethanol is strongly favored over the dehydration, and in contrast to most oxides, for example TiO₂(110), there is evidence for molecular hydrogen formation. This could imply that surface amines are less stable than surface hydroxyls so that hydrogen recombination and desorption are enabled. Therefore, nitrides may in general be favorable materials for hydrogen production from alcohol reforming, in particular if they simultaneously exhibit a wurtzite structure.

ASSOCIATED CONTENT

Supporting Information

The Supporting Information is available free of charge on the ACS Publications website at DOI: 10.1021/acs.jpcc.7b04946.

The raw data of a representative TPD of ethanol on MOCVD-grown GaN(0001), as well as some water traces for different ethanol coverages; the corrected TPD traces for ethanol on TiO₂(110); mass traces and TPD after photochemical experiments; and AFM pictures of the MOCVD-grown GaN(0001) surface to demonstrate the sample's morphology (PDF)

AUTHOR INFORMATION

Corresponding Author

*E-mail: ulrich.heiz@mytum.de. Phone: +49 (0) 89 289 13391. Fax: +49 (0) 89 289 13389.

ORCID

Martin Tschurl: 0000-0001-6618-7312

Author Contributions

||C.A.W. and S.L.K. contributed equally to this work.

Notes

The authors declare no competing financial interest.

ACKNOWLEDGMENTS

The authors thank the DFG through grant HE3435/22-1 and STU139/12-1 for financial support. C.A.W. thanks the Nanosystems Initiative Munich (NIM) for support. Furthermore, the authors thank Andrea Winnerl for the AFM measurements of the GaN(0001) samples.

REFERENCES

- (1) Haryanto, A.; Fernando, S.; Murali, N.; Adhikari, S. Current Status of Hydrogen Production Techniques by Steam Reforming of Ethanol: A Review. *Energy Fuels* **2005**, *19*, 2098–2106.
- (2) Ni, M.; Leung, D. Y.; Leung, M. K. A Review on Reforming Bio-Ethanol for Hydrogen Production. *Int. J. Hydrogen Energy* **2007**, *32*, 3238–3247.
- (3) Navarro, R. M.; Peña, M. A.; Fierro, J. L. G. Hydrogen Production Reactions from Carbon Feedstocks: Fossil Fuels and Biomass. *Chem. Rev. (Washington, DC, U. S.)* **2007**, *107*, 3952–3991.
- (4) Chladek, P.; Croiset, E.; Epling, W.; Hudgins, R. R. Characterization of Copper Foam as Catalytic Material in Ethanol Dehydrogenation. *Can. J. Chem. Eng.* **2007**, *85*, 917–924.
- (5) Nadeem, M.; Waterhouse, G.; Idriss, H. A Study of Ethanol Reactions on O₂-treated Au/TiO₂. Effect of Support and Metal Loading on Reaction Selectivity. *Surf. Sci.* **2016**, *650*, 40–50.
- (6) Shan, J.; Janvelyan, N.; Li, H.; Liu, J.; Egle, T. M.; Ye, J.; Biener, M. M.; Biener, J.; Friend, C. M.; Flytzani-Stephanopoulos, M. Selective Non-Oxidative Dehydrogenation of Ethanol to Acetaldehyde and

- Hydrogen on Highly Dilute NiCu Alloys. *Appl. Catal., B* **2017**, *205*, 541–550.
- (7) Bamwenda, G. R.; Tsubota, S.; Nakamura, T.; Haruta, M. Photoassisted Hydrogen Production from a Water-Ethanol Solution: a Comparison of Activities of Au-TiO₂ and Pt-TiO₂. *J. Photochem. Photobiol., A* **1995**, *89*, 177–189.
- (8) Murdoch, M.; Waterhouse, G. I. N.; Nadeem, M.; Metson, J. B.; Keane, M. A.; Howe, R. F.; Llorca, J.; Idriss, H. The effect of gold loading and particle size on photocatalytic hydrogen production from ethanol over Au/TiO₂ nanoparticles. *Nat. Chem.* **2011**, *3*, 489–492.
- (9) Kundu, S.; Vidal, A. B.; Nadeem, M. A.; Senanayake, S. D.; Idriss, H.; Liu, P.; Rodriguez, J. A.; Stacchiola, D. Ethanol Photoreaction on RuO₂/Ru-Modified TiO₂(110). *J. Phys. Chem. C* **2013**, *117*, 11149–11158.
- (10) Puga, A. V.; Forneli, A.; García, H.; Corma, A. Production of H₂ by Ethanol Photoreforming on Au/TiO₂. *Adv. Funct. Mater.* **2014**, *24*, 241–248.
- (11) Idriss, H.; Seebauer, E. Reactions of Ethanol over Metal Oxides. *J. Mol. Catal. A: Chem.* **2000**, *152*, 201–212.
- (12) Kim, Y. K.; Zhang, Z.; Parkinson, G. S.; Li, S.-C.; Kay, B. D.; Dohnálek, Z. Reactivity of FeO(111)/Pt(111) with Alcohols. *J. Phys. Chem. C* **2009**, *113*, 20020–20028.
- (13) Lusvardi, V.; Barteau, M.; Farneth, W. The Effects of Bulk Titania Crystal Structure on the Adsorption and Reaction of Aliphatic Alcohols. *J. Catal.* **1995**, *153*, 41–53.
- (14) Mattos, L. V.; Jacobs, G.; Davis, B. H.; Noronha, F. B. Production of Hydrogen from Ethanol: Review of Reaction Mechanism and Catalyst Deactivation. *Chem. Rev. (Washington, DC, U. S.)* **2012**, *112*, 4094–4123.
- (15) Vohs, J.; Barteau, M. Dehydration and Dehydrogenation of Ethanol and 1-Propanol on the Polar Surfaces of Zinc Oxide. *Surf. Sci.* **1989**, *221*, 590–608.
- (16) Gamble, L.; Jung, L. S.; Campbell, C. T. Decomposition and Protonation of Surface Ethoxys on TiO₂(110). *Surf. Sci.* **1996**, *348*, 1–16.
- (17) Farfan-Arribas, E.; Madix, R. J. Role of Defects in the Adsorption of Aliphatic Alcohols on the TiO₂(110) Surface. *J. Phys. Chem. B* **2002**, *106*, 10680–10692.
- (18) Kim, Y. K.; Kay, B. D.; White, J. M.; Dohnálek, Z. Alcohol Chemistry on Rutile TiO₂(110): The Influence of Alkyl Substituents on Reactivity and Selectivity. *J. Phys. Chem. C* **2007**, *111*, 18236–18242.
- (19) Li, Z.; Smith, R. S.; Kay, B. D.; Dohnálek, Z. Determination of Absolute Coverages for Small Aliphatic Alcohols on TiO₂(110). *J. Phys. Chem. C* **2011**, *115*, 22534–22539.
- (20) Hansen, J. Ø.; Huo, P.; Martinez, U.; Lira, E.; Wei, Y. Y.; Streber, R.; Lægsgaard, E.; Hammer, B.; Wendt, S.; Besenbacher, F. Direct Evidence for Ethanol Dissociation on Rutile TiO₂(110). *Phys. Rev. Lett.* **2011**, *107*, 136102.
- (21) Sturm, J.; Lee, C.; Bijkerk, F. Reactions of Ethanol on Ru(0001). *Surf. Sci.* **2013**, *612*, 42–47.
- (22) Lee, A. F.; Gawthorpe, D. E.; Hart, N. J.; Wilson, K. A Fast XPS Study of the Surface Chemistry of Ethanol over Pt(111). *Surf. Sci.* **2004**, *548*, 200–208.
- (23) Shekhar, R.; Barteau, M. A. Structure Sensitivity of Alcohol Reactions on (110) and (111) Palladium Surfaces. *Catal. Lett.* **1995**, *31*, 221–237.
- (24) Shur, M. S. GaN Based Transistors for High Power Applications. *Solid-State Electron.* **1998**, *42*, 2131–2138.
- (25) Morkoç, H.; Mohammad, S. N. High-Luminosity Blue and Blue-Green Gallium Nitride Light-Emitting Diodes. *Science* **1995**, *267*, 51–55.
- (26) Maeda, K.; Teramura, K.; Lu, D.; Takata, T.; Saito, N.; Inoue, Y.; Domen, K. Photocatalyst Releasing Hydrogen from Water. *Nature* **2006**, *440*, 295–295.
- (27) Ohno, T.; Bai, L.; Hisatomi, T.; Maeda, K.; Domen, K. Photocatalytic Water Splitting Using Modified GaN:ZnO Solid Solution under Visible Light: Long-Time Operation and Regeneration of Activity. *J. Am. Chem. Soc.* **2012**, *134*, 8254–8259.
- (28) Jensen, S. C.; Friend, C. M. The Dynamic Roles of Interstitial and Surface Defects on Oxidation and Reduction Reactions on Titania. *Top. Catal.* **2013**, *56*, 1377–1388.
- (29) Walenta, C. A.; Kollmannsberger, S. L.; Kiermaier, J.; Winbauer, A.; Tschurl, M.; Heiz, U. Ethanol Photocatalysis on Rutile TiO₂(110): The Role of Defects and Water. *Phys. Chem. Chem. Phys.* **2015**, *17*, 22809–22814.
- (30) Winnerl, A.; Pereira, R. N.; Stutzmann, M. Kinetics of Optically Excited Charge Carriers at the GaN Surface. *Phys. Rev. B: Condens. Matter Mater. Phys.* **2015**, *91*, 075316.
- (31) Kollmannsberger, S. L.; Walenta, C. A.; Winnerl, A.; Weiszer, S.; Pereira, R. N.; Tschurl, M.; Stutzmann, M.; Heiz, U. Doping-dependent Adsorption and Photon-stimulated Desorption of CO on GaN(0001). *J. Phys. Chem. C* **2017**, *121*, 8473–8479.
- (32) Smentkowski, V. S.; Yates, J. T. Universal Calibration of W5%Re vs W26%Re (Type-C) Thermocouples in the Temperature Range 32–2588 K. *J. Vac. Sci. Technol., A* **1996**, *14*, 260–265.
- (33) Ambacher, O.; Brandt, M. S.; Dimitrov, R.; Metzger, T.; Stutzmann, M.; Fischer, R. A.; Miehr, A.; Bergmaier, A.; Dollinger, G. Thermal Stability and Desorption of Group III Nitrides Prepared by Metal Organic Chemical Vapor Deposition. *J. Vac. Sci. Technol., B: Microelectron. Process. Phenom.* **1996**, *14*, 3532.
- (34) Tarsa, E. J.; Heying, B.; Wu, X. H.; Fini, P.; DenBaars, S. P.; Speck, J. S. Homoepitaxial Growth of GaN under Ga-stable and N-stable Conditions by Plasma-Assisted Molecular Beam Epitaxy. *J. Appl. Phys.* **1997**, *82*, 5472–5479.
- (35) Diale, M.; Auret, F.; van der Berg, N.; Odendaal, R.; Roos, W. Analysis of GaN Cleaning Procedures. *Appl. Surf. Sci.* **2005**, *246*, 279–389.
- (36) Winnerl, A.; Pereira, R. N.; Stutzmann, M. Kinetics of Optically Excited Charge Carriers at the GaN Surface: Influence of Catalytic Pt Nanostructures. *J. Appl. Phys.* **2015**, *118*, 155704.
- (37) Diebold, U. The Surface Science of Titanium Dioxide. *Surf. Sci. Rep.* **2003**, *48*, 53–229.
- (38) Lagerstedt, O.; Monemar, B. Variation of Lattice Parameters in GaN with Stoichiometry and Doping. *Phys. Rev. B: Condens. Matter Mater. Phys.* **1979**, *19*, 3064–3070.
- (39) Gupta, D.; Antony, B. Electron Impact Ionization of Cycloalkanes, Aldehydes, and Ketones. *J. Chem. Phys.* **2014**, *141*, 054303.
- (40) Tian, C.; Vidal, C. Cross Sections of Electron Impact Ionization of Ethylene. *Chem. Phys. Lett.* **1998**, *288*, 499–503.
- (41) Hudson, J. E.; Hamilton, M. L.; Vallance, C.; Harland, P. W. Absolute Electron Impact Ionization Cross-sections for the C1 to C4 Alcohols. *Phys. Chem. Chem. Phys.* **2003**, *5*, 3162–3168.
- (42) Yates, J. T., Jr.; Madey, T. E. Interactions between Chemisorbed Species: H₂ and CO on (100) Tungsten. *J. Chem. Phys.* **1971**, *54*, 4969–4978.
- (43) Kim, B.; Li, Z.; Kay, B. D.; Dohnálek, Z.; Kim, Y. K. The Effect of Oxygen Vacancies on the Binding Interactions of NH₃ with Rutile TiO₂(110)-1 × 1. *Phys. Chem. Chem. Phys.* **2012**, *14*, 15060–15065.
- (44) Hansen, J. Ø.; Bebensee, R.; Martinez, U.; Porsgaard, S.; Lira, E.; Wei, Y.; Lammich, L.; Li, Z.; Idriss, H.; Besenbacher, F.; et al. Unravelling Site-Specific Photo-Reactions of Ethanol on Rutile TiO₂(110). *Sci. Rep.* **2016**, *6*, 21990.
- (45) Wendt, S.; Matthiesen, J.; Schaub, R.; Vestergaard, E. K.; Lægsgaard, E.; Besenbacher, F.; Hammer, B. Formation and Splitting of Paired Hydroxyl Groups on Reduced TiO₂(110). *Phys. Rev. Lett.* **2006**, *96*, 066107.
- (46) Suzuki, S.; Fukui, K.-i.; Onishi, H.; Iwasawa, Y. Hydrogen Adatoms on TiO₂(110)-(1 × 1) Characterized by Scanning Tunneling Microscopy and Electron Stimulated Desorption. *Phys. Rev. Lett.* **2000**, *84*, 2156–2159.
- (47) Hammer, B.; Wendt, S.; Besenbacher, F. Water Adsorption on TiO₂. *Top. Catal.* **2010**, *53*, 423–430.
- (48) Chen, S.; Wang, L.-W. Thermodynamic Oxidation and Reduction Potentials of Photocatalytic Semiconductors in Aqueous Solution. *Chem. Mater.* **2012**, *24*, 3659–3666.

(49) Shen, M.; Henderson, M. A. Identification of the Active Species in Photochemical Hole Scavenging Reactions of Methanol on TiO₂. *J. Phys. Chem. Lett.* **2011**, *2*, 2707–2710.

(50) Martono, E.; Hyman, M. P.; Vohs, J. M. Reaction Pathways for Ethanol on Model Co/ZnO(0001) Catalysts. *Phys. Chem. Chem. Phys.* **2011**, *13*, 9880–9886.

(51) Kwak, G.; Yong, K. Adsorption and Reaction of Ethanol on ZnO Nanowires. *J. Phys. Chem. C* **2008**, *112*, 3036–3041.

(52) Halevi, B.; Vohs, J. M. TPD Study of the Reaction of CH₃CH₂SH and (CH₃CH₂)₂S₂ on ZnO(0001) and ZnO. *Catal. Lett.* **2006**, *111*, 1–4.

(53) Dulub, O.; Boatner, L. A.; Diebold, U. STM study of the Geometric and Electronic Structure of ZnO(0001)-Zn, (0001̄)-O, (101̄0), and (112̄0) Surfaces. *Surf. Sci.* **2002**, *519*, 201–217.

(54) Van de Walle, C. G.; Neugebauer, J. First-Principles Surface Phase Diagram for Hydrogen on GaN Surfaces. *Phys. Rev. Lett.* **2002**, *88*, 066103.

(55) Bermudez, V. Theoretical Study of Hydrogen Adsorption on the GaN(0001) Surface. *Surf. Sci.* **2004**, *565*, 89–102.

(56) Northrup, J. E. Hydrogen and Magnesium Incorporation on *c*-plane and *m*-plane GaN Surfaces. *Phys. Rev. B: Condens. Matter Mater. Phys.* **2008**, *77*, 045313.

(57) Li, S.-C.; Chu, L.-N.; Gong, X.-Q.; Diebold, U. Hydrogen Bonding Controls the Dynamics of Catechol Adsorbed on a TiO₂(110) Surface. *Science* **2010**, *328*, 882–884.

(58) Henderson, M. A. Structural Sensitivity in the Dissociation of Water on TiO₂ Single-Crystal Surfaces. *Langmuir* **1996**, *12*, 5093–5098.

(59) Fujino, T.; Katayama, M.; Inuzuka, K.; Okuno, T.; Oura, K.; Hirao, T. Surface Hydroxyl Formation on Vacuum-Annealed TiO₂(110). *Appl. Phys. Lett.* **2001**, *79*, 2716–2718.

(60) Shekhar, R.; Jensen, K. F. Temperature Programmed Desorption Investigations of Hydrogen and Ammonia Reactions on GaN. *Surf. Sci.* **1997**, *381*, L581–L588.

Supporting information for:
Anhydrous Ethanol Dehydrogenation on
MOCVD-grown GaN(0001)

Constantin A. Walenta,^{†,‡,§} Sebastian L. Kollmannsberger,^{†,§} Rui N. Pereira,[¶]
Martin Tschurl,[†] Martin Stutzmann,^{¶,‡} and Ueli Heiz^{*,†,‡}

[†]*Chair of Physical Chemistry, Department of Chemistry & Catalysis Research Center,
Technische Universität München, Lichtenbergstr. 4, 85748 Garching, Germany*

[‡]*Nanosystems Initiative Munich, Schellingstr. 4, 80799 München, Germany*

[¶]*Walter Schottky Institute and Physics Department, Technische Universität München, Am
Coulombwall 4, 85748 Garching, Germany*

[§]*The authors contributed equally to this work*

E-mail: ulrich.heiz@mytum.de

Phone: +49 (0) 89 289 13391. Fax: +49 (0) 89 289 13389

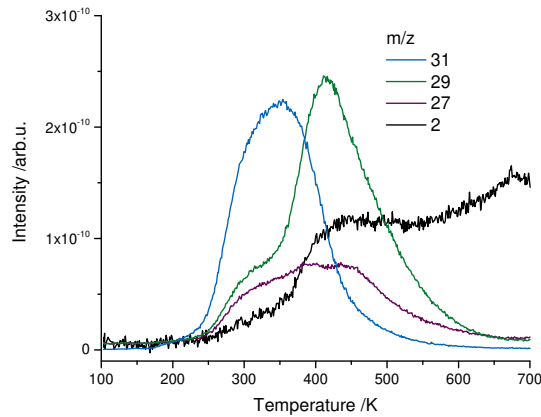


Figure S1: TPD traces for an ethanol dosage of 0.85 ML. Ethanol is detected on m/z 31, acetaldehyde on m/z 29, ethylene on m/z 27 and hydrogen on m/z 2. Without any raw data correction, both masses 29 and 27 appear within the cracking pattern of the ethanol as can be seen at a temperature of around 300 K. By applying the cracking pattern correction as mentioned above, the molecular yields are disentangled. Note, that the hydrogen quantification is corrected for the observed background.

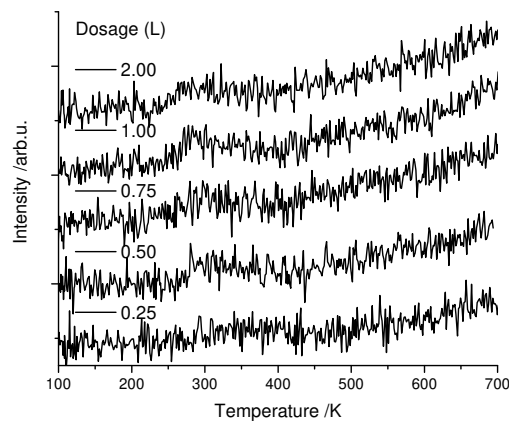


Figure S2: Water traces ($m/z = 18$) for different coverages of ethanol on GaN(0001). No distinct water formation is obtained. The rising background is attributed to originate from desorption from the sample holder and the small bump around 350 K is caused from the ethanol cracking pattern.

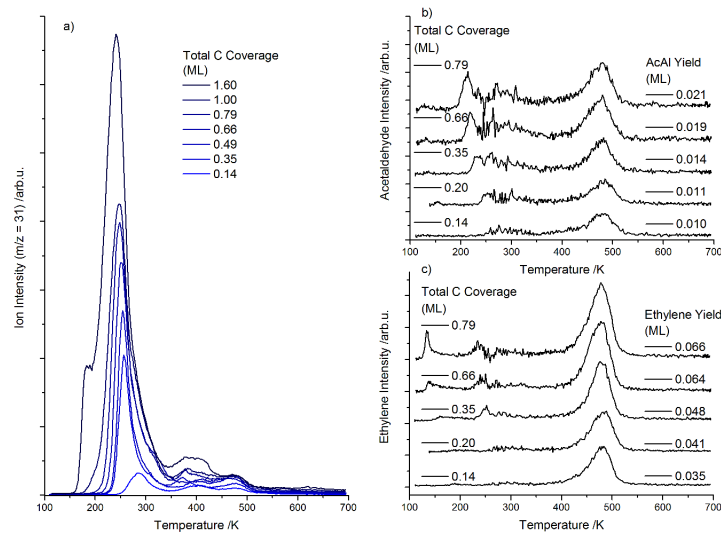


Figure S3: TPD results for different ethanol coverages on a reduced TiO₂(110)-surface. The results and desorption products are in very good agreement with the literature.^{S1–S5} The high temperature desorption products are further analyzed by integration. Note that the heavy noise results from an accumulation of noise in the cracking pattern analysis and the plots represent unsmoothed data. The H₂-trace (data not shown) is a straight line with the exception of some small signals at the multilayer temperature of ethanol and only for high multilayer ethanol coverages. These signals are assigned to the ethanol cracking pattern.

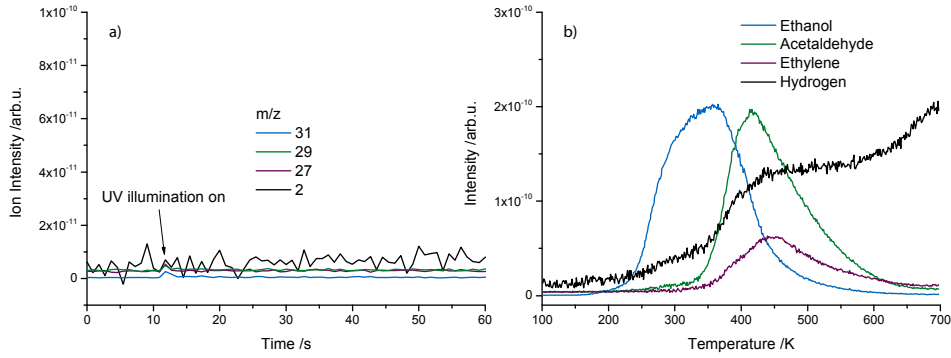


Figure S4: Photochemical experiments under isothermal conditions and an ethanol coverage of 0.82 ML. On the left side (a) a mass spectrum is shown, for which UV light (266.5 nm, more details are given in previous work^{S6}), was switched on after 11 s at a sample temperature of 100 K. No significant desorption yield is observed. On the right (b), a thermal desorption experiment after an illumination of 20 min is shown and the traces for the molecules are treated with the cracking pattern evaluation. The traces show no deviation from the measurements without illumination (Fig. S1).

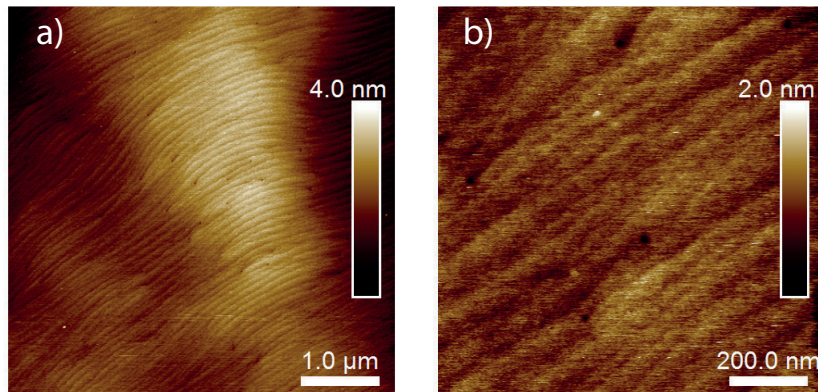


Figure S5: Ex-situ Atomic Force Microscopy (AFM) images of unintentionally doped GaN(0001) from Lumilog. The left image (a) shows an overview scan of 5 μm scale and the right image (b) a detail scan of 1 μm. The root mean square roughness is 0.641 nm for the samples and both images show typical dislocation features for MOCVD-grown GaN(0001) known from literature.^{S7–S10}

References

- (S1) Gamble, L.; Jung, L. S.; Campbell, C. T. *Surf. Sci.* **1996**, *348*, 1–16.
- (S2) Farfan-Arribas, E.; Madix, R. J. *J. Phys. Chem. B* **2002**, *106*, 10680–10692.
- (S3) Kim, Y. K.; Kay, B. D.; White, J. M.; Dohnálek, Z. *J. Phys. Chem. C* **2007**, *111*, 18236–18242.
- (S4) Li, Z.; Smith, R. S.; Kay, B. D.; Dohnálek, Z. *J. Phys. Chem. C* **2011**, *115*, 22534–22539.
- (S5) Hansen, J. Ø.; Huo, P.; Martinez, U.; Lira, E.; Wei, Y. Y.; Streber, R.; Lægsgaard, E.; Hammer, B.; Wendt, S.; Besenbacher, F. *Phys. Rev. Lett.* **2011**, *107*, 136102–136106.
- (S6) Walenta, C. A.; Kollmannsberger, S. L.; Kiermaier, J.; Winbauer, A.; Tschurl, M.; Heiz, U. *Phys. Chem. Chem. Phys.* **2015**, *17*, 22809–22814.
- (S7) Winnerl, A.; Pereira, R. N.; Stutzmann, M. *J. Appl. Phys.* **2015**, *118*.
- (S8) Schultz, T.; Schlesinger, R.; Niederhausen, J.; Henneberger, F.; Sadofev, S.; Blumstengel, S.; Vollmer, A.; Bussolotti, F.; Yang, J.-P.; Kera, S.; Parvez, K.; Ueno, N.; Müllen, K.; Koch, N. *Phys. Rev. B* **2016**, *93*, 125309.
- (S9) Tarsa, E. J.; Heying, B.; Wu, X. H.; Fini, P.; DenBaars, S. P.; Speck, J. S. *J. Appl. Phys.* **1997**, *82*, 5472–5479.
- (S10) Diale, M.; Auret, F.; van der Berg, N.; Odendaal, R.; Roos, W. *Appl. Surf. Sci.* **2005**, *246*, 279–389.

D.5. Ethanol surface chemistry on MBE-grown GaN(0001), GaO_x/GaN(0001), and Ga₂O₃($\bar{2}01$)

THE JOURNAL OF CHEMICAL PHYSICS **147**, 124704 (2017)

Ethanol surface chemistry on MBE-grown GaN(0001), GaO_x/GaN(0001), and Ga₂O₃($\bar{2}01$)

Sebastian L. Kollmannsberger,^{1,a)} Constantin A. Walenta,^{1,2,a)} Andrea Winnerl,³ Fabian Knoller,¹ Rui N. Pereira,³ Martin Tschurl,¹ Martin Stutzmann,^{2,3} and Ueli Heiz^{1,2,b)}¹Chair of Physical Chemistry, Department of Chemistry and Catalysis Research Center, Technische Universität München, Lichtenbergstrasse 4, 85748 Garching, Germany²Nanosystems Initiative Munich (NIM), Schellingstr. 4, 80799 Munich, Germany³Walter Schottky Institute and Physics Department, Technische Universität München, Am Coulombwall 4 85748 Garching, Germany

(Received 4 July 2017; accepted 8 September 2017; published online 28 September 2017)

In this work, ethanol is used as a chemical probe to study the passivation of molecular beam epitaxy-grown GaN(0001) by surface oxidation. With a high degree of oxidation, no reaction from ethanol to acetaldehyde in temperature-programmed desorption experiments is observed. The acetaldehyde formation is attributed to a mechanism based on α -H abstraction from the dissociatively bound alcohol molecule. The reactivity is related to negatively charged surface states, which are removed upon oxidation of the GaN(0001) surface. This is compared with the Ga₂O₃($\bar{2}01$) single crystal surface, which is found to be inert for the acetaldehyde production. These results offer a toolbox to explore the surface chemistry of nitrides and oxynitrides on an atomic scale and relate their intrinsic activity to systems under ambient atmosphere. *Published by AIP Publishing.* <https://doi.org/10.1063/1.4994141>

I. INTRODUCTION

Mimicking nature and driving a heterogeneous photocatalytic or photoelectrochemical reaction have become a major scientific and also industrial interest.^{1–5} In order to harvest a maximum of sunlight, semiconductors with optimized band positions are tailored via alloying and doping.^{6–8} However, these materials are quite complex, with multiple elements in the compound.^{8–10} An emerging group of such materials is alloys or solid solutions of oxides and nitrides, in general called oxy-nitrides.^{11–15} While the bulk properties of these materials have been tailored for their use in photo(electro-)catalysis, their surface chemistry is largely unknown. In the last decade, many of these materials have been investigated in electrocatalytic, photocatalytic, and photo-electrocatalytic studies, although mostly with limited efficiencies.^{16–19} Temperature-programmed desorption (TPD) studies in general have allowed for a more detailed investigation of surface reaction pathways and specific intermediates.^{20–22} Due to the interest in alcohols as a potential hydrogen carrier and its importance in both photocatalysis²³ and electrocatalysis,^{18,24} ethanol is the ideal molecule to investigate the surface reaction on oxynitride compounds. GaN and solid solutions of GaN:ZnO and GaN:InN have attracted much interest in the last years as stable materials in photo(electro)catalysis.^{25–31} However, the surface chemistry of these materials has not been widely studied.³² In this study, we investigate the ethanol surface chemistry of plasma-induced molecular beam epitaxy (PIMBE) grown GaN(0001) with different degrees of surface oxidation. Furthermore, a

Ga₂O₃($\bar{2}01$) single crystal is studied in order to compare our findings with results from a sample with a similar chemical surface composition.

II. EXPERIMENTAL

GaN(0001) is grown by plasma-induced molecular beam epitaxy (PIMBE) to a thickness of about 550 nm on Fe-doped semi-insulating Ga-polar GaN MOCVD (metal-organic chemical vapor deposition) templates (thickness 4 μ m) on α -Al₂O₃(0001) from Lumilog.^{33,34} The samples are non-intentionally doped Ga-face samples that show a free electron concentration of about 5×10^{16} cm⁻³ as determined by Hall measurements. The MBE (molecular beam epitaxy)-grown n-type GaN(0001) samples are etched 30 s in concentrated HCl and rinsed with Milli-Q water twice. Two MBE grown GaN(0001) samples and one Ga₂O₃ single crystal were used.

Prior to TPD measurements, one of the MBE grown samples [denoted GaN(0001) sample] was treated in cycles of Ar⁺-sputtering (0.5 keV, 1×10^{-6} mbar, $I_{\text{sputter}} = 2.0$ μ A, 100 K) for 15 min and 10 min, each time with a subsequent annealing step (800 K, 15 min). The other MBE sample [denoted GaO_x/GaN(0001)] was Ar⁺-sputtered for a total time of 50 min, again with consecutive annealing steps. In detail, five cycles of 5–20 min of sputtering (same conditions as above) followed by 800 K annealing were carried out. By these procedures, all carbon and chlorine contaminations were removed.

Furthermore, varying sputter time leads to a different surface oxidation^{34–36} as free Ga surface species are easily oxidized by oxygen or water from the residual background.^{37,38} The surface constitution was confirmed by Auger Electron Spectroscopy (AES) measurements. The Ga₂O₃($\bar{2}01$) single

^{a)}S. L. Kollmannsberger and C. A. Walenta contributed equally to this work.^{b)}Author to whom correspondence should be addressed: ulrich.heiz@mytum.de. Tel.: +49 (0)89 289 13391. Fax: +49 (0)89 289 13389.

124704-2 Kollmannsberger *et al.*J. Chem. Phys. **147**, 124704 (2017)

crystal (Tamura Cooperation, Tokyo, Japan) was chosen, since it is the natural growth direction of gallium oxide on (0001) facets.³⁹ The treatment before measurements includes 40 min Ar⁺-sputtering (1.0 keV, 5×10^{-6} mbar, $I_{\text{sputter}} = 10.0 \mu\text{A}$, 100 K), 30 min O₂ annealing (800 K, 2×10^{-6} mbar), and 30 min vacuum annealing at 800 K. The subsequent AES spectra did not show any contaminants.

The load lock compatible sample holder is of home-built design and fully made of tantalum. It is capable of heating and cooling samples between 100 K and 1000 K. Since in the upper most level two tantalum sheets are used to clamp the sample to the mount, also materials grown on electrical insulating substrates (i.e. sapphire) can be used. The temperature is measured with a spotwelded type-C thermocouple,⁴⁰ and the temperature difference between the measurement point on the back of the tantalum heating plate and the top of a sample grown on sapphire was determined to be less than 10 K over the entire thermal desorption run. The chamber consists of a quadrupole mass spectrometer (QMS, QMA 430, Pfeiffer Vacuum GmbH) with a skimmer that is differentially pumped, a molecular beam doser, a sputter gun (IQE 11/35, SPECS GmbH), and an Auger Electron Spectrometer (AES, CMA 100, Omicron Nanotechnology GmbH). In this setup, a typical base pressure of 8.0×10^{-11} mbar is achieved.

The purification of ethanol (absolute, HPLC grade, $\geq 99.8\%$, Sigma-Aldrich) was performed by several pump-freeze cycles. The ethanol molecules were adsorbed on the sample at 110 K. TPD experiments were performed using a constant heating rate of 1.2 K/s to 700 K. The cracking pattern correction of acetaldehyde accounts for fragment intensities of all desorbing products. The monolayer coverage is normalized to the integral of the highest coverage that shows no desorption of physisorbed ethanol.

X-ray photoelectron spectroscopy (XPS) was performed in a commercial system (Specs GmbH) using monochromatized Al K α radiation (= 1486.6 eV) to avoid an overlap of the Ga LMM Auger lines with the C 1s peak. Spectral fitting was performed using the Casa XPS analysis software and OriginPro. The curves were fitted using a Shirley background.

III. RESULTS

To elucidate the influence of gallium oxide surface species on the reactivity of ethanol to acetaldehyde, differently oxidized surfaces of PIMBE-grown GaN(0001) surfaces and a Ga₂O₃($\bar{2}01$) single crystal are investigated. The morphology of the PIMBE-grown GaN samples and the Ga₂O₃($\bar{2}01$) crystal was studied by *ex situ* AFM as shown in Figs. S1 and S2 of the [supplementary material](#). The morphology is in very good agreement with the literature for the GaN(0001) epitaxial films^{41–43} as well as for the Ga₂O₃($\bar{2}01$) single crystal.⁴⁴

The chemical compositions after the cleaning cycles were confirmed by *in situ* AES (Fig. S3 of the [supplementary material](#)). A detailed description of the determination of oxidation values from AES can be found in Table S1 of the [supplementary material](#). It is clearly evident that the different sample preparation leads to different surface compositions for the two MBE-grown GaN(0001) samples. On the GaN(0001) sample,

0.18 ML of “native oxide” is observed.^{45,46} XPS was also carried out on GaN(0001) to validate the cleaning cycle. The spectra in Fig. S4 of the [supplementary material](#) confirm the removal of residual carbon under the applied sputter conditions and indicate the oxidation of the sample. For the oxidized sample GaO_x/GaN(0001), a strong surface oxidation with 1.05 ML of “native oxide” is determined and in good agreement with the literature.⁴⁶ A successful cleaning from all contaminants was obtained for Ga₂O₃($\bar{2}01$). Furthermore, for the Ga₂O₃ single crystal, an oxygen rich first layer and a stoichiometric second layer are calculated from AES measurements. The oxygen content of the samples does not change with TPD runs.

In Fig. 1(a), the desorption characteristics of ethanol from a MBE-grown GaN(0001) surface are shown. It can be seen that the desorption maximum, appearing for low coverages at around 380 K, is shifting to lower temperatures (≈ 225 K) for higher coverages, until it saturates at 0.72 ML. Such a

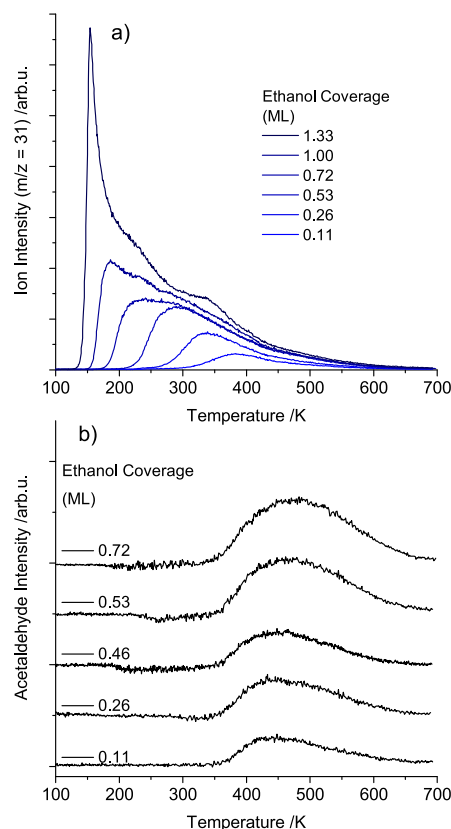


FIG. 1. TPD spectra from various coverages of ethanol dosed with a molecular beam doser on a MBE-grown GaN(0001) surface at 110 K (a). Fragmentation-corrected TPD spectra of the reaction product acetaldehyde (b). For the lowest coverage, the main desorption feature of ethanol appears at around 380 K and shifts to lower temperatures (≈ 225 K) with higher coverages. At coverages exceeding 0.72 ML, a second ethanol desorption peak at 180 K is observed. For the highest coverage, a sharp desorption maximum occurs at 150 K, which can be assigned to desorption of physisorbed ethanol. The desorption peak of acetaldehyde appears at 470 K. The acetaldehyde yield saturates at around 0.53 ML of initial ethanol dosage.

desorption behavior can be attributed to second-order desorption kinetics, which mostly result from dissociative adsorption.^{47–49} For the 1 ML coverage, a second low temperature peak at 180 K arises. For the highest coverage, a desorption peak at around 150 K can be assigned to desorption of physisorbed ethanol. The surface constitution was checked with AES before and after ethanol TPDs and showed no coking. Figure 1(b) shows the acetaldehyde yield from various ethanol coverages. The traces are corrected for fragmentation of desorbing hydrocarbons. The acetaldehyde desorption peak [Fig. 1(b)] occurs at around 470 K and the maximum yield is reached for 0.53 ML of adsorbed ethanol, since a higher initial ethanol dosage shows no increase in the acetaldehyde yield. In Fig. 2, the desorption features of ethanol from surface-oxidized GaO_x/GaN(0001) are given. The ethanol desorption maximum for the lowest coverage occurs at significantly higher temperatures compared to GaN(0001) and at a similar temperature (≈ 500 K) at which acetaldehyde is formed on GaN(0001). The shift of the leading edge of the desorption feature is similar to the ethanol desorption on the less oxidized sample. For the highest coverage, the desorption edge appears at around 280 K, and the multilayer feature can be assigned to the peak at 150 K. The product evaluation reveals that no acetaldehyde is produced on the surface oxidized GaN sample.

For Ga₂O₃($\bar{2}01$), the resulting ethanol TPD is shown in Fig. 3. As the sticking of ethanol is strongly reduced on Ga₂O₃ in comparison to GaN-based samples, a significantly higher dosage must be applied in order to achieve similar coverages. The Ga₂O₃($\bar{2}01$) surface exhibits a peak maximum at around 300 K for the lowest coverage. This maximum is increasing in intensity for higher coverages until another peak evolves at 250 K, indicating desorption from another site with lower binding energy. The peak at around 150 K, which rises for coverages exceeding 1 ML, can be assigned to desorption of physisorbed ethanol from the multilayer. Just like the strongly surface-oxidized GaN sample, the Ga₂O₃ surface shows no

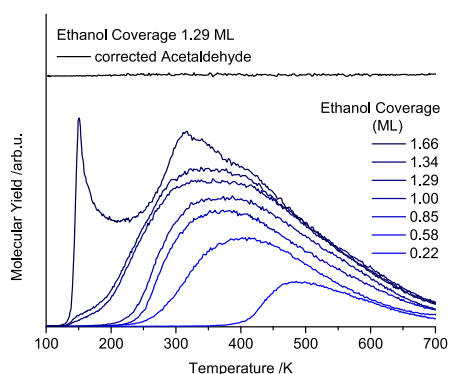


FIG. 2. Ethanol TPD spectra dosed with a molecular beam doser from GaO_x/GaN(0001) in the lower part and desorption yield of acetaldehyde at 1.29 ML in the upper part. For the lowest coverage, the peak maximum is located at around 500 K. With rising coverage, the leading edge shifts to 280 K for the saturated monolayer. For the highest coverages, physisorption of ethanol is observed at around 150 K. The acetaldehyde trace shows that no dehydrogenation products are formed.

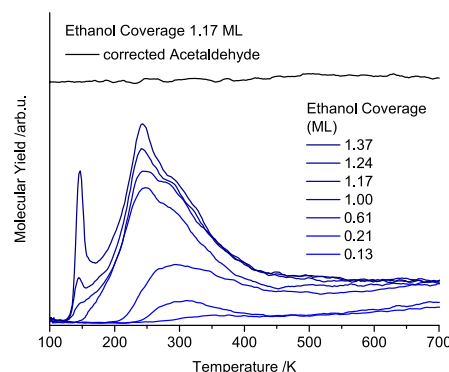
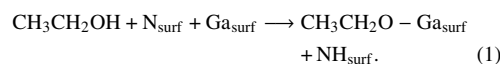


FIG. 3. Ethanol TPD spectra (smoothed) with Langmuir dosing from Ga₂O₃($\bar{2}01$) in the lower part and desorption yield of acetaldehyde at 1.17 ML in the upper part. For the lowest coverage, the peak maximum is located at around 300 K. With rising coverage, the desorption feature shifts to 250 K for the saturated monolayer. For coverages bigger than 1 ML, physisorption of ethanol is observed as can be seen from the peak at around 150 K. The high background at high temperatures originates from ethanol desorption from the sample holder, which is due to a combination of Langmuir dosing and a significantly reduced sticking of ethanol on Ga₂O₃ in comparison to GaN-based samples. No acetaldehyde formation is observed.

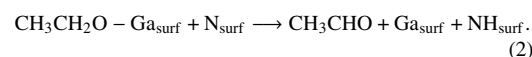
reactivity to produce acetaldehyde from ethanol, as can be seen in the upper part in Fig. 3. A larger background at higher temperatures is observed, which originates from ethanol desorption from the sample holder caused by the Langmuir dosing. It shall be mentioned that reaction pathways to products other than acetaldehyde are not observed for all samples studied. In this regard, conversion to CO or CO₂ (the CO traces are given in Fig. S5 in the supplementary material) does not occur, and very little amount of ethylene production is only visible on GaN(0001) (see Fig. S6 in the supplementary material).

IV. DISCUSSION

The surface reaction of ethanol to acetaldehyde on the MBE-grown GaN(0001) surface (Fig. 1) can be interpreted by the following mechanisms. In analogy to this study and others on metal oxides,^{50,51} this reactivity is always accompanied by a metal bound ethanolate intermediate,



This intermediate is also supported by two additional evidences: First, the shift of the leading edge to lower temperatures with increasing coverages is generally attributed to a second-order desorption kinetics from a dissociative adsorption.^{47–49} Furthermore, the acetaldehyde desorption is observed at higher temperatures than the ethanol one, indicating a more strongly bound ethanolate intermediate.⁵⁰ The dehydrogenation reaction is a formal α -H abstraction,



On the GaO_x/GaN(0001) surface, the thickness of the oxide layer obtained from the quantitative AES amounts to one complete monolayer of GaO_x on the GaN(0001) surface because it

124704-4 Kollmannsberger *et al.*J. Chem. Phys. **147**, 124704 (2017)

is known that the oxide growth takes place layer-by-layer and only on the surface.^{52,53} As observed in Fig. 2, the reactivity of ethanol vanishes completely and acetaldehyde production is not observed. The shift of the leading edge of the high temperature ethanol desorption peak indicates that the adsorption is dissociative.

Compared to the GaN(0001) surface, ethanol desorption takes place at higher temperatures. However, on the thin oxide film, no reactivity towards acetaldehyde is observed. This indicates that on GaN(0001) the surface nitrogen has a key role in the abstraction of α -H to facilitate the dehydrogenation reaction, whereas on the oxide this reaction channel is excluded. Consequently, the strongly bound ethoxy intermediates recombine with the proton to form ethanol.

In order to represent the gallia chemistry, the Ga₂O₃($\bar{2}01$) surface was studied (Fig. 3). No reaction of ethanol towards acetaldehyde was observed, similar to the reactivity of the oxidized GaO_x/GaN(0001) surface. However, for the bulk oxide, the adsorption properties of ethanol on the Ga₂O₃($\bar{2}01$) surface are changed, as ethanol desorbs at significantly lower temperatures of around 300 K. Furthermore, no distinct shift of the leading edge is observed and, in combination with the lower desorption temperature, a molecular adsorption for ethanol is likely to occur. This is in good agreement with findings for methanol adsorption on pristine Ga₂O₃ surfaces on powders and in theoretical studies.^{54,55} The adsorption property for high ethanol coverages of Ga₂O₃($\bar{2}01$) is similar to the GaN(0001) and the GaO_x/GaN(0001) surfaces, as all surfaces exhibit a multilayer feature at around 150 K.

To explain the difference in the reaction behavior of the oxide surfaces to GaN(0001), the different properties of the semiconductors have to be considered. All samples are n-type semiconductors, and thus, negative charges populate the surface states.⁴³ By oxidation of GaN to GaO_x/GaN(0001), these surface states are removed as shown by photoelectron spectroscopies⁵⁶ and electrochemistry.⁵⁷ This effect is attributed to be responsible for the blocking of the dehydrogenation pathway for ethanol. While the removal of surface states explains that α -H abstraction does not take place on GaO_x/GaN(0001), the ethoxy species does not even occur on Ga₂O₃($\bar{2}01$). However, the formation of such a more strongly bound ethoxy intermediate is generally a prerequisite for a subsequent chemical reaction.^{50,51}

V. CONCLUSION

In this work, AES, XPS, *ex situ* AFM, and TPD are used to investigate the influence of surface oxides on the reactivity of ethanol on MBE-grown GaN(0001). A thin GaO_x film on the GaN(0001) surface completely passivates the reactivity of ethanol to acetaldehyde. This demonstrates that the local chemical environment is responsible for the reactivity of ethanol. This can also be rationalized by the removal of the semiconductor's surface states upon oxidation.⁵⁶ The measurements on the Ga₂O₃($\bar{2}01$) single crystal confirm the missing reactivity for ethanol on gallia but also show that the adsorption properties of the molecule are influenced significantly by the bulk material. In contrast to the thin film, only non-dissociative molecular adsorption is observed on the

Ga₂O₃($\bar{2}01$) single crystal. However such an ethoxy formation is in general the initial step for a subsequent alcohol conversion.

SUPPLEMENTARY MATERIAL

See [supplementary material](#) for AFM images from the MBE-grown GaN(0001) surface and the Ga₂O₃($\bar{2}01$) single crystal, AES spectra of a MBE-grown GaN(0001) sample, an oxidized sample GaO_x/GaN(0001), and a Ga₂O₃ single crystal, a detailed description of the determination of "native oxide" proportion from AES measurements, and a XPS of the O 1s, the N 1s, the Ga 3d, and the C 1s signals. TPD traces representing the production of CO and ethylene for all three samples.

ACKNOWLEDGMENTS

The authors thank the DFG for financial support through Grant Nos. HE3435/22-1 and STU139/12-1. C.A.W. and S.L.K. thank the Zeidler Forschungsstiftung for a grant for the UnternehmerTUM MakerSpace GmbH, which enabled the manufacture of parts of the sample holder within the framework of the PhotoPlus start-up project.

- H. B. Gray, *Nat. Chem.* **1**, 7 (2009).
- P. D. Tran, L. H. Wong, J. Barber, and J. S. C. Loo, *Energy Environ. Sci.* **5**, 5902 (2012).
- W. Y. Teoh, J. A. Scott, and R. Amal, *J. Phys. Chem. Lett.* **3**, 629 (2012).
- T. A. Faunce, W. Lubitz, A. W. B. Rutherford, D. MacFarlane, G. F. Moore, P. Yang, D. G. Nocera, T. A. Moore, D. H. Gregory, S. Fukuzumi *et al.*, *Energy Environ. Sci.* **6**, 695 (2013).
- D. Kim, K. K. Sakimoto, D. Hong, and P. Yang, *Angew. Chem., Int. Ed.* **54**, 3259 (2015).
- K. Takanabe and K. Domen, *Green* **1**, 313 (2011).
- F. E. Osterloh, *Chem. Soc. Rev.* **42**, 2294 (2013).
- C. Pan, T. Takata, S. S. Khine Ma, K. Ueda, T. Minegishi, M. Nakabayashi, T. Matsumoto, N. Shibata, Y. Ikuhara, and K. Domen, *J. Mater. Chem. A* **4**, 4544 (2016).
- Q. Wang, T. Hisatomi, Q. Jia, H. Tokudome, M. Zhong, C. Wang, Z. Pan, T. Takata, M. Nakabayashi, N. Shibata *et al.*, *Nat. Mater.* **15**, 611 (2016).
- Y. Goto, J. Seo, K. Kumamoto, T. Hisatomi, Y. Mizuguchi, Y. Kamihara, M. Katayama, T. Minegishi, and K. Domen, *Inorg. Chem.* **55**, 3674 (2016).
- T. Hirai, K. Maeda, M. Yoshida, J. Kubota, S. Ikeda, M. Matsumura, and K. Domen, *J. Phys. Chem. C* **111**, 18853 (2007).
- K. Maeda and K. Domen, *J. Phys. Chem. C* **111**, 7851 (2007).
- M. Higashi, K. Domen, and R. Abe, *J. Am. Chem. Soc.* **134**, 6968 (2012).
- C. Pan, T. Takata, M. Nakabayashi, T. Matsumoto, N. Shibata, Y. Ikuhara, and K. Domen, *Angew. Chem., Int. Ed.* **54**, 2955 (2015).
- Z. Pan, T. Hisatomi, Q. Wang, M. Nakabayashi, N. Shibata, C. Pan, T. Takata, and K. Domen, *Appl. Catal., A* **521**, 26 (2016).
- S. S. Kocha, M. W. Peterson, D. J. Arent, J. M. Redwing, M. A. Tischler, and J. A. Turner, *J. Electrochem. Soc.* **142**, L238 (1995).
- Y. Kuang, Q. Jia, H. Nishiyama, T. Yamada, A. Kudo, and K. Domen, *Adv. Energy Mater.* **6**, 1501645 (2016).
- Y. Ohgi, A. Ishihara, K. Matsuzawa, S. Mitsushima, K.-i. Ota, M. Matsumoto, and H. Imai, *Electrochim. Acta* **68**, 192 (2012).
- M. G. Kibria, S. Zhao, F. A. Chowdhury, Q. Wang, H. P. T. Nguyen, M. L. Trudeau, H. Guo, and Z. Mi, *Nat. Commun.* **5**, 3825 (2014).
- B. Xu, J. Haubrich, C. G. Freyschlag, R. J. Madix, and C. M. Friend, *Chem. Sci.* **1**, 310 (2010).
- C. Lun Pang, R. Lindsay, and G. Thornton, *Chem. Soc. Rev.* **37**, 2328 (2008).
- M. A. Henderson, *Surf. Sci. Rep.* **66**, 185 (2011).
- S. Kundu, A. B. Vidal, M. A. Nadeem, S. D. Senanayake, H. Idriss, P. Liu, J. A. Rodriguez, and D. Stacchiola, *J. Phys. Chem. C* **117**, 11149 (2013).
- A. von Weber, E. T. Baxter, S. Proch, M. D. Kane, M. Rosenfelder, H. S. White, and S. L. Anderson, *Phys. Chem. Chem. Phys.* **17**, 17601 (2015).
- H. S. Jung, Y. J. Hong, Y. Li, J. Cho, Y.-J. Kim, and G.-C. Yi, *ACS Nano* **2**, 637 (2008).

124704-5 Kollmannsberger *et al.*J. Chem. Phys. **147**, 124704 (2017)

- ²⁶K. Maeda, T. Takata, M. Hara, N. Saito, Y. Inoue, H. Kobayashi, and K. Domen, *J. Am. Chem. Soc.* **127**, 8286 (2005).
- ²⁷K. Maeda, K. Teramura, T. Takata, M. Hara, N. Saito, K. Toda, Y. Inoue, H. Kobayashi, and K. Domen, *J. Phys. Chem. B* **109**, 20504 (2005).
- ²⁸T. Ohno, L. Bai, T. Hisatomi, K. Maeda, and K. Domen, *J. Am. Chem. Soc.* **134**, 8254 (2012).
- ²⁹H. Q. Doan, K. L. Pollock, and T. Cuk, *Chem. Phys. Lett.* **649**, 1 (2016).
- ³⁰B. AlOtaibi, H. P. T. Nguyen, S. Zhao, M. G. Kibria, S. Fan, and Z. Mi, *Nano Lett.* **13**, 4356 (2013).
- ³¹M. Ebaid, D. Priante, G. Liu, C. Zhao, M. S. Alias, U. Buttner, T. K. Ng, T. T. Isimjan, H. Idriss, and B. S. Ooi, *Nano Energy* **37**, 158 (2017).
- ³²V. Bermudez, *Surf. Sci. Rep.* **72**, 147 (2017).
- ³³U. Karrer, O. Ambacher, and M. Stutzmann, *Appl. Phys. Lett.* **77**, 2012 (2000).
- ³⁴S. L. Kollmannsberger, C. A. Walenta, A. Winnerl, S. Weiszer, R. N. Pereira, M. Tschurl, M. Stutzmann, and U. Heiz, *J. Phys. Chem. C* **121**, 8473 (2017).
- ³⁵H. Ishikawa, S. Kobayashi, Y. Koide, S. Yamasaki, S. Nagai, J. Umezaki, M. Koike, and M. Murakami, *J. Appl. Phys.* **81**, 1315 (1997).
- ³⁶R. Hunt, L. Vanzetti, T. Castro, K. Chen, L. Sorba, P. Cohen, W. Gladfelder, J. V. Hove, J. Kuznia, M. Khan *et al.*, *Phys. B* **185**, 415 (1993).
- ³⁷P. Lorenz, R. Gutt, T. Haensel, M. Himmerlich, J. A. Schaefer, and S. Krischok, *Phys. Status Solidi C* **7**, 169 (2010).
- ³⁸V. Bermudez and J. Long, *Surf. Sci.* **450**, 98 (2000).
- ³⁹V. Gottschalch, K. Mergenthaler, G. Wagner, J. Bauer, H. Paetzelt, C. Sturm, and U. Teschner, *Phys. Status Solidi A* **206**, 243 (2009).
- ⁴⁰V. S. Smentkowski and J. T. Yates, *J. Vac. Sci. Technol., B: Microelectron. Nanometer Struct.* **14**, 260 (1996).
- ⁴¹E. J. Tarsa, B. Heying, X. H. Wu, P. Fini, S. P. DenBaars, and J. S. Speck, *J. Appl. Phys.* **82**, 5472 (1997).
- ⁴²A. R. Smith, R. M. Feenstra, D. W. Greve, M. S. Shin, M. Skowronski, J. Neugebauer, and J. E. Northrup, *J. Vac. Sci. Technol., B: Microelectron. Nanometer Struct.* **16**, 2242 (1998).
- ⁴³A. Winnerl, R. N. Pereira, and M. Stutzmann, *J. Appl. Phys.* **118**, 155704 (2015).
- ⁴⁴K. Sasaki, M. Higashiwaki, A. Kuramata, T. Masui, and S. Yamakoshi, *Appl. Phys. Express* **6**, 086502 (2013).
- ⁴⁵B. S. Eller, J. Yang, and R. J. Nemanich, *J. Electron. Mater.* **43**, 4560 (2014).
- ⁴⁶J. Yang, B. S. Eller, and R. J. Nemanich, *J. Appl. Phys.* **116**, 123702 (2014).
- ⁴⁷J. T. Yates, Jr. and T. E. Madey, *J. Chem. Phys.* **54**, 4969 (1971).
- ⁴⁸Y. Lilach, I. Danziger, and M. Asscher, *Catal. Lett.* **76**, 35 (2001).
- ⁴⁹B. Kim, Z. Li, B. D. Kay, Z. Dohnalek, and Y. K. Kim, *Phys. Chem. Chem. Phys.* **14**, 15060 (2012).
- ⁵⁰Y. K. Kim, B. D. Kay, J. M. White, and Z. Dohnalek, *J. Phys. Chem. C* **111**, 18236 (2007).
- ⁵¹H. Idriss and E. Seebauer, *J. Mol. Catal. A: Chem.* **152**, 201 (2000).
- ⁵²N. J. Watkins, G. W. Wicks, and Y. Gao, *Appl. Phys. Lett.* **75**, 2602 (1999).
- ⁵³G. Hollinger, R. Skheyta-Kabbani, and M. Gendry, *Phys. Rev. B* **49**, 11159 (1994).
- ⁵⁴M. M. Branda, S. E. Collins, N. J. Castellani, M. A. Baltanás, and A. L. Bonivardi, *J. Phys. Chem. B* **110**, 11847 (2006).
- ⁵⁵V. M. Bermudez, *Langmuir* **24**, 12943 (2008).
- ⁵⁶V. M. Bermudez, *J. Appl. Phys.* **80**, 1190 (1996).
- ⁵⁷A. Winnerl, J. A. Garrido, and M. Stutzmann, *Appl. Phys. Lett.* **110**, 101602 (2017).

Supporting Information: Ethanol Surface Chemistry on MBE-grown GaN(0001), GaO_x/GaN(0001) and Ga₂O₃($\bar{2}01$)

Sebastian L. Kollmannsberger,^{1, a)} Constantin A. Walenta,^{1,2, a)} Andrea Winnerl,³ Fabian Knoller,¹ Rui N. Pereira,³ Martin Tschurl,¹ Martin Stutzmann,^{2,3} and Ueli Heiz^{1,2}

¹⁾Chair of Physical Chemistry, Department of Chemistry and Catalysis Research Center, Technische Universität München, Lichtenbergstrasse 4, 85748 Garching, Germany, E-mail: ulrich.heiz@mytum.de; Fax: +49 (0)89 289 13389; Tel: +49 (0)89 289 13391

²⁾Nanosystems Initiative Munich (NIM), Schellingstr. 4, 80799 Munich, Germany

³⁾Walter Schottky Institute and Physics Department, Technische Universität München, Am Coulombwall 4 85748 Garching

SUPPORTING INFORMATION

The Supporting Information contains the following content: AFM images from the MBE-grown GaN(0001) surface and the Ga₂O₃($\bar{2}01$) single crystal; AES spectra of a MBE-grown GaN(0001) sample, an oxidized sample GaO_x/GaN(0001) and a Ga₂O₃ single crystal; A detailed description of the determination of "native oxide" proportion from AES measurements; XPS of the O 1s, the N 1s, the Ga 3d and the C 1s signals; TPD traces representing the production of CO and ethylene for all three samples.

REFERENCES

- ¹E. J. Tarsa, B. Heying, X. H. Wu, P. Fini, S. P. DenBaars, and J. S. Speck, *J. Appl. Phys.* **82**, 5472 (1997).
- ²A. R. Smith, R. M. Feenstra, D. W. Greve, M. S. Shin, M. Skowronski, J. Neugebauer, and J. E. Northrup, *J. Vac. Sci. Technol.*, B **16**, 2242 (1998).
- ³A. Winnerl, R. N. Pereira, and M. Stutzmann, *J. Appl. Phys.* **118** (2015).
- ⁴K. Sasaki, M. Higashiwaki, A. Kuramata, T. Masui, and S. Yamakoshi, *Appl. Phys. Express* **6**, 086502 (2013).
- ⁵C. Argile and G. E. Rhead, *Surf. Sci. Rep.* **10**, 277 (1989).
- ⁶K. D. Childs, B. A. Carlson, L. A. Vanier, J. F. Moulder, D. F. Paul, W. F. Stickle, and D. G. Watson, *Handbook of Auger Electron Spectroscopy* (Physical Electronics Industries, 1995).
- ⁷O. Lagerstedt and B. Monemar, *Phys. Rev. B* **19**, 3064 (1979).
- ⁸N. J. Watkins, G. W. Wicks, and Y. Gao, *Appl. Phys. Lett.* **75**, 2602 (1999).
- ⁹G. Hollinger, R. Skheyta-Kabbani, and M. Gendry, *Phys. Rev. B* **49**, 11159 (1994).
- ¹⁰I. Shalish, Y. Shapira, L. Burstein, and J. Salzman, *Journal of Applied Physics* **89**, 390 (2001).

^{a)}Contributed equally to this work

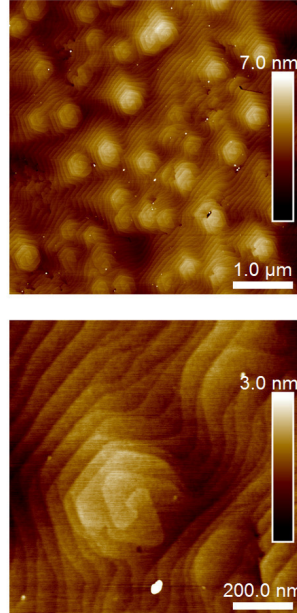


FIG. 1. AFM images of a PIMBE GaN(0001) surface. The morphology is in very good agreement with the general observations of the MBE-grown GaN(0001) epitaxial films in literature.¹⁻³

TABLE I. Determined proportion of Ga, N and O of the first and the second layer of the two differently prepared MBE grown GaN samples and the Ga₂O₃ sample. The values of the AES measurements are treated in a similar way as it has been reported for the evaluation of the chemical composition of thin films.⁵ In detail, the elemental sensitivities⁶ and an exponential decay for the signal intensity with the number of layers are considered. Furthermore, from the universal curve and the GaN lattice parameter⁷ it is interpreted that the Auger signal only results from the first four layers. Moreover, it is known that the oxidation of the GaN surface occurs in a layer by layer mode.^{8,9} For the Ga₂O₃ sample the assumption of an oxygen rich first layer is chosen from AES measurements. For the GaN samples an oxidation in accordance with the first layer of the Ga₂O₃ sample is applied. Accordingly, the third and the fourth layer are for all three samples stoichiometric.

| Material | Layer | Ga | N | O | "Native Oxide" /ML |
|--|--------|------|------|------|--------------------|
| GaN(0001) | first | 0.47 | 0.33 | 0.20 | 0.18 |
| | second | 0.50 | 0.50 | 0.00 | - |
| GaO _x /GaN(0001) | first | 0.30 | 0.00 | 0.70 | 1.00 |
| | second | 0.53 | 0.41 | 0.06 | 0.05 |
| Ga ₂ O ₃ ($\bar{2}01$) | first | 0.30 | 0.00 | 0.70 | - |
| | second | 0.40 | 0.00 | 0.60 | - |

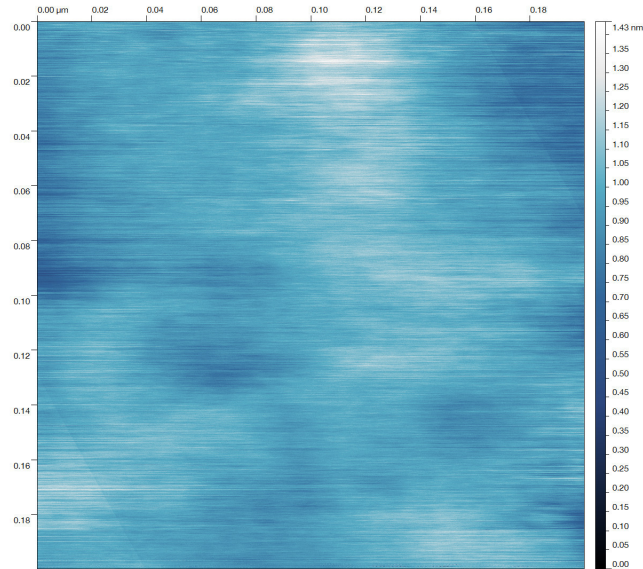


FIG. 2. AFM image of a Ga₂O₃ surface. Neither steps nor kink sites can be seen, which is in good agreement with observations of Ga₂O₃($\bar{2}01$) single crystals reported in literature.⁴

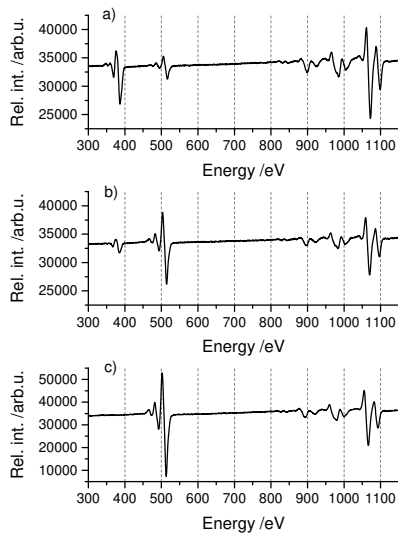


FIG. 3. AES spectra of a MBE-grown GaN(0001) sample (a)), an oxidized sample GaO_x/GaN(0001) (b)) and a Ga₂O₃ single crystal (c)).

4

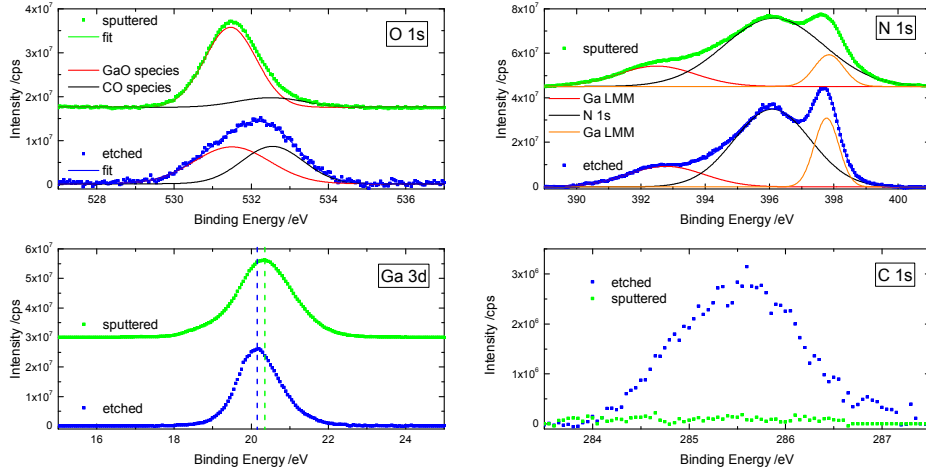


FIG. 4. XPS spectra of the O 1s, N 1s, Ga 3d and C 1s peaks of an etched and a sputtered GaN surface. The signals are intensity normalized to the Ga 3d peak and referenced to the position of the Ga-LMM Auger transitions. The O 1s peak shows that the etched sample exhibits two features, which can be assigned to gallium-oxygen and carbon-oxygen species.¹⁰ While the gallium-oxide peak is growing in intensity, the carbon-oxide feature gets significantly reduced upon sputtering. For the N 1s peak no significant changes upon sputtering are visible. The Ga 3d peak shifts upon sputtering to higher binding energy. This is attributed to surface oxidation, which is in good agreement with the literature.⁸ For the C 1s peak it can be seen that a carbon free surface can be obtained after 25 min of Ar sputtering.

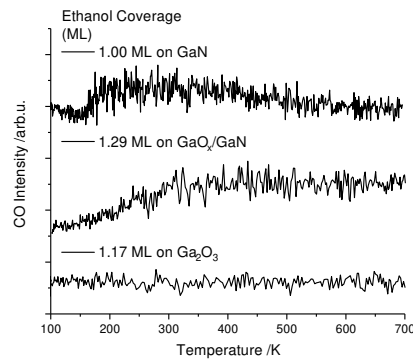


FIG. 5. Fragmentation-corrected CO traces of the TPD spectra for all three samples. It is found that CO and products exhibiting fragments at $m/z = 28$ are not significantly formed during a TPD run.

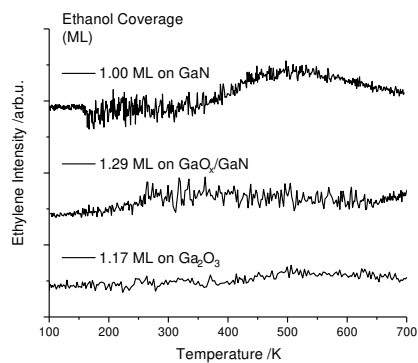


FIG. 6. Fragmentation-corrected ethylene ($m/z = 27$) traces of the TPD spectra for all three samples. While only a small ethylene yield may be visible on GaN, the sample with a higher degree of surface oxidation does not exhibit any reactivity in this reaction pathway at all. This is again similar to the reaction behavior of the Ga₂O₃ crystal.

D.6. Photocatalytic selectivity switch to C–C scission: α -methyl ejection of *tert*-butanol on TiO₂(110)



PCCP

PAPER

View Article Online
View Journal | View Issue



Cite this: *Phys. Chem. Chem. Phys.*,
2018, 20, 7105

Photocatalytic selectivity switch to C–C scission: α -methyl ejection of *tert*-butanol on TiO₂(110)[†]

Constantin A. Walenta,^{‡,ab} Sebastian L. Kollmannsberger,^{‡,a} Carla Courtois,^a
Martin Tschurl^{†,a} and Ueli Heiz^{*,ab}

The thermal and photochemical mechanistic pathways for tertiary alcohols on the rutile TiO₂(110)-surface are studied with the example of *tert*-butanol. While the thermal reaction is known to yield isobutene, the photochemical ejection of a methyl radical is observed at 100 K. The C–C scission, which is accompanied by the formation of acetone, is the only photochemical reaction pathway at this temperature and can be attributed to the reaction of photoholes that are created upon UV-light illumination at the surface of the n-type semiconductor. At 293 K the selectivity of the reaction changes, as isobutene is additionally formed photochemically. A comparison of the kinetics of the different reactions reveals further insights. Together with the quantitative evaluation of the reaction products at low temperatures and the comparison of the reaction pathways at different temperatures it is demonstrated how thermal effects can influence the selectivity of the reactions in photocatalysis.

Received 11th January 2018,
Accepted 6th February 2018

DOI: 10.1039/c8cp00223a

rsc.li/pccp

1 Introduction

While photocatalysis is currently increasingly studied in the context of energy production and storage, it is also an often used approach for the decomposition of organic pollutants.¹ In this regard, titania is one of the most often applied materials, as this substance offers a rich oxidation catalysis of organics. The underlying reaction pathways may also be exploited in other fields of chemistry as for example, biomass conversion to fuels or high-value chemicals. These chemical processes are still limited by a lack of selectivity and new reaction pathways are highly desired.² In this regard, primary, secondary and tertiary alcohols are structural motifs that are often found in the conversion of biomass. Furthermore, *tert*-butanol, which is studied in this work, is a common additive to fuels as a gasoline octane booster, although its effects on the environment are still under investigation.^{3,4} While titania exists in different modifications, rutile TiO₂(110) is by far the most researched surface.^{1,5} While the detailed

mechanisms *via* α -H abstraction of alkoxy species are known for methanol,^{6,7} ethanol⁸ and iso-propanol⁹ on this surface, tertiary alcohols have hitherto been neglected in photocatalytic studies on single crystal surfaces. This may be because textbooks about organic chemistry usually state that tertiary alcohols are inert towards oxidation.¹⁰ Nevertheless, attempts have been tried to use platinum-loaded TiO₂ (P25) particles for the photochemical conversion of *tert*-butanol.^{11,12} It was shown that the alcohol can indeed be converted into a variety of products. However, the exact reaction pathways remained elusive, which was also the case when this alcohol was added to steer the selectivity of the photooxidation towards aldehydes in a different study.¹³

The thermal chemistry of *tert*-butanol exhibits a dehydration pathway to isobutene *via* a concerted E2-elimination of water instead of an oxidation reaction.¹⁴ Furthermore, Dohnalek and co-workers have only recently reported a new thermal reaction pathway of phenylmethanol to methylbenzene and benzylradicals, because the benzene ring stabilizes the radical species.¹⁵ As in the case of *tert*-butanol an α -hydride elimination is disabled, similarly direct deoxygenation occurs in the thermal reaction.¹⁴ In this work, we study the photochemical reaction mechanism of the rutile reduced TiO₂(110) surface [r-TiO₂(110)] for *tert*-butanol. It is shown how the thermal and photochemical reaction steps contribute to the selectivity of the overall reaction outcome.

2 Experimental

The experiments were carried out in an ultrahigh vacuum (UHV) apparatus equipped for photochemical measurements

^a Chair of Physical Chemistry, Department of Chemistry and Catalysis Research Center, Technische Universität München, Lichtenbergstrasse 4, 85748 Garching, Germany. E-mail: ulrich.heiz@mytum.de; Fax: +49 (0)89 289 13389; Tel: +49 (0)89 289 13391

^b Nanosystems Initiative Munich (NIM), Schellingstr. 4, 80799 Munich, Germany

[†] Electronic supplementary information (ESI) available: detailed description of the product analysis, coverage dependent TPD experiments of *tert*-butanol, a product analysis of a TPD experiment as well as the coverage-dependent product distribution of the *tert*-butanol thermal experiments. Furthermore, the ratio of formed methyl-radical and methane is shown and isothermal illumination experiments at different temperatures are presented. See DOI: 10.1039/c8cp00223a

[‡] Contributed equally to this work.

as described previously.^{16,17} The cylindrical TiO₂(110) single crystal (Surface-net GmbH) is mounted on a 1 mm thick tantalum plate with tantalum clamps and a very thin gold foil to ensure good thermal conductivity. Crystal cleaning was accomplished by cycles of Ar⁺-sputtering (5.0×10^{-6} mbar, 20 min, 100 K, 11.8 μ A), annealing in oxygen (1×10^{-6} mbar, 820 K, 20 min) and vacuum annealing (820 K, 10 min) and no impurities were detected in the Auger electron spectra. The defect concentration of the reduced, blue crystal (denoted r-TiO₂(110)) was determined by H₂O temperature programmed desorption (TPD) to be about $6\% \pm 1\%$.¹⁸ Thermal and photo-desorption experiments were carried out in a line of sight geometry with respect to the quadrupole mass spectrometer (QMA 430, Pfeiffer Vacuum GmbH) with a distance of about 4 mm to the skimmer. UV illumination of the sample was accomplished by a frequency doubled OPO laser (GWU, premiScan ULD/400) that is pumped by the third harmonic of a Nd:YAG-laser (Innolas Spitlight HighPower 1200, 7 ns pulse width, 20 Hz repetition rate). The as-generated light pulses (700 μ J per pulse, 242 nm) illuminate the sample entirely. Laser induced thermal heating effects were not observed and *tert*-butanol did not show any absorption in the UV-vis spectra in the spectral region of the illumination. The *tert*-Butanol (2-methyl-2-propanol, Sigma-Aldrich, $\geq 99.5\%$) and *tert*-butanol-OD (2-methyl-2-propan(ol-d), Sigma Aldrich, 99 atom% D) were cleaned by pump-thaw cycles and dosed *via* background dosing. The coverages are referenced to the number of Ti⁴⁺-sites, for which a monolayer is normalized to the H₂O desorption yield from all Ti-sites (1 ML $\equiv 5.2 \times 10^{14}$ sites per cm⁻²). Further experimental details including

product identification, cracking pattern correction and ionization sensitivities are given in the ESI.† The photon-stimulated desorption (PSD) experiments are carried out by recording mass traces of products desorbing from the semiconductor under isothermal conditions at a given temperature.

3 Results and discussion

While the photochemical reaction behavior of tertiary alcohols has so far not been investigated on single crystalline surfaces, the thermal reaction pathway of *tert*-butanol is already quite well understood. In good agreement with the literature,^{14,19} it is found that *tert*-butanol reacts *via* dehydration to isobutene, which occurs at around 425 K. In experiments with the deuterated *tert*-butanol-OD, HDO is identified as a by-product at the reaction temperature of 425 K (Fig. S1 and S2, ESI†). The coverage dependent molecule yields (Fig. S3, ESI†) show that the thermal reactivity levels off after the coverage of all Ti-sites on the surface.¹⁴ When the n-type semiconductor r-TiO₂(110)-surface, which has been previously covered with 0.18 ML of *tert*-butanol, is illuminated with UV light, photon-generated holes reach the surface and methyl-radical ejection is observed at 100 K (Fig. 1a). While a similar photochemical methyl-ejection from organic compounds has been observed previously for ketones^{20–25} and acetaldehyde²⁶ on oxidized TiO₂(110) [o-TiO₂(110)] or in an oxygen atmosphere,²⁷ this pathway has so far not been identified for the reaction of alcohols. This signal is

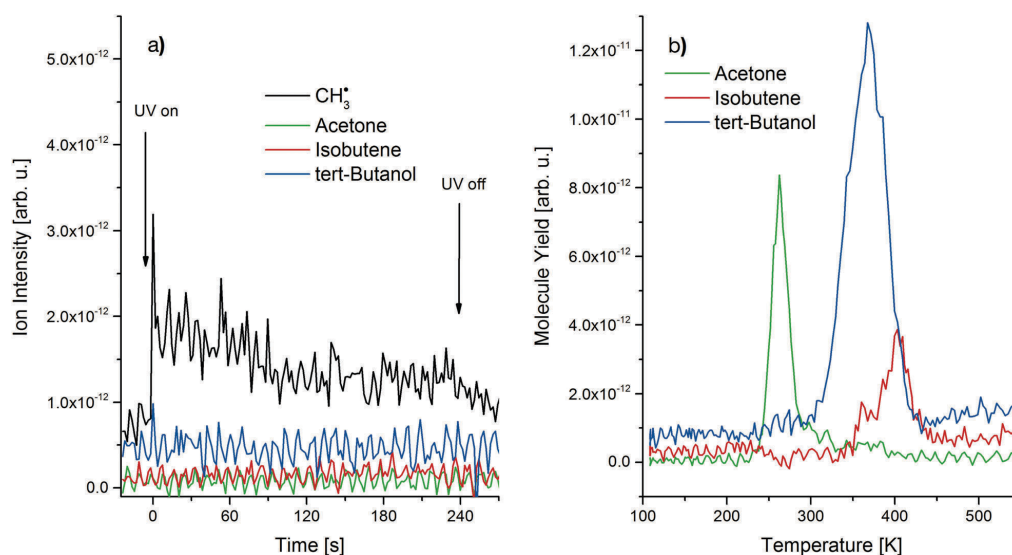


Fig. 1 (a) Isothermal photodesorption yield vs. time for 0.18 ML *tert*-butanol-OD at 100 K on a r-TiO₂(110) surface. When the sample is irradiated with UV light, a CH₃-radical is ejected from the *tert*-butanol, but further molecules do not desorb either due to the thermal or the photochemical reactions. In the right panel (b), a post-irradiation TPD experiment is shown after 20 min of UV illumination. The photo product acetone is observed around 270 K as well as the thermal dehydration product isobutene and unreacted *tert*-butanol.

indeed a methyl-radical as verified by a comparison of the masses 15 and 16 (Fig. S4, ESI†).

As for tertiary alcohols the usual photochemical reaction pathway^{6–8,29} via the abstraction of an α -H is intrinsically excluded, the reaction with photoholes instead initiates the cleavage of a C–C bond. More detailed insights into the reaction pathways are obtained by subsequent post-irradiation TPD experiments (see Fig. 1b for 20 min illumination). These experiments reveal the formation of three different species: acetone is identified as the resulting product from the photocatalytic methyl radical ejection. In addition, unreacted *tert*-butanol and isobutene, which is similarly observed in the TPDs without illumination (Fig. S2, ESI†), are detected. Auger electron spectroscopy after the TPD experiments (data not shown) indicates that neither the alcohols nor the ketones result in a coking of the TiO₂(110) surface and, consequently, the carbon balance can be closed.

While other reaction products are not observed, their ratio of acetone/*isobutene*/*tert*-butanol significantly changes over illumination times at 100 K (Fig. 2). With an increasing illumination duration, the acetone production increases, while both the *tert*-butanol and the *isobutene* yields diminish. Finally, the acetone production saturates after about 30 min, yielding 36% for an initial *tert*-butanol coverage of 0.18 ML.

This amounts to a conversion of 0.065 ML of *tert*-butanol. Alcoxy species have previously been found to be the photoactive species.^{6,7,30,31} While the actual active site for photooxidation still remains under discussion, we follow the interpretation of Henderson, who reports that methoxy formation occurs either on defects, co-adsorbed oxygen adatoms or terminal OH groups.³⁰ As on the *r*-TiO₂(110)-surface, only defects occur in significant amounts, and we assign the *tert*-butoxy formation to

occur predominantly in bridge-bonding oxygen (BBO) defects, as attributed by the saturation value, which is in excellent agreement with the concentration of BBO-vacancies of 0.06 ± 0.01 ML on the *r*-TiO₂(110)-surface as determined by water-TPD.¹⁸ Furthermore, scanning tunneling microscopy (STM) images of 2-butanol reveal the butoxy formation only occurs in the defect.³²

Interestingly, in the present work and the previously mentioned studies, some thermal dehydration-reactivity of the alcohol is still observed in the TPD after the photoproduct-accumulation experiment at cryogenic temperatures. As the thermal reaction has been attributed by Dohnalek and co-workers to also take place in the BBO-vacancies, these alkenes stem from diffusion of the alcohol into the cleared BBO-vacancies during the TPD experiments.

Therefore, the amount of acetone formed in the photo-reaction sites scales with the defect concentration, but not the sum of the overall reaction products. The thermal reaction pathway is not expected to be strongly affected by the photo-reaction. This is also supported by the behavior of the *isobutene* signal for different illumination times (Fig. 2), for which a drop from about 30% to only somewhat below 20% is observed.

In a subsequent experiment, the photoreaction was investigated at 293 K (Fig. 3a). This particular temperature was chosen, as on the one hand significant desorption of *tert*-butanol is not expected to occur. On the other hand, desorption of acetone should be enabled according to the post-irradiation TPD experiments (Fig. 1b) and the desorption behavior reported in the literature.^{9,33} Similar as in case of Fig. 1, the methyl radical ejection is observed from *tert*-butanol, while the desorption of *tert*-butanol is indeed completely suppressed. In addition, some acetone desorption is observed, although with significantly lower intensity during the beginning of the illumination. Unexpectedly, desorption of *isobutene* is also observed under UV illumination. While it has been shown that this molecule can even be photodesorbed below 100 K on the *r*-TiO₂(110) surface,²⁸ it is detected at least 50 K below its first desorption feature in the *tert*-butanol TPD experiment (Fig. S2, ESI†). When the resulting decay curves are normalized to their maximum value (Fig. 3b), the kinetics of the different processes can readily be compared with each other. All desorption traces show multi-exponential decay kinetics, which is generally found for photochemical processes on TiO₂ indicating complex reaction pathways.^{34,35}

However, the individual decay curves are significantly different from each other, which depends on the respective desorbing species: while *isobutene* clearly exhibits the fastest reaction kinetics, the ejection of methyl is somewhat faster than the acetone formation and desorption. This behavior indicates that different mechanisms play a role, which is a combination of the thermal and photochemical processes. The photochemistry at 100 K and 293 K as well as the thermal reactivity enable detailed insights into the different reaction mechanisms: the methyl radical ejection observed in all isothermal UV-illumination experiments is clearly a photon-induced reaction. However, this reaction is less efficient at 100 K than at 293 K, which

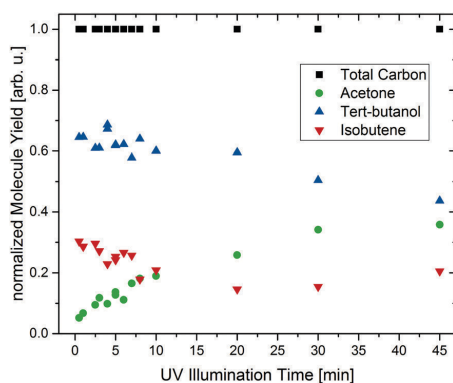


Fig. 2 Normalized integrated molecule yields vs. illumination time. Each of the data points represents the integrated molecule yields from a consecutive post-irradiation TPD run. Prior to this illumination, the *r*-TiO₂(110) surface is exposed to 0.18 ML *tert*-butanol-OD at 100 K. The carbon balance is closed, because coking is not observed in the experiments. With increasing UV illumination time, the photochemical yield of acetone increases, while both the *isobutene* and *t*-butanol yields are attenuated. After 30 min, the photoreaction saturates.

Paper

View Article Online

PCCP

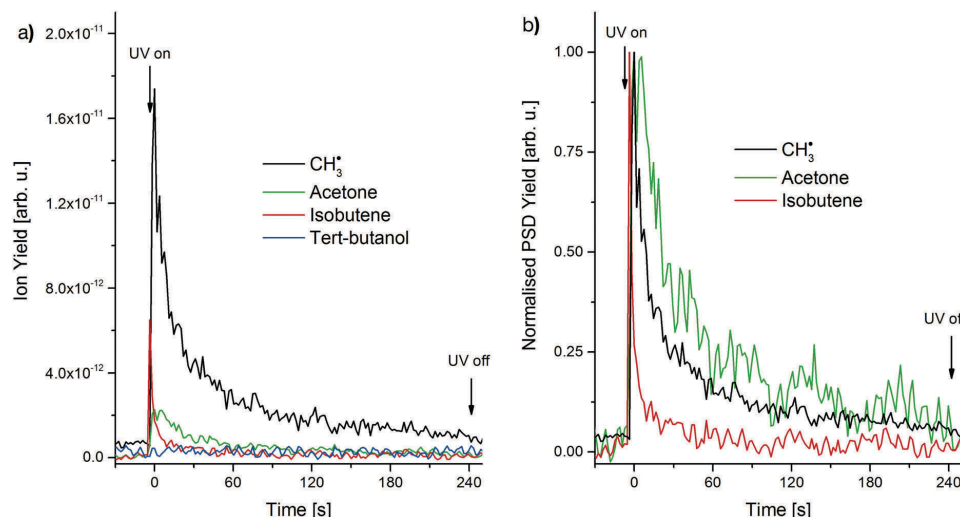
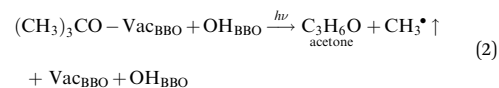
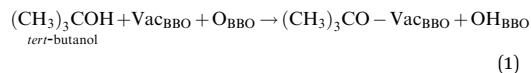


Fig. 3 (a) Isothermal photodesorption yield vs. time for 0.18 ML of *tert*-butanol-OD at 293 K on a *r*-TiO₂(110) surface. When the sample is irradiated with UV light, CH₃-radical ejection is observed similar to the experiment at cryogenic conditions. Furthermore, the photoreaction product acetone also desorbs under illumination at this temperature. In addition, isobutene formation and desorption is observed at 293 K. In panel (b), the normalized PSD yields from the same experiment as in (a) are shown for a qualitative comparison of decay rates. All the decay-rates follow a multi-exponential behavior. The acetone signal shows a small delay with respect to the methyl-radical ejection and then a slightly slower decay, which is attributed to thermal desorption behavior after the photoreaction to acetone. The isobutene decay is faster than the methyl-ejection, which may be attributed to a photochemical desorption as observed in the literature.²⁸

demonstrates that at least one reaction step, only accessible by thermal chemistry, is of importance. To study the temperature dependence further, PSD experiments of 0.18 ML *tert*-butanol are carried out at several temperatures between 239 K and 330 K (Fig. S5, ESI†). The analysis of this data shows (Fig. 4) that at 239 K about equal amounts of isobutene and acetone are formed. An increase in the temperature of the photoreaction enhances the formation of both products. However, while for isobutene only a modest increase in the yield is detected, the signal of acetone strongly rises. We attribute this observation to originate from the superposition of two different effects, which are an enhanced thermal desorption of acetone and the diffusion of *tert*-butanol to the photoactive site. The changes in product yields are further reflected in the selectivity of the photoreaction (Fig. 4b). While at low temperatures about 50% selectivity toward acetone is found, this value increases to over 80% at room temperature and above.

The absence of a distinct low-energy structure as the η^2 (C,O)-enolate for aldehydes and ketones^{20,21,27} suggests that the transfer of the hole immediately leads to the abstraction of a methyl group regardless of the exact adsorption geometry in the defect. While this process rules out temperature-induced geometric transformations, diffusion of the alcohol molecules into the defects plays an important role in the reactivity. This is supported by STM studies, which show that alcohol molecules are also bound on TiO₂ rows even when BBO vacancies are still accessible.^{32,36} Furthermore, the accompanied production of

acetone (eqn (2)) is also found to be slow at 100 K and the yield only saturates after 30 min of illumination.



On the other hand, the resultant increase in methyl ejection at 293 K is not only due to a higher diffusion rate of the alcohol molecules into the defects that remained empty, but also by a clearance of the defect by the thermal desorption of acetone. This subsequent desorption step of the ketone is also reflected by a slower decay of the acetone signal with respect to the methyl one, as for the latter this thermal reaction step does not occur.

In comparison with the products originating from methyl ejection, the desorption of isobutene is a very fast process, which is clearly evidenced by the rapid decay in the signal (Fig. 3b). While a very fast photodesorption behavior on the *n*-type semiconductor may be attributed to a photohole induced charge redistribution on the surface, the reaction is obviously temperature-dependent, as the formation of this molecule does not occur at 100 K. Otherwise, photodesorption of this molecule would have been observed at this temperature.²⁸ This temperature-dependence suggests, that a barrier to an activated

PCCP

View Article Online

Paper

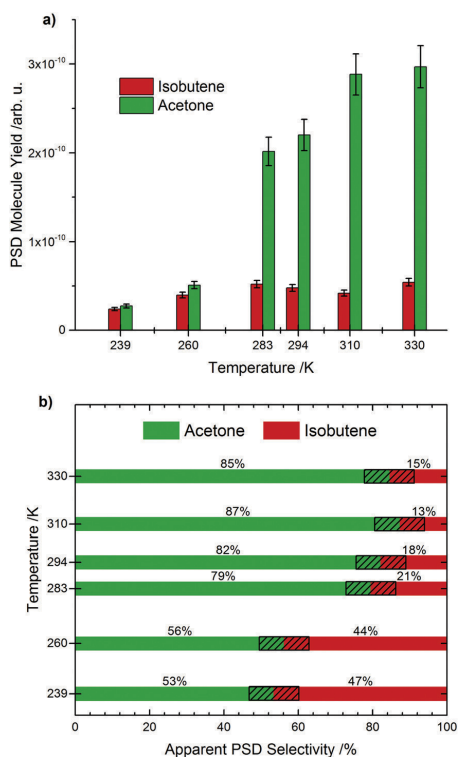


Fig. 4 (a) Resembles the integrated molecule yields of the first 100 s including all correction factors (see ESI†) for the different PSD yields from Fig. S5 (ESI†). For higher temperatures, the overall reaction yield is increased. In (b), the selectivities based on the integral yields are displayed. For higher temperatures, an enhanced apparent PSD selectivity towards acetone is obtained.

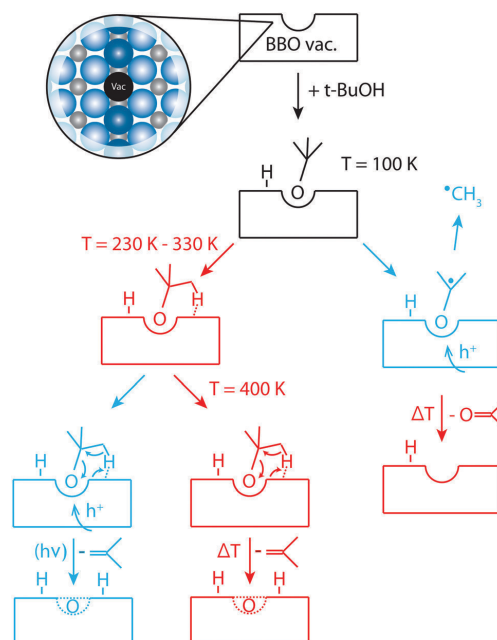
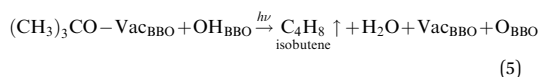
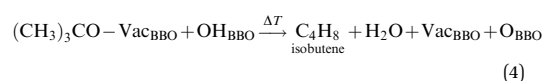
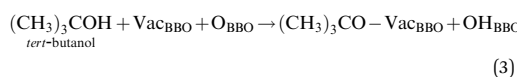


Fig. 5 Photochemical (blue) and thermal (red) reaction pathways of *tert*-butanol on the *r*-TiO₂(110) surface. When the photo-holes react at cryogenic conditions with *tert*-butanol, methyl ejection is observed. Consecutively, a thermal desorption of acetone is observed. When the photo-reaction is initiated at room temperature, thermally formed isobutene is observed at lower temperatures than that expected from the reaction temperature. The isobutene is either photo-desorbed in the illumination case or thermally desorbed. A representation of the BBO-vacancy from the surface normal is shown for the bare vacancy, while the BBO vacancy is shown in black. The Ti atoms are given in grey and the oxygen ones in blue.

transition state for the H₂O-elimination of *tert*-butanol exists, which can already be overcome at lower temperatures than that of the complete thermal reaction to isobutene. UV illumination seems to propel the consecutive chemical reaction steps and, as the desorption is not thermally hindered, the fastest kinetics of all the observed products results. In the thermal reaction pathway the production of isobutene by water-elimination has previously been attributed to be an E2-type reaction *via* a 5-membered cyclic structure involving the BBO-vacancy.¹⁴ Thus, it seems reasonable that this transition state is only formed after a certain temperature, while the formal abstraction of water is eventually done by the photoreaction (eqn (5)).



Both reactions, the formation of acetone by methyl ejection and the production of isobutene by dehydration, comprise thermal as well as photochemical steps, which are summarized in Fig. 5.

The water-free conditions also demonstrate, that such photoreactions do not necessarily need to occur *via* the generation of the OH-radical and the subsequent oxidation of the alcohol. Instead, a direct hole transfer to the organic molecule is observed. This mechanism may also work under aqueous conditions, as long as the defects are not blocked or oxygen ad-atoms exist on the semiconductor. In addition, our findings also explain perfectly the detected products from a previous study concerning the photooxidation of *tert*-butanol on co-catalyst loaded TiO₂ (Degussa P25) in a reactor at 373 K.^{11,12} In line with our observations, acetone was also identified as the main reaction product from the photoreaction, while isobutene was the

sole thermal decomposition product. Based on our study, we expected these properties to originate from the peculiar chemistry of TiO₂.

4 Conclusions

In summary, we have shown that the photooxidation for alcohols without an α -H moiety opens up new mechanistic pathways such as the splitting of C–C-bonds. In general, all photochemical processes observed can be associated with BBO-vacancy sites. Similar to ketones, the photooxidation of tertiary alcohols (*i.e.* tert-butanol) is attributed to be initiated by photoholes, which travel to the alcohol species to enable the ejection of a methyl radical. As the photochemical product evolution saturates at a certain amount, which can directly be related to the defect concentration, it is evidenced that the reaction occurs directly at the BBO-vacancy site. Increased reaction kinetics for the methyl ejection at higher temperatures suggest that diffusion and the clearance of defects play an important role in the reaction rate. While at 100 K only the reaction pathway to the formation of acetone occurs, an additional one is open for the illumination at 293 K. At this temperature, irradiation facilitates the formation of isobutene originating from a dehydration of the alcohol. However, the desorption of isobutene is observed at surprisingly low temperatures, as the thermal desorption is generally believed to take place immediately after the isobutene formation.^{14,28} The temperature-dependent behavior of this reaction can be attributed to a cyclic transition state involving the BBO-vacancy,¹⁴ and a redistribution of charges upon illumination, which may facilitate the reaction and product desorption. For all reaction channels, it is evident that both thermal as well as photochemical effects are important for the yield of a particular product. Furthermore, it is demonstrated that even a seemingly simple system such as rutile and a tertiary alcohol offers a rich chemistry with two different reaction pathways, dehydrogenation and dehydration, which can be tuned by the judicious choice of the appropriate reaction parameters.

Conflicts of interest

There are no conflicts to declare.

Acknowledgements

The authors thank the DFG for grant HE3435/22-1. C. A. W., S. L. K. and M. T. express gratitude to Christian Steiffen for keeping up the good mood during the experiments.

References

- M. A. Henderson, *Surf. Sci. Rep.*, 2011, **66**, 185–297.
- R. Rinaldi and F. Schüth, *Energy Environ. Sci.*, 2009, **2**, 610–626.

- F. Frusteri, F. Arena, G. Bonura, C. Cannilla, L. Spadaro and O. D. Blasi, *Appl. Catal., A*, 2009, **367**, 77–83.
- N. Rahmat, A. Z. Abdullah and A. R. Mohamed, *Renewable Sustainable Energy Rev.*, 2010, **14**, 987–1000.
- C. L. Pang, R. Lindsay and G. Thornton, *Chem. Rev.*, 2013, **113**, 3887–3948.
- M. Shen and M. A. Henderson, *J. Phys. Chem. Lett.*, 2011, **2**, 2707–2710.
- K. R. Phillips, S. C. Jensen, M. Baron, S.-C. Li and C. M. Friend, *J. Am. Chem. Soc.*, 2013, **135**, 574–577.
- C. A. Walenta, S. L. Kollmannsberger, J. Kiermaier, A. Winbauer, M. Tschurl and U. Heiz, *Phys. Chem. Chem. Phys.*, 2015, **17**, 22809–22814.
- D. Brinkley and T. Engel, *J. Phys. Chem. B*, 1998, **102**, 7596–7605.
- K. P. C. Vollhardt and N. E. Schore, *Organische Chemie*, Wiley-VCH Verlag GmbH & Co. KGaA, 5th edn, 2011.
- S. Preis and J. Falconer, *Water Sci. Technol.*, 2004, **49**, 141–145.
- S. Preis, J. L. Falconer, R. del Prado Asensio, N. C. Santiago, A. Kachina and J. Kallas, *Appl. Catal., B*, 2006, **64**, 79–87.
- V. Augugliaro, H. Kisch, V. Loddo, M. J. López-Muñoz, C. Márquez-Álvarez, G. Palmisano, L. Palmisano, F. Parrino and S. Yurdakal, *Appl. Catal., A*, 2008, **349**, 182–188.
- Y. Kim, B. D. Kay, J. White and Z. Dohnálek, *Catal. Lett.*, 2007, **119**, 1–4.
- L. Chen, R. S. Smith, B. D. Kay and Z. Dohnálek, *ACS Catal.*, 2017, **7**, 2002–2006.
- C. Walenta, S. Kollmannsberger, A. Winnerl, S. Weiszner, R. N. Pereira, M. Tschurl, M. Stutzmann and U. Heiz, *J. Phys. Chem. C*, 2017, **121**, 16291–16299.
- S. Kollmannsberger, C. A. Walenta, A. Winnerl, F. Knoller, R. N. Pereira, M. Tschurl, M. Stutzmann and U. Heiz, *J. Chem. Phys.*, 2017, **147**, 124704.
- M. A. Henderson, *Langmuir*, 1996, **12**, 5093–5098.
- Z. Li, R. S. Smith, B. D. Kay and Z. Dohnálek, *J. Phys. Chem. C*, 2011, **115**, 22534–22539.
- N. G. Petrik, M. A. Henderson and G. A. Kimmel, *J. Phys. Chem. C*, 2015, **119**, 12273–12282.
- N. G. Petrik, M. A. Henderson and G. A. Kimmel, *J. Phys. Chem. C*, 2015, **119**, 12262–12272.
- R. T. Zehr and M. A. Henderson, *Phys. Chem. Chem. Phys.*, 2010, **12**, 8085–8092.
- M. Shen and M. A. Henderson, *J. Phys. Chem. C*, 2011, **115**, 5886–5893.
- M. D. Kershish, D. P. Wilson and M. G. White, *J. Chem. Phys.*, 2013, **138**, 204703.
- M. A. Henderson, *Surf. Sci.*, 2008, **602**, 3188–3193.
- M. A. Henderson, *J. Phys. Chem. C*, 2008, **112**, 11433–11440.
- M. D. Kershish and M. G. White, *Phys. Chem. Chem. Phys.*, 2013, **15**, 17976–17982.
- M. A. Henderson, *J. Phys. Chem. C*, 2013, **117**, 14113–14124.
- M. Setvin, X. Shi, J. Hulva, T. Simschitz, G. S. Parkinson, M. Schmid, C. Di Valentin, A. Selloni and U. Diebold, *ACS Catal.*, 2017, 7081–7091.
- M. Shen and M. A. Henderson, *J. Phys. Chem. C*, 2012, **116**, 18788–18795.

[View Article Online](#)

PCCP

Paper

- 31 G. Kolesov, D. Vinichenko, G. A. Tritsarlis, C. M. Friend and E. Kaxiras, *J. Phys. Chem. Lett.*, 2015, **6**, 1624–1627.
- 32 Z. Zhang, O. Bondarchuk, B. D. Kay, J. M. White and Z. Dohnálek, *J. Phys. Chem. C*, 2007, **111**, 3021–3027.
- 33 M. A. Henderson, *J. Phys. Chem. B*, 2004, **108**, 18932–18941.
- 34 M. A. Henderson, M. Shen, Z.-T. Wang and I. Lyubinetsky, *J. Phys. Chem. C*, 2013, **117**, 5774–5784.
- 35 T. L. Thompson and J. T. Yates, *Chem. Rev.*, 2006, **106**, 4428–4453.
- 36 M. Shen, D. P. Acharya, Z. Dohnálek and M. A. Henderson, *J. Phys. Chem. C*, 2012, **116**, 25465–25469.

Electronic Supplementary Material (ESI) for Physical Chemistry Chemical Physics.
This journal is © the Owner Societies 2018

Supporting Information: Photocatalytic Selectivity Switch to C-C Scission: α -Methyl Ejection of tert-Butanol on TiO₂(110)

Constantin A. Walenta,^{†,‡,¶} Sebastian L. Kollmannsberger,^{†,¶} Carla Courtois,[†]

Martin Tschurl,[†] and Ueli Heiz^{*,†,‡}

[†] Chair of Physical Chemistry, Department of Chemistry & Catalysis Research Center,
Technische Universität München, Lichtenbergstr. 4, 85748 Garching, Germany

[‡] Nanosystems Initiative Munich, Schellingstr. 4, 80799 München, Germany

[¶] The authors contributed equally to this work

*corresponding author: ulrich.heiz@mytum.de

Data Analysis:

During the thermal and photo-desorption experiments, the potential products were monitored with several masses: Isobutene with masses 56, 41 and 39; acetone with 58 and 43; tert-butanol with 59 and 31; tert-butanol-OD with 59, 31 and 32. The methyl-radical was detected during the experiments on mass 15. Further molecules and corresponding masses including H₂ (2), HD (3), CH₄ (16), H₂O (18), HDO (19), CO (28), CO₂ (44) were recorded, but found to be insignificant with the exception of water (see Fig. S2). To quantify the results, the coverages of tert-butanol normalized to the H₂O-TPD of a

monolayer according to the convention in the literature.¹ The tert-butanol-OD was quantified using masses 31 and 32, because some isotope exchange could not be avoided in the gas line and on the single crystal. Isobutene and acetone were quantified using masses 56 and 58 as well as by considering the fragmentation of tert-butanol and the respective other molecules. For the quantification, all molecule yields were corrected for their fragmentation pattern, their transmission through the quadrupole mass spectrometer, and their ionization cross-sections (see Fig. S3 and S4).²⁻⁴

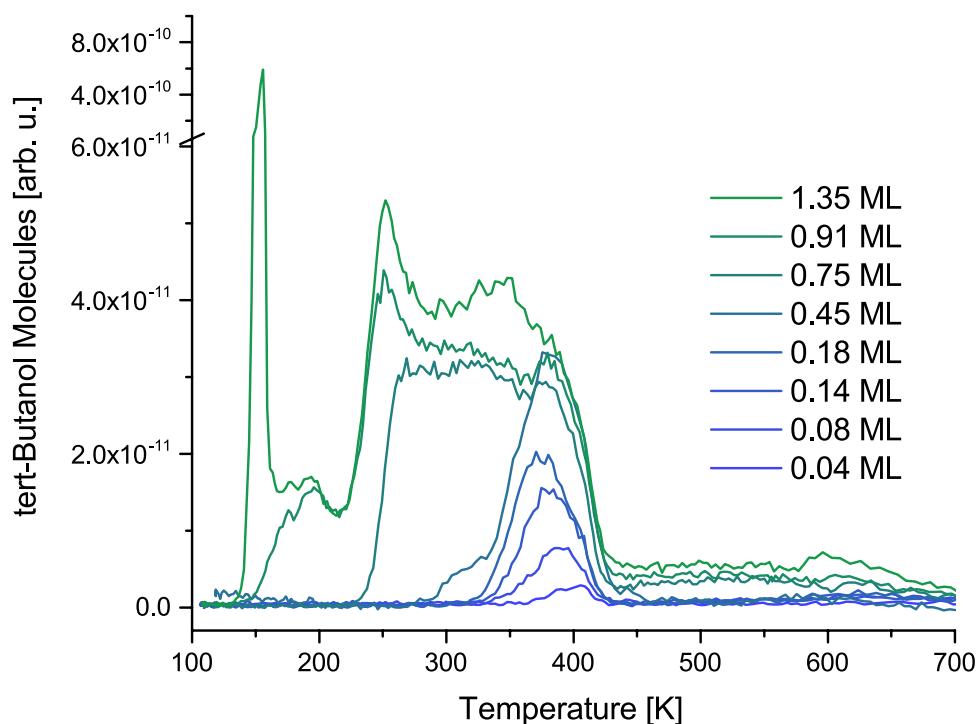


Figure S1: Coverage dependent TPD-series of tert-butanol-OD on a reduced TiO₂(110)-surface [r-TiO₂(110)]. At small coverages, a desorption feature at around 400 K arises, that is attributed to tert-butanol binding to the Ti-lattice sites. With higher coverages this feature saturates and a shoulder is growing to a peak at 250 K, which is assigned to the desorption from bridge-bonding oxygen (BBO) surface atoms. Another feature appearing below 200 K is attributed to multilayer desorption. The coverages are referenced to the

coverage determination of Dohnalek and co-workers and in very good agreement with their work.¹

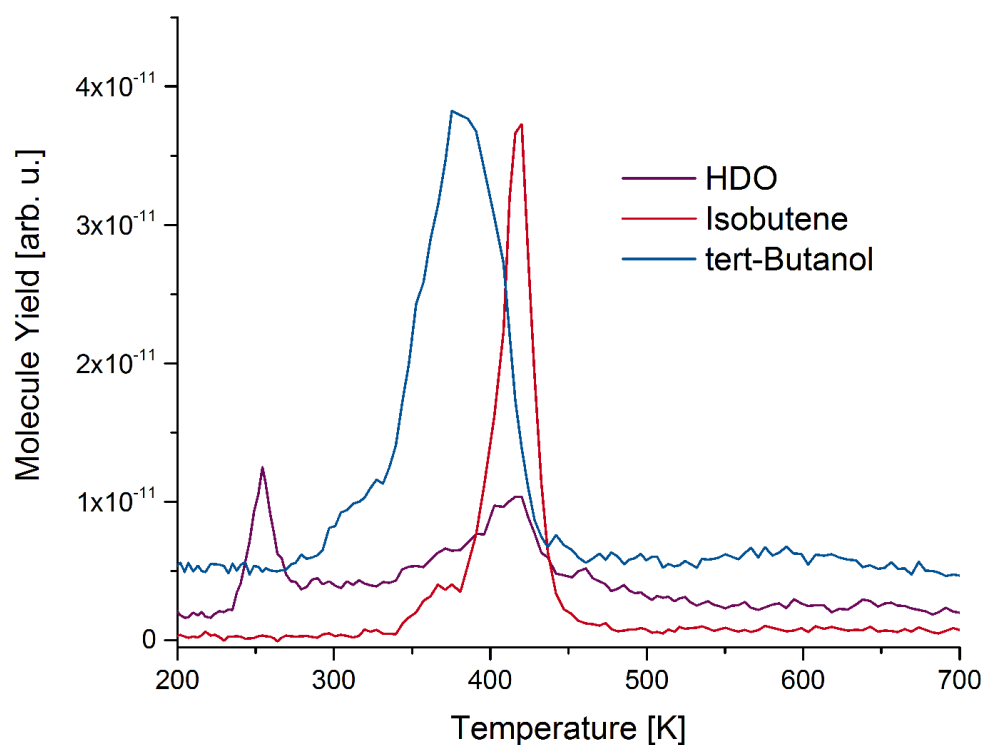


Figure S2: TPD of 0.45 ML tert-butanol-OD on r-TiO₂(110). Tert-butanol desorbs from the Ti-lattice sites, while a dehydration pathway to isobutene is observed at around 425 K, which is in agreement with previous studies.⁵⁻⁶ Additionally, the HDO ($m/z = 19$) was also monitored and two peaks occur: One is attributed to the direct dehydration pathway of tert-butanol-OD at 425 K, for which HDO is the by-product. In addition, another peak is observed at 250 K, which is attributed to the desorption of BBO-sites. It arises from water adsorption from the background and some dissociative adsorption, since some exchange to background adsorption from water is obtained.

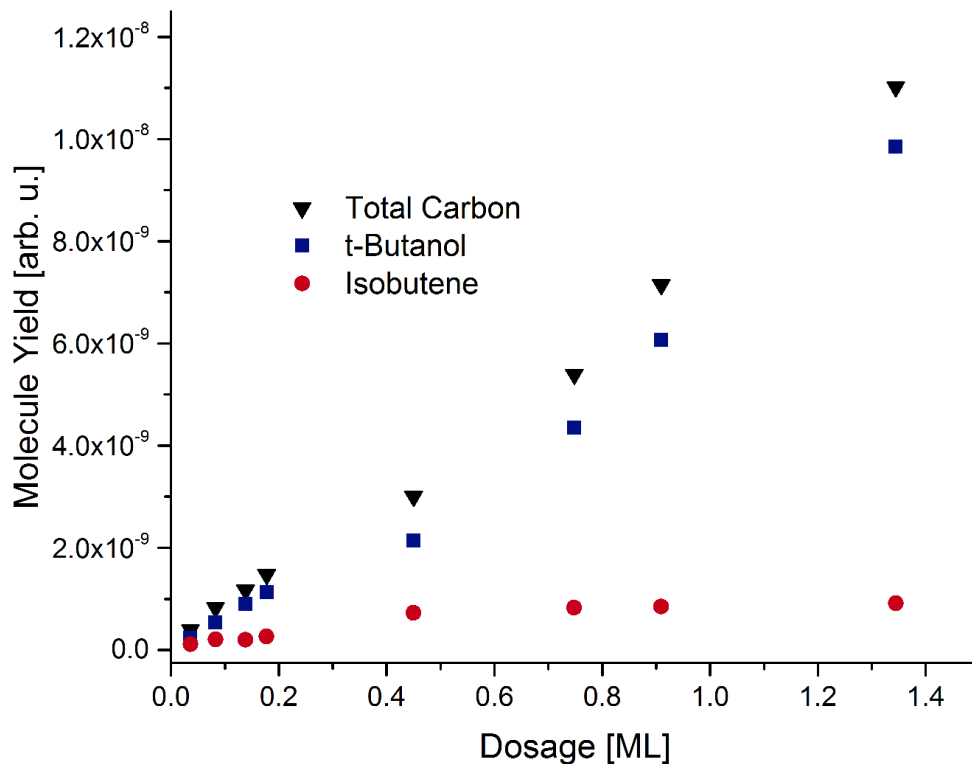


Figure S3: Integrated amounts of tert-butanol-OD and Isobutene for different coverages. While tert-butanol is shown in blue squares, the amount of isobutene is given in red circles. Auger electron spectroscopy and earlier studies¹ indicate that there are no carbon deposits for all alcohols on $r\text{-TiO}_2(110)$. Hence, the carbon balance can be closed, which is addressed by black triangles showing the total carbon dosage by addition of the carbon containing desorbing molecules.

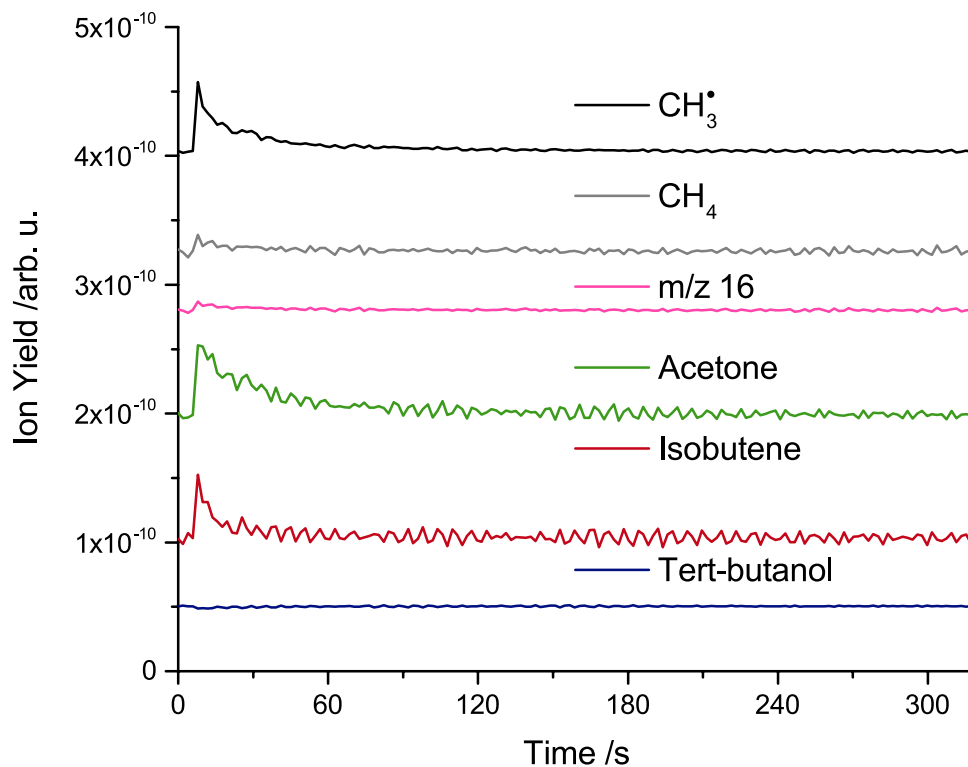


Figure S4: Isothermal photodesorption yield vs time for 0.18 ML of tert-butanol at 295 K on the $r\text{-TiO}_2(110)$ surface. Note, that for the fully stated molecules, cracking pattern contributions are already accounted for. The traces are offset for clarity. The signal of m/z 15 is more than 8 times as much as for m/z 16. This is a clear indicator, that really a methyl radical is ejected during the photoreaction, while only trace amounts of methane are observed. The purple trace represents the raw data for mass 16. Note, that all correction factors as described above are included in that data, which increases also the noise in this data set.

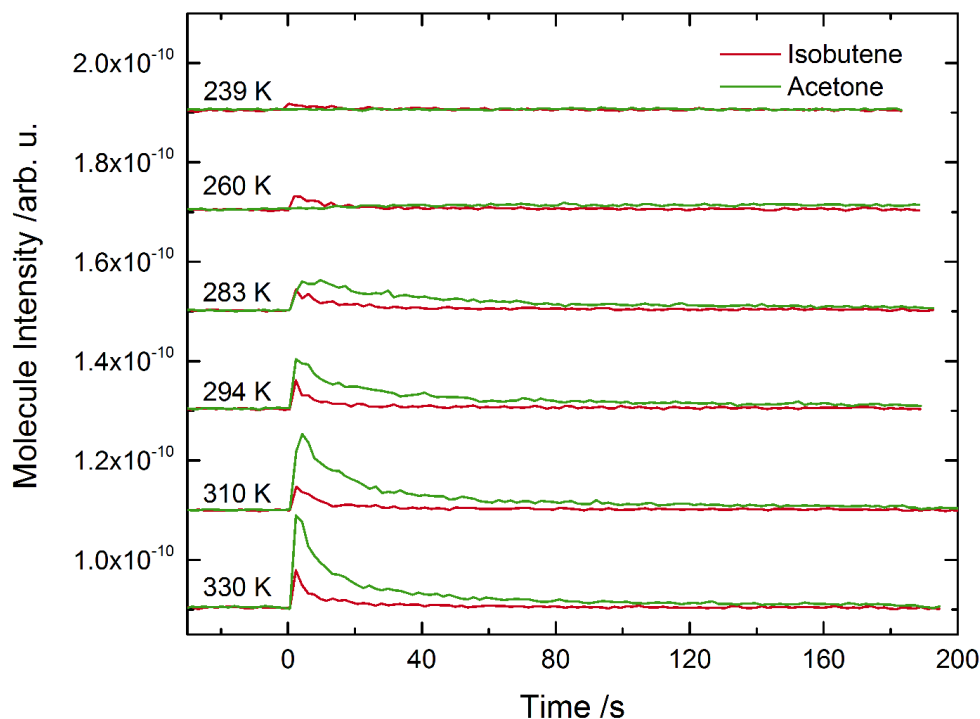


Figure S5: Isothermal photodesorption yield vs time for 0.18 ML of tert-butanol at different temperatures on a r-TiO₂(110) surface. The UV illumination is started at 0 s and ended after 180 s. For all temperatures, some desorption of both isobutene and acetone is observed, while no tert-butanol desorbs by irradiation. By increasing the temperature, both the overall apparent desorption rate is increased as well as the selectivity towards acetone. The traces are offset for clarity.

Notes and references:

- 1 Li, Z.; Smith, R. S.; Kay, B. D.; Dohnálek, Z., *J. Phys. Chem C*, 2011, **115**, 22534-22539.
- 2 Bull, J. N.; Harland, P. W.; Vallance, C., *J. Phys. Chem. A*, 2012, **116**, 767-777.
- 3 Irikura, Y.-K. K. K. K. In *BEB*, Proc. 2nd Int. Conf. on Atom. Molec. Data and Their Applications, Bell, K. A. B. K. L., Ed. AIP, New York, NY: 2000.

- 4 Hudson, J. E.; Hamilton, M. L.; Vallance, C.; Harland, P. W., *Phys. Chem. Chem. Phys.*, 2003, **5**, 3162-3168.
- 5 Kim, Y. K.; Kay, B. D.; White, J. M.; Dohnálek, Z., *J. Phys. Chem. C*, 2007, **111**, 18236-18242.
- 6 Kim, Y. K.; Kay, B. D.; White, J. M.; Dohnálek, Z., *Catal. Lett.*, 2007, **119**, 1-4.

E. Unpublished Manuscripts

E.1. Thermal control of selectivity in photocatalytic, water-free alcohol photo-reforming

Thermal control of selectivity in photocatalytic, water-free alcohol photo-reforming

Sebastian L. Kollmannsberger,^{†,¶} Constantin A. Walenta,^{†,‡,¶} Carla Courtois,[†]
Martin Tschurl,[†] and Ueli Heiz^{*,†,‡}

[†]*Chair of Physical Chemistry, Department of Chemistry & Catalysis Research Center,
Technische Universität München, Lichtenbergstr. 4, 85748 Garching, Germany*

[‡]*Nanosystems Initiative Munich, Schellingstr. 4, 80799 München, Germany*

[¶]*The authors contributed equally to this work*

E-mail: ulrich.heiz@mytum.de

Phone: +49 (0) 89 289 13391. Fax: +49 (0) 89 289 13389

Abstract

The selective oxidation of alcohols has not only recently attracted great attention. In this work we focus on the photo-reforming of methanol, ethanol, cyclohexanol, benzyl alcohol and tert-butanol on well defined Pt_x/TiO₂(110) in the UHV. It is found, that with the exception of tert-butanol, alcohol oxidation produces the respective water-free aldehydes and ketons along with the formation of stoichiometric molecular hydrogen with 100% selectivity. Molecular stoichiometric mechanisms are presented for this type of reactions and the photo-oxidative coupling reactions. A strong influence of temperature on the selectivity is demonstrated and the role of the metal particles is further clarified.

Introduction

Selective oxidation of alcohols has attracted extensive attention in the last decade.¹⁻³ In this regard tuning the selectivity of photocatalytic reactions is currently heavily studied.^{4,5} A key step to high selectivities is the fundamental understanding of photocatalytic mechanisms. Therefore, studies on perfectly defined semiconductor single crystals are of utmost importance. Titania based systems do not only represent the most heavily used semiconductors in photocatalytic applications, but $\text{TiO}_2(110)$ is also a well-available, heavily studied single crystalline material. Therefore, it represents an ideal material to elucidate fundamental mechanisms in photocatalysis. Similarly, Pt is a very prominent and often used co-catalyst for the photocatalytic hydrogen evolution.⁶ In alcohol reforming, the photocatalytic synthesis of highly industrial relevant products as benzaldehyde, formaldehyde or cyclohexanone is particularly attractive. Benzaldehyde is among the most important molecules in cosmetics and flavor industries.⁷ Formaldehyde is, besides of its application as building block chemical, also needed as precursor for potential ultra-low emission fuels.⁸ In particular the formation of water-free formaldehyde as an alternative to the commonly used formox process, which requires a complex procedure to be freed from water and other impurities is of great interest.⁹ Cyclohexanone is a precursor molecule for the production of nylon-6 and is industrially synthesized by either a high temperature and high pressure oxidation of cyclohexane or a two step process starting from phenol.¹⁰ Consequently, the development of a one step photo-process may be observed with great attention. Ethanol oxidation is highly relevant, as it is easily available in large amounts from biomass conversion and its photo-oxidation to produce solar hydrogen from bio ethanol is environmentally benign.¹¹

As it is generally known that photo-oxidation of primary and secondary alcohols proceeds via an abstraction of the $\alpha\text{-H}$,¹²⁻¹⁵ the investigation of a tertiary alcohol like tert-butanol is therefore mechanistically interesting, because the conventional pathway is not feasible. Therefore, we have chosen these four alcohols, whose conversions are industrially relevant and the mechanistically interesting tert-butanol for the photocatalytic reforming.

While alcohol oxidations have been explored in great depth on bare $\text{TiO}_2(110)$ single crystal surfaces in single coverage experiments,^{14–26} investigations with co-catalyst loaded semiconductors under catalytic conditions are scarce. However, such studies enable unique insights into mechanistic details. In the following we demonstrate the determination of stoichiometric mechanisms for the photo-oxidation of alcohols, photo-oxidative coupling reactions, the formation of hydrogen and temperature induced selectivity changes as well as the description of the role of the metal particles.

Experimental

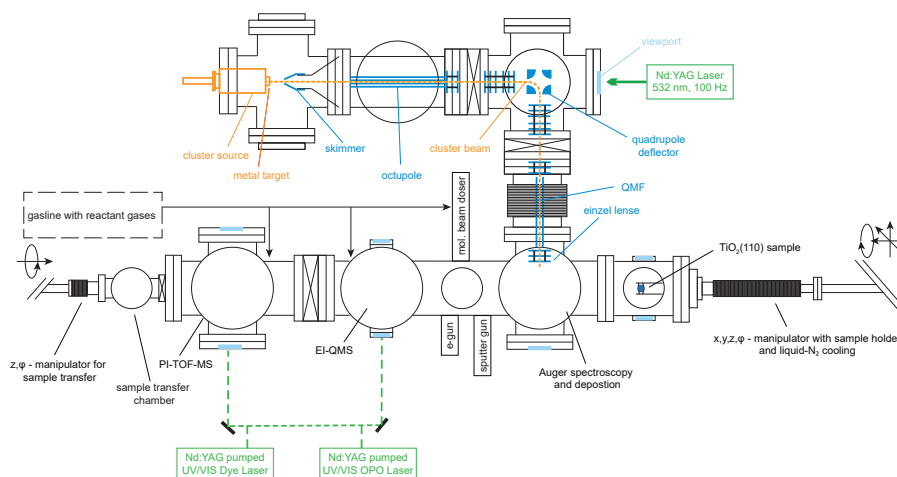


Figure 1: Chamber scheme of the UHV apparatus including the laser vaporization cluster source and the laser system.

The experimental setup for photocatalytic measurements, which is shown schematically in figure 1, consists of a UHV chamber with a background pressure better than 9.8×10^{-11} mbar and a laser vaporization cluster source for the deposition of size selected metal clusters. The main chamber includes a manipulator (VAB Vakuum GmbH), a surface preparation and surface analysis part, a reaction part with an electron ionisation quadrupole mass spectrom-

eter (EI-QMS) (QMA 430, Pfeiffer Vacuum GmbH) and a homebuilt photo ionisation time of flight mass spectrometer (PI-TOF-MS), which enables the selective ionisation of isobar molecules.²⁷ Furthermore, a sample transfer chamber and a gasline with reactant gases, which contains a leak valve and a molecular beam doser, are attached to the chamber.

The sample holder, which is described in detail elsewhere,¹⁴ enables liquid nitrogen cooling and heating. The laser system consists of a Nd:YAG pumped dye laser and a Nd:YAG pumped UV/Vis OPO laser. The photoexcitation of the semiconductor is carried out with a wavelength of 242 nm, obtained by the frequency doubled OPO laser (GWU, premiScan ULD/400) which is pumped by the third harmonic of a Nd:YAG-laser (Innolas Spitlight HighPower 1200, 7 ns pulse width, 20 Hz repetition rate).

The rutile TiO₂(110) single crystal (SurfaceNet GmbH) was prepared by cycles of Ar⁺-sputtering (1.5 keV, 1×10^{-5} mbar, 30 min), oxygen annealing (800 K, 1×10^{-6} mbar, 20 min) and vacuum annealing (800 K, 10 min) until no contamination was detected in Auger electron spectroscopy (AES). The resulting TiO₂(110) has a light blue color with a bridge-bonded oxygen (BBO) vacancy concentration determined with H₂O TPD, of $6 \pm 1\%$ of Ti-lattice sites.²⁸

The laser vaporization cluster source is operated by a Nd:YAG laser (532 nm, 100 Hz, Innolas), which ablates a Pt target (99.95% purity, ESG Edelmetalle, Germany). The resulting plasma is cooled by a He pulse and expanded into the vacuum. The resulting cationic clusters are guided and bent into a quadrupole mass filter (QMF) (Extrel, USA) to enable cluster size selection.²⁹ The QMF is operated with the AC-potential only in this work and acts as an ion guide discarding all masses lower than Pt₈. With these settings a size-distribution from Pt₇ to Pt₃₅ with a maximum from Pt₁₁ to Pt₁₃ (see SI Fig. S1) results. The deposition of 1% ML Pt (respective to the surface atoms) onto the TiO₂(110) single crystal occurs under soft-landing conditions ($< 1\text{eV}/\text{atom}$ in kinetic energy), as checked with retarding field analysis. The cluster loadings are determined by recording the cluster current during deposition with a picoammeter (Keithley, 6587). The samples are named Pt_{*x*}/TiO₂(110) in the

following.

Methanol (Chromasolv, $\geq 99.9\%$, Sigma-Aldrich), ethanol (absolute, HPLC grade, $\geq 99.8\%$, Sigma-Aldrich), cyclohexanol (99%, Sigma-Aldrich), tert-butanol (2-methyl-2-propanol, $\geq 99.5\%$, Sigma-Aldrich) and benzyl alcohol (99.8%, Sigma-Aldrich) were degasified by several freeze-pump-thaw cycles prior to their insertion via a leak valve into the UHV chamber.

Results

In order to study the process of alcohols in photo-reforming, UV illumination experiments have been carried out in alcohol background pressure.

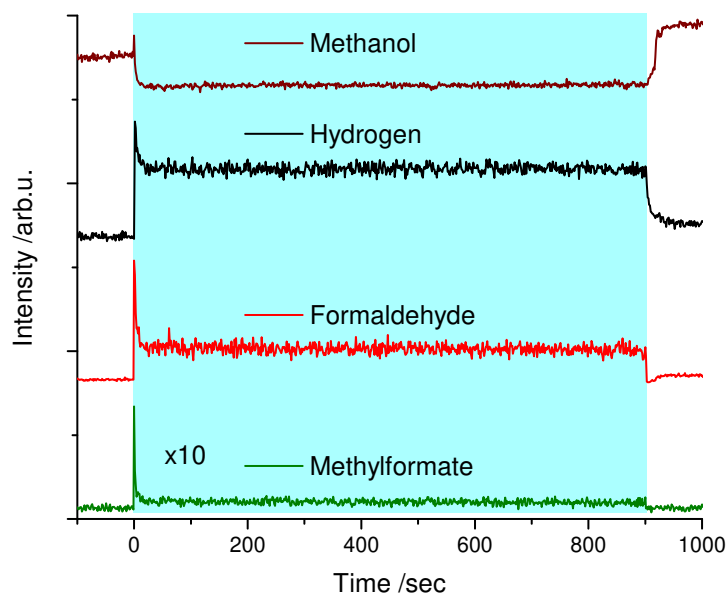


Figure 2: Methanol ($m/z = 32$), hydrogen ($m/z = 2$), formaldehyde ($m/z = 30$) and methyl formate ($m/z = 60$) signals at 262 K in a methanol background pressure of 7×10^{-8} mbar. The blue region highlights the period of laser irradiation (242 nm, 195 μJ). Note that the methyl formate signal is multiplied with a factor of 10 for better visibility.

Figure 2 shows the QMS traces of methanol, hydrogen, formaldehyde and methyl formate

during laser irradiation of the $\text{Pt}_x/\text{TiO}_2(110)$ at 262 K in a methanol background pressure of 7×10^{-8} mbar. On the one hand, the intensity of the methanol fragment drops drastically with the start of the illumination and goes back to the initial value when the illumination is stopped. On the other hand, the irradiation leads to an immediate rise of the molecular hydrogen, the formaldehyde and the methyl formate intensities. After about 10 sec a steady state in the formation of formaldehyde and all other molecules is reached, which is then constant over the whole illumination time. From a baseline corrected integral of the constant region of formation, a turn over frequency (TOF) is determined. The QMS is calibrated for methanol to obtain quantitative values from the ion currents. In this quantitative analysis of the respective molecule, its fragmentation pattern, its electron impact ionization cross sections (see SI Table S1) and the m/z dependent transmission through the QMS are considered. Moreover, for the determination of TOFs the amount of active sites is attributed to the number of BBO vacancies (see Discussion). The TOFs of the other alcohols are determined in identical experiments with the same procedure of quantification.

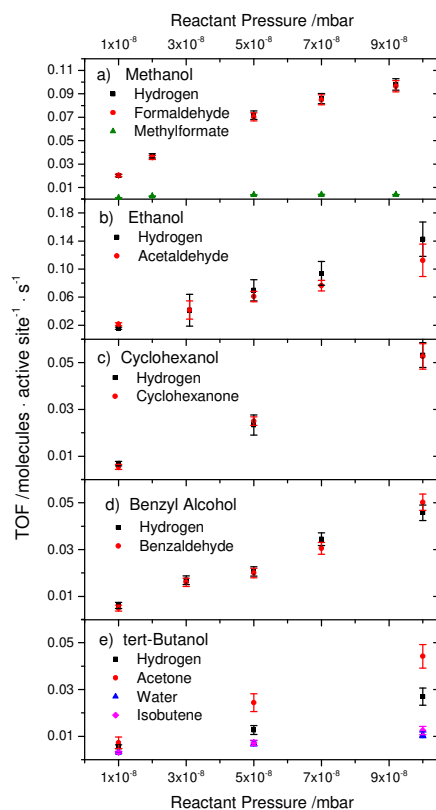


Figure 3: Pressure-dependent TOFs for photocatalytic reforming of a) methanol, b) ethanol, c) cyclohexanol, d) benzyl alcohol and e) tert-butanol. The temperature is 260 K in a), 280 K in b),c),e) and 300 K in d). In general the TOFs rise linearly in the investigated pressure range and a saturation behavior is not observed. Note that other products than the displayed ones are not observed.

In figure 3 the pressure dependent TOFs of the five different alcohols are depicted in the range from 1×10^{-8} mbar to 1×10^{-7} mbar. Higher pressures were not studied to ensure that ion-molecule reactions after electron impact ionization in the QMS do not deteriorate a quantitative determination of the products. From all α -H containing alcohols the respective aldehyde or ketone and H_2 , corresponding to the stoichiometry of the reaction, are observed. With higher reactant pressure the TOFs rise linear, with the exception of methanol, for which a flattening may be observed. Furthermore, other by-products are not detected at the investigated temperature for all α -H containing alcohols. This is again different for methanol, for

which photo-reforming leads to the formation of methyl formate. The TOF of this reaction shows a saturation behavior, starting at a pressure of 5×10^{-8} mbar (see SI Fig. S2 for zoom in methyl formate TOF). A comparison of both carbon-based products (i.e. methyl formate and formaldehyde) as a function of laser power reveals that a further photon is needed for the reaction to methyl formate (see SI Fig. S3). For ethanol other reaction pathways can be ruled out, as different mass fragments (see SI Fig. S4) do not exhibit any change in signal during illumination after cracking pattern correction. Similarly, also for cyclohexanol and benzyl alcohol a selectivity of 100% toward the ketone and the aldehyde occurs.

An exception to those α -H containing alcohols is tert-butanol, for which the standard oxidation pathway of the other alcohols is excluded. Therefore, only $1/2$ H_2 is obtained from the oxidation of one tert-butanol to acetone, accompanied by stoichiometric methyl-radical ejection. Furthermore, an additional side reaction forming isobutene and water is observed. The photo-reforming of each alcohol is stoichiometric in long time experiments (≥ 30 min) and without any changes in the TOFs.

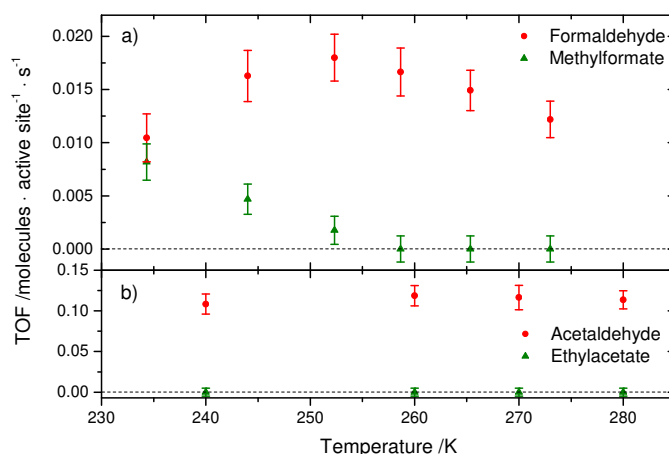


Figure 4: Temperature dependent TOFs for a) methanol (1×10^{-8} mbar) and b) ethanol (1×10^{-7} mbar) photo-reforming. Methanol (a)) shows a temperature induced selectivity change from formaldehyde to methyl formate. Instead, ethanol (b)) does not exhibit a reaction to ethyl acetate and the TOFs are temperature independent in the investigated temperature range from 240 K to 280 K.

For all alcohols the reaction has been investigated for their temperature-dependence under isobaric condition. Figure 4 shows the product distribution for methanol and ethanol oxidation as a function of temperature but otherwise constant conditions. For methanol photoreforming about the same amount of formaldehyde and methyl formate is produced at 235 K (figure 4a). However, the selectivity of the reaction changes drastically with higher temperatures. The TOF to methyl formate drops to zero at around 260 K, while that to formaldehyde remains high. More precisely this means that a temperature-dependent selectivity toward $A_{\text{formaldehyde}}$, defined as $S_{\text{formaldehyde}} = \frac{A_{\text{formaldehyde}}}{A_{\text{total product}}}$, is obtained from 56% at 235 K and 100% at 273 K. While the reaction becomes more selective, the conversion of methanol declines at temperatures higher than 250 K.

For the conversion of ethanol it can be seen, that no by-product is observed over the whole investigated temperature range (figure 4b). As a result a 100% selectivity to acetaldehyde is always achieved. Furthermore, a change in the TOF is only visible at temperatures lower than 200 K (see SI Fig. S5), while it stays constant at elevated values. The differences in the TOFs of formaldehyde and acetaldehyde of about a factor 10 are only related to different background pressure of the respective reactant, which was chosen to completely rule out a consecutive photo-reaction for ethanol.

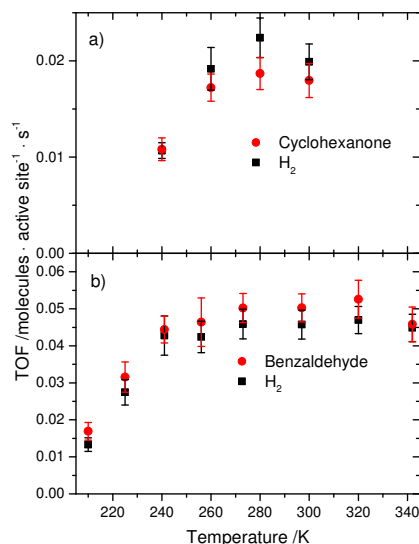


Figure 5: Temperature dependent TOFs for a) cyclohexanol (1×10^{-8} mbar) and b) benzyl alcohol (5×10^{-8} mbar) photo-reforming. Secondary products are not observed from cyclohexanol and benzyl alcohol reforming. The TOFs in a) and b) rise with temperature and saturate at around 260 K.

Figure 5a shows the cyclohexanone TOFs in the range from 240 K to 300 K and figure 5b the benzaldehyde TOFs in the range from 210 K to 340 K. A rise of the turnover is observed for both alcohols in the lower temperature region up to ≈ 260 K. In the region above this temperature the investigated TOFs remain almost constant. Furthermore, a 100% selectivity to cyclohexanone and nearly a 100% selectivity to benzaldehyde during the respective photo-reforming is found. For the latter molecule, a minor by-product is detected at a $m/z=92$ fragment (see SI Fig. S6a), which can be attributed to benzyl benzoate. Its very low signal-to-noise intensity excludes a reliable product quantification. Therefore, only a qualitative evaluation is shown in the SI (Fig. S6b).

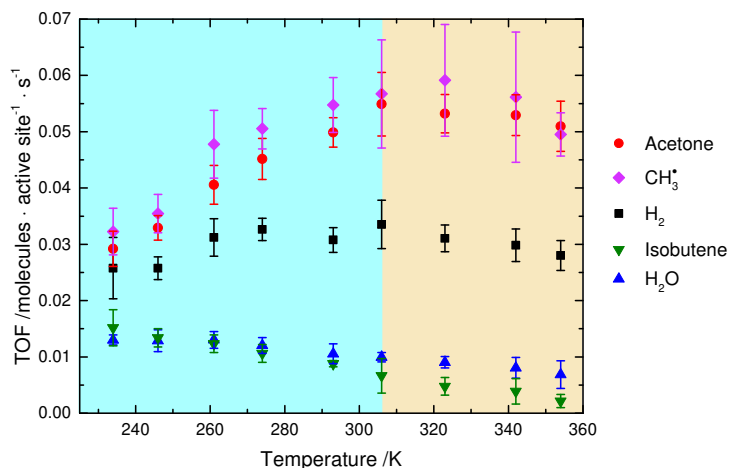


Figure 6: Temperature dependent TOFs for tert-butanol (1×10^{-7} mbar) photo-reforming. The lower temperature region up to ≈ 305 K, in which the turn over to acetone rises, is depicted in blue. The upper temperature region, with a constant or slight decrease of the acetone TOF, is depicted in ochre. Over the whole investigated temperature region, the turnover of isobutene and H_2O declines with rising temperature.

For the temperature-dependent TOFs of tert-butanol photo-reforming a complex behavior occurs. On the one hand, a rise in the TOFs of acetone, methyl radical and H_2 is observed with rising temperatures from 230 K to 305 K (blue region in Figure 6). Afterwards the turnover of those products is constant or decreases slightly (ochre region). On the other hand, the TOFs of isobutene and H_2O show a slow decrease over the entire temperature range. Consequently, the selectivity to acetone is increasing strongly from 66% at 234 K to 96% at 306 K (blue region) and only very weakly in the ochre part.

Discussion

Active Site

There is still an ongoing discussion, whether the photocatalytic alcohol oxidation proceeds via a thermally formed alkoxy species^{16–20} or via a photoinduced one.^{21–25} However, the majority of studies favor a thermal process over a photochemical one. In this regards,

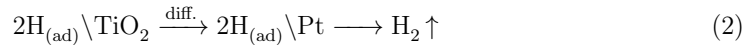
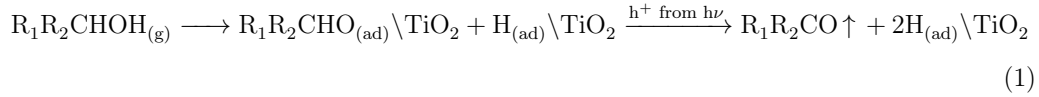
laser power-dependent TOFs previously supplied strong evidence that methanol oxidation is an one photon process (see also SI Fig. S7).⁷ Moreover, during a dark case ethanol dosing to a Pt_x/TiO₂(110) at 277 K a short-term hydrogen evolution occurs (see SI Fig. S8), which can be attributed to recombination of hydrogen atoms from thermal ethoxy formation. Furthermore, SFG measurements and DFT calculations suggest that molecularly and dissociatively adsorbed methanol are present at Ti_{5c}-sites.³⁰ Based on these evidences, we assume a photo-oxidation of thermally formed alkoxy in the following.

In addition, as only about 15% of a monolayer are always converted into the oxidation product on a bare TiO₂(110),^{14,15,26} a complete conversion of all Ti_{5c} bound alcohol species can be ruled out. Consequently, a connection to a special reactive site seems logical. As the BBO vacancy is negatively charged (instead of two Ti⁴⁺ two Ti³⁺ are observed)³¹ a hole, which is coming to the surface under illumination, would likely be attracted from this site. Consequently a photo-reaction at the BBO vacancy or in the vicinity of the BBO vacancy seems highly probable. Following this argumentation, we have chosen to use the amount of BBO vacancies for the determination of TOFs.

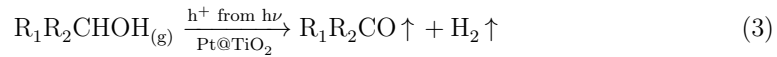
Oxidation Reaction

Photocatalytic alcohol reforming on Pt_x/TiO₂(110) produces water-free aldehyde or ketone of the respective alcohol and stoichiometrically molecular hydrogen as shown previously for methanol.⁷ The first step is the thermal reaction by dissociative adsorption, resulting in the formation of an alkoxy and a hydrogen atom. The following photo-oxidation of the alkoxy species proceeds via a hole-mediated α -H abstraction. The resulting aldehyde or ketone desorbs thermally for high enough temperatures. The remaining two hydrogen atoms diffuse on the TiO₂(110) surface, recombine at a Pt cluster and finally desorb, which are all thermal processes. The reaction equations are shown for the general alcohol oxidation eq.1, hydrogen

recombination eq.2 and the total reaction eq.3.



and the total reaction:



This mechanism is used for the interpretation of all α -H containing alcohols. From the determined TOFs it can be seen, that a stoichiometric aldehyde or ketone to hydrogen ratio is observed.

Pressure Dependence

In the investigated pressure range a linear rise of the TOFs is visible for all investigated alcohols, despite of methanol, at a temperature of maximal TOF. From this linear rise an adsorption limitation can be concluded.³² Consequently, the alcohol photo-reforming is a first order reaction with the reactant pressure in the investigated pressure range. A saturation of the reactive surface sites with reactant is not obtained.

Table 1: Rate constants (k) at a temperature (T) of maximal rate, referenced to the alcohol pressure.

| Product | k [$\times 10^5$] | T [K] |
|---------------------|---------------------|-------|
| Formaldehyde | 16.6 ± 1.8 | 260 |
| Acetaldehyde | 10.6 ± 1.2 | 280 |
| Acetone | 4.6 ± 0.3 | 280 |
| Isobutene | 1.5 ± 0.4 | 280 |
| Acetone + Isobutene | 6.1 ± 0.7 | 280 |
| Cyclohexanone | 5.1 ± 0.1 | 280 |
| Benzaldehyde | 4.6 ± 0.2 | 300 |

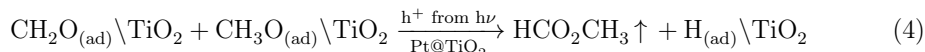
In order to compare the rates of the different alcohol photo-reforming reactions, the reaction rate k , normalized to the pressure of the alcohol, is determined (see table 1). For tert-butanol the summarized acetone and isobutene TOF reflects the rate of tert-butanol conversion. As methyl formate formation does not change the methanol conversion significantly at the investigated temperature, it is omitted for the determination of the reaction rate constant. Although the temperature is the lowest for formaldehyde production, the largest rate constant is obtained. In general, a decrease of the rate constant with the steric demand of the alcohol is visible, which can be ascribed to a steric hindrance of the active site required geometry, which is in good accordance with the adsorption-limitation of the reaction rate.

Temperature Dependence

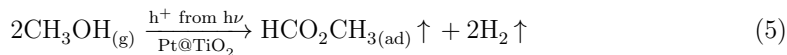
At the applied substrate pressure the TOF rises for all investigated alcohols in a low temperature regime, after which it stays constant or slightly decreases at higher temperatures. This behavior can be explained with the relationship of temperature and pressure. When the TOF rises with temperature an increasing product formation due to faster product desorption occurs. As soon as the curve flattens not enough substrate is any longer available at the surface to enable a further increase in the TOF. This adsorption limitation can be counteracted with higher substrate pressures resulting in a later flattening of the curve.³³ The activation energies, which can be obtained from the slope of the linear region in an Arrhenius plot are very low ($< 20 \frac{\text{kJ}}{\text{mol}}$) (see SI Fig. S9 and Table S2). This is as expected for photocatalytic reactions³⁴ and is a strong evidence for a limitation by product desorption. Furthermore, the observed adsorption limitation at higher temperatures is in very good accordance with the determined pressure dependent behavior.

Oxidative coupling reaction

A further reaction pathway is found for methanol, for which a coupling to methyl formate occurs. This consecutive oxidation reaction is the only additionally observed pathway for methanol photo-reforming. The formation of this coupling product is in good agreement with non steady-state photocatalytic studies on bare $\text{TiO}_2(110)$,^{19,22,24} but the exact coupling mechanism producing methyl formate is still under discussion. It is suggested that either a formyl or a hemiacetal intermediate is formed to produce methyl formate.^{19,22,35} Both pathways represent photo-activated mechanisms, in which a photon is needed for the coupling of formaldehyde and methanol, as it is also observed by the illumination dependence in this study (see Fig. S3). The resulting reaction equation is in eq.4:



The total reaction is given by:



A strong temperature dependence is observed for the selectivity toward methyl formate. It is related to the residence time of formaldehyde on the TiO_2 surface, which has to be long enough in order to enable the consecutive reaction. As the formaldehyde desorption maximum from a reduced $\text{TiO}_2(110)$ surface is at around 260 K,^{16,24,36} the drop in the methyl formate TOF can be related to a higher desorption rate resulting in a significant decrease in the residence time of the molecule. For photo-reforming of benzyl alcohol a similar coupling mechanism occurs resulting in the production of benzyl benzoate, but with a strongly reduced rate. Similarly to the formation of methyl formate, the consecutive photooxidation step is strongly dependent on temperature and only in a small window little amount of benzyl benzoate is detected.

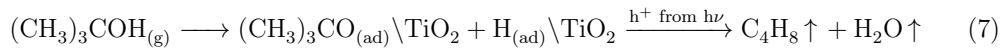
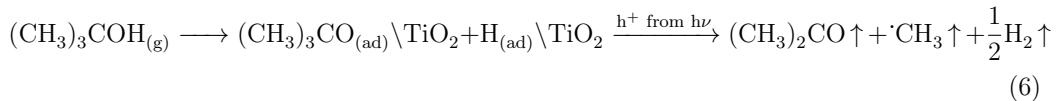
In contrast to formaldehyde and benzaldehyde the second photo-oxidation step does not

occur for adsorbed acetaldehyde. This is in good accordance with previous work of Henderson and Friend, who showed that photo-oxidation of acetaldehyde is not possible on reduced $\text{TiO}_2(110)$ in contrast to the photo-oxidation of formaldehyde.^{36,37} Our study demonstrates that the pathway of photoinduced decomposition of acetaldehyde on reduced $\text{TiO}_2(110)$ proposed by Yang and coworkers³⁸ is not relevant under catalytic conditions.

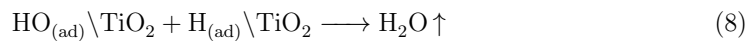
From cyclohexanol photo-reforming a coupling product would only be possible if a ring opening would occur. However, such a reaction can be ruled out as no product besides cyclohexanone is detected.

Tert-butanol photo-reforming

In contrast to the α -H containing alcohols, tert-butanol photo-oxidation leads to methyl ejection and the desorption of hydrogen and acetone. Furthermore, isobutene and water are formed via a photo activated thermal reaction pathway. Both pathways are reflected in the stoichiometry of the photo-reaction and were observed also on the bare TiO_2 previously,³⁹ but without the evolution of molecular hydrogen. The reaction on Pt-loaded TiO_2 are given in equation 6 and 7.



with the formation of water resulting from a dehydroxylation of the semiconductor:



The selectivity of tert-butanol photo reforming shows also a pronounced temperature-dependence. While the acetone pathway is thermally hindered, which is attributed to a limitation for the thermal butoxy formation, the isobutene formation declines continuously with rising temperature. This is due to the required transition state of the photothermal reaction, which has previously been attributed to be a 5-membered cyclic structure involving the BBO-vacancy.³⁹ While the transition state may be thermodynamically favored, the probability for molecules exhibiting this particular geometry declines with rising temperature, because of entropic reasons.

Conclusion

In summary, water-free alcohol photo-reforming on Pt_x/TiO₂(110) at room temperature is shown for five alcohols (methanol, ethanol, cyclohexanol, benzyl alcohol and tert-butanol) under anaerob conditions. The main reaction products of all α -H containing alcohols is the respective aldehyde or ketone and stoichiometric molecular hydrogen. The photo-oxidation mechanism proceeds via an hole-mediated α -H abstraction of dissociative adsorbed alcohol on the TiO₂ surface and recombination of abstracted hydrogen at Pt_x clusters, a mechanism, which was recently described by us.⁷ In particular, the reaction of tert-butanol excludes a pathway via the conventional photoelectrochemical-type mechanisms, but is in perfect agreement with the reaction model suggested by us. For all α -H containing alcohols 100% selectivity toward the aldehyde or the ketone is obtained with an optimization of the reaction temperature. For methanol photo-reforming a consecutive photo-oxidation yielding the coupling product methyl formate is obtained. As for higher temperatures the residence time of formaldehyde is decreased, the production rate of the coupling product declines strongly. While this consecutive photo-reaction is also enabled for benzaldehyde yielding benzyl benzoate, but significantly less pronounced than for formaldehyde, all other investigated alcohols do not exhibit this reaction.

However, for tert-butanol a completely different reaction behavior is observed. Instead of an α -H removal a methyl radical is ejected, leading to acetone as main product from tert-butanol photo-reforming. Furthermore, isobutene and stoichiometric water results from tert-butanol photo-reforming and the selectivity of this reaction changes with temperature, as the rate of acetone formation strongly increases with rising temperature.

In summary, it is shown that the temperature plays a major role in the selectivity of photocatalytic reactions. Consequently, the temperature-control of photocatalyzed processes is prerequisite to achieve an optimized reaction control.

Our work further demonstrates that photocatalytic gasphase alcohol oxidation produces the respective water-free aldehydes and ketons with high selectivities and suggests that these reactions can also be conducted under industrially-relevant conditions.

Acknowledgement

The authors thank the DFG through grant HE3435/22-1. C.A.W., S.L.K., C.C. and M.T. express gratitude to Christian Steiffen for keeping up the good mood during the experiments.

Supporting Information Available

The following files are available free of charge.

The Supplementary Information includes the size distribution of the deposited Pt clusters. Furthermore, a table of the electron impact ionization cross sections of the investigated molecules is shown. Moreover a zoom in the pressure-dependent TOFs to methyl formate is depicted. An incident light energy dependent photocatalytic methanol reforming experiment is presented. Furthermore the CH_3 fragment intensity is compared to the acetaldehyde turn over in a pressure dependent ethanol photo-reforming experiment. The low temperature region of the ethanol photo-reforming TOFs is presented. The water, oxygen, benzaldehyde and benzyl benzoate QMS traces are shown for a temperature-dependent benzyl alcohol

photo-reforming experiment and the coupling product benzyl benzoate is depicted qualitative. Laser power dependent TOFs are shown for methanol photo-reforming. Molecular hydrogen evolution from ethanol in non-illumination conditions is presented. Arrhenius plots are given for acetaldehyde, cyclohexanone, benzaldehyde and acetone. The activation energies are summarized in a table.

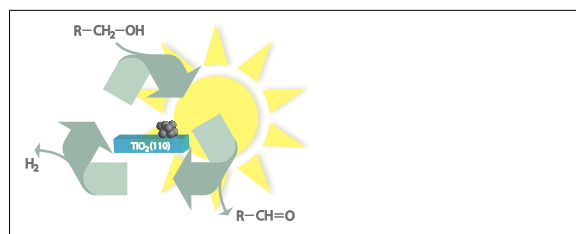
References

- (1) Davis, S. E.; Ide, M. S.; Davis, R. J. *Green Chem.* **2013**, *15*, 17–45.
- (2) Parmeggiani, C.; Cardona, F. *Green Chem.* **2012**, *14*, 547–564.
- (3) Vinod, C. P.; Wilson, K.; Lee, A. F. *J. Chem. Technol. Biot.* **2011**, *86*, 161–171.
- (4) Sanwald, K. E.; Berto, T. F.; Eisenreich, W.; Gutiérrez, O. Y.; Lercher, J. A. *J. Catal.* **2016**, *344*, 806 – 816.
- (5) Yang, X.; Zhao, H.; Feng, J.; Chen, Y.; Gao, S.; Cao, R. *J. Catal.* **2017**, *351*, 59 – 66.
- (6) Chen, X.; Shen, S.; Guo, L.; Mao, S. S. *Chem. Rev.* **2010**, *110*, 6503–6570.
- (7) Pina, C. D.; Falletta, E.; Rossi, M. *J. Catal.* **2008**, *260*, 384 – 386.
- (8) Omari, A.; Heuser, B.; Pischinger, S. *Fuel* **2017**, *209*, 232 – 237.
- (9) Su, S.; Zaza, P.; Renken, A. *Chem. Eng. Technol.* **1994**, *17*, 34–40.
- (10) Claus, P.; Berndt, H.; Mohr, C.; Radnik, J.; Shin, E.-J.; Keane, M. A. *J. Catal.* **2000**, *192*, 88 – 97.
- (11) Ni, M.; Leung, D. Y.; Leung, M. K. *Int. J. Hydrogen Energy* **2007**, *32*, 3238–3247.
- (12) Pillai, U. R.; Sahle-Demessie, E. *J. Catal.* **2002**, *211*, 434 – 444.

- (13) Tomita, O.; Otsubo, T.; Higashi, M.; Ohtani, B.; Abe, R. *ACS Catal.* **2016**, *6*, 1134–1144.
- (14) Walenta, C. A.; Kollmannsberger, S. L.; Kiermaier, J.; Winbauer, A.; Tschurl, M.; Heiz, U. *Phys. Chem. Chem. Phys.* **2015**, *17*, 22809–22814.
- (15) Brinkley, D.; Engel, T. *J. Phys. Chem. B* **1998**, *102*, 7596 – 7605.
- (16) Shen, M.; Henderson, M. A. *J. Phys. Chem. Lett.* **2011**, *2*, 2707–2710.
- (17) Shen, M.; Henderson, M. A. *J. Phys. Chem. C* **2012**, *116*, 18788–18795.
- (18) Kolesov, G.; Vinichenko, D.; Tritsarlis, G. A.; Friend, C. M.; Kaxiras, E. *J. Phys. Chem. Lett.* **2015**, *6*, 1624–1627.
- (19) Phillips, K. R.; Jensen, S. C.; Baron, M.; Li, S.-C.; Friend, C. M. *J. Am. Chem. Soc.* **2013**, *135*, 574–577.
- (20) Nadeem, A. M.; Muir, J. M. R.; Connelly, K. A.; Adamson, B. T.; Metson, B. J.; Idriss, H. *Phys. Chem. Chem. Phys.* **2011**, *13*, 7637 – 7643.
- (21) Guo, Q.; Xu, C.; Ren, Z.; Yang, W.; Ma, Z.; Dai, D.; Fan, H.; Minton, T. K.; Yang, X. *J. Am. Chem. Soc.* **2012**, *134*, 13366–13373.
- (22) Guo, Q.; Xu, C.; Yang, W.; Ren, Z.; Ma, Z.; Dai, D.; Minton, T. K.; Yang, X. *J. Phys. Chem. C* **2013**, *117*, 5293–5300.
- (23) Ma, Z.; Guo, Q.; Mao, X.; Ren, Z.; Wang, X.; Xu, C.; Yang, W.; Dai, D.; Zhou, C.; Fan, H. et al. *J. Phys. Chem. C* **2013**, *117*, 10336–10344.
- (24) Yuan, Q.; Wu, Z.; Jin, Y.; Xu, L.; Xiong, F.; Ma, Y.; Huang, W. *J. Am. Chem. Soc.* **2013**, *135*, 5212–5219.
- (25) Zhou, C.; Ren, Z.; Tan, S.; Ma, Z.; Mao, X.; Dai, D.; Fan, H.; Yang, X.; LaRue, J.; Cooper, R. et al. *Chem. Sci.* **2010**, *1*, 575–580.

- (26) Xu, C.; Yang, W.; Guo, Q.; Dai, D.; Chen, M.; Yang, X. *J. Am. Chem. Soc.* **2013**, *135*, 10206–10209.
- (27) Winbauer, A.; Kollmannsberger, S. L.; Walenta, C. A.; Schreiber, P.; Kiermaier, J.; Tschurl, M.; Heiz, U. *Anal. Chem.* **2016**, *88*, 5392–5397.
- (28) Henderson, M. A. *Langmuir* **1996**, *12*, 5093–5098.
- (29) Heiz, U.; Vanolli, F.; Trento, L.; Schneider, W.-D. *Rev. Sci. Instrum.* **1997**, *68*, 1986–1994.
- (30) Liu, S.; Liu, A.; Wen, B.; Zhang, R.; Zhou, C.; Liu, L.-M.; Ren, Z. *J. Phys. Chem. Lett.* **2015**, *6*, 3327–3334.
- (31) Zhang, Z.; Bondarchuk, O.; Kay, B. D.; White, J. M.; Dohnálek, Z. *J. Phys. Chem. B* **2006**, *110*, 21840–21845.
- (32) Moulijn, J. A.; van Leeuwen, P. W. N. M.; van Santen, R. *Catalysis: An Integrated Approach to Homogeneous, Heterogeneous and Industrial Catalysis*; Studies in Surface Science and Catalysis; Elsevier, 1993; Vol. 79; pp 69 – 86.
- (33) Goodman, D. W. *J. Vac. Sci. Technol.* **1982**, *20*, 522–526.
- (34) Cant, N. W.; Cole, J. R. *J. Catal.* **1992**, *134*, 317 – 330.
- (35) Lang, X.; Wen, B.; Zhou, C.; Ren, Z.; Liu, L.-M. *J. Phys. Chem. C* **2014**, *118*, 19859–19868.
- (36) Cremer, T.; Jensen, S. C.; Friend, C. M. *J. Phys. Chem. C* **2014**, *118*, 29242–29251.
- (37) Zehr, R.; Henderson, M. *Surf. Sci.* **2008**, *602*, 2238–2249.
- (38) Xu, C.; Yang, W.; Guo, Q.; Dai, D.; Yang, X. *Phys. Chem. Chem. Phys.* **2016**,
- (39) Walenta, C. A.; Kollmannsberger, S. L.; Courtois, C.; Tschurl, M.; Heiz, U. *Phys. Chem. Chem. Phys.* **2018**, –.

Graphical TOC Entry



Supporting information for:
Thermal control of selectivity in
photocatalytic, water-free alcohol
photo-reforming

Sebastian L. Kollmannsberger,^{†,¶} Constantin A. Walenta,^{†,‡,¶} Carla Courtois,[†]
Martin Tschurl,[†] and Ueli Heiz^{*,†,‡}

[†]*Chair of Physical Chemistry, Department of Chemistry & Catalysis Research Center,
Technische Universität München, Lichtenbergstr. 4, 85748 Garching, Germany*

[‡]*Nanosystems Initiative Munich, Schellingstr. 4, 80799 München, Germany*

[¶]*The authors contributed equally to this work*

E-mail: ulrich.heiz@mytum.de

Phone: +49 (0) 89 289 13391. Fax: +49 (0) 89 289 13389

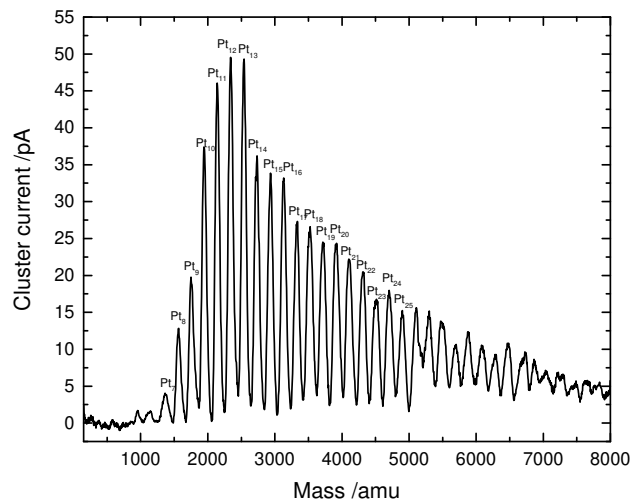


Figure S1: Size-distribution from Pt₇ to Pt₃₅ with a maximum from Pt₁₁ to Pt₁₃ from the laser vaporization cluster source. The cluster size is about 1 nm and the distribution shows a log-normal behaviour.^{S1}

Table S1: Electron impact ionization cross sensitivity values at 70 eV and m/z fragments used for quantification.

| substance | ICS [\AA^2] | m/z fragment |
|----------------|------------------------|--------------|
| methanol | 4.61 ^{S2} | 31 |
| formaldehyde | 4.14 ^{S3} | 30 |
| acetaldehyde | 6.7 ^{S2} | 44 |
| benzaldehyde | 20.1 ^{S4} | 106 |
| cyclohexanone | 17.6 ^{S4} | 70 |
| methyl-radical | 2.99 ^{S5} | 15 |
| acetone | 9.0 ^{S2} | 58 |
| isobutene | 11.889 ^{S6} | 56 |
| water | 2.275 ^{S6} | 18 |
| hydrogen | 1.021 ^{S6} | 2 |
| methyl formate | 6.8 ^{S7} | 60 |

The QMS ion current is calibrated via the desorption integral of a saturation coverage of the Ti-lattice sites with methanol in a TPD experiment. To obtain quantitative values for other molecules than methanol the fragmentation pattern, the electron impact ionization cross sensitivities (ICS) and the m/z dependent transmission through the QMS must be considered. The fragmentation pattern are obtained from mass spectra from the National Institute of Standards and Technology for all molecules^{S8} besides methyl.^{S9} The ICS values and the m/z fragments used for the quantification can be found in table S1.

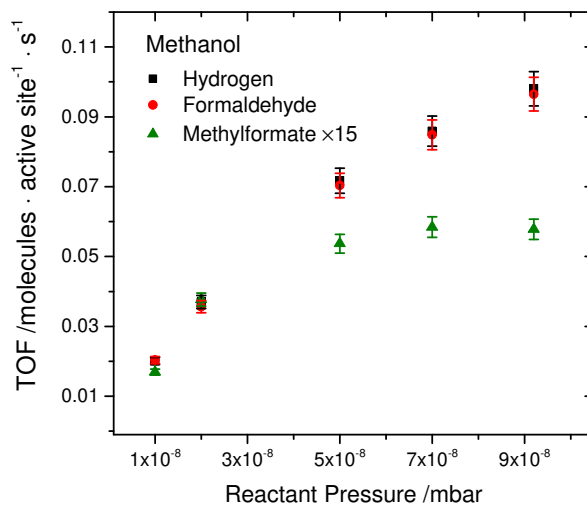


Figure S2: Pressure-dependent methanol photo-reforming at 260 K. Note that the methyl formate TOFs are multiplied with a factor of 15 for better visibility.

The TOFs of methyl formate from methanol photo-reforming show a saturation behavior, starting at a pressure of 5×10^{-8} mbar (see Figure S2).

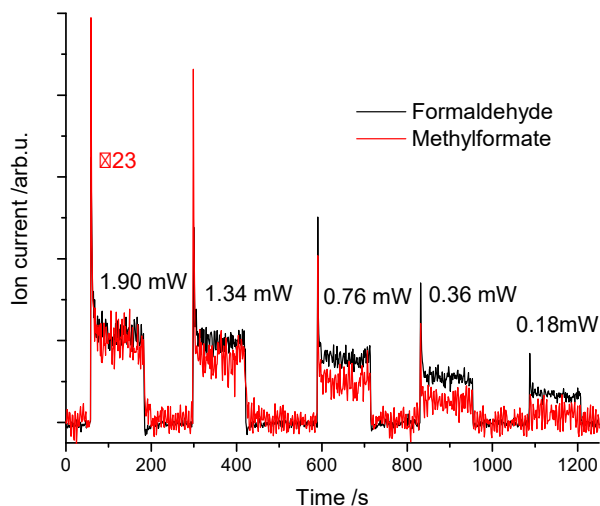


Figure S3: Laser power-dependent photo-catalytic methanol conversion. Note that the $m/z = 60$ trace is enlarged by a factor of 23 to optimize the comparability between the two products. The indicated energies refer to the light energy directly before the UHV chamber.

From laser power-dependent photo-catalytic methanol conversion (Figure S3), it can be seen that the yield of the coupling product methyl formate is stronger reduced than the yield of formaldehyde with lower laser power. Consequently, the coupling of an adsorbed formaldehyde and a methoxy is a consecutive photo-catalytic process.

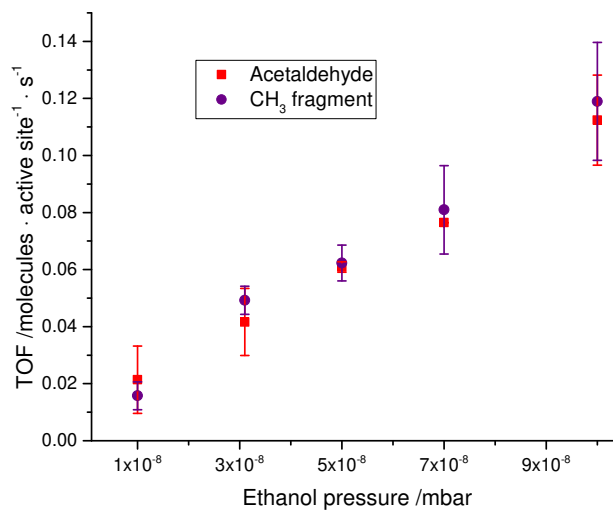


Figure S4: Pressure-dependent TOFs for ethanol photo-reforming at 280 K. Plotted are the acetaldehyde TOFs obtained from evaluation of the $m/z=15$ QMS signal (CH_3 -fragment) and the $m/z=44$ QMS signal. As both are identically the formation of other molecules containing CH_3 -fragments can be ruled out.

From ethanol photo-reforming other reaction products containing CH_3 -fragments are ruled out by comparison of the acetaldehyde TOFs obtained from two different m/z QMS signals, as shown in figure S4.

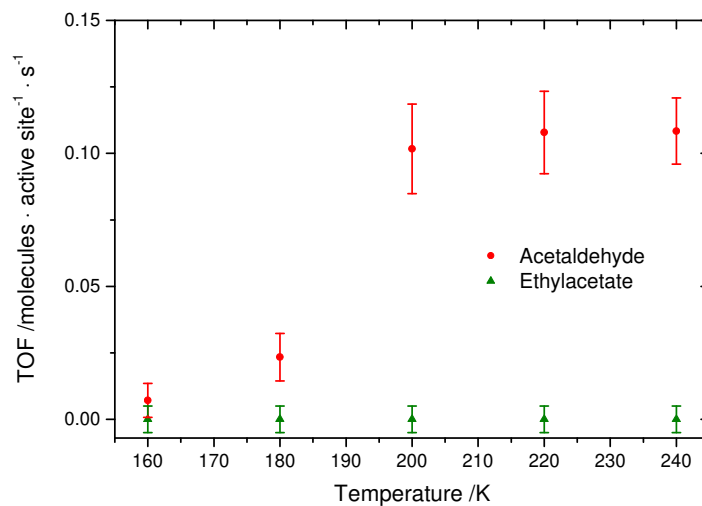


Figure S5: Low temperature region of acetaldehyde and ethylacetate TOFs from ethanol photo-reforming at 1×10^{-7} mbar.

It can clearly be seen from figure S5, that the acetaldehyde TOFs rise from 160 K to 200 K. From this temperature on the following TOFs are constant. Furthermore it is visible, that no ethylacetate is formed.

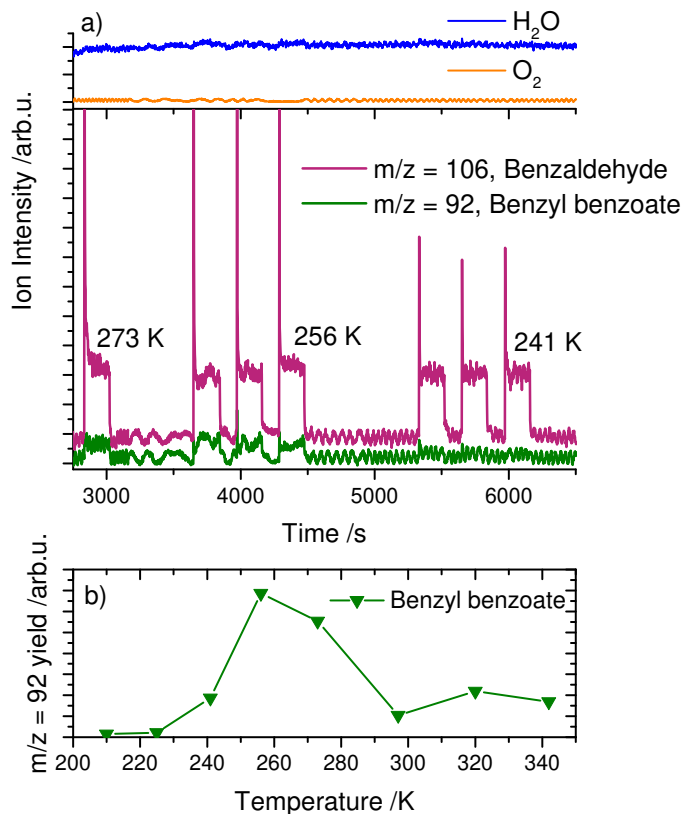


Figure S6: Temperature-dependent benzyl alcohol photo-reforming at 5×10^{-8} mbar. In a) the water, oxygen, benzaldehyde and benzyl benzoate raw data QMS traces are shown for three different temperatures. b) shows a qualitative evaluation of the coupling product benzyl benzoate.

For benzyl alcohol it is found that the $m/z=92$ fragment is formed in a small temperature range from ≈ 240 K to ≈ 300 K, which can either result from toluene (deoxygenation of benzyl alcohol^{S10}) or from benzyl benzoate (coupling product). Note that no oxygen or water desorption is observed during catalysis (see SI Fig. S6a). Consequently, the formation of toluene can be ruled out as a potential side product to this pathway does not occur and poisoning effects are also not observed. Therefore, a coupling reaction to benzyl benzoate is proposed. However, we refrain from a quantitative analysis as the $m/z=92$ fragment is only a minor fragment of benzyl benzoate resulting in a large error, when being quantified.

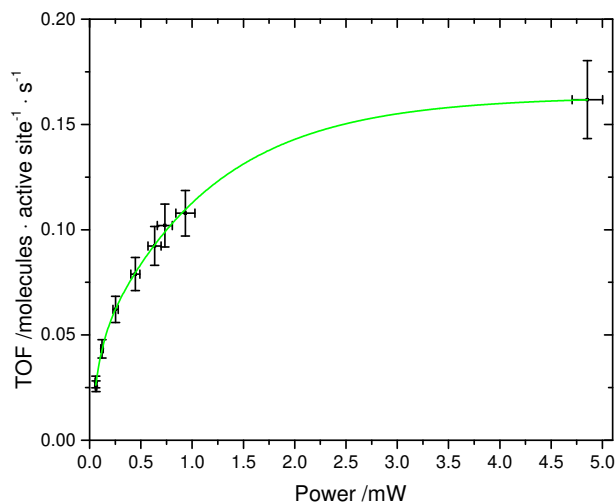


Figure S7: Laser power-dependent formaldehyde TOFs from methanol photo-reforming at 1×10^{-7} mbar and 255 K.

The laser power-dependent TOFs for methanol photo-reforming are depicted in figure S7 and show a first order behavior in the low power region, followed by a zero order regime. These findings supply strong evidence that methanol oxidation is an one photon process.

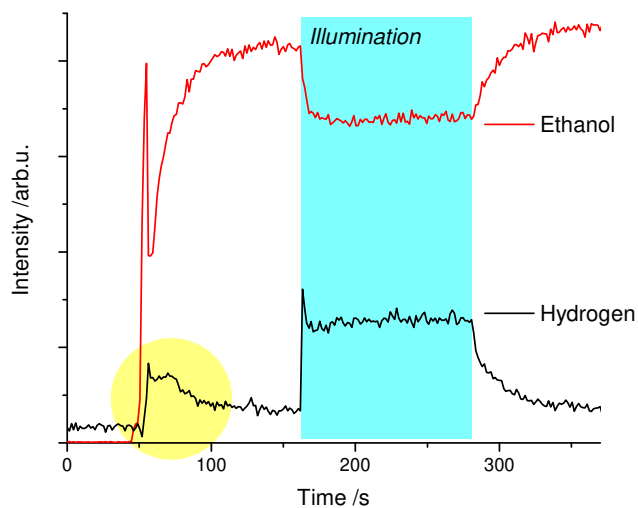


Figure S8: Molecular hydrogen evolution, highlighted in yellow, from ethanol in non-illumination conditions at 277 K and 1×10^{-7} mbar. The subsequent illumination is shown only for comparison purposes.

Figure S8 shows a molecular hydrogen evolution from ethanol in the dark. The catalyst is illuminated for 30 min in vacuum after a previous ethanol photo-reforming. Subsequently an ethanol pressure of 1×10^{-7} mbar is introduced into the chamber, starting at about 50 s in figure S8. An immediate molecular hydrogen evolution occurs, which results from thermal ethoxy formation, which occurs on the $\text{TiO}_2(110)$ surface.

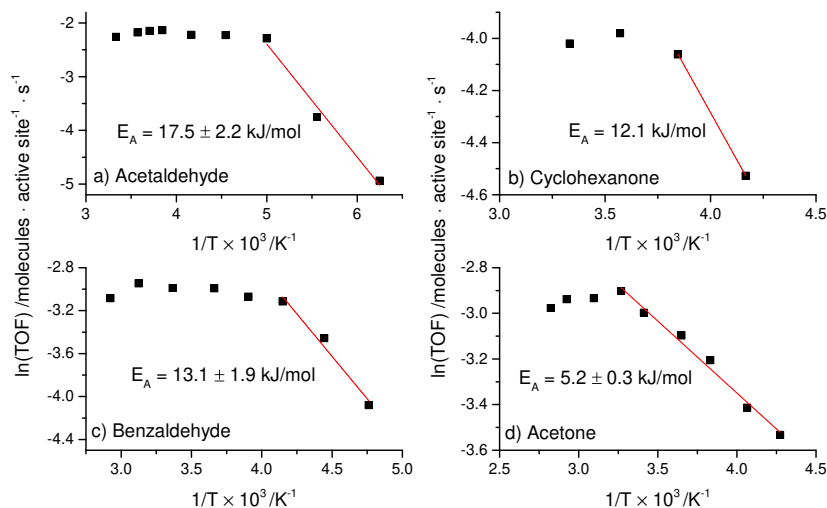


Figure S9: Arrhenius plots for a) acetaldehyde (at 1×10^{-7} mbar), b) cyclohexanone (at 1×10^{-8} mbar), c) benzaldehyde (at 5×10^{-8} mbar) and d) acetone (at 1×10^{-7} mbar) photo-reforming of the respective alcohol. The activation energy E_A is determined from the slope of the linear rise in the Arrhenius plot.

The obtained activation energies (see figure S9) are all less than $20 \frac{\text{kJ}}{\text{mol}}$ and are summarized in table S2. We refrain from an Arrhenius type activation energy evaluation of the formaldehyde formation, as this reaction competes with the methyl formate formation.

Table S2: Activation energies of acetaldehyde, cyclohexanone, benzaldehyde and acetone formation from figure S9

| Product | E_A [$\frac{\text{kJ}}{\text{mol}}$] |
|---------------|--|
| Acetaldehyde | 17.5 ± 2.2 |
| Cyclohexanone | 12.1 |
| Benzaldehyde | 13.1 ± 1.9 |
| Acetone | 5.2 ± 0.3 |

References

- (S1) Crampton, A. S.; Rötzer, M. D.; Schweinberger, F. F.; Yoon, B.; Landman, U.; Heiz, U. *J. Catal.* **2016**, *333*, 51–58.
- (S2) Bull, J. N.; Harland, P. W.; Vallance, C. *J. Phys. Chem. A* **2012**, *116*, 767–777.
- (S3) Gupta, D.; Antony, B. *J. Chem. Phys.* **2014**, *141*, 054303.
- (S4) Harrison, A. G.; Jones, E. G.; Gupta, S. K.; Nagy, G. P. *Can. J. Chem.* **1966**, *44*, 1967–1973.
- (S5) Peng, X.; Viswanathan, R.; Smudde Jr., G. H.; Stair, P. C. *Rev. Sci. Instrum.* **1992**, *63*, 3930–3935.
- (S6) Kim, Y.-K.; Irikura, K. K.; Rudd, M. E.; Ali, M. A.; Stone, P. M.; Chang, J.; Coursey, J. S.; Dragoset, R. A.; Kishore, A. R.; Olsen, K. J.; Sansonetti, A. M.; Wiersma, G. G.; Zucker, D. S.; Zucker, M. A. Electron-Impact Ionization Cross Section for Ionization and Excitation Database. <http://physics.nist.gov/ionxsec>, 2004 version 3.0; 2018, February 12.
- (S7) Hudson, J. E.; Weng, Z. F.; Vallance, C.; Harland, P. W. *Int. J. Mass Spectrom.* **2006**, *248*, 42 – 46.
- (S8) Linstrom, P., Mallard, W., Eds. *NIST Chemistry WebBook, NIST Standard Reference Database Number 69*, retrieved December 12, 2017 ed.; National Institute of Standards and Technology: Gaithersburg MD, 20899, 2017.
- (S9) Langer, A.; Hipple, J. A.; Stevenson, D. P. *J. Chem. Phys.* **1954**, *22*, 1836–1844.
- (S10) Chen, L.; Smith, R. S.; Kay, B. D.; Dohnalek, Z. *ACS Catal.* **2017**, *7*, 2002–2006.

E.2. Why Co-Catalyst-Loaded Rutile Facilitates Photocatalytic Hydrogen Evolution

Why Co-Catalyst-Loaded Rutile Facilitates Photocatalytic Hydrogen Evolution

Constantin A. Walenta^{a,b,†}, Sebastian L. Kollmannsberger^{a,†}, Carla Courtois^a, Rui N. Pereira^c, Martin Stutzmann^{b,c}, Martin Tschurl^a, Ueli Heiz^{a,b,*}

^aChair of Physical Chemistry, Department of Chemistry & Catalysis Research Center, Technische Universität München, Lichtenbergstr. 4, 85748 Garching, Germany

^bNanosystems Initiative Munich, Schellingstr. 4, 80799 München, Germany

^cWalter Schottky Institute and Physics Department, Technische Universität München, Am Coulombwall 4, 85748 Garching

*corresponding author: email ulrich.heiz@tum.de

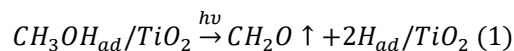
† The authors contributed equally to this work

Abstract:

As the conduction band edge of rutile is close to the reduction potential of hydrogen, there is a long-lasting discussion, whether molecular hydrogen can be evolved from this semiconductor. Our study on methanol photoreforming in the ultra-high vacuum reveals that photocatalysts comprising a TiO₂(110) single crystal decorated with platinum clusters indeed enable the evolution of H₂. This is attributed to a new type of mechanism, in which the co-catalyst acts as a recombination center for hydrogen and not as a reduction site of a photoreaction. This mechanism is an alternative pathway to the commonly used photoelectrochemical type mechanism, and must particularly be considered for systems, in which the reducible semiconductors enable the surface diffusion of hydrogen species.

Hydrogen generated from renewable feedstocks is envisioned to act as a potential fuel for clean transportation.^[1] In the last decade research focusing on increasing the efficiency of hydrogen production has tremendously been intensified by following both conventional and novel approaches.^[2] Photocatalytic water splitting facilitated by co-catalyst loaded semiconductor particles is one promising way for clean hydrogen production. Recently, such systems have been reported to exceed efficiencies of over 1% in a scalable solar-to-hydrogen production.^[3] Surprisingly, detailed mechanistic insights are still scarce despite of the intense research efforts undertaken in the past. Such knowledge, however, may be vital for the development of devices, which economically outperform electrolyzers driven by a solar cell. So far, there is general agreement that two different effects contribute to the hydrogen evolution rate, the charge carrier dynamics and the chemical reactions. For the latter, both partial reactions are usually treated somewhat independently from each other, following the concepts of photoelectrocatalysis. For most of the systems it is believed that the oxidation reaction is the rate-determining step, while the evolution of hydrogen occurs on a much faster time scale. The latter is usually viewed as a two-electron reduction of H⁺. If such a separate picture of both half-reactions is valid, the choice of particular semiconductor materials is subject to certain restrictions, for example the position of the band edges with respect to the electrochemical potential of the two half-reactions. In this regard, there is still a lively discussion whether rutile is capable of enabling the evolution of molecular hydrogen or if its conduction band edge is too low in energy.^[4] Evidenced by the study of the photocatalysis of methanol as model reaction, we show that H₂ evolution is indeed possible on a rutile single crystal decorated with small platinum clusters as co-catalysts. Experiments under well-defined conditions and in comparison with the bare semiconductor reveal the exact reaction mechanism, which does not occur along the (generally expected) reduction of H⁺ by photoelectrons. The mechanism also explains, why only very little amounts of co-catalyst already facilitate efficient H₂ formation.^[5] We believe that this mechanism has to be considered in other photocatalytic systems, in particular for those that enable hydrogen surface diffusion.

The photochemical behavior of methanol and other alcohols on bare TiO₂(110) is already heavily investigated, which makes them excellent systems for studying the hydrogen evolution reaction. As alcohols are known to efficiently facilitate the hole-reaction, they have vastly been used in different studies as hole-scavenger in the past.^[6] From studies in UHV it is known that on a reduced titania crystal the main photochemical reaction pathway is a disproportionation reaction yielding formaldehyde and the hydroxylated semiconductor (see Eq. 1).^[7] At best only very small amounts of molecular hydrogen are detected.^[8]



As the semiconductor stays significantly hydroxylated until the desorption of water at elevated temperatures (above 500 K), catalyst poisoning is observed.

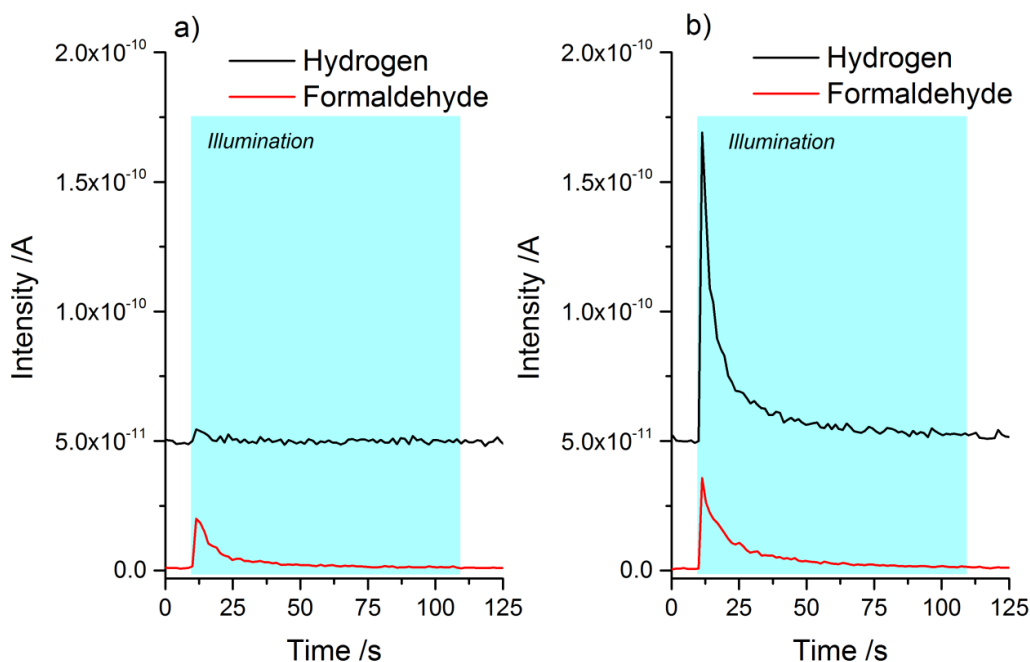


Figure 1: Photochemical products of 1 L methanol on $r\text{-TiO}_2(110)$ [a] and on $\text{Pt}_x/\text{TiO}_2(110)$ [b] at 260 K. Upon UV illumination (shown as blue background), methoxy species are photooxidized to formaldehyde, which desorbs thermally. In [a] only trace amounts of H_2 are formed upon illumination, while the catalyst poisoning is observed in subsequent runs (see Fig. S6 and S7). The conditioned Pt-loaded photocatalyst [b] shows an almost identical decay curve for formaldehyde desorption, but significant production of H_2 is additionally visible during illumination. Note, that the traces represent ion intensities and not numbers of molecules.

In contrast, the deposition of small platinum clusters on the semiconductor completely changes the behavior (see Fig. 1). While the rate constant of the formaldehyde production, which is reflected in the respective decay curve (see the description in chapter 4.3 in the SI), remains the same, strong production of molecular hydrogen is observed. The kinetics of this hydrogen production are very similar to the formaldehyde production, which suggests that the latter is the rate-determining step and that hydrogen diffusion and recombination is much faster. Contrary to the reaction on the bare semiconductor, catalyst poisoning is not observed after the deposition of Pt clusters. Besides a conditioning of the co-catalyst in the first cycle, due its reaction with the methanol, the kinetics stay the same in subsequent cycles (see Figure S10).

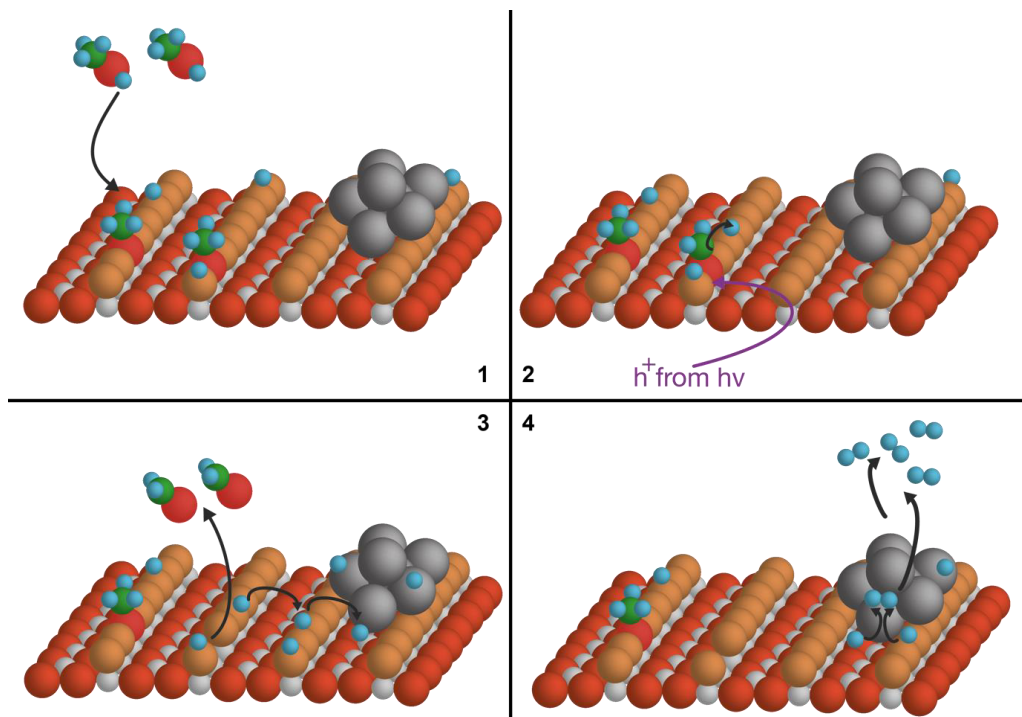


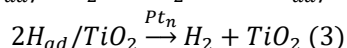
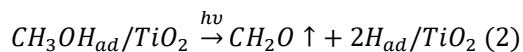
Figure 2: Scheme of the mechanism of photocatalytic methanol conversion at 260 K at a co-catalyst-loaded $r\text{-TiO}_2(110)$ -surface on an atomic scale. The reaction takes place in a bridge-bonding oxygen (BBO) vacancy, in which the thermally formed methoxy species (1) get oxidized by the photoholes^[9] (2) and the formaldehyde desorbs (3). The formed atomic hydrogen diffuses on the surface (3), recombines at a co-catalyst and thermally desorbs (4), facilitating an overall charge neutral disproportionation reaction, which is triggered by the irreversible photooxidation step.

The comparison of the photocatalytic reaction behavior of the bare semiconductor with the Pt-loaded one leads to the following reaction mechanism, which is illustrated in Figure 2. From the alcohol chemistry on the bare semiconductor it is known that methoxy species are formed in titania defects and methoxys act as photoactive species for a hole-mediated $\alpha\text{-H}$ abstraction.^[7a] Upon co-catalyst loading, this photoreaction mechanism remains unaltered, as evidenced by the unchanged apparent rate constant of formaldehyde production. However, the appearance of the intense H_2 signal demonstrates that the role of the co-catalyst is to enable the recombination of hydrogen atoms of the hydroxylated TiO_2 crystal (Eq. 2 & 3). While the desorption of H_2 may be facilitated by the recombination heat of photon-generated charges at or in the vicinity of the co-catalysts, an electron-consuming reduction of H^+ can be excluded due to the conservation of charges. Further evidence is supplied by the reaction conditions of our experiments, where in contrast to electrochemical systems solvated H^+ moieties are not present due to the absence of a solution phase.

The comparison of Eq. 2 and 3 with Eq. 1 demonstrates that the release of H_2 occurs via the recombination of hydrogen atoms on the co-catalyst, which can already be facilitated thermally (see Fig. S14).

As the contribution of photogenerated electrons is not required for yielding the respective products, the overall reaction is in fact a hole-mediated disproportionation

reaction of the alcohol rather than two different redox reactions, with the first step being the same as Eq. 1:



As seen in Eq. 2, the reaction requires only one photon, which is further evidenced in the illumination dependent TOFs, which show a first-order behavior transferring into a saturation regime at higher illumination intensities (Fig. S12).

This mechanism does not only consider the charge balance and catalytic reaction behavior, but is also in good agreement with findings from semiconductor physics. As the TiO_2 single crystal represents a bulk oxide n-type semiconductor, surface band bending must strongly be considered, which is different to nano-structured systems. On an n-type semiconductor, photoholes highly tend to migrate to the surface, while photogenerated electrons preferentially move towards the bulk. A consumption of these photoholes causes a flattening of the semiconductor bands, which results in an increased rate of defect regeneration by corresponding photoelectrons. The resulting neutral charge balance is fully compatible with the mechanism described above.

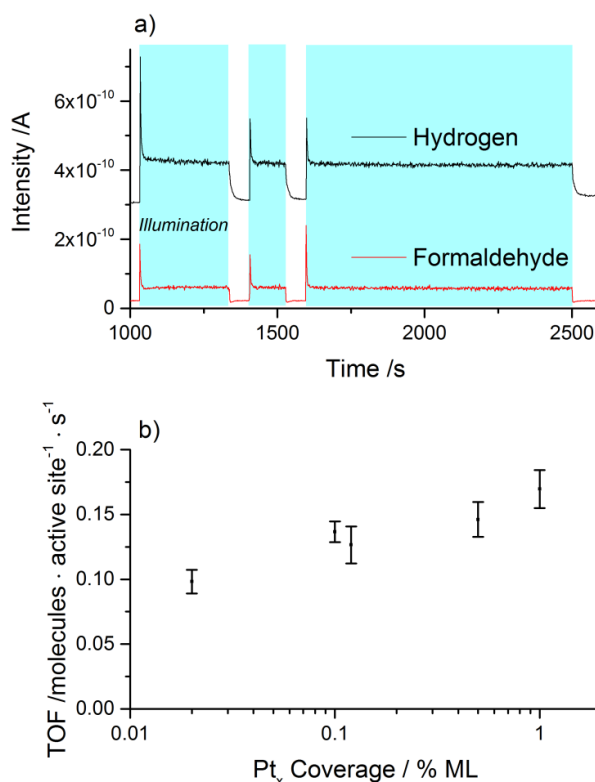


Figure 3: Photocatalytic conversion of methanol on Pt-loaded r-TiO₂(110). In a), the photocatalytic conversion of methanol to formaldehyde and hydrogen is shown. The reaction immediately starts with UV illumination and also stops immediately in the dark. In b), the cluster coverage is varied on the semiconductor and the reaction even occurs with an appreciable TOF for a Pt cluster coverage of 0.02 % of a monolayer. Note, that

the tail in the H₂ trace after the illumination also evidences a thermal recombination reaction of hydrogen.

The absence of poisoning in Pt_x/TiO₂(110) enables to perform the reaction under steady-state conditions (Fig. 3a) and to determine the turnover frequency (TOF) of the photocatalyst. Surprisingly, it is found that higher coverages of co-catalysts only lead to very small changes in the TOF (Figure 3b). In this regard, changing the Pt loading over almost two orders of magnitude (from 0.02% to 1% of a monolayer) only leads to a 2-fold increase in the TOF. If a typical spherical rutile nanoparticle of 20 nm in diameter is considered, this coverage amounts to weight loadings of less than 0.01 to over 0.3 w% of platinum (assuming the bulk density of rutile TiO₂ and Pt₁₅ as the average cluster size). Indeed, in a recent study of colloidal systems it was reported that very little amounts of platinum loading already result in high hydrogen production rates.^[5] This is also in good agreement with previous work of Haruta and co-workers, who observed a maximum, but in the lower loading regime they found a similar increase in H₂ production.^[10]

With the hole-mediated disproportionation reaction mechanism, a straightforward interpretation of this observation can readily be given: As the platinum co-catalysts only act as recombination centers for hydrogen, charge carrier dynamics do not significantly influence the reaction step of hydrogen formation. Instead, the migration of hydrogen atoms to the co-catalysts plays a crucial role. In this regard, it has only recently been shown that the diffusion of hydrogen is efficiently facilitated over large distances on TiO₂, which has been attributed to the redox properties of the semiconductor.^[11] As a result, the distance of the co-catalyst to the center of photoreaction is not of paramount importance for the H₂ evolution rate.

The coverage dependence again demonstrates, how strongly formaldehyde formation is governing the overall reaction rate. As the density of oxygen vacancies, which were previously identified as active sites for the hole-mediated reaction, is about 6% (see Fig. S2), it is over two orders of magnitude higher than the lowest cluster coverage. Therefore, the vital role of these defects in the reaction rate makes the avoidance of their blocking essential. Whether the defects are preserved may also depend on the method of co-catalyst preparation. In this study, clusters are randomly distributed on the surface due to the applied deposition method.^[12]

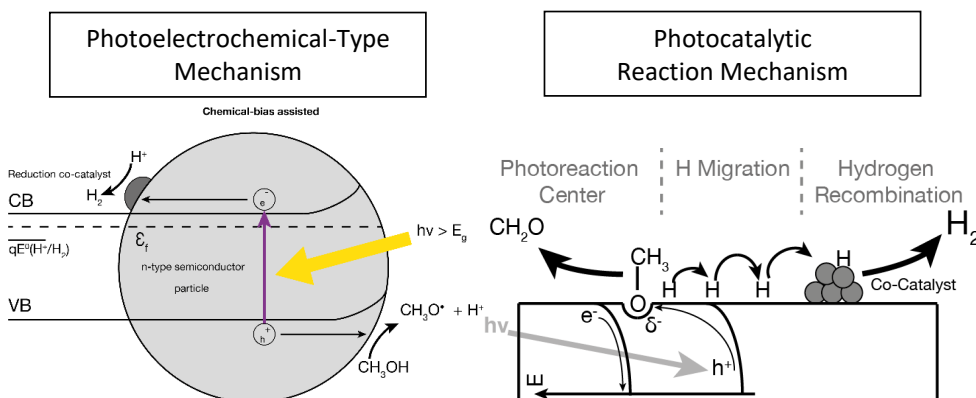


Figure 4: Different mechanistic pathways for photocatalytic reactions. In the left part, the conventional model (adapted from Domen and coworkers^[2b, 6]) based on

photoelectrochemistry is displayed. In this picture, H₂ evolution consumes two photoelectrons on the HER co-catalyst, while the other half-cell reaction is facilitated by two photoholes. The band edge positions have to align to the chemical standard reduction potentials to facilitate the photoelectrochemical reaction. In the right panel, the photocatalytic mechanism is shown. By light absorption, the methoxy species is photooxidized by one hole in the partially negatively charged defect, leading to formaldehyde desorption from the photoreaction center. The co-generated H-atoms migrate on the surface to the co-catalysts (in this case Pt clusters), which act as a recombination centers, rather than reduction sites for protons from solution. As the dissociative adsorption of methanol already occurs thermally in the dark on the semiconductor, only one photon is needed for the photocatalytic reaction in case of TiO₂. Depending on the reaction, the catalyst material and the reaction conditions, one of these two mechanisms may serve as a correct description for the reaction pathway.

The photon-stimulated desorption of oxygen, which is a powerful tool to probe the concentration of accessible BBO-defects^[13], further confirms this assumption as it does not significantly change after cluster deposition and even catalysis (see Fig. S15). For example, this is different to the formation of clusters via the evaporation of metals on the semiconductor with subsequent annealing, which was found to strongly inhibit the photooxidation of CO in case of Pt^[14] or the O₂ photodesorption in case of gold^[15]. This is a clear indication that the migration to or the formation of metal centers in or near defects will inhibit the formation of the oxidized product and, thus, the entire reaction.

In summary, some important consequences result from these findings:

1. The new mechanism, which differs from the generally adopted photoelectrochemical picture, (see Figure 4) is an alternative possibility for the evolution of molecular hydrogen. While the established pathway still may be dominant in certain systems, the new mechanism extends the range of possible semiconductor materials. In particular, hydroxyl-forming oxides may be potential candidates and their conduction band edges do not necessarily have to match the reduction potential of hydrogen, as it is illustrated here in the case for rutile decorated with co-catalysts.^[4b]
2. The amount of co-catalyst for the H₂ evolution has only a very weak influence on the TOF. While vital for the formation of molecular hydrogen, a coverage of 0.02% (which amounts to a loading of 0.01 w% for typical 20 nm rutile particles) result in a considerable strong H₂ signal. This effect can readily be explained with the reaction mechanism: As the co-catalysts only enables hydrogen recombination, its loading only plays a minor role in comparison to the formation of formaldehyde, which is the rate-determining step.
3. As oxygen vacancies enable the α -H abstraction, it is vital that the co-catalyst does not block them. Consequently, the procedure of co-catalyst preparation may be essential for the photoreaction yield.^[16] The optimal preparation procedure may differ for different metals, depending on the metal mobility on the semiconductor.^[12b]
4. The mechanism also illustrates that there may exist intrinsic differences of photocatalysis in comparison to photoelectrocatalysis other than the absence of voltage. These differences may be associated with disadvantages (e.g. significant contributions of the back reaction), but also with advantages as both half-reactions are not strictly separated from each other.

While these findings are obtained for the hydrogen evolution reaction from alcohol reforming, the thermal reaction steps (abstraction of the first hydrogen atom^[17], H-migration^[17] and –recombination) may similarly contribute to the hydrogen evolution reaction in the photocatalytic water splitting.

Experimental Methods

All experiments were performed in an ultra-high vacuum apparatus^[18] with an attached laser-vaporization cluster source. A detailed description of the experiments and the apparatus is given in the supporting information. In brief, a reduced TiO₂(110) single crystal is prepared by sputter and annealing cycles and Pt clusters are soft-landed on the sample. Methanol is either dosed at cryogenic temperatures or via a constant background, while all relevant masses are monitored with a QMS. Given a certain temperature, the photoreaction is facilitated by a nanosecond pulsed OPO-Laser, operated at 241.8 nm. The reaction is shown to be independent of UV wavelength and pulsed or continuous excitation, as long as the photon energy is above the band gap (see SI).

Acknowledgements

We thank the DFG through grants HE3435/22-1 and STU139/12-1 for financial support.

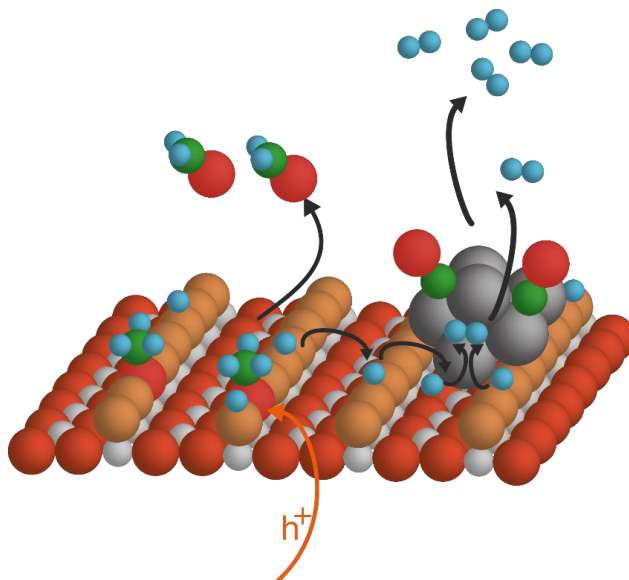
References:

- [1] J. A. Turner, *Science* **2004**, *305*, 972-974.
- [2] a) K. Maeda, K. Teramura, D. Lu, T. Takata, N. Saito, Y. Inoue, K. Domen, *Nature* **2006**, *440*, 295-295; b) T. Hisatomi, J. Kubota, K. Domen, *Chem. Soc. Rev.* **2014**, *43*, 7520-7535.
- [3] Q. Wang, T. Hisatomi, Q. Jia, H. Tokudome, M. Zhong, C. Wang, Z. Pan, T. Takata, M. Nakabayashi, N. Shibata, Y. Li, I. D. Sharp, A. Kudo, T. Yamada, K. Domen, *Nat. Mater.* **2016**, *15*, 611-615.
- [4] a) S. Chen, L.-W. Wang, *Chem. Mater.* **2012**, *24*, 3659-3666; b) T. R. Esch, T. Bredow, *Surf. Sci.* **2017**, *665*, 20-27.
- [5] K. Wang, Z. Wei, B. Ohtani, E. Kowalska, *Catal. Today* **2017**.
- [6] D. M. Fabian, S. Hu, N. Singh, F. A. Houle, T. Hisatomi, K. Domen, F. E. Osterloh, S. Ardo, *Energ. Environ. Sci.* **2015**, *8*, 2825-2850.
- [7] a) M. Shen, M. A. Henderson, *J. Phys. Chem. Lett.* **2011**, *2*, 2707-2710; b) K. R. Phillips, S. C. Jensen, M. Baron, S.-C. Li, C. M. Friend, *J. Am. Chem. Soc.* **2013**, *135*, 574-577.
- [8] C. Xu, W. Yang, Q. Guo, D. Dai, M. Chen, X. Yang, *J. Am. Chem. Soc.* **2013**, *135*, 10206-10209.
- [9] G. Kolesov, D. Vinichenko, G. A. Tritsarlis, C. M. Friend, E. Kaxiras, *J. Phys. Chem. Lett.* **2015**, *6*, 1624-1627.
- [10] G. R. Bamwenda, S. Tsubota, T. Nakamura, M. Haruta, *J. Photochem. Photobiol. A* **1995**, *89*, 177-189.

- [11] W. Karim, C. Spreafico, A. Kleibert, J. Gobrecht, J. VandeVondele, Y. Ekinci, J. A. van Bokhoven, *Nature* **2017**, *541*, 68-71.
- [12] a) N. Isomura, X. Wu, Y. Watanabe, *J. Chem. Phys.* **2009**, *131*, 164707; b) A. Sasahara, C. L. Pang, H. Onishi, *J. Phys. Chem. B* **2006**, *110*, 17584-17588.
- [13] C. N. Rusu, J. T. Yates, *Langmuir* **1997**, *13*, 4311-4316.
- [14] A. Linsebigler, C. Rusu, J. T. Yates, *J. Am. Chem. Soc.* **1996**, *118*, 5284-5289.
- [15] Z. Zhang, W. Tang, M. Neurock, J. T. Yates, *J. Phys. Chem. C* **2011**, *115*, 23848-23853.
- [16] G. M. Haselmann, D. Eder, *ACS Catal.* **2017**, *7*, 4668-4675.
- [17] Z. Zhang, O. Bondarchuk, B. D. Kay, J. M. White, Z. Dohnálek, *J. Phys. Chem. B* **2006**, *110*, 21840-21845.
- [18] C. A. Walenta, S. L. Kollmannsberger, J. Kiermaier, A. Winbauer, M. Tschurl, U. Heiz, *Phys. Chem. Chem. Phys.* **2015**, *17*, 22809-22814.

Keywords: Alcohol Photoreforming; Hydrogen Production; Photocatalysis; Reaction Mechanisms; Renewable Hydrogen

Table of Contents:



A new mechanism for the photocatalytic hydrogen production is reported, which differs significantly from the common picture derived from photoelectrocatalysis. It reveals that the photoreaction only enables the hydrogen abstraction, while the actual formation of H₂ occurs only thermally on the co-catalyst.

Supporting Information: Why Co-Catalyst-Loaded Rutile Facilitates Photocatalytic Hydrogen Evolution

Constantin A. Walenta^{a,b,†}, Sebastian L. Kollmannsberger^{a,†}, Carla Courtois^a, Rui N. Pereira^c, Martin Stutzmann^{b,c}, Martin Tschurl^a, Ueli Heiz^{a,b,*}

^aChair of Physical Chemistry, Department of Chemistry & Catalysis Research Center, Technische Universität München, Lichtenbergstr. 4, 85748 Garching, Germany

^bNanosystems Initiative Munich, Schellingstr. 4, 80799 München, Germany

^cWalter Schottky Institute and Physics Department, Technische Universität München, Am Coulombwall 4, 85748 Garching

*corresponding author: email ulrich.heiz@tum.de

† The authors contributed equally to this work

1. Catalyst Preparation

A rutile TiO₂(110) single crystal (Surface-net GmbH) was cleaned by several cycles of sputtering (Ar, 1.0 keV, $7 \cdot 10^{-6}$ mbar) and annealing at 850 K in vacuum, which results in an atomically flat surface, while the crystal shows a light blue color indicating a slightly reduced surface [r-TiO₂(110)]. Over the course of the experiments, the crystal was sputtered (same conditions), annealed in oxygen atmosphere ($1 \cdot 10^{-6}$ mbar, 820 K) for 20 min and vacuum annealed at 820 K for 10 min. This recipe is known to result in a clean surface with a constant bridge-bonding oxygen (BBO) vacancy concentration.^[1]

The Pt (99.95% purity, ESG Edelmetalle, Germany) clusters are generated by a laser vaporization source coupled with a quadrupole mass spectrometer (Extrel, USA). In this work, the quadrupole mass spectrometer was operated with the AC-potential only, acting as an ion guide. The resulting size-distribution is then determined by the pressure and voltage settings and kept constant over the course of the experiments.^[2] The Pt clusters are deposited on the r-TiO₂(110) surface under soft-landing conditions (< 1 eV/atom in kinetic energy). The resulting catalyst is therefore named Pt_x/TiO₂(110) in the following. Between the experiments, a few cycles in sputtering, lasting in total more than 1h, were employed to facilitate a clean surface. The surface purity is verified by D₂-TPD, since also the smallest contamination of Pt clusters on the surface leads to a desorption feature in a TPD between 200 K and 300 K.

The platinum cluster coverages investigated in this work are displayed in Table 1. The coverages are given in %ML respective to the $1.5 \cdot 10^{15}$ surface atoms of the TiO₂(110) surface.^[3] They are determined by the neutralization current of soft-landed cationic Pt clusters measured by a picoammeter (Keithley 6587).

Table 1: Cluster coverages used in this work on the TiO₂(110) surface.

| %ML [cm ²] | Number of clusters [e/nm ²] | Number of clusters [e/cm ²] |
|------------------------|---|---|
| 0.02 | 0.003 | $3 \cdot 10^{11}$ |
| 0.1 | 0.015 | $1.5 \cdot 10^{12}$ |
| 0.12 | 0.018 | $1.8 \cdot 10^{12}$ |
| 0.5 | 0.075 | $7.5 \cdot 10^{12}$ |
| 1.0 | 0.15 | $1.5 \cdot 10^{13}$ |

Methanol (Chromasolv, $\geq 99.9\%$ purity) and Methanol-d₃ (Sigma Aldrich, 99.8 atom % D) are cleaned via several pump-freeze cycles and either introduced by dosing or in a constant background.

2. Catalyst Characterization

The absence of contaminants from the r-TiO₂(110) surface is deduced from Auger Electron Spectroscopy (AES) as shown in Figure S1. Further, the surface of a light blue crystal shows a certain BBO vacancy concentration. The vacancies can be observed either by STM^[4] or by titration experiments.^[3, 5] In this study, the BBO-vacancy density was about $6 \pm 1\%$ of the Ti-lattice sites as determined by temperature programmed desorption (TPD) of H₂O (Fig. S2).

The cluster size distribution is checked before every experiment and determined by a mass scan over all sizes. The resulting mass spectrum is displayed in Figure S3. The clusters are deposited randomly on the surface and show no preferential adsorption as evidenced by Kelvin Probe Force Microscopy and STM.^[6]

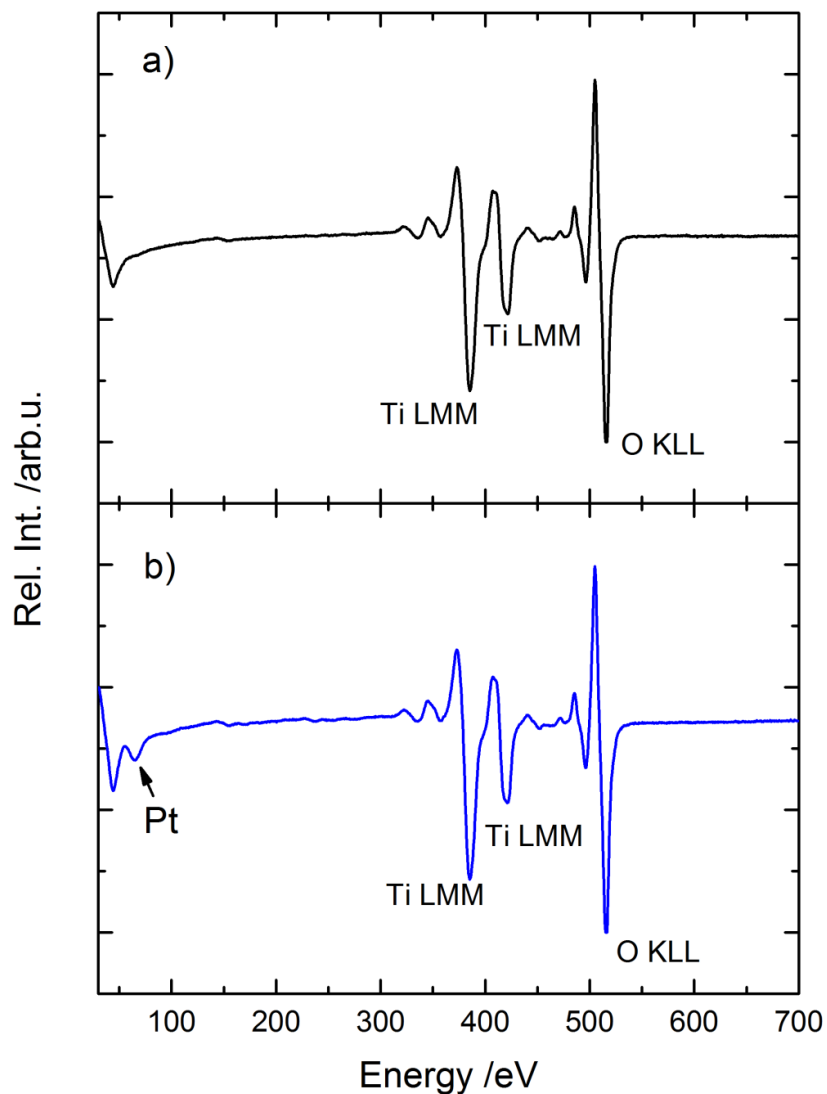


Fig. S1: Auger Electron Spectrum of the r-TiO₂(110) surface (a) and Pt_x/r-TiO₂(110) (b). Titanium and oxygen are observed for the rutile TiO₂(110) surface, while a small feature of Pt NOO Peak is observed at 64 eV. The coverage of 1% Pt_x/ML.

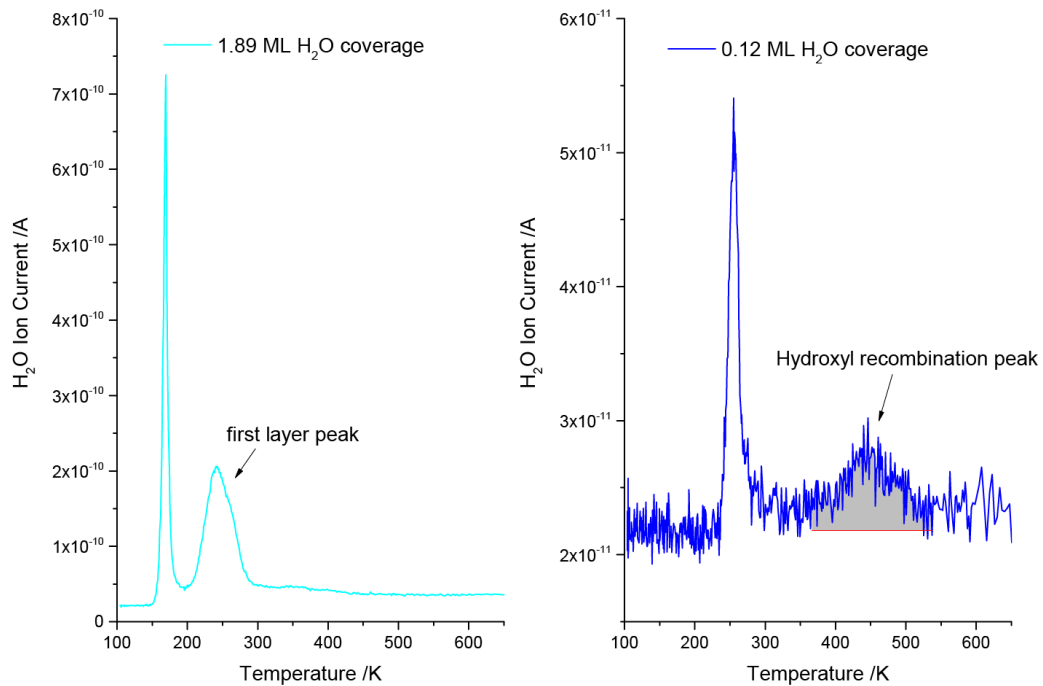


Fig. S2: TPD spectra of H_2O on the $\text{r-TiO}_2(110)$ surface. In S2a, the TPD of 1.89 ML of H_2O dosed on the surface is shown and is in excellent agreement with literature.^[5a, 7] The first layer peak is assigned to water desorbing from Ti-lattice sites, while the feature at around 170 K is attributed to water on BBO-sites and multilayer adsorption. Figure S2b shows a smaller coverage, where the hydroxyl recombination peak is clearly observed around 460 K. The grey area indicate the integrated area, that is compared to the integral of the first layer peak in S2a, to obtain a BBO-vacancy concentration of $6 \pm 1\%$ of Ti-lattice sites.

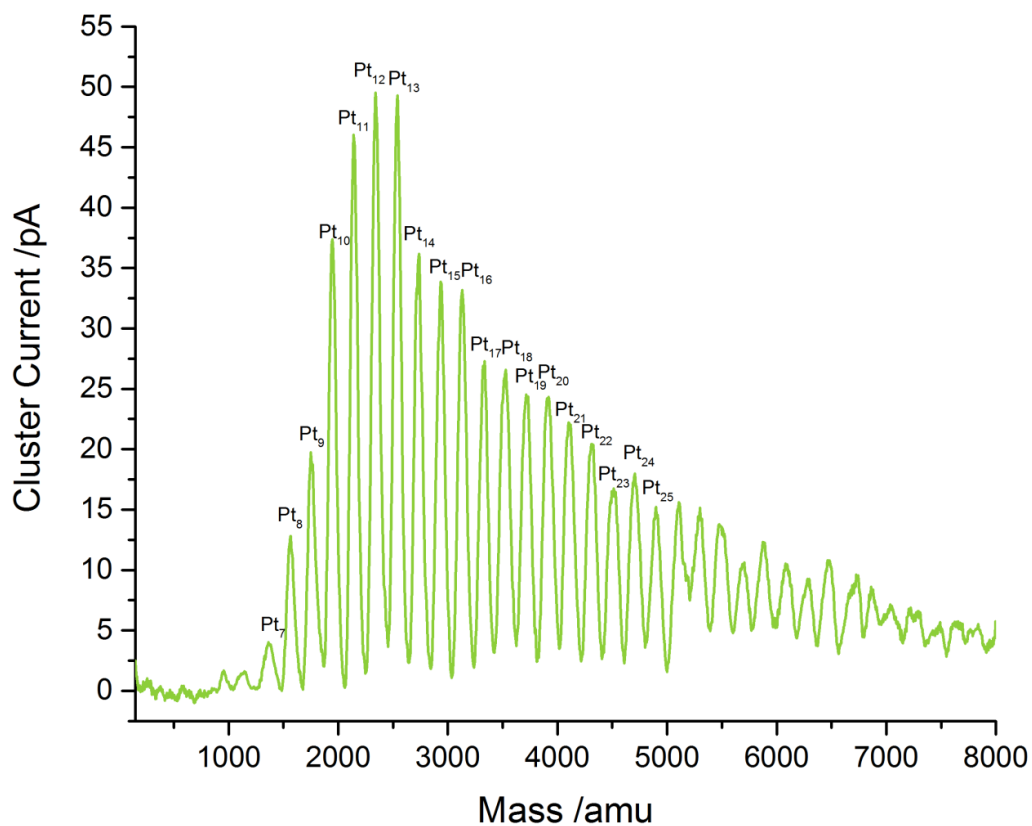


Fig. S3: Mass spectrum of the cluster size distribution of Pt clusters from the laser vaporization source. The spectrum is taken after the quadrupole mass filter and shows a size-distribution of Pt₇ up to Pt₃₂. When depositing in the ion guide mode, all masses lower than Pt₈ are discarded. The clusters show a log-normal distribution and have a size about 1 nm in diameter.^[2]

3. Thermal Reaction Products

To understand photocatalytic mechanism on an atomic scale, first the methanol chemistry on $r\text{-TiO}_2(110)$ is explored (see Fig. S4) which is found to be in very good agreement with literature.^[8]

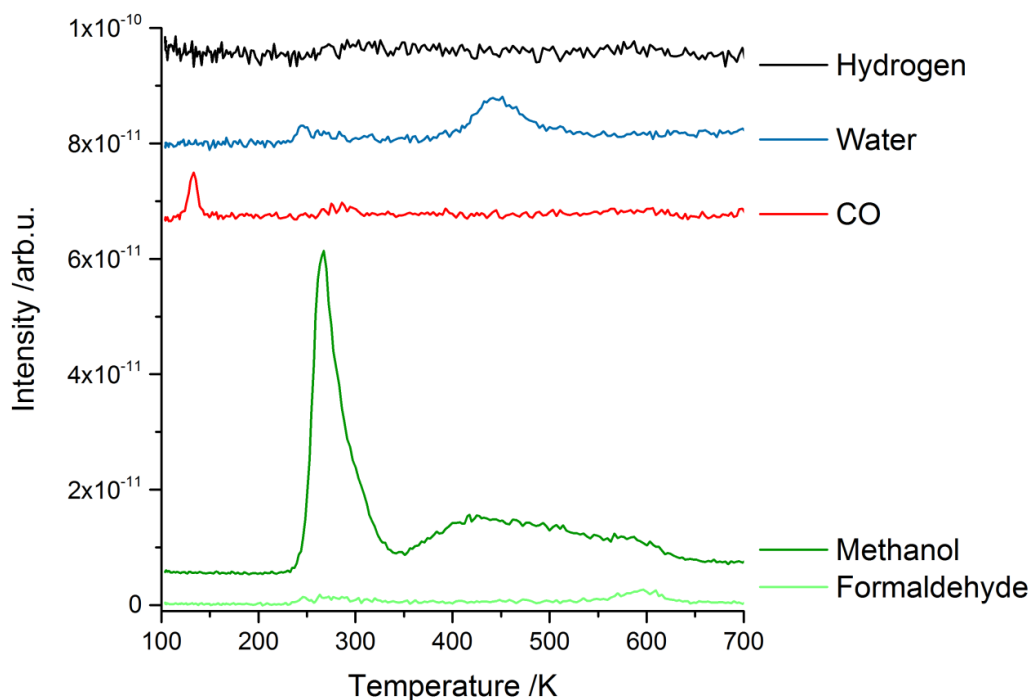


Fig. S4: TPD of 1 L of methanol on $r\text{-TiO}_2(110)$. Molecular methanol mainly desorbs at 270 K from Ti-lattice sites. The high temperature feature at 480 K is associated with recombinative desorption of dissociated methanol and trace amounts of formaldehyde are obtained around 600 K. No molecular hydrogen formation is observed from methanol. The excess hydrogen from formaldehyde formation typically forms water on oxides, as observed from the water desorption at 470 K. The small CO signal at 125 K is attributed to background adsorption. The traces are offset for clarity.

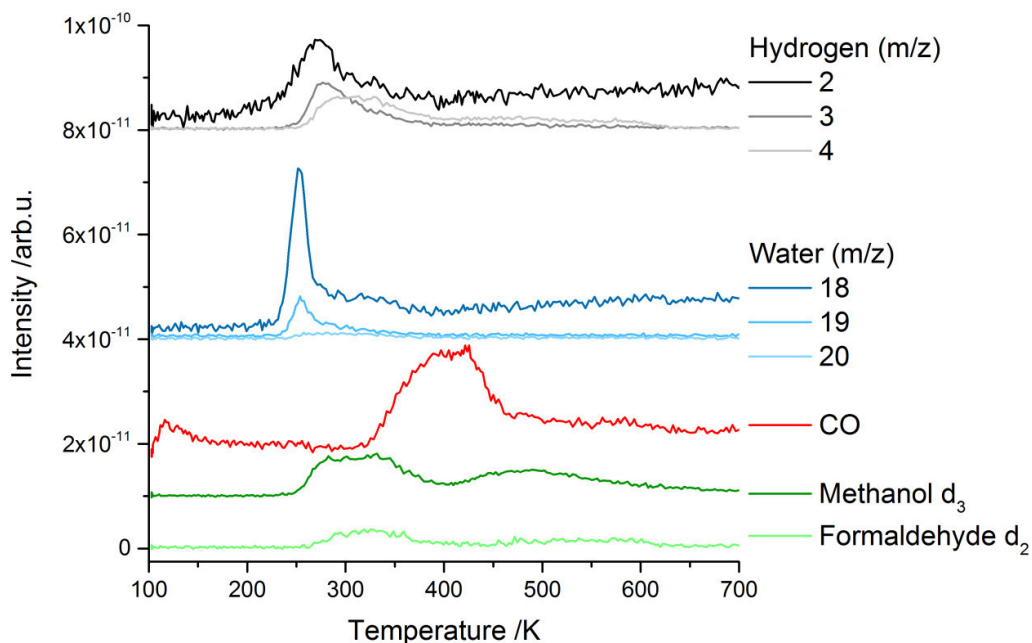


Fig. S5: TPD of 1 L of methanol- d_3 on $Pt_x/r-TiO_2(110)$. In this experiment, isotopically labeled methanol CD_3OH is used to explore the thermal reactions on Pt-loaded $TiO_2(110)$. While the methanol signal is less intense, both molecular and dissociative adsorption are observed on the TiO_2 surface. No intact desorption of methanol or formaldehyde from Pt is observed. Instead, the dehydrogenation products hydrogen and CO ultimately desorb at higher temperature. Methanol- d_3 on Pt is completely decomposed and Hydrogen desorbs between 250 K and 350 K. Additionally, CO is observed between 350 and 500 K, as is expected for a CO TPD from Pt nanoparticles on $TiO_2(110)$.^[9] Additionally, some water is observed at 240 K. The traces are grouped and offset for clarity.

4. Photocatalytic Activity-Measurements

For the photocatalytic measurements, the catalyst is prepared and moved to the QMS. The pulse energy of the laser is monitored and the reactant is dosed at cryogenic conditions, unless stated otherwise. The crystal is heated to the reaction temperature and then the UV-illumination is started.

To determine turnover-frequencies (TOFs), the catalyst is exposed to a continuous background of a certain methanol pressure and the UV illumination is facilitated and blocked. Areas of constant photoconversion of methanol to H₂ (*m/z*=2) and formaldehyde (*m/z*=30) are chosen and both signals are integrated over time. For both species, transmission of the calibrated QMS, ionization cross sections and cracking pattern contributions are taken into account. The following integral area is normalized by the integral of a methanol TPD peak of the Ti-lattice sites (1 ML = 5.2 • 10¹⁴).^[7a] To calculate the TOF or site time yield (STY), this integral is divided by the number of active sites for formaldehyde production (0.06 ML, in this case for the BBO-vacancies^[8c] [see Fig. S2]) to yield a number of molecules per active site per second. Stoichiometry was checked for every catalytic experiment (see Fig. S8).

This TOF is possibly still limited by mass transport, but pressures higher than 4 • 10⁻⁷ were not investigated to ensure the proper detection by QMS.

The apparent quantum yield (AQY) can be calculated by relating the number of evolved molecules per second to the photon flux:^[10]

$$AQY (\%) = \frac{\text{Product molecules (s}^{-1}\text{)}}{\text{Photons (s}^{-1}\text{)}} \times 100 \quad (1)$$

In this work, the amount of product molecule (either formaldehyde or hydrogen) is divided by the number of incident photons from the laser.

In the classical picture, two charges are needed to oxidize methanol to formaldehyde as well as reduce protons to H₂.^[10b, 11] For the lowest photon fluxes (compare to Fig. S9), a quantum yield of 3.2% is obtained, while in the saturation regime (see Fig. S9), the quantum yield is about 0.11%.

4.1 Methanol Photocatalysis on TiO₂(110)

In Figure S6, an isothermal measurement of 1 L methanol on the TiO₂(110) is shown at 260 K. Upon irradiation, photoholes travel to the surface in the n-type semiconductor and oxidize methoxy species on the surface.^[8c, 12] Consecutive dosages of reactants after the first photoreaction, show only trace amounts of formaldehyde and no hydrogen, as would be expected from site-blocking of the hydroxyl groups from ethanol photochemistry (sterically or electronically).^[11]

A second type of measurements performed in this study are continuous reactant-dosage measurements, where a certain background pressure of methanol is applied to the prepared catalyst, then the sample is tempered to the reaction temperature of 260 K and then the irradiation experiments are started, while the surface is clearly saturated with methanol. Such an experiment on a bare r-TiO₂(110) surface is shown in Figure S7. In a background of 1 • 10⁻⁷ mbar methanol at 260 K, irradiation of the

photocatalyst is started. As expected from Fig. S6, also under the catalytic conditions the catalyst shows poisoning after the first initial irradiation.

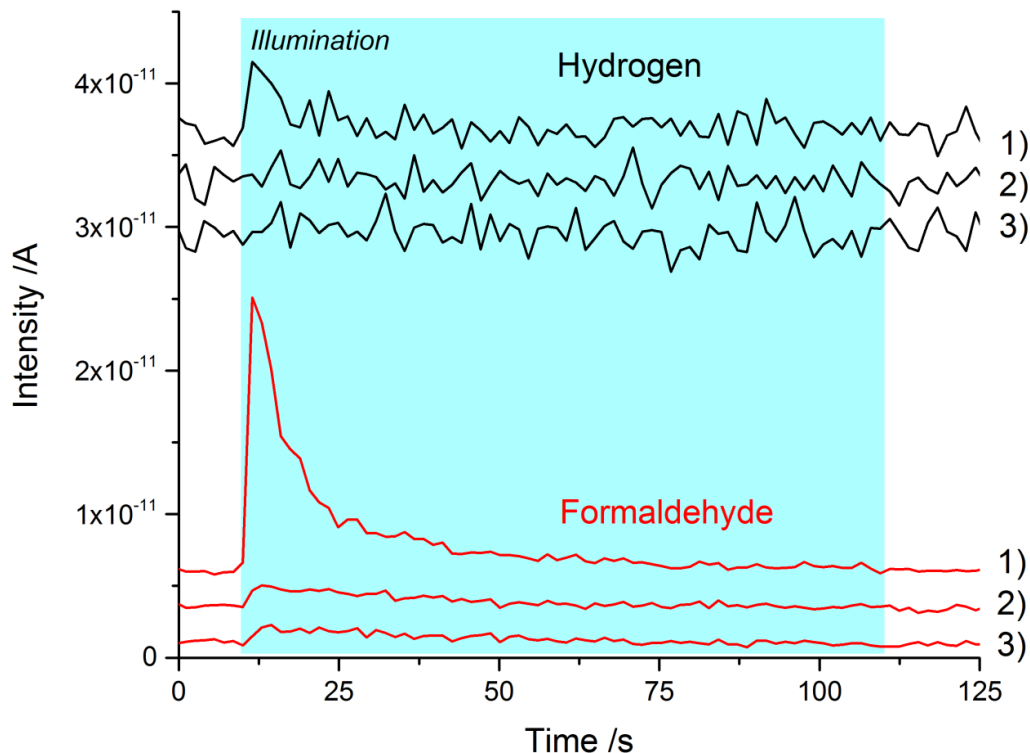


Fig. S6.: Isothermal mass traces of photoreaction of methanol on the $r\text{-TiO}_2(110)$ surface at 260 K. In experiment 1), 1 L methanol is adsorbed on the crystal at 110 K and then the crystal is tempered at 260 K. The blue box shows the time of UV-illumination. Upon excitation of the n-type semiconductor, photoholes travel to the surface and oxidize the methoxy to formaldehyde.^[8c, 12] At this temperature, the formed formaldehyde desorbs thermally, while only a very small trace amount of H_2 is observed.^[7b] For alcohols in general, the aldehyde formation is obtained, while the resulting hydroxyls from stoichiometry are known to poison the catalyst by site-blocking (sterically or electronically).^[1] This is shown by a consecutive coverage of the catalyst after 1) at cryogenic temperature by 1 L of Methanol. In the next started photoreaction at 260 K in 2), only a very small signal is obtained for formaldehyde and hydrogen is not obtained at all. This also holds true for further coverages as shown in traces 3).

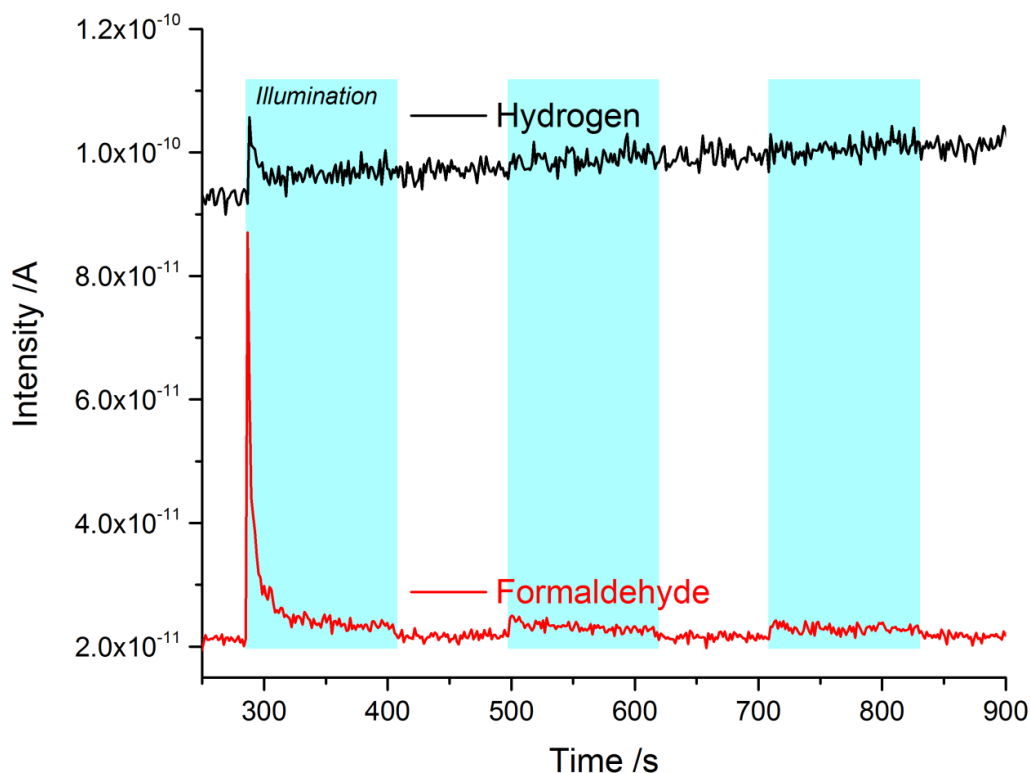


Fig. S7.: Isothermal experiment at 260 K on a $r\text{-TiO}_2(110)$ -surface in a constant methanol background of $1 \cdot 10^{-7}$ mbar. In agreement with Fig. S6, upon the first irradiation formaldehyde and some trace amounts of hydrogen desorb. Upon the second and third illumination, only a very small conversion of formaldehyde is obtained, since most sites are blocked by hydroxyls (sterically or electronically). No appreciable hydrogen signal is obtained during those irradiations.

4.2 Methanol Photocatalysis on $\text{Pt}_x/\text{TiO}_2(110)$

Photocatalytic measurements were performed on the $r\text{-TiO}_2(110)$ surface with different loadings of Pt clusters on the surface. Then a background pressure of methanol is applied and the reaction temperature is chosen. The photocatalytic reaction is then started by the UV illumination.

The reaction is stoichiometric at every pressure in the range of up to $4 \cdot 10^{-7}$ mbar, as shown in Fig. S8.

Varying the incident pulse energy of the UV illumination shows, that a saturation regime is achieved and for the small pulse energies, a linear dependency on the incident light is obtained (Fig. S10). In Figure S11, it is shown that the photocatalytic reaction is independent on the used wavelength, when the energy of the photon is higher than the semiconductor's band gap and furthermore independent on pulsed or continuous illumination, at least to a ns-Laser with 20 Hz. In Fig. S13 the thermal H_2 peak from dissociatively adsorbed methanol is shown prior to a photocatalytic experiment with Pt loaded $\text{TiO}_2(110)$. The comparison of O_2 photon-stimulated desorption (PSD) on a bare surface and after the used photocatalyst gives evidence

that it is possible to empty all active sites for the oxidation reaction, that takes place in the BBO defects.^[8c]

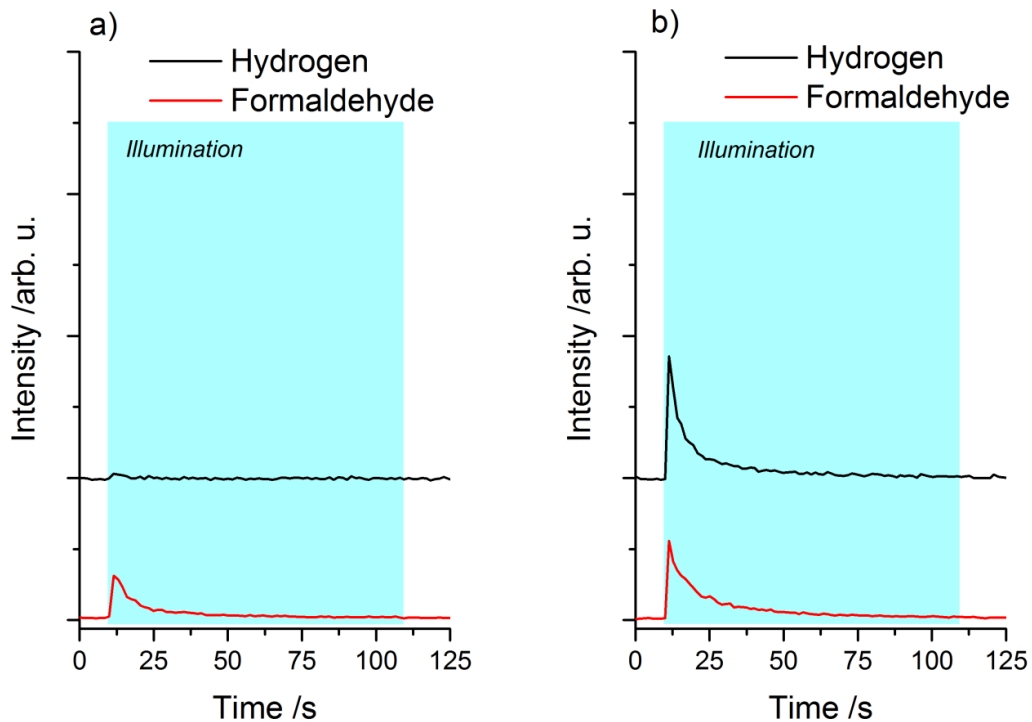


Fig. S8.: Quantified photochemical products of 1 L methanol on $r\text{-TiO}_2(110)$ [a] and on $\text{Pt}_x/\text{TiO}_2(110)$ [b] at 260 K. The converted raw data of Fig. 1 to ion intensity shows, that the signal of hydrogen and formaldehyde are almost stoichiometric for the Pt-loaded semiconductor [b]. The difference of the initial formaldehyde intensity between the bare and co-catalyst loaded TiO_2 is due to a reduction of photoactive sites as it can be seen from kinetic considerations (see section 4.3.). This reduction is attributed to a hydroxylation of bare titania as the resulting hydrogen moieties from thermal methoxy formation in the dark are blocking (either electronically or sterically) active sites.

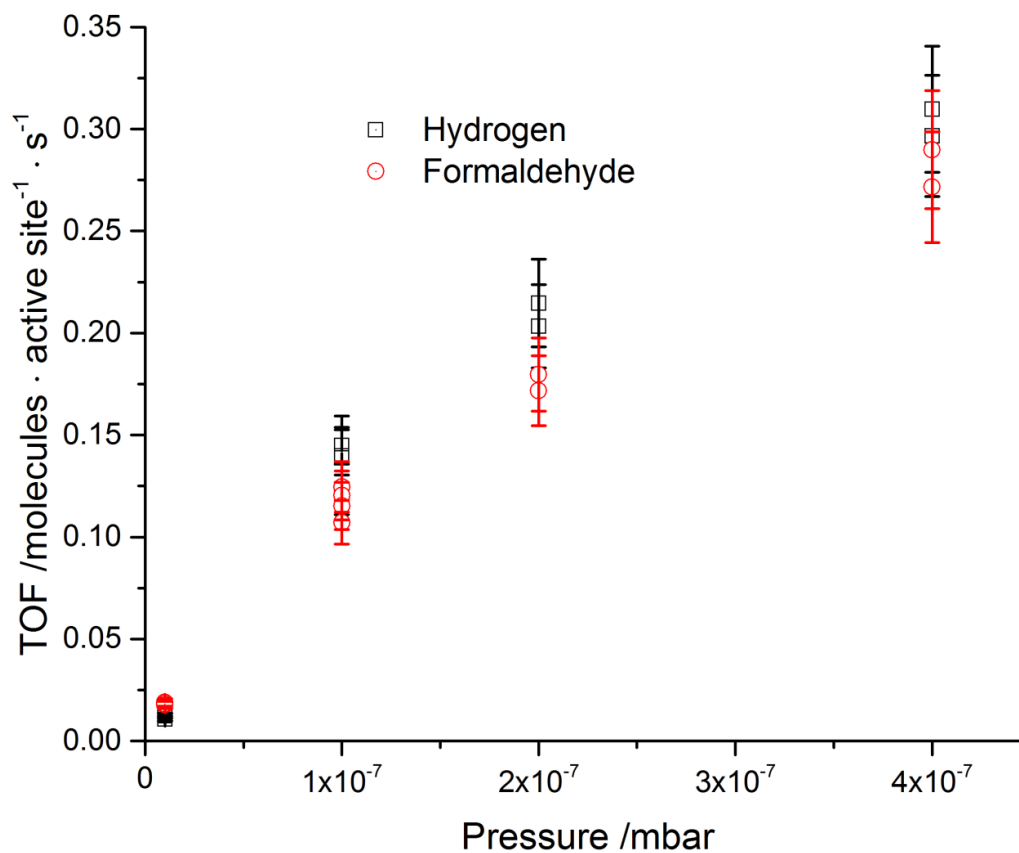


Fig. S9: Background pressure-dependent TOF for Pt_x/r-TiO₂(110) for photocatalytic measurements. The catalyst was prepared with a coverage of 1‰ clusters per TiO₂(110) surface atoms and methanol was introduced in the chamber background at 260 K. The reaction stoichiometry is independent of the pressure. Every square and circle pair resembles a photocatalytic experiment. Pressures higher than 4 · 10⁻⁷ mbar were avoided to ensure the integrity of the ultra-high vacuum.

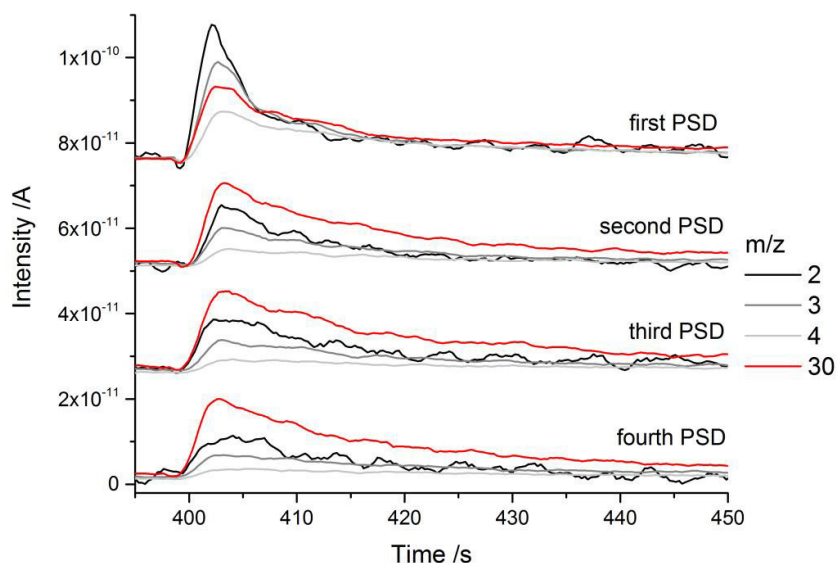


Fig. S10: Consecutive photocatalytic experiments with methanol on $\text{Pt}_x/\text{r-TiO}_2(110)$. The Pt coverage is 0.75% cluster per surface atom and the reaction is carried out at 260 K after adsorption of 1L methanol- d_3 . In contrast to Fig. S6, no catalyst poisoning is observed after an initial conditioning of the catalyst. Formaldehyde is measured with mass 30, while all hydrogen species are measured on the masses 2, 3 and 4. Between the cycles, the surface is recovered with 1 L of methanol- d_3 . In the first experiments, more H_2 is observed, which is attributed to dissociative methanol adsorption and an unknown degree of pre-hydroxylation of the semiconductor. In all runs, the formaldehyde intensity and kinetic decay stays the same and after the conditioning in the first shot, the same holds true for all hydrogen traces.

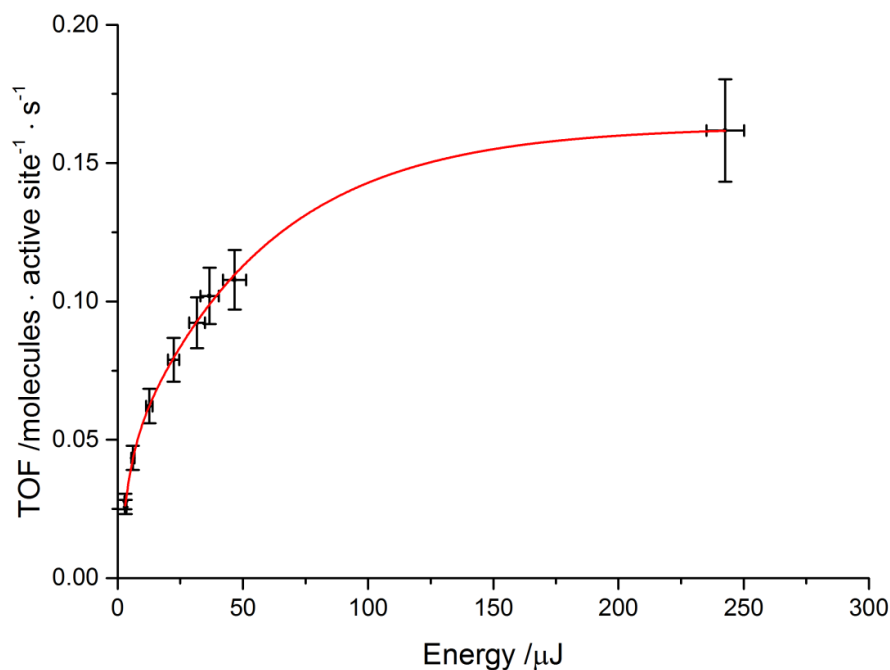


Fig. S11: Formaldehyde-TOF in dependency of the incident light energy. When the OPO-Laser is operated at 241.8 nm, typically a pulse energy of 250 μJ is obtained. When the laser beam intensity is reduced to pulse energies below 35 μJ , a linear dependence is obtained. The red line is only a guide to the eye to show that the photoexcitation saturates. The error bars in energy are determined by the standard deviation of the laser power, while the TOF errors bars are of 10%, except for the one at 250 μJ , which is a standard deviation of four measurements.

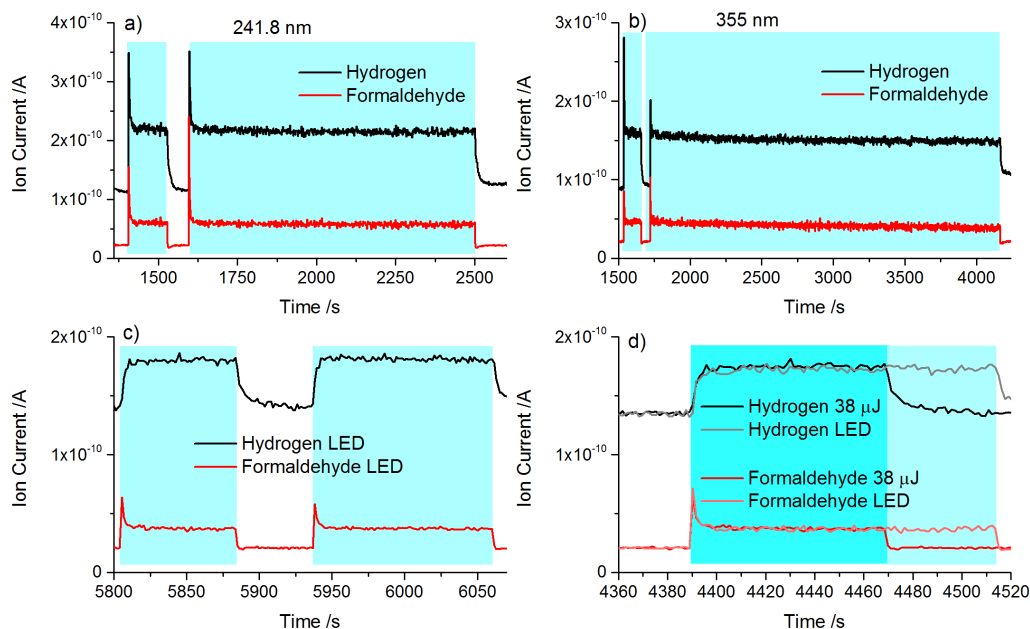


Fig. S12: Photocatalytic experiments depending on wavelength and illumination conditions with $\text{Pt}_x/\text{TiO}_2(110)$ and a cluster coverage of 1% is shown in a background of $1 \cdot 10^{-7}$ mbar methanol. In a), the sample is illuminated with $750 \mu\text{J}$ at 241.8 nm, and with illumination the reaction starts immediately. The reaction stops immediately, when the light is switched off and also runs constant. In panel b), the pulse energy is also hold constant at $250 \mu\text{J}$, but the wavelength is changed to 355 nm. The same amounts of hydrogen and formaldehyde are obtained, also in the second illumination over a time of 45 min. In c), the light source is exchanged from the ns-Laser with 20 Hz to a continuous light source. In this case, this light source is a UV-LED that emits light around 367 nm (see Fig. S11 for details), well above the band gap value for rutile TiO_2 of 3.0 eV. The photocatalytic reaction of Methanol shows the same behavior as in a) and b). In panel d), a direct comparison of the LED to laser excitation is shown, while the pulse energy of the laser is only $38 \mu\text{J}$ at 241.8 nm and the characteristics show no appreciable difference.

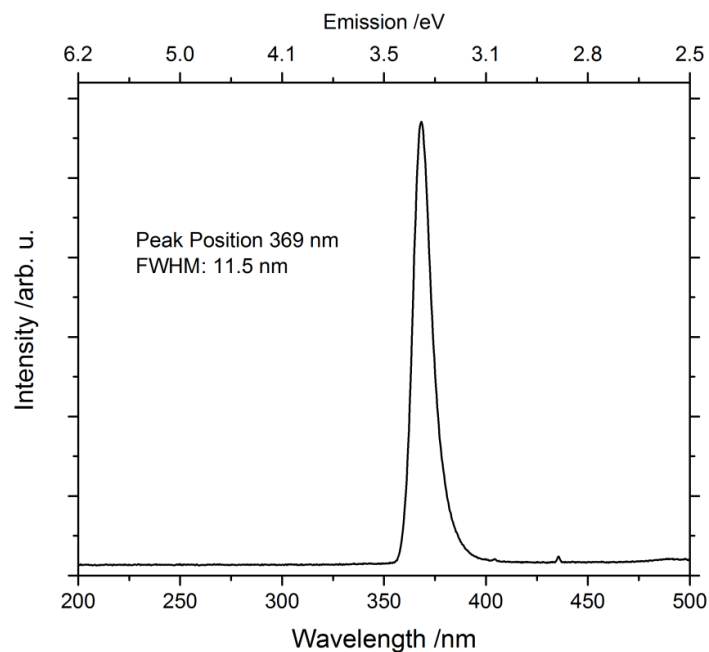


Fig. S13: Light emission characteristics of the UV-LED. The emission is centered around 369 nm with a full-width half maximum of 11.5 nm.

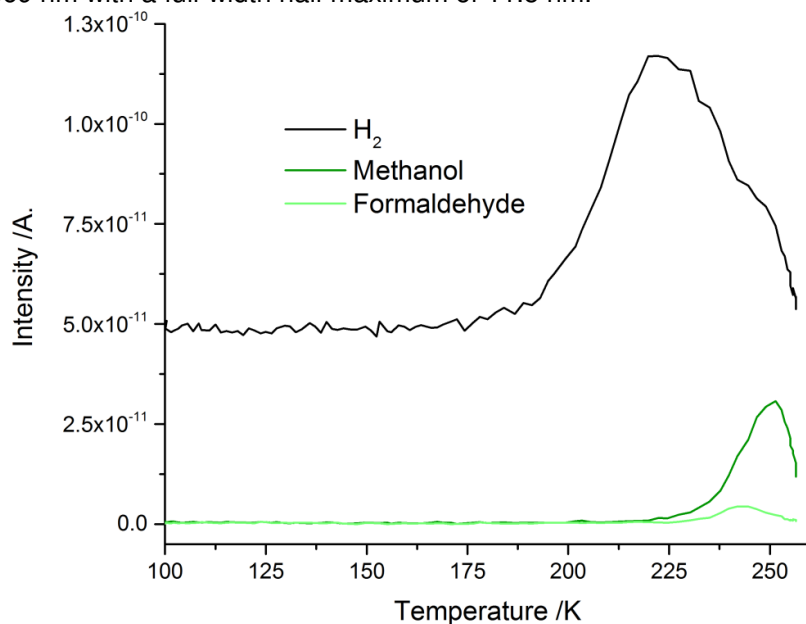


Fig. S14: TPD of Methanol in a background of $1 \cdot 10^{-7}$ mbar on 1% Pt_x/TiO₂(110) from 100 K to the reaction temperature at 260 K. After the oversaturation of the surface at cryogenic temperatures, some methanol desorption occurs around 250 K as it is expected from Fig. S4. In agreement with Fig. S5, hydrogen desorption from the Pt clusters is observed, too. As methanol adsorbs dissociatively on the TiO₂(110), which is known from STM studies^[13], the abstracted hydrogen atoms thermally recombine at the Pt clusters and desorb.

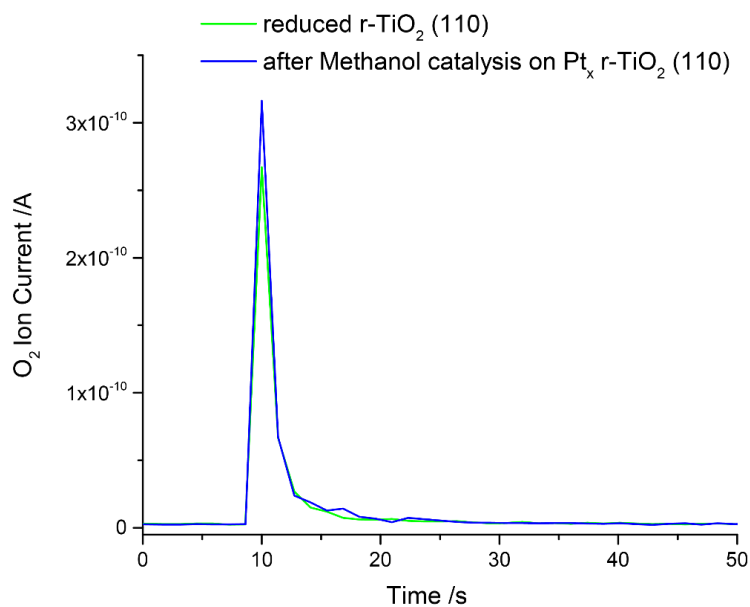


Fig. S15: O₂-Photon Stimulated Desorption at 100 K of the r-TiO₂(110)-surface and the Pt_x/TiO₂(110) catalyst after 2 h of photocatalysis. The green trace represents a O₂ PSD from bare surface, that is in excellent agreement with literature. After the catalytic experiment, the methanol background is turned off and the sample was illuminated for another 15 min to deplete all the methanol from BBO-vacancies. After illumination is turned off, the sample was cooled down to 100 K and exposed to 20 L of oxygen, to saturate the BBO-defect sites. Upon UV illumination, the same intensity and kinetics for the O₂ PSD are observed as for the bare sample, indicating that the amount of defect sites stays constant and that the methanol at least in the BBO-vacancies was completely converted.

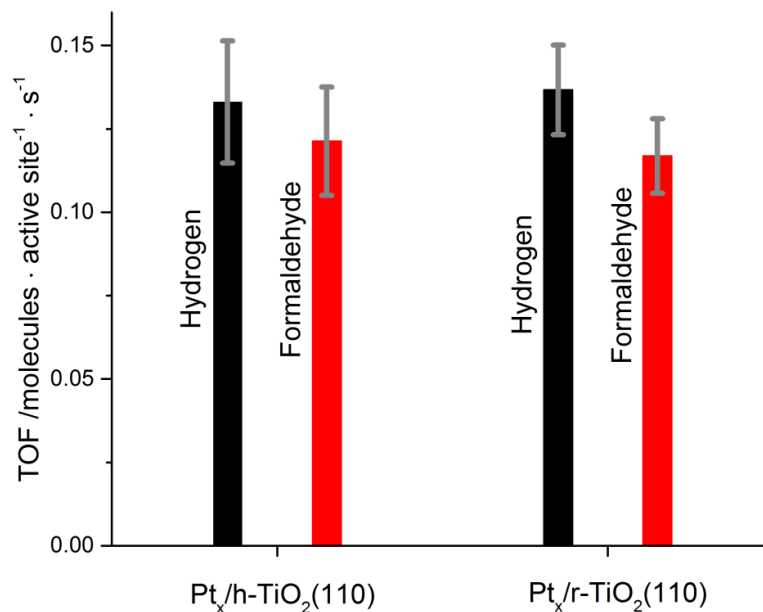


Figure S16: TOFs at 260 K for a background of $1 \cdot 10^{-7}$ mbar methanol on 1% Pt_x/TiO₂(110) for a reduced and pre-hydroxylated TiO₂(110). The h-TiO₂(110) was prepared in the same way as in a previous study by Kim *et al.*^[14]

4.3 Decay Rate Discussions for Single Coverage Experiments

The overall reaction (Eq. 2 and 3) of methanol can be written in the following kinetic description:

$$r = -\frac{d[\text{methanol}]_t}{dt} = \frac{d[\text{formaldehyde}]_t}{dt} = k * [hv] * [\text{methanol}]_t \quad (\text{Eq. S1})$$

Whereas under constant illumination, $k' = k * [hv]$. For the decay of product, the typical exponential decay function is yielded:

$$[\text{methanol}]_t = [\text{methanol}]_0 * \exp(-k't) \quad (\text{Eq. S2})$$

with $[\text{methanol}]_0$ being the initial methanol concentration in photoactive sites.
As

$$[\text{formaldehyde}]_t = [\text{methanol}]_0 - [\text{methanol}]_t \quad (\text{Eq. S3})$$

this results in the following expression for the integral product yield:

$$[\text{formaldehyde}]_t = [\text{methanol}]_0 * (1 - \exp(-k't)) \quad (\text{Eq. S4})$$

and its differential form, which represents the signal in the desorption measurements, being:

$$\frac{d[\text{formaldehyde}]_t}{dt} = [\text{methanol}]_0 * k' * \exp(-k't) \quad (\text{Eq. S5})$$

Therefore, it is evident that the rate constants (k' and k for constant photon fluxes) are reflected in the respective exponential decays, which are similar for the bare and the co-catalyst loaded semiconductor.

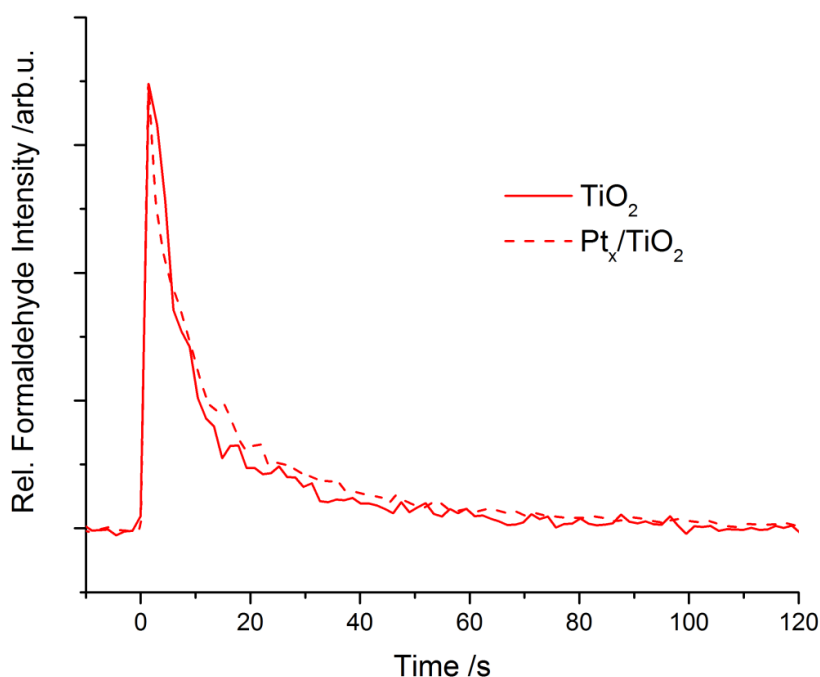


Fig. S17: Isothermal illumination experiments at 100 K of the r- $\text{TiO}_2(110)$ -surface and the $\text{Pt}_x/\text{TiO}_2(110)$ catalyst of 1 L of methanol with normalized intensities. It can be seen, that a loading with Pt co-catalysts does not change the exponential decay significantly within the accuracy of the measurements.

Note, that the rate constant cannot be directly modelled without the knowledge of the respective individual reaction steps, which are highly complex. Details in such a modelling can be seen in K.R. Philipps *et al.* in the Supporting Information.^[12]

References:

- [1] C. A. Walenta, S. L. Kollmannsberger, J. Kiermaier, A. Winbauer, M. Tschurl, U. Heiz, *Phys. Chem. Chem. Phys.* **2015**, *17*, 22809-22814.
- [2] A. S. Crampton, M. D. Rötzer, F. F. Schweinberger, B. Yoon, U. Landman, U. Heiz, *J. Catal.* **2016**, *333*, 51-58.
- [3] U. Diebold, *Surf. Sci. Rep.* **2003**, *48*, 53-229.
- [4] E. Wahlström, E. K. Vestergaard, R. Schaub, A. Rønnau, M. Vestergaard, E. Lægsgaard, I. Stensgaard, F. Besenbacher, *Science* **2004**, *303*, 511-513.
- [5] a) M. A. Henderson, *Langmuir* **1996**, *12*, 5093-5098; b) G. Lu, A. Linsebigler, J. T. Yates, *J. Phys. Chem.* **1994**, *98*, 11733-11738.
- [6] a) A. Sasahara, C. L. Pang, H. Onishi, *J. Phys. Chem. B* **2006**, *110*, 17584-17588; b) N. Isomura, X. Wu, Y. Watanabe, *J. Chem. Phys.* **2009**, *131*, 164707; c) S. Bonanni, K. Aït-Mansour, H. Brune, W. Harbich, *ACS Catal.* **2011**, *1*, 385-389.
- [7] a) Z. Li, R. S. Smith, B. D. Kay, Z. Dohnálek, *J. Phys. Chem. C* **2011**, *115*, 22534-22539; b) C. Xu, W. Yang, Q. Guo, D. Dai, M. Chen, X. Yang, *J. Am. Chem. Soc.* **2013**, *135*, 10206-10209.
- [8] a) M. A. Henderson, S. Otero-Tapia, M. E. Castro, *Faraday Discuss.* **1999**, *114*, 313-329; b) M. Shen, D. P. Acharya, Z. Dohnálek, M. A. Henderson, *J. Phys. Chem. C* **2012**, *116*, 25465-25469; c) M. Shen, M. A. Henderson, *J. Phys. Chem. Lett.* **2011**, *2*, 2707-2710.
- [9] A. Linsebigler, C. Rusu, J. T. Yates, *J. Am. Chem. Soc.* **1996**, *118*, 5284-5289.
- [10] a) A. Kudo, Y. Miseki, *Chem. Soc. Rev.* **2009**, *38*, 253-278; b) T. Hisatomi, J. Kubota, K. Domen, *Chem. Soc. Rev.* **2014**, *43*, 7520-7535.
- [11] a) B. Ohtani, *J. Photochem. Photobiol. C* **2010**, *11*, 157-178; b) B. Ohtani, *Chem. Lett.* **2008**, *37*, 216-229.
- [12] K. R. Phillips, S. C. Jensen, M. Baron, S.-C. Li, C. M. Friend, *J. Am. Chem. Soc.* **2013**, *135*, 574-577.
- [13] Z. Zhang, O. Bondarchuk, J. M. White, B. D. Kay, Z. Dohnálek, *J. Am. Chem. Soc.* **2006**, *128*, 4198-4199.
- [14] B. Kim, Z. Li, B. D. Kay, Z. Dohnalek, Y. K. Kim, *Phys. Chem. Chem. Phys.* **2012**, *14*, 15060-15065